



MAGNETIC REPORTER GENES FOR MRI-BASED STEM CELL TRACKING

Thesis submitted in accordance with the requirements of the
University of Liverpool for the degree of Doctor in Philosophy

by

Sofia Melo Pereira

January 2015

ACKNOWLEDGMENTS

This work has been supported by an EU Marie Curie Reintegration Grant contract number PERG08-GA-2010-276909, with support from the Institute of Translational Medicine, University of Liverpool.

A special thanks to my supervisors Dr Patricia Murray and Dr Arthur Taylor for creating a very interesting project and seeing the potential in me to fulfil it. All the wisdom and support given were essential to achieve this goal. Also, thank you to Prof David Edgar for all support given during lab meetings.

Thank you to Maria Christofi and Zohra Butt for helping me to put this project together. For the entire stem group, a big thank you for all the support given over the years, especially to Aleksandra Rak-Raszewska, Virginie Mournetas and Ilaria Santeramo for all their work and life related advices and for making my PhD years much lighter and enjoyable. You will always be in my heart.

I would also like to thank Dr. Stuart Marshall-Clarke and Miss Carolyn Rainer for all the help and availability using the FACS Aria and Mr George Miller for his help with the ICP analysis.

Finally, thank you to my parents and Miguel, my favourite people in the world, I owe everything to you. Also, my sincere respect for all animals sacrificed during the course of this project.

ABSTRACT

Introduction: Over the past decades, several labelling techniques have been used in an attempt to track stem cells using magnetic resonance imaging (MRI). However, very few of these were able to definitely determine the precise location of stem cells within a living organism and monitor throughout a long term period, without loss or diffusion of the signal. A novel MRI cell tracking method described in 2005 proposed that reporter genes that could effectively increase the iron content of a target cell would allow a stronger contrast when imaged via MR. Being a fundamental part of the iron metabolism, transferrin receptor-1 (TfR-1) and ferritin heavy chain-1 (Fth-1) were naturally suggested to have the potential to increase the iron load of cells when overexpressed. More recently, there has been some interest in the reporter gene MagA, which is a known iron transporter found in magnetotactic bacteria.

Aim: To evaluate the suitability of using TfR-1, Fth-1 and MagA as potential magnetic reporter genes for MRI-based cell tracking.

Methods: Several cell and stem cell lines were transduced with a 2nd generation HIV-based lentiviral system containing one or more magnetic reporters. Viral transduction resulted in genome incorporation of bicistronic construct(s) with TfR-1 gene alongside a gene encoding a green fluorescent reporter (GFP) and/or Fth-1 and MagA gene alongside a red fluorescent reporter (RFP). This allowed for identification and monitoring of positive cells with complementing imaging modalities: MRI and fluorescence based methods. Transgenes were evaluated for integration stability over passages and their influence on iron homeostasis was assessed; also, integration and/or overexpression were confirmed at the mRNA and protein level. Finally, the influence of magnetic reporters on intracellular iron retention and MRI contrast capacity was tested both *in vitro* and in

a model organism, the chick embryo.

Results: After analysing all three potential magnetic reporters, TfR-1 was found to be the most promising, as its overexpression induced an adjustment of iron homeostasis in Chinese hamster ovary K1 cells, leading to higher intracellular iron accumulation relative to controls. The same adjustment was found in mouse mesenchymal stem cells (mMSC), but only when TfR-1 was overexpressed in conjunction with Fth-1, also leading to an increase in iron retention capacity. However, a limitation was found when overexpressing Fth-1 in mMSC, as permanent iron supplementation was needed in order to keep these cells viable. In contrast with previous studies, MagA gene integration posed some restrictions in certain cell lines studied. The results presented here show that while some cell types are able to stably maintain MagA expression over several passages, others fail to survive and die shortly after transduction, suggesting that a potential toxic effect may be originating from MagA gene integration. From the surviving cells, two were compared side by side and contradictory results were obtained, demonstrating that MagA would only be a suitable magnetic reporter for some cell types.

Conclusion: The results obtained with this project are of relevance for reporter gene-based MRI cell tracking as they show that no single magnetic reporter is capable of generating detectable MRI contrast for a global cohort of cell lines. On the contrary, overexpression of endogenous genes or integration of foreign genes should be performed with caution and analysed on a case by case basis. Finally, for some cell type and magnetic reporter gene combinations, this study suggests that MRI could be a promising method for the longitudinal monitoring of engrafted cells, especially when the cells have been cultured in media supplemented with low concentrations of iron.

TABLE OF CONTENTS

Acknowledgments	I
Abstract	II
List of Figures	VIII
List of Tables	XV
List of Equations	XVI
List of Supplementary Data	XVII
List of Hyperlinks	XVIII
Abbreviations	XIX
Chapter 1 Introduction	1
Overview.....	1
1.1 Stem cell tracking and MRI	2
1.1.1 Magnetic resonance imaging	3
1.1.2 Exogenous vs. endogenous iron oxide-based contrast agents for MRI	5
1.1.3 Metalloprotein-based MRI reporter genes	6
1.2 Iron metabolism.....	8
1.2.1 Regulation of intracellular iron – IRP/IRE regulatory system.....	10
1.3 Transferrin Receptor-1	13
1.3.1 Transferrin receptor-1 molecular structure and biochemistry	14
1.3.2 Cellular internalization of iron through transferrin/TfR-1 complex	15
1.3.3 Transferrin receptor-2.....	16
1.4 Ferritin	17
1.4.1 Ferritin molecular structure and biochemistry	18
1.4.2 Ferritin internalization of iron	19
1.5 Magnetotactic bacteria, magnetosomes and MagA	20
1.5.1 Magnetosome formation	22
1.5.2 MagA gene.....	23
1.6 Aims	25
Chapter 2 Materials and Methods	27
Overview.....	27
2.1 Molecular cloning	27

2.1.1 Reporter genes cDNA	27
2.1.2 Extraction of total RNA.....	28
2.1.3 DNase treatment of RNA.....	29
2.1.4 Synthesis of cDNA by reverse transcriptase.....	29
2.1.5 cDNA amplification by polymerase chain reaction	29
2.1.6 Electrophoresis by FlashGel® System.....	31
2.1.7 Cloning transgenes cDNA into pCR®II-TOPO®	32
2.1.8 Transformation of chemically competent cells by heat-shock	32
2.1.9 Analysis of transformed colonies	33
2.1.10 Cloning of lentiviral constructs.....	33
2.1.11 Nucleic acid purification and precipitation	35
2.1.12 Electrophoresis of agarose gels.....	35
2.1.13 Ligation	36
2.1.14 Sequence analysis.....	38
2.2 Cell Culture	39
2.2.1 Cell lines.....	39
2.2.2 Routine cell culture	39
2.2.3 Cryopreservation and recovery of cells.....	40
2.3 Generation of reporter cell lines	41
2.3.1 Production optimization of lentiviral particles.....	43
2.3.2 Transfection of the producer cell line	45
2.3.3 Concentration of lentiviral particles.....	45
2.3.4 Determination of viral titres and efficiency of transduction.....	46
2.3.5 Transduction of stem cells.....	47
2.3.6 Fluorescence Activated Cell Sorting	48
2.4 Evaluation of intracellular iron	49
2.4.1 Cell viability when exposed to ferric citrate	49
2.4.2 Intracellular iron quantification	50
2.5 Expression of transgenes at mRNA and Protein Level.....	52
2.5.1 Reverse transcription quantitative Real-Time PCR	52
2.5.2 Immunofluorescence.....	56
2.5.3 Western Blotting	57

2.6 Transmission electron microscopy (TEM) analysis	61
2.7 Cell viability capacity.....	62
2.8 Multilineage differentiation	62
2.9 Animal work.....	64
2.10 Magnetic Resonance Imaging.....	65
2.10.1 Sample preparation.....	65
2.10.2 Imaging	65
2.11 Error bars and statistical analysis	66
Chapter 3 Stable Integration of Reporter Genes into Established Cell Lines	67
3.1 Introduction	67
3.1.1 Transfection methods	67
3.1.2 Lentiviral-mediated transduction.....	69
3.1.3 Choice of lentiviral vectors	71
3.2 Results.....	73
3.2.1 Generation of lentiviral constructs.....	73
3.2.2 Production of lentiviral particles	79
3.2.3 Determination of viral titer of lentiviral particles	81
3.2.4 Transduction efficiency between cell lines	83
3.2.5 Optimization of Intracellular Iron Loading	87
3.3 Discussion	91
Chapter 4 Transferrin Receptor-1 as a Reporter Gene for MRI Tracking of Cells.....	94
4.1 Introduction	94
4.1.1 Studies targeting transferrin receptor-1	94
4.1.2 Transferrin receptor-1 as an MRI reporter gene.....	95
4.2 Results.....	98
4.2.1 Evaluation of reporter gene integration	98
4.2.2 Cell viability	103
4.2.3 Iron homeostasis	104
4.2.4 Intracellular Iron Uptake <i>in vitro</i>	112
4.2.5 MRI	114
4.3 Discussion	122
4.4 Supplementary data	127

Chapter 5 Ferritin Heavy Chain-1 and Transferrin Receptor-1 as Reporter Genes for MRI	
Tracking of Cells	129
5.1 Introduction	129
5.1.1 Studies targeting ferritin heavy chain-1	129
5.1.2 Ferritin heavy chain-1 gene as an MRI reporter gene	130
5.2 Results.....	134
5.2.1 Reporter gene integration in normal cell culture conditions.....	134
5.2.2 Reporter gene integration with iron supplementation.....	141
5.2.3 Cell viability	145
5.2.4 Overexpression of reporter genes at mRNA and protein level	147
5.2.5 Intracellular Iron Uptake <i>in vitro</i>	154
5.2.6 MRI	155
5.3 Discussion	163
5.4 Supplementary data	171
Chapter 6 MagA as a Reporter Gene for MRI tracking of cells	173
6.1 Introduction	173
6.1.1 MagA gene as an MRI reporter gene	173
6.2 Results.....	177
6.2.1 Reporter gene integration in stem cell lines	177
6.2.2 Reporter gene integration in CHO K1 cell line.....	181
6.2.3 Iron homeostasis	186
6.2.4 Reporter gene stability with iron supplementation.....	191
6.2.5 Intracellular Iron Uptake <i>in vitro</i>	193
6.2.6 MRI	198
6.3 Discussion	208
6.4 Supplementary data	216
Chapter 7 General Discussion And Conclusion	217
Bibliography	227
Appendix I cDNA sequences	242
Appendix II Buffers, solutions, media, other material.....	245
Appendix III Plasmid maps.....	251

LIST OF FIGURES

- Figure 1** – Illustration of IRP/IRE regulatory system acting on a post-transcriptional level of two groups of genes involved in iron metabolism, ferritin and transferrin receptor-1 genes. When iron is depleted, IRPs bind to IREs present in UTRs and repress the translation, in case of ferritins, or promote mRNA stability in case of transferrin receptor-1. On the other hand, when the IRPs recognize there is an excess of iron, they unbind from the IRE, promoting the translation of ferritins and the endonucleolytic cleavage of transferrin receptor-1 mRNAs. 12
- Figure 2** – Transmission electron microscopy of a *Magnetospirillum magneticum* with a magnetosome chain (A) and of isolated magnetosomes (B) with intact membranes, indicated by the arrow. Scale bars are 100 nm. Reproduced with permission from Benoit *et al.* (2009) (A) and from Schüler (2004) (B). 21
- Figure 3** – Simplified illustration showing a hypothesized mechanism for membrane invagination, iron biomineralization of magnetosomes and MagA function as an iron transporter protein. Illustration based on Komeili *et al.* (2006). 23
- Figure 4** – Illustration of transfection of the producer cell line HEK 293T(N) with transfer, packaging and envelope plasmids, which comprise a 2nd generation HIV-based lentiviral system. After collecting the lentiviral particles from the media, cells of interest can be transduced in a target cell line. 42
- Figure 5** – Plasmid maps of parental vectors dT (A) and GFP (B) and lentiviral constructs dT_F (C), GFP_T (D) and dT_M (E). Some key features are represented, such as the fluorophore of each plasmid (dTomato or eGFP transgene) connected to the gene of interest (Fth-1/TfR-1/MagA) through an IRES to allow bicistronic expression of both genes. Also represented is the promoter elongation factor 1-alfa (EF1- α) to initiate the constitutive expression and the HIV-long terminal repeats (LTR), which flank the region to be incorporated into the host's cell genome. 79
- Figure 6** – Flow cytometry analysis of red (dT) and green (GFP) fluorescent populations of HEK 293T(N) cells after being transduced with the same volume of viral supernatant, produced with different plasmid ratios. Error bars represent SEM ($n=3$) (M&M, p.43). 80
- Figure 7** – Flow cytometry analysis of red (dT, dT_F and dT_M) and green (GFP, GFP_T) fluorescent cells in relation to the volume of lentiviral particles used for transduction of HEK 293T(N) cells. A 40% fluorescent threshold was set and the chosen value for titration is annotated with a *. Error bars represent SEM (number of biological replicates are indicated in the legend) (M&M, p.46). 82
- Figure 8** – Viral titer of different lentiviral preparations determined in HEK 293T(N) cells. Error bars represent SEM (number of biological replicates are indicated in the X-axis) (M&M, p.47). 83
- Figure 9** – Flow cytometry analysis of populations of fluorescent cells after transduction with different viral preparations, such as dT (A), GFP (B), dT_F (C), GFP_T (D) and dT_M (E) in several types of cells, demonstrating the variation of transduction efficiency between cell lines. As previously, the chosen value to calculate the viral titer was below the 40% fluorescent threshold and is annotated with a *. Error bars represent SEM where possible (numbers of biological replicates are indicated on the graphs) (M&M, p46). 84

- Figure 10** – Viral titer of different lentiviral preparations specifically determined for each cell line (**A**). Error bars represent SEM where possible. Numbers of biological replicates are indicated in the table in **B** (M&M, p47). 86
- Figure 11** – Cell viability evaluation of several cell lines, when exposed to increasing amounts of ferric citrate for a period of 24h (**A**). Absorbance is shown in relation to control cells (cultured without supplementation). The best logistic fit for each cell line is represented in the cell's correspondent colour. The 0.2 and 2 mM marks display the chosen concentrations of ferric citrate used in further experiments, supported by the table in **B**. EC50 and EC80 represent the ferric citrate concentration (mM) that causes 50 and 80% cell reduction relative to control. Error bars represent SEM ($n=3$) (M&M, p49). 87
- Figure 12** – Measurement of intracellular iron content of mMSC, mKSC, HEK 293T(N) and CHO K1 with different supplements: FC-0.2 mM of ferric citrate, AC-50 μ M L-ascorbic acid, HL-1.28 mM human holo-transferrin. Error bars represent SEM ($n=3$). 90
- Figure 13** – Control (C17s) and TFR-1/FTH-1 transfected cells (C17-12s) were supplemented with iron (1 mM of ferric citrate and 1 mg/ml holo-transferrin) for 48h before transplantation into an adult mouse brain. **a** – schematic representation of a coronal section of a mouse brain, indicating the injection site (is), control regions in the cortex (ctx) and striatum (str). **b** and **c** – Magnetic resonance (7 T) T_2^* -weighted images of *ex vivo* mouse brain sections, 20 days after injection. A clear contrast is observed between injected cells and the surrounding brain tissue; analysing regions of interest within the injection site, a significant signal loss is detected for C17-12s ($n=3$), when compared to C17s ($n=2$). Reproduced with permission from Deans *et al.* (2006). 97
- Figure 14** – Representative pictures of CHO K1 cells, at P3 (**A**) and P8 (**B**) post-transduction, and control cells (untransduced) at an equivalent passage. GFP corresponds to GFP transduced cells and GFP_T to TfR-1 transduced cells. All green fluorescent pictures were taken with the same exposure conditions. Scale bars correspond to 100 μ m. 99
- Figure 15** – Flow cytometry histograms of (**A**) CHO K1 cells, at P3 and P8 after transduction. Histograms show the number of events (cells) counted (y-axis) versus the fluorescence intensity (x-axis). Green fluorescence (GF) gate represents GFP-positive cell population plotted in **B**. The Xmean (**C**) represents the mean fluorescence obtained from the gated region (GFP cells). Error bars represent SEM ($n=3$); a.u. - arbitrary units; (M&M, p.48). 100
- Figure 16** – RT-qPCR relative quantification of GFP, Viral_T and CHO_T targets in control, GFP and GFP_T transduced CHO K1 cells at P1 and P3 post-transduction. GFP and Viral_T expression values are normalised to P1 (**A**) and endogenous CHO_T to control cells (**B**). A very significant statistical decrease of endogenous TfR-1 is observed only in TfR-1 overexpressed cells (GFP_T), both at P1 and P3. Error bars represent SEM ($n=3$) (M&M, p.52). 102
- Figure 17** – Viability of GFP and GFP_T transduced CHO K1 cells at P1 and P4 post-transduction. Data points are normalised to Control (untransduced) cells. Error bars represent SEM ($n=3$) (M&M, p.61). 103
- Figure 18** – RT-qPCR relative quantification of transgenes GFP (**A**) and Viral_T (**B**) when GFP and GFP_T transduced cells were exposed to 0 and 0.2 mM of iron. Error bars represent SEM ($n=3$) (M&M, p.52). 105
- Figure 19** – Relative quantification of endogenous TfR-1 (CHO_T) expression obtained via

RT-qPCR (**A** and **C**) and of total (endogenous + viral) TfR-1 (Total_T) protein levels obtained via WB (**B** and **D**), when control, GFP and GFP_T transduced cells were exposed to different iron concentrations of 0 and 0.2 mM (M&M, p.50). Graphs **A** and **B** evaluate target expression levels when each cell line is exposed to different iron concentrations and graphs **C** and **D** the difference between cell lines when exposed to the same iron concentration. Error bars represent SEM ($n=3$) (M&M, p.52 for RT-qPCR and p.57 for WB)..... 106

Figure 20 – Representative immunofluorescence pictures of GFP_T transduced CHO K1 cells, showing nuclear staining with DAPI (**A**), green fluorescence (GF) obtained by GFP reporter (**B**) and the detection of TfR-1 proteins, visualized by red fluorescence (RF) (**C**). The overlay between these conditions shows that GFP reporter is mainly expressed in the nucleus (**D**), TfR-1 is present outside the nuclear region, more likely localized at the cellular membrane (**E**) and that there is a mixed population in (**F**), where only the high expressing GFP cells also have an overexpression of TfR-1. A higher magnification of the insets is presented on the right hand side pictures. Scale bars: 25 μ m; (M&M, p.56)..... 109

Figure 21 – Relative quantification of Fth-1 (Total_F) expression obtained via RT-qPCR (**A** and **C**) and the respective protein levels obtained via WB (**B** and **D**), when Control, GFP and GFP_T transduced cells were exposed to different iron concentrations of 0 and 0.2 mM. Graphs **A** and **B** evaluate Total_F expression levels when each cell line is exposed to different iron concentrations and graphs **C** and **D** the difference between cell lines when exposed to the same iron concentration. Error bars represent SEM ($n=3$) (M&M, p.52 for RT-qPCR and p.57 for WB)..... 111

Figure 22 – Intracellular iron content of CHO K1 cells determined with the Ferrozine assay (**A**). Control, GFP and GFP_T transduced cells were supplemented with different iron concentrations of 0, 0.2 and 2 mM for 4 days prior to measurement (Iron supplementation, p.50). Fold-differences between GFP_T cells and Control or GFP are presented for each supplementation condition in **B**. Error bars represent SEM ($n=3$) (M&M, p.50)..... 113

Figure 23 – MR imaging of cell pellets of CHO K1 cells. **A** is a T2-weighted representative MR image obtained with the MRI of control with no iron supplementation (0 mM), GFP and GFP_T both supplemented with 0.2 and 2 mM of iron (Iron supplementation, p.50). Relaxation times T1 and T2 were quantified on a specific region of the cell pellet and are represented in **B** and **C**, respectively. Error bars represent SEM ($n=3$) (M&M, p.65). 115

Figure 24 – Fluorescence and MR imaging of GFP (**A**, **C** and **E**) and GFP_T (**B**, **D** and **F**) transduced CHO K1 cells, 2 days after injection in the midbrain of a chick embryo (E5). Cells were injected after culture with or without iron supplementation (0, 0.2 and 2 mM of iron for 3 days) (Iron supplementation, p.50). In the fluorescence imaging panel, bright field (BF) and green fluorescence (GF) are projection images from the whole embryo; overlays are presented for both left and right views and were used as a reference guidance for MR imaging; scale bars correspond to 1 mm. In the MRI panel, anatomical images are displayed as transverse sections along the rostrocaudal axis of the embryo (left to right); 10 sections are displayed for each embryo. All images are representative from the results obtained and were equally processed with ImageJ software. Arrows indicate T2 shortening effect; b – bubble of air. Position of the embryo: F – front; B – back; R – right; L – left; number of biological and technical replicates is

	indicated in the table above (M&M, p.65).	120
Figure 25	– Representative pictures of mMSC at P1 post-transduction. Control cells (untransduced) are displayed at an equivalent passage. dT corresponds to dTomato transduced cells; dT_F to Fth-1 transduced cells; GFP to GFP transduced cells; GFP_T to TfR-1 transduced cells and dT_Fth-1+GFP_T to cells transduced in conjunction with Fth-1 and TfR-1. All sets of pictures were taken with the same exposure conditions. A higher magnification of the insets is presented on the right hand side panel. RF - Red fluorescence; GF - Green fluorescence; RF/GF - Merge. Scale bars correspond to 100 μ m.	136
Figure 26	– Viability assay on transduced mMSC at P1 post-transduction with normal cell culture conditions. Data points and statistics are presented in relation to Control (untransduced) cells. Error bars represent SEM ($n=3$) (M&M, p.61).....	138
Figure 27	– RT-qPCR relative quantification of dTomato, Viral_F, GFP and Viral_T targets in transduced mMSC at P1 and P3 post-transduction (without FACS sorting). Expression values of target genes are plotted against P1 without (A) and with (B) iron supplements from 24h post-transduction. Error bars represent SEM ($n=3$) (M&M, p.52).	140
Figure 28	– Representative pictures of mMSC at P7 post-transduction and FACS sorted, as well as control cells (untransduced) at an equivalent passage. All sets of pictures were taken with the same exposure conditions. RF-Red fluorescence; GF-Green fluorescence; RF/GF - Merge. Scale bars correspond to 100 μ m.	143
Figure 29	– Flow cytometry histograms (A and D) of mMSC cells, at P8 post-transduction and after FACS sorting. Histograms show the number of events (cells) counted (y-axis) versus the fluorescence intensity (x-axis). Red/ green fluorescence (RF/GF) gate represents dTomato/GFP-positive cell population plotted in B and E . The Xmean (C and F) represents the mean fluorescence obtained from the gated region (dTomato/ GFP cells). Error bars represent SEM ($n=3$). a.u-arbitrary units; M&M, p.48.	144
Figure 30	– Viability of transduced mMSC at P1 and P8 post-transduction when supplemented with iron. Cells at P8 were already FACS sorted. Data points and statistics are presented in relation to Control (untransduced) cells, cultured in the same conditions. Error bars represent SEM ($n=3$) (M&M, p.61).....	146
Figure 31	– RT-qPCR relative quantification of endogenous and viral TfR-1 transcripts (Total_T, A and B) and of endogenous and viral Fth-1 transcripts (Total_F, C and D) in Control and transduced mMSC at P1 and P3 post-transduction. Expression values of target genes are normalized in relation to P1 (A and C) and to Control cells (B and D). Error bars represent SEM ($n=3$) (M&M, p.52).	149
Figure 32	– WB relative quantification of Total_T (A) and Total_F (B) targets in Control and transduced mMSC at P8 post-transduction and after FACS sorting. Error bars represent SEM ($n=3$) (M&M, p. 57).	151
Figure 33	– Representative immunofluorescence pictures of Control, GFP and GFP_T in panel A and dT, dT_F and negative control in panel B , at P8 post-transduction and after FACS sorting. Nuclear region is shown by DAPI staining. In panel A , green fluorescence (GF) is originated from the GFP reporter and the detection of TfR-1 proteins is visualized with a red fluorescent antibody. On the contrary, in panel B , red fluorescence (RF) is obtained due to the presence of dTomato reporter and the detection of TfR-1 proteins is visualized with a green fluorescent antibody. dT_F+GFP_T condition was not possible to be evaluated by IF due to the presence of both GFP and dTomato reporters. All pictures sets	

were taken with the same exposure conditions. Negative controls targeting only the secondary Abs used are included to prove specificity to the primary Ab. Scale bars: 25 μm ; M&M, p.56..... 152

- Figure 34** – Intracellular iron content of mMSC cells determined with the Ferrozine assay. Control and transduced cells were supplemented with different iron concentrations of 0.2 mM from 24 post-transduction or 2 mM for 4 days prior to measurement (Iron supplementation, p.50). A non-supplemented (0 mM) Control was also included. Error bars represent SEM ($n=3$) (M&M, p.50). 154
- Figure 35** – MR imaging of cell pellets of mMSC cells. **A** is a T2-weighted representative MR image obtained with the MRI of Control with no iron supplementation (0 mM); Control and dT_F+GFP_T, dT and dT_F, GFP and GFP_T both supplemented with 0.2 mM from 24h post-transduction or with 2 mM of iron for 4 days (Iron supplementation, p.50). Relaxation times T1 and T2 were quantified on a specific region of the cell pellet and are represented in **B** and **C**, respectively. Error bars represent SEM ($n=3$) (M&M, p. 65). 156
- Figure 36** – Fluorescence and MR imaging of dT and dT_F (A and B), GFP and GFP_T (C and D) and dT_F+GFP_T and dT (0 mM) (E and F) transduced mMSC cells, 2 days after injection in the midbrain of a chick embryo (E5). Cells received 2 mM of iron supplementation for 3 days prior to injection, with the exception of dT (0 mM) (F), which did not receive any supplementation (Iron supplementation, p.50). In the fluorescence imaging panel, bright field (BF) and red/green fluorescence (RF/GF) are projection images from the whole embryo; overlays are presented for both left and right views and were used as a reference guidance for MR imaging; scale bars correspond to 1 mm. In the MRI panel, anatomical images are displayed as transverse sections along the rostrocaudal axis of the embryo (left to right); 10 sections are displayed for each embryo. All images are representative from the results obtained and were equally processed with ImageJ software. Arrows indicate T2 shortening effect; b – bubble of air; * – blood. Position of the embryo: F – front; B – back; R – right; L – left; number of biological and technical replicates is indicated in the table above (M&M, p.65)..... 161
- Figure 37** – Transmission electron microscopy (TEM) of HEK 293FT cells overexpressing MagA, where electron dense spots are visible (and highlighted in the inset) and have been suggested to correspond to iron oxide nanoparticles. Reproduced with permission from Zurkiya *et al.* (2008)..... 174
- Figure 38** – RT-qPCR relative quantification of dTomato (**A**) and MagA (**B**) transgenes, evaluated in four dT_M transduced cell lines (MOI=1), including HEK 293T(N) as a reference, over a period of 40 days. Error bars represent SEM ($n=3$) (M&M, p.52). 178
- Figure 39** – Cell proliferation of HEK 293T(N), mESC, mMSC and mKSC during a period of 8 days after being transduced with dT (**A**) or dT_M (**B**) lentiviral constructs. Data points are plotted in relation to control cells. The threshold line represents 50% of cell counts. Error bars represent SEM ($n=3$) (M&M, p.61). 180
- Figure 40** - Representative pictures of CHO K1 (**A**) and HEK 293T(N) (**B**) cells at P7 post-transduction, and Control cells (untransduced) at an equivalent passage. dT corresponds to dTomato transduced cells and dT_M to MagA transduced cells. All red fluorescent pictures were taken with the same exposure conditions. Scale bars correspond to 100 μm 182
- Figure 41** – Flow cytometry histograms (**A**) of CHO K1 and HEK 293T(N) cells, at P3 after

transduction. Histograms show the number of events (cells) counted (y-axis) versus the fluorescence intensity (x-axis). Red fluorescence (RF) gate represents the dTomato-positive cell population plotted in (B). The Xmean (C) represents the mean fluorescence obtained from the gates region (RF cells). Error bars represent SEM ($n=3$). a.u.–arbitrary units; M&M, p.48. 183

- Figure 42** – RT-qPCR relative quantification of dTomato and MagA transgene expression at P1 and P3 in dT_M transduced CHO K1 cells or HEK 293T(N). For the evaluation of transgene expression over two passages, HEK 293T(N) cells were not FACS sorted. Expression values are plotted against P1. Error bars represent SEM ($n=3$) (M&M, p.52). 185
- Figure 43** – Proliferation assay on dT and dT_M transduced CHO K1 cells at P1 and P4. Data points are plotted in relation to Control (untransduced) cells. Error bars represent SEM ($n=3$). A statistical difference is found in dT_M (P1) cells when compared to Control and dT cells of the same passage (M&M, p.61). 186
- Figure 44** – Relative quantification of transferrin receptor-1 (Total_T) expression obtained via RT-qPCR (A and C) and the respective protein levels as obtained via WB (B and D), when Control, dTomato (dT) and MagA (dT_M) transduced cells were exposed to different iron concentrations of 0, 0.2 and 2 mM (Iron supplementation, p.50). Graphs A and B evaluate Total_T expression levels when each cell line is exposed to different iron concentrations and graphs C and D the difference between cell lines when exposed to the same iron concentration. Error bars represent SEM ($n=3$) (M&M, p.52 for RT-qPCR and p.57 for WB). 188
- Figure 45** – Relative quantification of ferritin heavy chain1 (Total_F) expression obtained via RT-qPCR (A and C) and the respective protein levels as obtained via WB (B and D), when Control, dTomato (dT) and MagA (dT_M) transduced cells were exposed to different iron concentrations of 0, 0.2 and 2 mM ((Iron supplementation, p.50)). Graphs A and B evaluate Total_F expression levels when each cell line is exposed to different iron concentrations and graphs C and D the difference between cell lines when exposed to the same iron concentration. Error bars represent SEM ($n=3$); (M&M, p.52 for RT-qPCR and p.57 for WB). 189
- Figure 46** – RT-qPCR relative quantification of transgenes dTomato (A) and MagA (B) when dTomato (dT) and MagA (dT_M) transduced cells were exposed to 0, 0.2 or 2 mM of iron. Error bars represent SEM ($n=3$) (M&M, p.52). 192
- Figure 47** – Intracellular iron content of CHO K1 (A) and HEK 293T(N) (B) cells determined with the Ferrozine assay. Control, dTomato (dT) and MagA (dT_M) transduced cells were supplemented with different iron concentrations of 0, 0.2 and 2 mM for 4 days prior to measurement (Iron supplementation, p.50). Error bars represent SEM ($n=3$) (M&M, p.50). 194
- Figure 48** – Prussian blue and DAB staining of HEK 293T(N) Control, dTomato (dT) and MagA (dT_M) cells exposed to different iron concentrations of 0, 0.2 and 2 mM (Iron supplementation, p.50), M&M, p.51. 196
- Figure 49** – Electron microscopy images of HEK 293T(N) cells. (A) Control cells exposed to no iron supplementation and (B) dTomato (dT) and (C) MagA (dT_M) transduced cells supplemented with 0.2 mM of iron. Electron dense spots in A inside mitochondria and B and C are found in the cytoplasm. Scale bars: 200 nm; M&M, p.60. 197
- Figure 50** – MR imaging of cell pellets of CHO K1 (A,C and E) and HEK 293T(N) (B, D and F)

cells. **A** and **B** are T2-weighted representative MR images obtained with MRI of Control with no iron supplementation (0 mM), dTomato (dT) and MagA (dT_M) both supplemented with 0.2 and 2 mM of iron (Iron supplementation, p.50). Relaxation times T1 and T2 were quantified on a specific region of the cell pellet and represented in **C-D** and **E-F**, respectively. Error bars represent SEM ($n=3$) (M&M, p.65). 199

Figure 51 – Fluorescence and MR imaging in CHO K1 (A, B, C and D) and HEK 293T(N) (E, F, G and H) cells, 2 days after injection in the midbrain of a chick embryo (E5). dTomato (dT) and MagA (dT_M) cells were injected with or without iron supplementation (2 mM of iron for 3 days) (Iron supplementation, p.50). In the fluorescence imaging panel, bright field (BF) and red fluorescence (RF) are projection images from the whole embryo; overlays are presented for both left and right views and were used as a reference guidance for MR imaging; scale bars correspond to 1 mm. In the MRI panel, anatomical images are displayed as transverse sections along the rostrocaudal axis of the embryo (left to right); 10 sections are displayed for each embryo, with the exception of D which has 12 images, to visualize the signal at the bottom of the neck. All images are representative from the results obtained and were equally processed with ImageJ software. Arrows indicate T2 shortening effect; b – bubble of air. Position of the embryo: F – front; B – back; R – right; L – left; number of biological and technical replicates is indicated in the table above (M&M, p.65)..... 205

LIST OF TABLES

Table 1 – Conditions of PCR reaction and cycling for cDNA fragment amplification.	30
Table 2 – Description of primers used to amplify cDNA fragments by PCR, with the respective annealing temperatures and resulting product size. Note that in the primer sequences, the red nucleotides represent either the start codon (ATG) or the stop codon (TTA, TCA). The green sequence is a Kozac sequence that was purposely introduced before the start site of TfR-1 and MagA cDNA to help initiate the translation process. This was not performed for Fth-1 cDNA because a native Kozac sequence is already present. Novel restriction enzymes are highlighted in bold.	31
Table 3 – Conditions used for ligation reactions.	37
Table 4 – Primers used for sequence analysis of the constructs generated. F – Forward orientation; R – Reverse orientation.	38
Table 5 – Relative amounts of each individual plasmid and mass ratios tested for transfection optimization. Note that in the negative control (1:0:0) the packaging and envelope plasmids are not included for the transfection of HEK 293T(N) cells.	43
Table 6 – Sequence of primers used for amplification of cDNA by Real-Time PCR and resultant amplification product. <i>H-Homo sapiens</i> , <i>M-Mus musculus</i> , <i>C-Cricetulus griseus</i> ; GAPDH primers were designed to amplify a cDNA region common to both mouse and human variants; Pabpn1 and Vezt were taken from Bahr <i>et al.</i> (2009).	54
Table 7 – Description of primary and secondary Abs used in immunofluorescence (IF) and western blot (WB).	57
Table 8 – Cloning strategies, including the amplification method, electrophoresis of amplified fragments and colony restriction digests performed to create and evaluate individual constructs containing Fth-1 (A and B), TfR-1 (C and D) and MagA (E and F) cDNAs. Half arrows represent forward (F) or reverse (R) primers. Components of the lentiviral vectors: red – dTomato gene; grey – IRES; dark green - EF1- α promoter; light green – GFP gene.	74

LIST OF EQUATIONS

Equation 1 – Fenton reaction (Fenton, 1894).	9
Equation 2 – Calculation of individual viral titre, which is the number of transducing units (TU), <i>i.e.</i> , single lentiviral particles, that exist per volume unit of harvested viral supernatant. F corresponds to the ratio of fluorescent cells, N is the total number of cells at the time of transduction (5×10^4), V the volume (ml) of diluted vector added to each well and D the fold-dilution of vector used for transduction (Kutner <i>et al.</i> , 2009).	47

LIST OF SUPPLEMENTARY DATA

- Supplementary figure 1** – Representative western blots and correspondent total protein gels from control, GFP and transferrin receptor-1 (GFP_T) transduced CHO K1 cells, supplemented for 4 days with 0 or 0.2 mM of iron. Orange rectangle highlights total TfR-1 (endogenous + viral, here described as Total_T) protein expression, with a predicted molecular weight (MW) of 100 kDa; white rectangle corresponds to actin expression with 42 kDa and blue rectangle to Fth-1 (or Total_F) with 21 kDa. Protein quantification was normalized using total protein gels and confirmed using actin as a reference protein (M&M, p.57). 127
- Supplementary figure 2** – Representative immunofluorescence pictures of Control, GFP and GFP_T transduced CHO K1 cells, showing nuclear staining with DAPI, green fluorescence (GF) originating from the GFP reporter and the detection of TfR-1 proteins, visualized with a red fluorescent antibody (RF). A clear protein overexpression of TfR-1 is found in GFP_T. All pictures sets were taken with the same exposure conditions. RF pictures with a longer exposure time are shown in the insets. A negative control targeting only the secondary Ab is included to confirm the specificity to the primary Ab. Scale bars: 25 µm; (M&M, p.56). 128
- Supplementary figure 3** – Representative differentiation pictures of Control, dT, GFP, dT_F, GFP_T and dT_F+GFP_T incubated with 0.2 mM of iron 24h post-transduction, along with a non-supplemented Control. Differentiation potential of these cells was directed towards the formation of osteocytes, adipocytes or chondrocytes (M&M, p.62). 171
- Supplementary figure 4** – Representative western blot and correspondent total protein gels from Control, dT, GFP, ferritin heavy chain-1 (dT_F), transferrin receptor-1 (GFP_T) and dT_F+GFP_T transduced mMSC cells, iron supplemented since 24h after transduction. Orange rectangle highlights total TfR-1 (endogenous + viral, described as Total_T) protein expression, with a predicted molecular weight (MW) of 100 kDa; white rectangle corresponds to actin expression with 42 kDa and blue rectangle to Fth-1 (endogenous + viral, Total_F) with 21 kDa. Sometimes another band is detected when targeting Fth-1, which may correspond to a post-translational modification of this protein. Protein quantification was normalized using total protein gels and confirmed using actin as a reference protein (M&M, p. 57). 172
- Supplementary figure 5** – Representative western blots (**A** and **B**) and correspondent total protein gels (**C** and **D**) from Control, dTomato (dT) and MagA (dT_M) transduced CHO K1 (**A** and **C**) and HEK 293T(N) (**B** and **D**) cells, supplemented for 4 days with 0, 0.2 or 2 mM of iron. Orange rectangle highlights TfR-1 (or Total_T) protein expression, with a predicted molecular weight (MW) of 100 kDa; white rectangle corresponds to actin expression with 42 kDa and blue rectangle to Fth-1 (or Total_F) with 21 kDa. Sometimes another band is detected when targeting Fth-1, which may correspond to a post-translational modification of this protein. Please note that because actin was not stable in different blots, particularly in the case of CHO K1 cells (**A**), protein quantification was normalized using only total protein gels for this cell line (M&M, p. 57). 216

LIST OF HYPERLINKS

NCBI - <http://www.ncbi.nlm.nih.gov/>

UniProt KB P02794 - <http://www.uniprot.org/uniprot/P02794>

Permission from Benoit *et al.* (2009) - <https://s100.copyright.com/CustomerAdmin/PLF.jsp?ref=209848d3-dd50-4059-9e73-3b8fe1cd7970>

Permission from Schüler (2004) - <https://s100.copyright.com/CustomerAdmin/PLF.jsp?ref=effb77f4-3a42-4485-a7a5-55d75dd01c73>

pCR2.1MS-magA plasmid, Addgene, 21751 – <http://www.addgene.org/21751/>

pHIV-dTomato plasmid, Addgene, 213734 – <https://www.addgene.org/21374/>

pHIV-eGFP plasmid, Addgene, 21373 – <https://www.addgene.org/21373/>

Packaging plasmid psPAX2, Addgene, 12260 – <https://www.addgene.org/12260/>

Envelope plasmid pMD2.G, Addgene, 12259 – <https://www.addgene.org/12259/>

Gene therapy clinical trials worldwide – <http://www.wiley.com/legacy/wileychi/genmed/clinical/>

Permission from Deans *et al.* (2006) <https://s100.copyright.com/CustomerAdmin/PLF.jsp?ref=b8af3bd3-a2d9-4259-9bc8-c1db1a198906>

Permission from Zurkiya *et al.* (2008) – <http://s100.copyright.com/CustomerAdmin/PLF.jsp?ref=73a790f3-5535-4f62-970c-299461cf71e4>

M. magnetotacticum MS-1 bacterial strain (GenBank AB001699.1) – <http://www.ncbi.nlm.nih.gov/nuccore/AB001699.1>

M. magneticum AMB-1 bacterial strain (GenBank D32253.1) – <http://www.ncbi.nlm.nih.gov/nuccore/D32253>

Mus musculus Ferritin heavy chain 1 mRNA (NM_010239.2) – http://www.ncbi.nlm.nih.gov/nuccore/NM_010239.2

Mus musculus Transferrin Receptor-1 mRNA (NM_011638.4) – http://www.ncbi.nlm.nih.gov/nuccore/NM_011638.4

ABBREVIATIONS

a.u. – Arbitrary units.

AAVs – Adeno-associated viral vectors

Ab – Antibody

Blast – Basic local alignment search tool

CHO K1 - Chinese Hamster Ovary cell line K1

CIP - Calf Intestinal Alkaline Phosphatase

D – Dapi

DAB – 3,3'-Diaminobenzidine

DMEM – Dulbecco's Modified Eagle's Medium

DMT1 – Divalent metal transporter 1

DMT-1 – Divalent Metal Transporter-1

DOX – Doxycycline

E – Embryonic day

EC₁₀ – Effective concentration at 10% inhibition

EF1- α – Elongation factor 1- α promoter

eGFP – Enhanced green fluorescent protein

ETR – Engineered transferrin receptor-1

FCS – Foetal calf serum

FTH-1 – Human ferritin heavy chain-1

Fth-1 – Mouse ferritin heavy chain-1

FTL-1 – Human ferritin light chain-1

Ftl-1 – Mouse ferritin light chain-1

GAPDH – Glyceraldehyde-3-phosphate dehydrogenase

GF – Green fluorescence

GO – Gene Ontology

HEK 293T(N) – Human embryonic kidney cells 293-T(N)

HEPES – 4-(2-hydroxyethyl)-1-piperazineethanesulfonic acid

hESC – Human embryonic stem cells

HIV – Human immunodeficiency virus

hMSC – Human mesenchymal stem cells

ICP – Inductively coupled plasma

IF – Immunofluorescence

IM – Insertional mutagenesis

IRE – Iron responsive element

IRES – Internal ribosome entry site

IRP – Iron regulatory protein

LIF – Leukaemia Inhibitor factor

LIP - Labile iron pool

LTR – Long terminal repeats

LV – Lentivirus-based vectors

MAI – Magnetosome Island

MCS – Multiple cloning site
MEM – Minimum Essential Medium Eagle
MEMRI – Manganese-Enhanced MRI
mESC – Mouse embryonic stem cells
mKSC – Mouse kidney-derived stem cells
mMSC – Mouse mesenchymal stem cells
MOI – Multiplicity of infection
MRI – Magnetic resonance imaging
MtF – Mitochondrial ferritin
n – Number
NCBI – National centre for biotechnology information
NTC – Non-template controls
p – *p*-value
PBS - Dulbecco's Phosphate Buffered Saline
PET - Positron emission tomography
pg - Picogram
RF – Red fluorescence
RFP - Red fluorescent protein
RT – Room temperature
RT-qPCR – Reverse transcription quantitative Real-Time PCR
RVs – Retroviral vectors
SD – Standard deviation
SEM – Standard error (SE) of mean (M)
SIN – self-inactivating
SPECT - Single-proton emission computed tomography
SPIONs - Superparamagnetic iron oxide nanoparticles
T – Tesla
TBP/Tbp - TATA box protein (human/ mouse)
TE – Echo times
TEM – Transmission electron microscopy
TET – Tetracycline
TFR-1 – Human transferrin receptor-1
Tfr-1 – Mouse transferrin receptor-1
TR – Repetition times
TU - Transducing units
UTR - Untranslated region
UV – Ultraviolet
VSV-G – vesicular stomatitis virus G
WB – Western Blot
WPRE – Woodshuck post-transcriptional regulatory element
WST-8 – [2-(2-methoxy-4-nitrophenyl)-3-(4-nitrophenyl)- 5-(2,4-disulfophenyl)-2H-tetrazolium
WT – Wild type

CHAPTER 1

INTRODUCTION

OVERVIEW

The field of regenerative medicine using stem cell-based treatments has overcome many challenges over the past few decades. However, the fate of stem cells following administration into model organisms still needs to be further studied and understood. In order to gain some answers, one possibility is to visualize stem cell spatial localization through magnetic resonance imaging (MRI). The monitoring of stem cells *in vivo* would be a great advantage not only to allow a specialized treatment of injured deep internal organs, but also to unravel and understand important key points during the course of tissue regeneration. This could be achieved by modifying the stem cells so that they overexpress iron-binding proteins, or 'magnetic reporters', thus enabling their detection via MRI. This chapter covers the basic biology of iron metabolism, which ferritin and transferrin receptor-1 are a fundamental part of, as well as the origin and function of the MagA gene in magnetotactic bacteria. A review of the use of these genes as magnetic reporters in MRI-based cell tracking will be introduced in the subsequent chapters.

1.1 STEM CELL TRACKING AND MRI

The most routinely used technology for the study of stem cells is fluorescence optical imaging and there are a number of reporter genes readily available, such as red or green fluorescent proteins (RFP/GFP) (Gould and Subramani, 1988). Another optical imaging system uses luminescence derived from specific organisms and is therefore designated as bioluminescence imaging, a technology that captures visible light emission from cells or tissues. This is only possible due to presence of specific reporters as, for example, firefly luciferase, originally derived from the North American firefly (de Wet *et al.*, 1985), that and upon activation via D-luciferase substrate emits a 560 nm emission peak (Sadikot and Blackwell, 2004). However, a pitfall commonly associated with these optical reporters is the low depth penetration capacity, which is essential for regenerative studies focused on injured deep internal organs.

In order to understand stem cell-based regenerative processes, one needs to effectively monitor cell survival, migration and differentiation potential (Bhirde *et al.*, 2011). Therefore, over the past years, there has been an increasing interest in technologies which are able to explore in-depth the human body. Some examples are positron emission tomography (PET) (Bailey *et al.*, 2005), contrast-enhanced ultrasonography (US) (Jang and Lee, 2004), X-ray computed tomography (X-ray CT) (Herman, 2009), MRI, amongst others. All these technologies greatly differ in imaging resolution capacity, contrast used and user safety, but they effectively monitor non-invasively functional processes within an organism (Engstrom *et al.*, 2003). In particular, the use of MRI for stem cell tracking has mainly relied on iron as

a contrast agent to visualize cells of interest. New techniques have been emerging in an attempt to provide optimum iron load into the cells either by labelling with exogenous contrast agents or by modifying the cells through genetic engineering. On one hand, the exogenous materials introduced into the cells are very often composed of iron oxide covered with a biocompatible synthetic shell, like, for example, superparamagnetic iron oxide nanoparticles (SPIONs) (Peacock *et al.*, 2012; Renshaw *et al.*, 1986). On the other hand, genetic engineering of the cell focuses mainly on introducing or overexpressing one or more components of the iron metabolic pathway (Deans *et al.*, 2006; Genove *et al.*, 2005) or other synthetic or foreign genes (Iordanova *et al.*, 2010; Zurkiya *et al.*, 2008) in order to augment intracellular iron load, using iron present within a cell or in its surroundings.

1.1.1 Magnetic resonance imaging

MRI has been used since the mid-1980s and is a well suited technology with an adequate spatial resolution for deep internal organ, tissue and molecular imaging (Cherry, 2004). Also, it is one of the best choices for non-invasive imaging. Perhaps the most important feature is that MRI acts without emitting ionizing radiation, but other aspects are also of great significance, such as: i) high spatial resolution and tissue contrast, providing precise and detailed information about organ morphology and function; ii) unlimited tissue penetration and iii) the potential use of a broad range of contrast mechanisms. Usually, clinical MRI scanners use between 1.5 and 3 Tesla (T), which might pose as problem in the required resolution for detection of small amounts of high-iron contrast stem cell

populations (Harney and Meade, 2010). This could be simply overcome by using scanners with high-field strengths such as 4.7, 9.4, 11.7 or 14T (Louie *et al.*, 2000).

The mechanism behind conventional MR imaging is the detection of signals from relaxation mechanisms, produced by the magnetization of hydrogen nuclei (^1H), present in mobile water protons, either in the form of spin-lattice relaxation time (T1), spin-spin relaxation time (T2 or T2*). Once the sample is positioned in a static magnetic field, the magnetic moment characteristic of ^1H tends to align with the direction of the magnetic field. The signal detection is directly proportional to the concentration of nucleus imaged in a certain region and decreases exponentially with the time constant T2 or T2* (Haacke *et al.*, 1999).

A few compounds may enhance MRI contrast, by affecting the relaxation properties of the nuclei present in their surroundings. On one hand, the use of gadolinium containing agents may result in positive contrast, primarily affecting T1 time constant and promoting signal intensity. On the other hand, a negative contrast can be achieved with the use of compounds made of superparamagnetic iron oxides, mainly affecting T2 (or T2*) time constant, resulting in signal loss. This signal loss is due to the strong magnetic moment associated with iron oxide particles and its interaction with the surrounding water protons (Ahrens and Bulte, 2013; Jung and Jacobs, 1995).

More information about the physical properties of MRI and the use of iron oxide-based contrast agents can be found in Henkelman *et al.* (2001), Hawrylak *et al.* (1993) and Bulte and Kraitchman (2004).

1.1.2 Exogenous vs. endogenous iron oxide-based contrast agents for MRI

The most commonly used method to generate contrast for MRI is to label cells *in vitro* with exogenous iron oxide-based contrast agents, like SPIONs (Patel *et al.*, 2010). This method of labelling has proven to be effective and robust for stem cell tracking of small populations and not only is a good choice for short-term studies up to 6 weeks, it also has been shown not to interfere with cell viability or proliferation capacity (Bulte *et al.*, 2001; Taylor *et al.*, 2012). Nevertheless, if long-term regenerative studies are an essential requirement for stem cell-based treatments, exogenously incorporating iron inside a cell does pose some limitations. After an initial cell labelling with SPIONs, cell proliferation causes the label to be diluted by 50% following each cell division (Taylor *et al.*, 2014). Also, even though exogenous labelling materials are biocompatible to some extent, they are still foreign objects to the cell and might be easily rejected, via exocytosis, or degradation. Exocytosis of the label could lead to it being incorporated by neighbouring host cells, giving rise to false positives (Bulte and Kraitchman, 2004). Another potential cause of false positive signal could arise from phagocytosis of dead stem cells by neighbouring host cells or macrophages, leading to the transfer of the magnetic label. At last, even though SPIONs have been proven not to interfere with cell viability or proliferation, it has been reported that in some cell types it can inhibit cell differentiation (Chen *et al.*, 2010; Kostura *et al.*, 2004).

On the other hand, the use of endogenous iron through the expression of genes that may influence the intracellular iron content of a cell may prove to have

certain advantages over other labelling methods. For instance, stem cells expressing metalloprotein-based reporter genes can also be monitored non-invasively, in theory through long periods of time. If these genes are integrated into the cell's genome, it is much less likely to undergo a loss of signal during cell proliferation or even to be rejected by the cell. In the case of cell death, reporter gene expression will immediately arrest and its products will probably be more easily dissolved by the normal metabolism, avoiding the risk of false positive signal (Rodriguez-Porcel *et al.*, 2009). Also, other genes of interest can be associated with the magnetic reporter gene, creating suitable vectors for gene therapy (Liu *et al.*, 2009). In the case of basic research, the gene of interest can be a fluorescent protein and in this case MRI contrast can be confirmed with optical imaging. An obvious limitation to this contrast method is the low sensitivity of detection, when compared to materials like SPIONs (Gilad *et al.*, 2007b). If iron availability is not present in surrounding areas to the cell in sufficient amounts, magnetic reporter gene overexpression may not incorporate sufficient iron volumes to generate MRI contrast. Nonetheless, metalloprotein-based reporter genes have been suggested to be sufficient to provide a good MRI contrast for stem cell tracking (Deans *et al.*, 2006; Genove *et al.*, 2005).

1.1.3 Metalloprotein-based MRI reporter genes

The next generation of MRI-based approaches for cell tracking rely on new technologies for cellular imaging. As previously described, metalloprotein-based reporter genes can involve several components of the iron metabolism pathway or iron-related proteins in order to induce an up-regulation of intracellular iron. Some

of those components targeted so far are proteins such as: the transferrin receptor-1 (Moore *et al.*, 1998); the tyrosinase enzyme (Alfke *et al.*, 2003); a synthetic lysine-rich protein (Gilad *et al.*, 2007a); both subunits of the ferritin complex used either together or separately (Cohen *et al.*, 2005; Genove *et al.*, 2005) and even synthetically modified ferritin (Iordanova *et al.*, 2013); and, lastly, foreign genes such as the bacterial iron transporter protein, MagA (Goldhawk *et al.*, 2009; Zurkiya *et al.*, 2008).

1.2 IRON METABOLISM

Iron is a vital and indispensable element to life, as it is necessary to produce heme and non-heme iron proteins involved in several cellular processes. The most important example is iron present in haemoglobins of erythrocytes, which comprise about 60-70% of total body iron and are essential for oxygen transport. Iron is also present in cytochromes, which take part in the electron transport during aerobic cellular respiration, and is a key constituent in enzyme production and DNA synthesis, amongst other functions (Ponka and Lok, 1999). When iron is depleted within a cell it may lead to cell arrest and death (Muckenthaler *et al.*, 2008). Nevertheless, however important this nutrient is, when present in excess, it becomes toxic, leading to the formation of highly reactive oxygen radical species, damaging cell membranes, proteins and ultimately affecting the integrity of nucleic acids (Hentze and Kuhnt, 1996).

Iron is often found in two interconvertible oxidation states: ferrous iron (Fe^{2+}) and ferric iron (Fe^{3+}). At normal physiological conditions, ferrous iron readily converts into ferric iron. This process is known as the Fenton reaction (Equation 1) and the resultant oxidation leads to the formation of hydroxyl radicals ($\text{HO}\cdot$) and hydroxide ions (OH^-). When ferric iron is reduced back into ferrous iron, it forms a hydroperoxyl radical (HO_2) and another oxygen-radical species (H^+) in the process (Ponka *et al.*, 1998; Powell, 1998).



Equation 1 – Fenton reaction (Fenton, 1894).

This essential element can only be obtained through diet, and therefore, the balance to meet the needs between consumption and storage starts by regulation of iron absorption at the intestinal level, and later, by the expression of proteins involved in iron storage and transport (Bothwell, 1995). Initially, at a broad level and in response to specific liver signalling, iron is absorbed through metal transporters localized on the intestine duodenal mucosa membrane, like ferroportin and the divalent metal transporter-1 (DMT1) (Ganz and Nemeth, 2012; Hentze *et al.*, 2004). Iron is then released from intestinal enterocytes into the plasma serum and captured by a protein called transferrin. This protein is responsible for the bloodstream circulation and transport of iron to all cells in the body. Transferrin can be loaded with one or two units of iron and is called mono or diferric transferrin, respectively. The latter is also commonly known as holo-transferrin and it is the predominant state present in the bloodstream. When this protein does not contain any bound iron, it is called apo-transferrin. The bond between iron and transferrin, although efficient, is easily reversible to allow the metal to be released upon demand (Aisen, 2004). Due to iron's high reactivity when present in physiological oxygen conditions, its metabolism is tightly controlled and well-coordinated by post-transcriptional expression of genes that make part of the iron regulatory protein/ iron responsive element (IRP/IRE) regulatory system.

1.2.1 Regulation of intracellular iron – IRP/IRE regulatory system

Inside the cell there is transient free iron, known as the labile iron pool (LIP). The magnitude of LIP is tightly controlled by the cell and this transient iron is bound to low molecular weight molecules, ready to be used in a variety of cellular processes (Thomson *et al.*, 1999). The depletion or excess of iron within the LIP is easily detected in the cytoplasm by iron regulatory proteins, IRP1 and IRP2. The importance of IRPs in development is demonstrated by the occurrence of embryonic lethality when IRP1 and IRP2 genes are knocked-out in mice (Smith *et al.*, 2006). The IRPs bind to iron responsive elements (IRE), which are hairpin structures present in untranslated regions (UTR) of mRNAs from genes involved in iron metabolism (Wilkinson and Pantopoulos, 2014). Many genes are involved in the uptake, utilization, storage and export of iron at the cellular level (Muckenthaler *et al.*, 2008). Two of the most important genes are responsible for iron uptake (transferrin receptor genes) and storage (ferritin genes) and therefore both contain iron responsive elements in their mRNA UTR. Transferrin receptors act at the cellular membrane interacting with mono or diferric transferrin from the bloodstream. Both ferritin and transferrin receptors can serve either as iron donors or acceptors; however, ferritin has the capacity not only to receive and accept large quantities of iron, but also to act as an intracellular storage molecule (Aisen *et al.*, 2001).

When iron is depleted inside a cell, IRPs bind to an IRE located at the 5'UTR of ferritin mRNAs, repressing translation, in order to stop the acquisition and

storage of iron present in the LIP. In contrast, it also binds to an IRE found in the 3'UTR of transferrin receptor-1 transcripts to promote mRNA stability and prevent degradation. Consequently, this increases the translation and the number of receptors available, allowing more interactions with holo-transferrin molecules, thus increasing the levels of intracellular iron. On the other hand, when elevated iron levels are detected by IRPs, this regulatory protein unbinds from the 5'UTR IRE of ferritins and its expression is readily induced, capturing the majority of iron in the form of a soluble non-toxic ferrihydrite mineral (Harrison and Arosio, 1996), before the Fenton reaction can take place. Meanwhile, the opposite happens for transferrin receptor-1 transcripts, and IRPs unbind from the 3'UTR IRE, allowing its cleavage by endonucleases and subsequent degradation (Ford *et al.*, 1984; Ponka *et al.*, 1998; Rouault, 2006). With those mechanisms, the translation of ferritins and transferrin receptor-1 is efficiently controlled at the post-transcriptional level. Figure 1 illustrates this process.

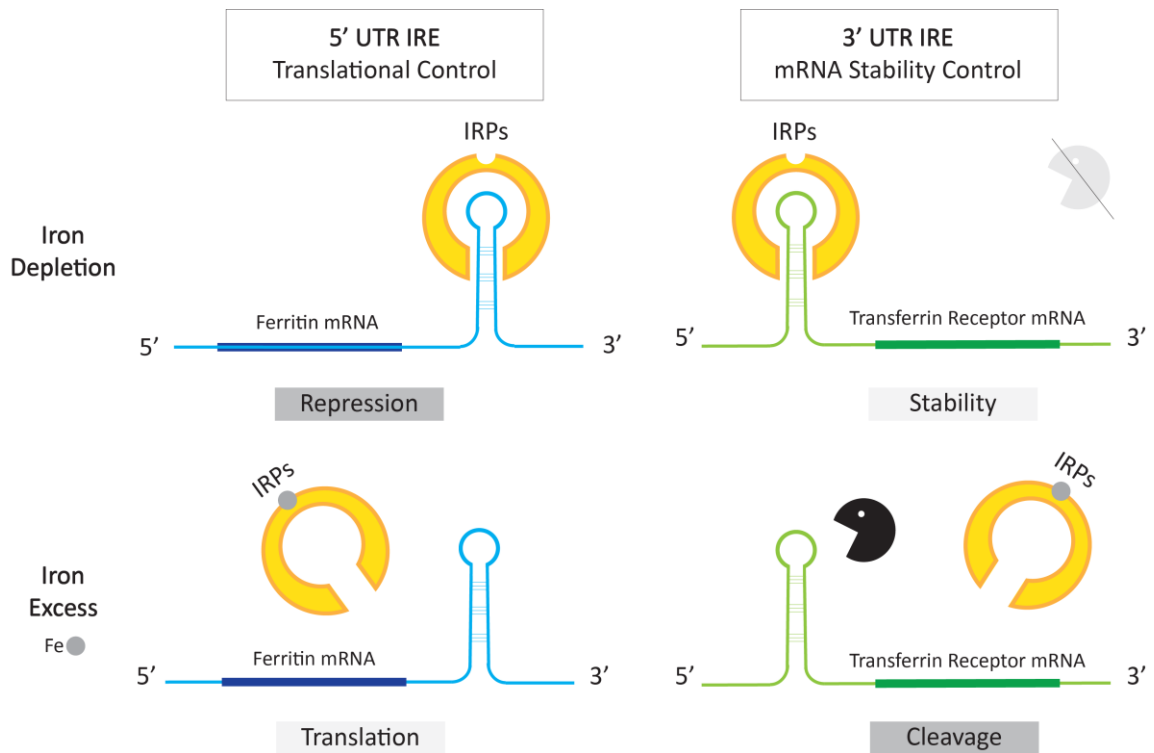


Figure 1 – Illustration of IRP/IRE regulatory system acting on a post-transcriptional level of two groups of genes involved in iron metabolism, ferritin and transferrin receptor-1 genes. When iron is depleted, IRPs bind to IREs present in UTRs and repress the translation, in case of ferritins, or promote mRNA stability in case of transferrin receptor-1. On the other hand, when the IRPs recognize there is an excess of iron, they unbind from the IRE, promoting the translation of ferritins and the endonucleolytic cleavage of transferrin receptor-1 mRNAs.

1.3 TRANSFERRIN RECEPTOR-1

As previously stated, iron is transported by transferrin to virtually all tissues within an organism. However, intracellular iron incorporation is proportional to the number of receptors available at the cellular membrane; therefore, cells expressing more transferrin receptor-1 (TfR-1) usually have higher iron acquisition capacities than cells expressing low levels of TfR-1. Examples of cells with high numbers of TfR-1 include immature erythroid cells, which contain the highest mass of total TfR-1 in an organism, as well as non-proliferating cells, such as hepatocytes and endothelial cells of the blood-brain barrier (Gatter *et al.*, 1983; Ponka and Lok, 1999). Also, rapidly proliferating cells, both normal and malignant, have been shown to have a higher number of transferrin receptor-1 (Inoue *et al.*, 1993), which may be due to a greater need of iron for synthesis of DNA (Jordan and Reichard, 1998). Because TfR-1 is known to be expressed in high levels in cancer cells, several studies analyse this receptor for targeted drug delivery therapies (Moore *et al.*, 2001; Qian *et al.*, 2002; Wang *et al.*, 2010).

It has been shown that external factors may also contribute to an up-regulation of TfR-1 expression levels. This is the case when adult MSC were labelled *in vitro* with SPIONs and ultrasmall SPIONs (USPIONs). An up-regulation of TfR-1 was observed in this cell line only when transfection agents were not used. The authors hypothesized that this enhanced up-regulation of TfR-1 was due to a higher iron uptake (Schäfer *et al.*, 2007).

1.3.1 Transferrin receptor-1 molecular structure and biochemistry

The transferrin receptor-1 gene is 33 kb and is located on chromosome 3 in humans, and chromosome 16 in mice, and is transcribed into a ~5 kb mRNA. In mice, only one variant of this gene exists, while in humans two variants can be found, encoding for the same protein, only differing in the 5'UTR (data available from National centre for biotechnology information - [NCBI](#)). The 3'UTR is one of the most important regions in TfR-1 mRNA and it was first discovered by Owen and Kühn (1987). This region is remarkably large, composed of about 2500 bp in total, and five conserved fragments, corresponding to the IREs involved in post-transcriptional control of the receptor (Appendix I, mouse TfR-1 mRNA sequence, p.242).

At the protein level, mammalian TfR-1 is a homodimer with two identical transmembrane subunits, each with a molecular weight of approximately 85 kDa, and joined by two disulphide bonds (Jing and Trowbridge, 1987). The crystal structure was first shown by Lawrence *et al.* (1999) and revealed three different regions: i) a globular extracellular portion, where transferrin binds; ii) a hydrophobic intramembranous region to anchor the protein within the cell membrane; and finally iii) a cytoplasmic region, essential for normal endocytosis. More importantly, within the globular extracellular portion, three different domains were identified: a protease-like domain, an apical domain and a helical domain (Lawrence *et al.*, 1999). It is important to note that in this extracellular domain, there is a trypsin-sensitive site, and if proteolytic cleavage occurs, transferrin binding activity

is lost (Rutledge *et al.*, 1994). Complete knock-out of TfR-1 leads to death during embryonic development, as this gene is essential for normal development of erythrocytes as well as the nervous system (Levy *et al.*, 1999).

1.3.2 Cellular internalization of iron through transferrin/TfR-1 complex

At physiological pH (7.4), once iron-bound transferrin reaches the cell membrane, it interacts with TfR-1. Each subunit of TfR-1 binds to one transferrin molecule and the transferrin/TfR-1 complex is internalized by receptor-mediated endocytosis. This binding between transferrin and TfR-1 only takes place if transferrin is loaded with iron, in the form of mono or diferric transferrin. The binding with diferric transferrin is about 30 times stronger than with monoferric transferrin. If transferrin is present without iron (apo-transferrin), it is not recognised by TfR-1, thus avoiding an inefficient competition between mono/diferric transferrin and apo-transferrin (Young *et al.*, 1984). Then, by an energy-dependent process, the endocytic vesicle environment turns rapidly acidic, where the pH decreases to about 5.6 (Gomme *et al.*, 2005; Hémadi *et al.*, 2004). At this low pH concentration and also aided by TfR-1, iron molecules (in the form of Fe^{2+}) are released from transferrin and cross the endosomal membrane through the divalent metal transporter DMT-1, also known as Nramp2 (Fleming and Andrews, 1998). The iron-free Transferrin/TfR-1 complex is then recycled to the cell membrane, where at physiological pH, TfR-1 unbinds from apo-transferrin. Apo-transferrin is then ready for a new cycle of iron transport. It is estimated that each transferrin molecule experiences more than 100 cycles during its life-time (Aisen, 1998).

1.3.3 Transferrin receptor-2

A second transferrin receptor, designated as TfR-2, was first revealed by Kawabata *et al.* (1999), and it has a much lesser impact on cellular iron acquisition. It has a high homology (45% identity) with the classical TfR-1 and internalizes iron in a similar manner, but at a 25-fold lower rate when compared to TfR-1 (Kawabata *et al.*, 1999). Contrary to TfR-1, it is responsible for non-transferrin-bound iron uptake (Graham *et al.*, 2008) and its tissue distribution is very different. TfR-2 is expressed in two transcripts: α -TfR-2 is found mainly in the liver and in liver-derived cell lines, while β -TfR-2 is found in several cell types but at low expression levels (Aisen *et al.*, 2001; Kawabata *et al.*, 1999; Trinder and Baker, 2003). It is also important to note that TfR-2 does not contain any IREs and its expression is regulated at the post-transcriptional level by the binding to diferric transferrin (Robb and Wessling-Resnick, 2004).

1.4 FERRITIN

As previously discussed, ferritin is a highly specialised molecule whose primary function is to store ferric iron (Fe^{3+}) inside its protein shell in a biochemically safe configuration. Its function is so important that the three-dimensional conformation appears highly conserved throughout evolution. Also, it is expressed ubiquitously in most eubacteria, archaea, plants and animals, with the exception of yeasts. Ferritins are commonly known as the cell's iron deposit, storing around 20-30% of the total iron present in an organism. They can then release iron in a controlled fashion upon cellular demand (Harrison and Arosio, 1996; Harrison *et al.*, 1987; Theil, 1987). Ferritins are mainly found in the cell's cytoplasm, but they can be found as well inside lysosomes, the nucleus and mitochondria (mitochondrial ferritin or MtF). This distribution enables ferritin not only to protect nuclear and mitochondrial DNA from toxic effects resulting from iron oxidation, but also to be broadly distributed to easily provide iron where and whenever needed (Corsi *et al.*, 2002; Koorts and Viljoen, 2007; Levi and Arosio, 2004). Also, some common functions associated with ferritins include the participation in the iron recycling process in macrophages and storage of iron in hepatocytes not only during short, but also during long-term periods (Theil, 1990). According to the Gene Ontology (GO) database, besides the well-known cellular iron homeostasis function, ferritins are also involved in various biological processes, such as the immune response, cell proliferation (Wu *et al.*, 1999) and transmembrane and post-Golgi vesicle-mediated transport ([UniProt KB P02794](#)).

1.4.1 Ferritin molecular structure and biochemistry

Ferritins are protein complexes formed of two different subunits: H or *heavy* subunit and L or *light* subunit. At the gene level, H and L subunits derive from two different genes, ferritin heavy chain-1 (Fth-1) and ferritin light chain-1 (Ftl-1), and are located in different chromosomes: Fth-1 gene is found on chromosome 11 and 19 and Ftl-1 gene is found on chromosome 19 and 7, in humans and mice, respectively (data available from [NCBI](#)). The complete knock-out of Fth-1 in mouse was proven to be embryonically lethal, but if one of the alleles is present the mice were healthy and fertile (Ferreira *et al.*, 2000). Both genes have homologous coding sequences but greatly differ in their UTRs. The 5'UTR of Fth-1 has been vastly studied over the years and several regulatory regions have been described. Amongst four described so far, the most important one is the IRE, which is a highly conserved 28 base-pair sequence (Appendix I, mouse Fth-1 mRNA sequence, p.242). This *cis*-acting element forms a stem-loop structure which interacts with *trans*-acting IRPs according to iron availability, as previously described (Torti and Torti, 2002; Worwood, 1990). Ferritin expression is not only controlled post-transcriptionally via IRP/IRE regulatory system, but it is also subject to a strict genetic control, depending on the particular tissue and conditions associated with oxidative stress (Arosio and Levi, 2002; Boyd *et al.*, 1985).

At the protein level, each ferritin is a heteropolymer composed of variable ratios of heavy and light subunits, of 21 and 19 kDa, respectively. Ferritins usually assemble subunits in different ratios giving rise to a large variety of isoferritins. In

mammals, ferritins consisting of just one subunit can be assembled, although homopolymers are rarely formed (Santambrogio *et al.*, 1993). Multiple copies of ferritins are usually present within a cell and 24 subunits are needed to form an empty ferritin shell whose outer and inner diameter are about 12 and 8 nm, respectively. Ferritin is known as apo-ferritin when iron is not present inside its core. Each apo-ferritin molecule can store up to 4500 Fe³⁺ atoms (Harrison and Arosio, 1996).

1.4.2 Ferritin internalization of iron

Studies have demonstrated that the heavy-subunit is the main controller of ferritin function and has a ferroxidase activity centre, which is essential for iron oxidation and incorporation. In contrast, the light-subunit facilitates the heavy-subunit activity and is responsible for iron nucleation and mineralization (Levi *et al.*, 1988; Treffry *et al.*, 1997). Therefore, the heavy-subunit incorporates iron several-fold faster than the light-subunit, even though the light subunit is more stable to physical denaturation (Lawson *et al.*, 1989; Santambrogio *et al.*, 1992). To sequester iron in a non-toxic way, the ferroxidase centre of the heavy-subunit interacts with ferrous iron (Fe²⁺) to promote its oxidation, also consuming peroxides used in the Fenton reaction, and thus avoiding the production of hydroxyl radicals. For that reason, ferritin is also known to be a dynamic inhibitor of free radical production with an antioxidant action (Arosio *et al.*, 2009; Chasteen and Harrison, 1999).

1.5 MAGNETOTACTIC BACTERIA, MAGNETOSOMES AND MAGA

More commonly known as magnetotactic bacteria, *Magnetospirillum sp.* is a gram-negative bacterium. The two most studied species are *M. magneticum* and *M. gryphiswaldense*. They are found in freshwater, have motility, mostly due to flagella, and in their pure form are known to perform aerobic respiration (Bazylinski and Frankel, 2004). This type of bacteria is also thought to migrate and self-orientate according to the earth's magnetic field (Blakemore, 1975). This is only possible due to a specialized organelle, known as the magnetosome (Stolz *et al.*, 1986), also routinely described as a bacterial magnetic particle or intracellular superparamagnetic nanocrystal. The organelle derives from invaginations of the prokaryotic inner plasma membrane and is able to accumulate biomineralized iron, if an iron-rich environment is present (Komeili *et al.*, 2006). During the mineralization process, iron incorporation can occur either by the formation of crystals of magnetite (Fe_3O_4), giving rise to iron oxide magnetosomes (Frankel *et al.*, 1979), or crystals of greigite (Fe_3S_4), creating iron sulphite magnetosomes (Mann *et al.*, 1990). Both of these types are typically between 35 and 120 nm in diameter, depending on stage of maturity, and are protected by a thin lipid bilayer (Bazylinski *et al.*, 1994) (Figure 2).

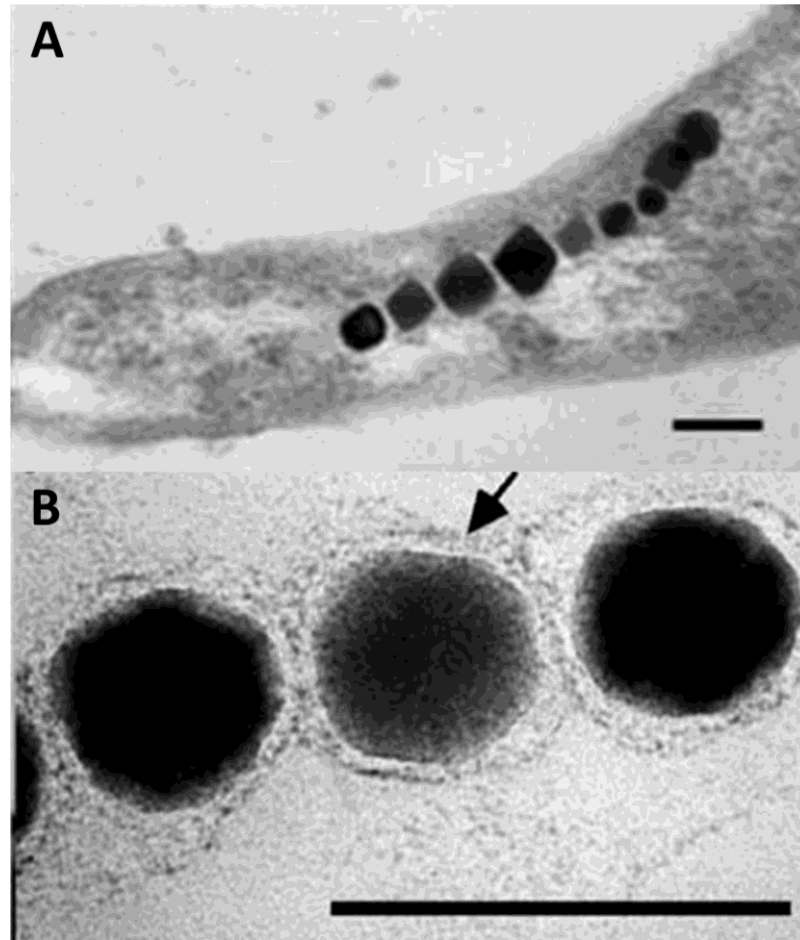


Figure 2 – Transmission electron microscopy of a *Magnetospirillum magneticum* with a magnetosome chain (A) and of isolated magnetosomes (B) with intact membranes, indicated by the arrow. Scale bars are 100 nm. Reproduced with permission from Benoit *et al.* (2009) (A) and from Schüler (2004) (B).

Different species of magnetotactic bacteria have specific types and morphologies of magnetosomes, but share some characteristics such as a high chemical purity, narrow sizes and specific arrangements within the cell. Usually, magnetosomes form a linear chain and align according to the cytoskeletal filaments. This alignment allows the organisms to orientate relative to an external magnetic field (Komeili *et al.*, 2006). The rare features of this prokaryotic organelle make it an interesting candidate of MRI cell tracking studies. Over the past decade,

magnetotactic bacteria or harvested and purified magnetosomes (Lang and Schüler, 2006) have been used as biogenic magnetic nanoparticles for several applications in biotechnology (Yoshino *et al.*, 2010), cancer therapeutics (Mannucci *et al.*, 2014) and even robotics research (Martel *et al.*, 2009).

1.5.1 Magnetosome formation

A large number of genes have been identified in an organized and conserved genomic region named the magnetosome island or MAI, that have been shown to be of great importance in magnetosome formation and function. In the magnetotactic bacterium AMB-1 strain, the MAI was predicted to comprise approximately 2% of the whole genome content (Fukuda *et al.*, 2006; Ullrich *et al.*, 2005). This cluster of genes effectively coordinates the cytoplasmic membrane invagination, vesicle formation, iron absorption, transport and incorporation, and finally, magnetite crystallization (Komeili *et al.*, 2006; Murat *et al.*, 2010). Also, an iron responsive study revealed hundreds of up-regulated and down-regulated genes are involved in magnetosome regulation (Suzuki *et al.*, 2006). Amongst these genes, there is a particular interest in MagA, firstly identified by Matsunaga *et al.* (1992), which encodes for an iron transporter localized both in the cytoplasmic and magnetosome membranes (Matsunaga *et al.*, 1992; Nakamura *et al.*, 1995b) (Figure 3).

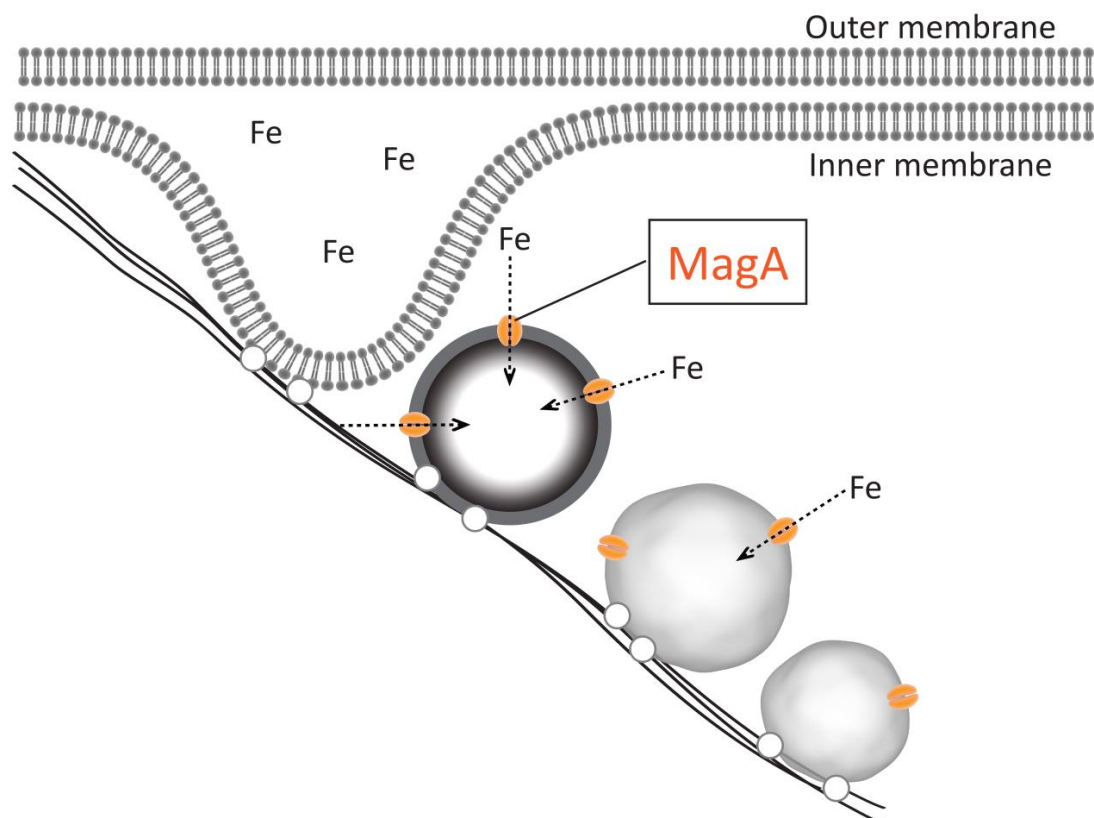


Figure 3 – Simplified illustration showing a hypothesized mechanism for membrane invagination, iron biomineralization of magnetosomes and MagA function as an iron transporter protein. Illustration based on Komeili *et al.* (2006).

1.5.2 MagA gene

As previously stated, MagA was identified as an iron transporter of magnetotactic bacteria and in magnetotactic bacterium AMB-1 strain, the MagA gene is translated into a protein homologous to the potassium efflux membrane-binding protein found in *Escherichia coli* (Nakamura *et al.*, 1995b). The MagA coding sequence from *Magnetospirillum magnetotacticum* MS-1 strain, which is of nearly 1.3 kb, can be found in Appendix I (p.242). Gene expression analysis led to the finding that MagA transcription is higher when iron concentrations are low. Also, MagA accumulates iron inside the magnetosome vesicles in an energy-dependent manner, acting like an H^+/Fe^{2+} antiporter and

therefore, MagA is believed to be a vital element in magnetosome synthesis (Nakamura *et al.*, 1995a; Nakamura *et al.*, 1995b). Conversely, a recent study where a targeted deletion of the MagA gene was performed in both *M. magneticum* and *M. gryphiswaldense* suggests that MagA is not essential for magnetosome formation. This study showed that both mutants were able to form magnetosomes as efficiently as wild-type bacteria. Further investigation revealed that the MagA gene is not localized within the MAI, the genomic region that contains all essential genes for magnetosome formation (Uebe *et al.*, 2012).

1.6 AIMS

The field of cell tracking using MRI as the base technology is of great interest and has been explored over the past decades. However, a labelling or tracking method that proves to be both efficient and stable in a long term-basis and that can also be used to detect cells in deep-set organs *in vivo* is yet to be further explored.

The main focus of this work was to compare three magnetic reporter genes, transferrin receptor-1, ferritin heavy chain-1 and MagA genes, previously reported to provide an efficient iron load when overexpressed in target cells, thus giving rise to a stronger MRI contrast. In order to do this:

1. Magnetic reporter genes were stably introduced into established cell/ stem cell lines, using a HIV-lentiviral approach, alongside fluorescent reporter genes, allowing for bicistronic expression of both genes.
2. Several iron concentrations and derived supplements were evaluated to adjust optimum supplementation conditions to transduced cells in order to maximize the cell iron load capacity and, thus, MRI contrast capability.
3. Transferrin receptor-1 was individually evaluated as a potential magnetic reporter gene in a model cell line, Chinese Hamster Ovary K1 (CHO K1) cell line.

4. Ferritin heavy chain-1 and transferrin receptor-1 were assessed as magnetic reporters both individually and together in mouse mesenchymal stem cells (mMSC).
5. MagA was individually evaluated as a potential magnetic reporter both in stem cell lines such as, mouse embryonic stem cells (mESC), mMSC and mouse kidney stem cells (mKSC), and in established cell lines like CHO K1 and human embryonic kidney (HEK) 293T(N) cells.
6. Once the different magnetic reporters (or respective controls) were introduced in a specific cell line, some common parameters were assessed: i) reporter gene integration, over passages and when exposed to different iron concentrations; ii) cell viability at different time-points; iii) differences in iron homeostasis when confronted with the overexpression of iron-related proteins; iv) intracellular iron uptake *in vitro* and finally, v) MRI imaging of cell pellets and of chick embryos, which were used as the animal model for this study.

CHAPTER 2

MATERIALS AND METHODS

OVERVIEW

This chapter describes molecular biology techniques and cell culture procedures that were used to generate and evaluate the reporter cell lines. The production and integration of self-inactivating (SIN) replication-defective VSV-G pseudotyped HIV-based lentiviral particles, as well as the protocols for the assessment of the transgenes at the mRNA and protein expression levels are described. Also, the potential of these transgenes to serve as magnetic reporters in stem cells was evaluated by determining the iron content and MRI contrast of cells. Finally, the viability, proliferation and differentiation capacity of these cells was explored. Buffers, solutions, media, restriction enzymes, equipments and other underlined material are detailed in Appendix II (p.245). Manufacturer's protocols are only described in case modifications were made.

2.1 MOLECULAR CLONING

2.1.1 Reporter genes cDNA

Three reporter genes were chosen for this research, *Mus musculus* ferritin heavy chain 1 (Fth-1) and transferrin receptor-1 (TfR-1) and *Magnetospirillum magnetotacticum* (MS-1 Strain) MagA. Mouse Fth-1 and TfR-1

cDNAs were synthesized from an RNA sample of the D1 mesenchymal stem cell line (see section 2.2.1 Cell lines, p.39). Iron responsive elements, present in both cDNAs, were identified using the online software *SIREs Web Server 2.0* (Campillos *et al.*, 2010) and excluded from amplification. Magnetotactic bacteria MagA cDNA was extracted from a commercial pCR2.1MS-magA plasmid ([Addgene, 21751](#)). Sequences of cDNAs can be found in Appendix I (p.242).

2.1.2 Extraction of total RNA

Cells cultured in a 35 mm dish were used for RNA extraction with TRIzol® Reagent. Growth medium was removed from the culture dish and 1 ml of TRIzol® Reagent was added and the cells were lysed by pipetting up and down. The homogenate was transferred to a 1.5 ml microcentrifuge tube to which 200 µl of chloroform was added. This solution was then shaken by hand for about 15 s, incubated for 2 min at room temperature (RT) and finally centrifuged at 12,000 xg for 15 min at 4°C. This resulted in the formation of three clearly separated phases of which the top one contained the RNA. This phase was carefully transferred to a clean tube and mixed with 500 µl of 100% 2-propanol, incubated at RT for 10 min and then centrifuged in the same conditions as described previously to pellet the RNA. The supernatant was carefully removed and the pellet was washed with 1 ml of 75% ethanol and centrifuged at 7500 xg for 5 min at 4°C. After discarding the supernatant, the RNA pellet was air-dried and dissolved in the appropriate volume of molecular biology water.

2.1.3 DNase treatment of RNA

A DNase treatment was performed to remove any traces of DNA contamination: 8 μ l of total RNA were mixed with 1x RQ1 DNase 10x Reaction Buffer and 1 U of RQ1 RNase-Free DNase per μ g of RNA and incubated for 30 min at 37°C. Afterwards, 1 μ l of RQ1 DNase Stop Solution was added to the mix and incubated at 65°C for 15 min, in order to completely stop the reaction. From this point, samples were either handled on ice or stored at -80°C until further use.

2.1.4 Synthesis of cDNA by reverse transcriptase

The synthesis of the first-strand cDNA from total RNA was performed with SuperScript™III Reverse Transcriptase. Briefly, a maximum of 5 μ g of total RNA were added to a solution containing 200 ng of random hexamers, 10 mM deoxyribonucleotide (dNTP) mix and molecular biology water up to 13 μ l, denatured at 65°C for 5 min, followed by a quick chill on ice. A mix of 5x First Strand Buffer, 0.1 M dithiothreitol (DTT) and 200 U of SuperScript™III-RT were then added. The resulting solution was mixed gently and incubated for 5 min at room temperature, followed by incubation at 50°C for 60 min. Afterwards, the reaction was inactivated by heating up to 70°C for 15 min. The solution was stored at -20°C until further use.

2.1.5 cDNA amplification by polymerase chain reaction

Fth-1, TfR-1 and MagA cDNA fragments were amplified by polymerase chain reaction (PCR) in a 2720 Thermal Cycler, using a set of specific primers (Sigma),

Fth-1_F/Fth-1_R for Fth-1, TfR-1_Kozak_F/TfR-1_R for TfR-1 and MagA_Kozac_F/MagA_R for MagA cDNA amplification, as well as a proof-reading polymerase, to ensure there were no amplification errors (Table 1). The primers and the annealing temperatures (Ta) used here and in section 2.1.10 Cloning of lentiviral constructs (p.33) are detailed in Table 2. Ta was determined by subtracting 5°C from the melting temperature (Tm) of each set of primers. The gene-specific primers were designed with restriction enzyme BamHI or EcoRI at the 5' end.

Table 1 – Conditions of PCR reaction and cycling for cDNA fragment amplification.

PCR Set up	1x Reaction Mix	Cycling conditions
cDNA / plasmid DNA	2 µl / 10 ng/µl	
Forward primer (10 µM)	1 µl	95°C, 1 min – 1x
Reverse primer (10 µM)	1 µl	95°C, 45 s
dNTPs (10 mM)	1 µl	Ta, 45 s
AccuBuffer (10x) + MgSO ₄ (1.5 mM)	5 µl	72°C, 2 min
<u>Accuzyme™ DNA polymerase</u> (2.5 U/µl)	1 µl	72°C, 5 min -1x
H ₂ O	Vol up to 50 µl	

30x

Table 2 – Description of primers used to amplify cDNA fragments by PCR, with the respective annealing temperatures and resulting product size. Note that in the primer sequences, the red nucleotides represent either the start codon (ATG) or the stop codon (TTA, TCA). The green sequence is a Kozac sequence that was purposely introduced before the start site of TfR-1 and MagA cDNA to help initiate the translation process. This was not performed for Fth-1 cDNA because a native Kozac sequence is already present. Novel restriction enzymes are highlighted in bold.

	cDNA	Primer	Sequence (5'-3')	Ta (°C)	Product (bp)
Amplification from plasmid or cDNA	Fth-1	Fth-1_F*	GGGATCCCCGCCGCCACC ATG AC	59	575
		Fth-1_R*	GGATCC CTT AGCTCTCATCACCGT		
	TfR-1	TfR-1_Kozak_F	GGAG CCACC ATGATGGATCAAGCCAG	55	2319
		TfR-1_R	GCATGTTACAT TTA AAACTCATTGTC		
	MagA	MagA_Kozac_F*	GGGATCC CCACC ATGGACCTGCATCATC	57	1314
		MagA_R*	CGGGAT CCTC AGATTCCAGT		
Amplification from PCR [®] II-TOPO [®]	Fth-1	Fth-1_EcoRI_F**	GGATTAG GAAT TCCCGCCG	57	586
		Fth-1_BamHI_R*	GCAACTGGGATCC CTT AGCTC		
	TfR-1	TfR-1_Kozak_BamHI_F*	GACGGATCCA CCACC ATGATGGAT	60	2322
		TfR-1_BamHI_R*	GCAATCGGGAT CCTT AAACTC		
	MagA	MagA_EcoRI_F**	GGG GAAT CC CCACC ATGG	59	1319
		MagA_BamHI_R*	GCGTACGGGAT CCTC AGATTC		

* - A BamHI restriction site was introduced to the primer.

** - An EcoRI restriction site was introduced to the primer.

2.1.6 Electrophoresis by FlashGel[®] System

The resulting PCR products were confirmed by running a mix of 1 µl of PCR product, 1 µl of FlashGel[®] Loading Dye and 3 µl of water in a 1.2% FlashGel[®] Cassette using the FlashGel[®] System. In order to estimate the cDNA fragment sizes, either FlashGel[®] DNA Marker 100 bp-4 kb or FlashGel[®] QuantiLadder were used. Each single band was recovered according to the manufacturer's instructions with the use of FlashGel[®] Recovery Kit.

2.1.7 Cloning transgenes cDNA into pCR®II-TOPO®

cDNA fragments of each transgene were cloned into pCR®II-TOPO®. As suggested in the TOPO TA Cloning Kit, an A-tail was added to the purified PCR fragments by the addition of 1x BIOTAQ Buffer, 0.5 µl of dNTPs (10 mM) and 2.5 U of BIOTAQ™ DNA Polymerase up to a reaction volume of 10 µl and incubating for 10 to 15 min at 72°C. Afterwards, ligation reactions were prepared by adding 4 µl of PCR fragments, with 1 µl of salt solution and 1 µl of TOPO vector. This solution was mixed gently and incubated at room temperature for 5 min.

2.1.8 Transformation of chemically competent cells by heat-shock

Approximately 2 µl of ligation reaction were mixed with One Shot® Match™-T1^R Competent Cells (provided with the TOPO TA Cloning Kit) and processed according to manufacturer's instructions. Afterwards, 50 µl of the culture were plated in pre-warmed selective LB-Agar plates (100 µg/ml ampicillin selection) supplemented with 40 mg/ml of X-gal and incubated overnight at 37°C. The purpose for the supplementation of LB plates with X-gal is to allow the blue/ white screening of colonies. If an insert is cloned to pCR®II-TOPO® vector, it will disrupt the LacZ gene present within the multiple cloning site (MCS) and consequently the β-galactosidase enzyme will not be produced, giving rise to a white colony. On the other hand, if the LacZ gene is kept undisrupted because no insert was cloned into MCS, the production β-galactosidase enzyme will form a blue precipitate when exposed to X-gal substrate, leading to the formation of a blue colony (see Appendix III for more details on the vector, p.251).

2.1.9 Analysis of transformed colonies

Several white colonies were individually picked and grown in the presence of the appropriate antibiotic. Each colony was diluted in 3 ml of LB medium with 100 µl/ml of ampicillin and incubated at 37°C overnight, with shaking (200 rpm). High quality plasmid DNA mini-preparations were then made using QIAprep® spin miniprep kit, following the protocol provided by the manufacturer. The plasmid DNA preparations were measured for DNA concentration with a NanoDrop™ 1000 spectrophotometer, and were then used for colony restriction analysis, sequencing of positive clones and cloning into lentiviral vectors.

For colony restriction analysis, 250 ng of plasmid DNA were digested with 5 U of the appropriate restriction enzyme(s) in 1x of the corresponding buffer, up to a final reaction volume of 20 µl. The digests were left for at least 2h with the incubation temperature respecting the manufacturer's instructions for each enzyme. Afterwards, one or two clones containing plasmids with the expected sizes evaluated by gel electrophoresis of the digestion products were selected for confirmation by sequencing. All sequencing analysis was performed by *DNA Sequencing and Services* (University of Dundee) and the primers used for sequencing are detailed in Table 4 (section 2.1.13 Ligation, p.36).

2.1.10 Cloning of lentiviral constructs

Mouse Fth-1 and bacteria MagA PCR fragments were individually cloned into the MCS of pHIV-dTomato vector ([Addgene, 21374](#)) and TfR-1 PCR fragment into

the MSC of pHIV-eGFP vector ([Addgene, 21373](#)). To do this, 4.5 µg of vector (pHIV-dTomato) was opened through two rounds of digests for at least 2 h, at 37°C: first digest was with 5 U of restriction enzyme EcoRI-HF™ and the 1x corresponding buffer, up to a volume of 20 µl with molecular biology water, followed by a phenol:chloroform purification and ethanol precipitation step (see section 2.1.11 Nucleic acid purification and precipitation, p.35), and digested once again with 5U of restriction enzyme BamHI, under the same conditions. In the case of pHIV-eGFP, 4.5 µg of vector were simply digested with BamHI. Digestions were confirmed by running 1 µl of digestion product, in a 1.2% FlashGel Cassette. Both vectors were then subjected to phosphatase treatment with 10 U of Calf Intestinal Alkaline Phosphatase (CIP), for 1h at 37°C, to prevent vector re-circularisation.

Inserts previously cloned in pCR®II-TOPO® were amplified by PCR using a new set of primers, in which, for Fth-1 and MagA, an EcoRI restriction enzyme was present in the forward primer and a BamHI restriction enzyme in the reverse primer; in the case of TfR-1, both primers presented BamHI restriction sites. All primers with introduced restriction sites were followed by a non-specific nucleotide tail (Table 2, p.31) to allow an efficient digest of the enzymes in the PCR fragment ends. After cDNA amplifications as described before, the entire PCR products were cleaned using a PCR Cleaning Kit, following the manufacturer's instructions. Then, Fth-1 and MagA cDNA fragments were subjected to two subsequent restriction digestions, while TfR-1 cDNA fragment was subject to a single digestion, as performed for the plasmid vector pHIV-dTomato and pHIV-eGFP, respectively. The

resulting products (vector and inserts) were then purified by agarose gel electrophoresis.

2.1.11 Nucleic acid purification and precipitation

This procedure was used to clean nucleic acid solutions (DNA or RNA). Molecular grade water was used to bring the solution to a final volume of 100 µl and an equal volume of solution consisting of Phenol: Chloroform: Isoamyl alcohol (25:24:1) was added. The sample was vortexed and centrifuged at 15,682 *xg* for 2 min, at room temperature; the upper aqueous phase (with the nucleic acids) was collected and transferred into a clean tube.

Nucleic acids were precipitated by adding 2.5x volumes of pure ethanol and 1:10 volume of 3 M sodium acetate pH 5.2 to the previous solution. After a quick vortex, the solution was left at -80°C for at least 30 min and then centrifuged at 15,682 *xg*, for 25 min at 4°C. The supernatant was discarded and the pellet washed with 100 µl 70% ethanol and centrifuged once again at 15,682 *xg*, for 10 min at room temperature. After removing the supernatant, the pellet was air-dried and resuspended in the appropriate amount of molecular grade water, usually 10 to 20 µl.

2.1.12 Electrophoresis of agarose gels

This technique was mainly used to visualise and verify the integrity of nucleic acids, to estimate the size of fragments when comparing to a known molecular-weight marker, to confirm the complete digestion of a restriction enzyme

with its substrate or to recover a specific DNA band. Agarose powder was added to 1x TAE buffer, to make a final gel concentration of 1% (w/v), boiled in a microwave oven and left to cool for a while; then, 10,000x dilution of SYBR®Safe DNA Gel Stain/Ethidium Bromide was added for visualization of nucleic acids under ultraviolet (UV) light. The solution was poured into a gel tray, where it was left to solidify. Afterwards, digested PCR fragments were mixed with 5x HyperLadder™ loading buffer, to 1x final concentration, to increase the density to the sample and for visual control of the electrophoresis. An electric potential of 100 V was applied to the gel immersed in 1x TAE buffer. Samples were observed under UV light and sizes of fragments were estimated by comparison with a molecular-weight maker, HyperLadder™I (200 bp-10 kb) or HyperLadder™IV (100 bp-1000 bp), depending on the expected size of the sample. Specific size bands, corresponding to pHIV-dTomato, pHIV-eGFP linear vectors, Fth-1, TfR-1 and MagA cDNAs, were carefully extracted from the agarose gel and purified using QIAquick gel extraction kit.

2.1.13 Ligation

The ligation reactions between plasmid vectors and each cDNA were performed at molar ratios of 1:3 and 1:7 (vector DNA:insert DNA), up to a maximum of 200 ng of DNA in a 10 µl solution, prepared according to Table 3. The ligations were left for 16 h, at 4°C. Two controls were performed: 1:0 corresponds to the digested vector with phosphatase treatment and 1:0 P to the digested vector with no phosphatase treatment.

Table 3 – Conditions used for ligation reactions.

Ligation Set up	Molar Ratios		Controls	
	1:3	1:7	1:0	1:0 P
Plasmid Vector DNA	1	1	1	1
Insert DNA	3	7	0	0
10x Ligation Buffer	1	1	1	1
<u>T4 DNA Ligase</u> (1 U/ μ l)	1	1	1	1
H ₂ O	4	0	7	7
Total Volume	10 μ l			

Half of each ligation reaction was transformed into One Shot[®] Stbl3[™] Chemically Competent *E. coli* cells, according to the manufacturer's protocol. Transformed colonies were selected by growth in the presence of 100 μ g/ml ampicillin, screened for positive clones and processed for sequencing as described above (section 2.1.9 Analysis of transformed colonies, p.33). Positive lentiviral constructs were also sent for sequencing of the whole vector (Table 4) to confirm the presence of all key features detailed in Appendix III, pHIV-dTomato and pHIV-eGFP plasmid maps.

Table 4 – Primers used for sequence analysis of the constructs generated. F – Forward orientation; R – Reverse orientation.

Vector Sequenced	Primer - Orientation		Sequence (5'-3')
pCR2.1MS-magA (Addgene, 21751)			
pCR®II-TOPO_Fth-1	T7	F	TAATACGACTCACTATAGGG
pCR®II-TOPO_TfR-1	M13	R	CAGGAAACAGCTATGAC
pCR®II-TOPO_MagA			
	Seq_insert	F	CTCAAGCCTCAGACAGTG
	Seq_insert	R	GGCTTCGGCCAGTAACG
	Seq1	F	CTGGAAGCTTCTTG
	Seq2	F	CCAGGCCCTGAAGC
pHIV-dTomato_Fth-1/ pHIV-eGFP_TfR-1/ pHIV-dTomato_MagA	Seq3	F	CGTAAAAAGGCCGCG
	Seq4	F	CTACGATACGGG
	Seq5	F	GGGGTTCCGCGCA
	Seq6	F	GATGCGGTTTTGGCAG
	Seq7	F	GAGGAAGAGCAAAAC
	Seq8	F	GAGACAGATCCATTCG
	Seq9	F	CGCTGCTTTCGATAAG

2.1.14 Sequence analysis

The sequencing output was analysed using Chromas Lite Software, Version 2.01 and homology searches of DNA databases were performed through NCBI, using the basic local alignment search tool (BLAST).

2.2 CELL CULTURE

2.2.1 Cell lines

In total, six adherent cell lines were used in the course of this study, specifically:

- Human embryonic kidney (HEK) 293 T(N) cells, purchased from System Biosciences (LV900A-1);
- Mouse Brachyury (Bra)-GFP knock-in embryonic stem cells, here simply described as mESC, were kindly provided by Dr Georges Lacaud, from Paterson Institute for Cancer Research (Manchester). Detailed information about this cell line can be found in Fehling *et al.* (2003);
- Mouse mesenchymal stem cells (mMSC) (D1 ORL UVA), purchased from ATCC (CRL-12424™);
- Mouse kidney-derived stem cells H6 (mKSC), established by the Stem Cell Research group (University of Liverpool). More information about this cell line can be found in Mora *et al.* (2012);
- Chinese hamster ovary (CHO) cell line K1, purchased from ATCC (CCL-61™).

2.2.2 Routine cell culture

Cell culture procedures were performed in sterile conditions in a *Biomat class II safety cabinet* and solutions were pre-warmed to 37°C before use.

All surfaces, materials and mediums in direct or indirect contact with the working area were either sterile or disinfected with 70% ethanol.

Cells were cultured in specific medium for each cell type, always grown at 37°C in a humidified incubator with 5% CO₂ and passaged every 2-3 days when they reached a density of around 70-80%. HEK 293T(N), mMSC and mKSC were grown in cell culture medium A, mESC in cell culture medium B and CHO K1 in cell culture medium C. For subculturing, the culturing medium was discarded and the cells were detached from the dish by treatment with 1% trypsin/EDTA for 2 min. Trypsin treatment was stopped by adding 2x times the trypsin volume with culture medium containing 10% foetal calf serum (FCS). After a 3 min and 233xg centrifugation, the supernatant was discarded and the cells resuspended in the appropriate amount of fresh growth medium. This solution was used to make 1:3 or 1:5 dilutions, in case the cell line was to be maintained in culture, or the cells were counted using a haemocytometer or a *TC20™ Automated Cell Counter* and a specific number of cells were seeded in new plates/ dishes. For mESC and CHO K1 cells, the plates/ dishes were treated with 0.1% (w/v) gelatine solution at room temperature for at least 15 min, prior to seeding.

2.2.3 Cryopreservation and recovery of cells

For cryopreservation of cells, trypsin treatment was performed as described previously. After discarding the supernatant of pelleted cells, cells were resuspended in freezing medium, at approximately 10⁶ cell density per ml of medium. The cell suspension was then transferred into cryovials (1ml each),

inserted into a freezing container filled with 2-propanol and incubated at -80°C for 2 days, after which they were transferred to a liquid nitrogen tank.

In order to thaw cryopreserved cells, the vial was quickly thawed in a 37°C water bath and its contents immediately transferred to 5 ml of the appropriate medium. The suspension was centrifuged at 500xg for 3 min and the supernatant was discarded. The cells were resuspended in the proper amount of culture medium and maintained as described above.

2.3 GENERATION OF REPORTER CELL LINES

The lentiviral expression vectors pHIV-dTomato and pHIV-eGFP are a third generation vectors, suitable for 2nd and 3rd generation packaging systems. Here, a second generation packaging system was used, which involves the use of three plasmids for the production of viral particles (expression or transfer plasmid, an envelope plasmid and a packaging plasmid). The system is divided in several DNA units to ensure the user's safety and avoid unwanted self-assembly of viral particles. These HIV-based plasmids are also self-inactivating, *i.e.*, once they infect (or transduce) a cell they become inactive and cannot replicate. In particular, pHIV-dTomato and pHIV-eGFP were chosen due to certain desirable characteristics, such as a constitutive elongation factor 1-alpha (EF1- α) promoter, a MCS to introduce genes of interest upstream an internal ribosome entry site (IRES) and fluorescent reporters dTomato and eGFP, respectively. The IRES present between the target gene and the fluorescent reporter allows bicistronic expression of both

genes. More information about the plasmids can be found in Appendix III (p.251).

Here, the packaging plasmid psPAX2 ([Addgene, 12260](#)) and the envelope plasmid pMD2.G ([Addgene, 12259](#)) were transiently cotransfected with the expression vector of interest to the producer cell line HEK 293T(N) to produce lentiviral particles. These particles, in turn, were used to transduce several cell lines in this research (Figure 4). The following procedures of transfection, concentration and titration of lentiviral particles were based on a protocol described by Kutner *et al.* (2009). All solutions, materials and surfaces that were in direct contact with the lentiviral particles were disinfected with 1% Virkon.

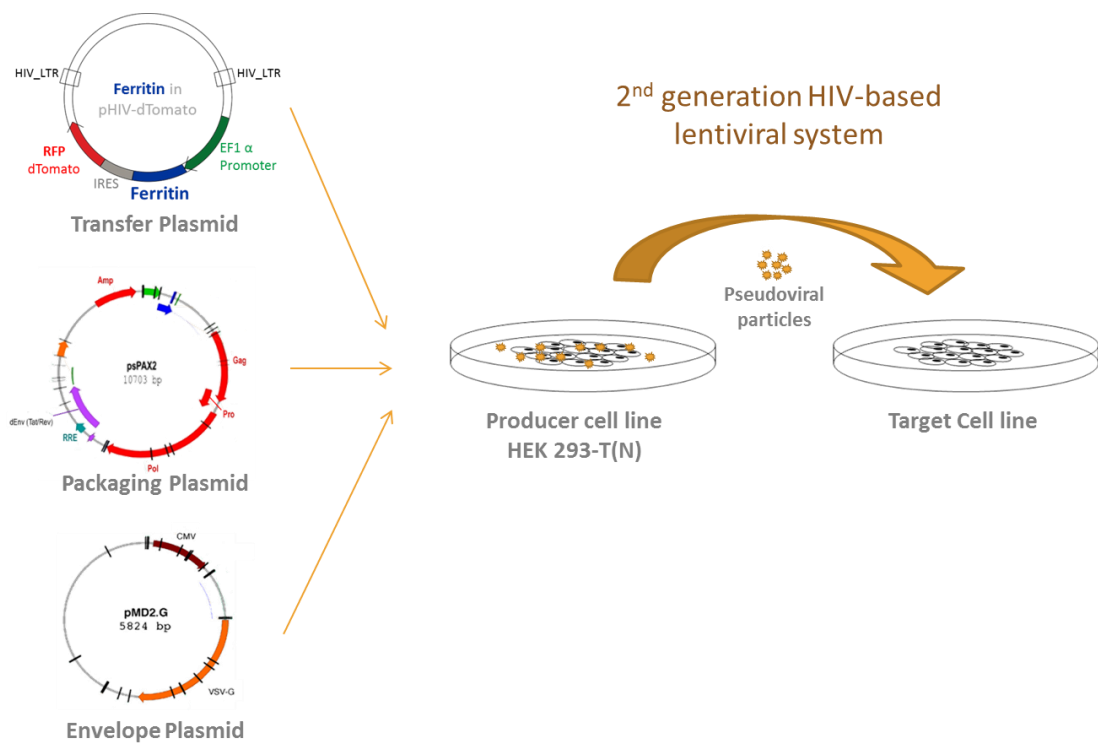


Figure 4 – Illustration of transfection of the producer cell line HEK 293T(N) with transfer, packaging and envelope plasmids, which comprise a 2nd generation HIV-based lentiviral system. After collecting the lentiviral particles from the media, cells of interest can be transduced in a target cell line.

2.3.1 Production optimization of lentiviral particles

The relative amounts of the transfer, packaging and envelope plasmids involved in the production of lentiviral particles have to be optimized on a case-by-case basis before transfection with the final constructs can be performed. For this, 3.8×10^5 HEK 293T(N) cells were seeded per well in a 6-well-plate, in order to obtain around 40-50% density at the start of the experiment. After allowing the cells to attach for 3-4 h, the growth medium was replaced with 2 ml of fresh cell culture medium in each well. The transfection was tested with the lentiviral expression vectors pHIV-dTomato or pHIV-eGFP as transfer plasmids and analysing five different mass ratios, together with a negative control (1:0:0). Transfer, packaging and envelope plasmids were mixed up to a total amount of 2 μg , as presented in Table 5.

Table 5 – Relative amounts of each individual plasmid and mass ratios tested for transfection optimization. Note that in the negative control (1:0:0) the packaging and envelope plasmids are not included for the transfection of HEK 293T(N) cells.

Expression constructs	Mass ratios	Relative amounts (μg)			Water
		Transfer vector	Packaging (psPAX2)	Envelope (pMD2.G)	
pHIV-dTomato/ pHIV-eGFP	1:0:0	2	0	0	Up to a final volume of 54 μl
	1:1:1	0.667	0.667	0.667	
	3:2:1	1	0.667	0.333	
	4:2:1	1.143	0.571	0.286	
	7:2:1	1.4	0.4	0.2	
	10:10:1	0.952	0.952	0.095	

The transient transfection into HEK 293T(N) cells was performed by calcium phosphate precipitation, where 6 μ l of 2.5 M of calcium chloride were added to the solution containing the plasmids, resulting in a total volume of 60 μ l. An equal amount of 2x HEPES (4-(2-hydroxyethyl)—1-piperazineethanesulfonic acid) was carefully added to this solution, one drop at the time. This final solution was left to rest for approximately 20 min and then added to a single well in the 6-well-plate, again in a dropwise mode. After approximately 30 min, calcium phosphate precipitates were visualized under the light microscope. The cells were incubated for 16 h, at which point the medium was replaced with fresh growth medium. The cells were left to grow under the same conditions for another 48 h. During this time, replication defective lentiviral particles are secreted into the culture medium. Therefore, this medium was harvested into a 15 ml tube and centrifuged at 500xg for 10 min to pellet dead cells and large debris. The supernatant was then filtered into a clean tube using a 0.45 μ m PES filter. The supernatant containing lentiviral particles was divided into 500 μ l aliquots frozen in crushed dry ice and stored at -80°C until further use.

To evaluate production efficiencies, cells of interest were seeded in a 24-well-plate at 10-20% density at the beginning of the experiment. Cells were given 300 μ l of fresh cell culture medium supplemented with 8 μ g/ml of polybrene. 200 μ l of lentiviral supernatant for each production condition were added to the cells and these were incubated for 16 h. The medium was replaced with fresh culture medium and incubated for another 48 h, in the same conditions.

Afterwards, the cells were washed twice with 1x Dulbecco's Phosphate Buffered Saline (PBS), fixed with 4% formaldehyde for 10 min and washed again with PBS. Analysis was performed by flow cytometry (see section 2.3.6 Fluorescence Activated Cell Sorting, p.48).

2.3.2 Transfection of the producer cell line

For the production of high titers of pseudoviral particles, HEK 293T(N) cells were seeded in a 6-well-plate. Each of the expression constructs (pHIV-dTomato_Fth-1/ pHIV-eGFP_TfR-1/ pHIV-dTomato_MagA) and the parental vectors (pHIV-dTomato/pHIV-eGFP) to serve as controls, were mixed with the envelope and packaging plasmids up to a total amount of 2 µg, with a mass ratio of 4:2:1. The transient transfection was carried out as described before. The resulting supernatant containing lentiviral particles was either concentrated by ultracentrifugation (see below) or aliquoted and frozen.

2.3.3 Concentration of lentiviral particles

To concentrate lentiviral particles, supernatant containing the viral particles was pooled in 50 ml tubes. Equal volumes were distributed between the Ultra-Clear SW28 ultracentrifuge tubes and 1/10 of the final volume of 20% (w/v) sucrose solution were then slowly added to the bottom of the tube, up to a maximum of 38.5 ml. The tubes were carefully placed and balanced in a pre-cooled *Beckman SW28 Ultracentrifuge Rotor*. The ultracentrifugation was carried out at 82,700xg at 4°C, during 2 h. Afterwards, the tubes were carefully removed and the supernatant

discarded. The tubes were left upside down in a paper towel for 10 min and then air-dried for a few minutes until a transparent pellet was observable. To slowly dissolve the pellet, 100 µl of PBS were added to centre bottom of the tube. The tubes were incubated on ice and vortexed gently every 20 min up to a period of 2 h. After this period, tubes were centrifuged for 1 min at 500 *xg* and pellets were resuspended by pipetting up and down. The concentrated lentiviral particles were divided into 50 µl aliquots, frozen in crushed dry ice and stored at -80°C until further use.

2.3.4 Determination of viral titres and efficiency of transduction

In order to determine the viral titre, HEK 293T(N) cells together with the target cells to be transduced were seeded in 6-well-plates at a density of 5×10^4 cells per well. Cells were given approximately 3-4h to attach. The growth medium was then replaced with 2 ml of fresh growth medium supplemented with 8 µg/ml of polybrene. For the titration of supernatant containing lentiviral particles several volumes (from 0.05 to 200 µl) of viral supernatant were added to each 6-well-plate and incubated at 37°C in a humidified incubator with 5% CO₂ for 16 h. The medium was then replaced with fresh culture medium and incubated for another 48 h, under the same conditions. After this period, the cells were harvested and centrifuged for 3 min at 500*xg*; the supernatant was discarded and cells were washed with 1 ml of PBS and centrifuged as before. After removing the supernatant, the cells were resuspended in 1 ml of PBS and kept in ice until further use.

Titration of transducing lentiviral particles was performed by evaluating the percentage of transduced cells using flow cytometry, translating this into single transducing units (TU), calculated according to Equation 2:

$$TU/ml = \frac{FN}{V} * D$$

Equation 2 – Calculation of individual viral titre, which is the number of transducing units (TU), *i.e.*, single lentiviral particles, that exist per volume unit of harvested viral supernatant. F corresponds to the ratio of fluorescent cells, N is the total number of cells at the time of transduction (5×10^4), V the volume (ml) of diluted vector added to each well and D the fold-dilution of vector used for transduction (Kutner *et al.*, 2009).

With the viral titre for concentrated and unconcentrated lentiviral particles having been established, cells were transduced at a precise multiplicity of infection, or MOI. For example, to transduce cells at a MOI=1, the number of TU needed to infect a known number of cells was calculated, so that there was 1 lentiviral particle per cell. In the case of MOI=5, there would be 5 lentiviral particles per cell.

2.3.5 Transduction of stem cells

To stably integrate reporter genes into the genome of different stem cell lines, typically 1×10^3 cells were seeded in a 48-well-plate and once attached, medium was replaced with specific growth medium mixed either with unconcentrated or concentrated lentiviral particles. The medium was also supplemented with 8 $\mu\text{g/ml}$ of polybrene to allow a more efficient virus-cell interaction. The cells were incubated in these conditions for 16 h; afterwards, the medium was replaced with fresh medium and cultured as usual. Please note that in order to have biological replicates, transduction of cells were performed on an

individual basis in at least in three independent experiments ($n=3$). Also, after the transduction process, cells were not subcultured for a minimum period of 7 days, at which point it was designated as P1 post-transduction.

2.3.6 Fluorescence Activated Cell Sorting

Fluorescence activated cell sorting (FACS) was initially used for the functional titration of lentiviral preparations. This was possible due to the presence of a fluorescent reporter in the lentiviral constructs.

When possible, transduced cells were expanded up to $2-4 \times 10^6$ cells and sorted at the earliest passage possible. Cells were harvested and resuspended in medium, transferred into round-bottom glass tubes and kept in ice until sorted. FACS was performed using a *BD FACSAria* (BD Biosciences) instrument. Sorted cells were collected in culture medium and seeded with supplementation of 1% Penicillin/Streptomycin to avoid possible infections.

Cells were routinely analysed for percentage of fluorescent cells using a *BD FACScalibur* (BD Biosciences) instrument, using a 488 nm laser and the appropriate fluorescence detectors depending on the transgene used (FL1 for eGFP or FL2 for dTomato). When appropriate, compensation thresholds were optimized to analyse double transduced cells (containing both GFP and dTomato transgenes). Non-transduced cells were used as a baseline control, a threshold set to less than 1% fluorescence. FACS output was analysed using *Cyflowic™ Software* (CyFlo Ltd, Finland).

2.4 EVALUATION OF INTRACELLULAR IRON

2.4.1 Cell viability when exposed to ferric citrate

A colorimetric assay was performed to evaluate the cell viability of cells when exposed to increasing concentrations of ferric citrate, to assess suitable levels of iron supplementation. In order to do so, 5×10^3 cells of each cell line studied were seeded in a 96-well-plate and allowed to grow overnight under normal cell culture conditions. The medium was then removed and replaced with culture medium supplemented with 2-fold increasing concentrations of ferric citrate (9.8, 19.5, 39.1, 78.1, 156, 312.5, 625, 1250, 2500 and 5000 μM). A positive and a negative control were present, cells with no supplementation and cells exposed to 0.1% Triton X-100 represented the highest and lowest possible number of viable cells. A blank (medium only) was also measured for normalization of the data. All conditions were done in triplicates to precisely determine the standard deviation for each condition. The cells were exposed to these conditions for 24 h. Cell counts were measured using a Cell Counting Kit-8, based on the compound WST-8 [2-(2-methoxy-4-nitrophenyl)-3-(4-nitrophenyl)-5-(2,4-disulfophenyl)-2H-tetrazolium] which forms a colorimetric dye once its reduced by dehydrogenases present in living cells, and thus, the amount of colour formed is proportional to the live cells in study. The cell medium was therefore removed and a cell counting solution plus culture medium (1:10, respectively) were added to the cells and incubated for a range of 1-5 h; the absorbance was measured in an *Anthos labtec instruments spectrophotometer LP400* at wavelengths of 450 nm for detection and 620 nm as a

reference. The output was then analysed in terms of percentage of cell number in relation to the concentration of toxic agent.

2.4.2 Intracellular iron quantification

Iron supplementation

Controls and transduced cells were seeded at a specific density and incubated either with iron supplemented media or simply in standard medium. Iron supplementation conditions included 0.2 or 2mM of ferric citrate, 50µM of L-ascorbic acid and 1.28 mM of human holo-transferrin. From here on, these will be designated simply as iron supplements. Note that in the standard medium the iron supplementation present is 300nM of ferric nitrate (DMEM) plus an unknown concentration of iron-related supplements (including transferrin) present in the Foetal Calf Serum.

Ferrozine Assay

Controls and transduced cells were seeded in 6-well-plates at a specific density, depending on the cell type and incubated with iron supplements or simply in standard medium for 4 days. The medium was refreshed 24h before measurement. Cells were then washed twice with PBS, trypsinized with 500 µl, harvested into a microcentrifuge tube and diluted in 1 ml of complete media. At this point, cells were centrifuged in a table-top centrifuge for 3 min, at 700 *xg*. The supernatant was discarded and cell pellet resuspended in 1 ml of media. The cell density was measured and then $1.4-2.5 \times 10^6$ cells were placed in a new tube. The

number of cells used for iron quantification was dependent on the cell line used, but it was kept constant for all experimental conditions. Cells were once again centrifuged in the same conditions and were resuspended in 50 μ l of 1.2M HCl, followed by the addition of 50 μ l 4.5% Potassium permanganate. At the same point, dilutions of a known iron standard (1, 0.5, 0.25, 0.125, 0.06 and 0.03 μ g) were prepared with the same reagents, in order to build a standard curve. A blank tube, only with a mix of the two reagents was also prepared. All the above conditions were heated at 60°C, for 2 h, under a fume hood. After allowing the tubes to cool down, they were centrifuged at 6400 xg , for 1 min. 20 μ l of Ferrozine reagent were mixed with the solution and let to develop for at least 30 min. To remove any cell debris, one last centrifugation was performed at 5100 xg for 3 min and 100 μ l of supernatant were placed in a 96-well-plate in order to read the absorbance at 570 nm in an *Anthos labtec instruments spectrophotometer LP400*. For each biological condition, three technical replicates were performed. The data was treated by removing the blank value from all conditions and the iron content per cell was calculated based on the standard curve and the total number of cells.

Prussian blue and DAB Staining

Control and transduced cells were seeded in a 24-well-plate, incubated with standard medium (no iron) and standard medium supplemented with either 0.2 mM or 2 mM of ferric citrate and were left to proliferate until confluent. Afterwards, cells were washed with PBS and fixed with 4% formaldehyde for 10 min. For Prussian blue staining, an iron stain kit was used and a 1:1 mixture of

4% potassium ferrocyanide solution with 4% hydrochloric acid was added to the cells for 30 min at RT. Cells were then washed several times with PBS and incubated for 15 min with 3,3'-Diaminobenzidine (DAB) enhancement solution. The reaction was stopped by washing the cells several times with distilled water.

2.5 EXPRESSION OF TRANSGENES AT MRNA AND PROTEIN LEVEL

2.5.1 Reverse transcription quantitative Real-Time PCR

Experimental set-up

This method was used to evaluate relative mRNA expression between cells. At least three biological replicates were performed for each cell line, *i.e.*, individually transduced cells at different time points. Cells were either processed at day 0 (before transduction) or control cells were included, to confirm the total absence of the transduced genes.

Primer design

The expression of genes of interest as well as endogenous reference genes, specific to each species, was measured. Primer pairs were specifically designed for Real-Time quantitative PCR amplification, using NCBI Primer Blast and the following optimal parameters: T_m of 60°C (except for primers F_IRES and T_IRES which was 65°C), size product between 60-150 bp, length of 18-25 bp, GC content between 40-60% and unique annealing to the targeted gene (Udvardi *et al.*, 2008). In case of Fth-1 and TfR-1, to specifically distinguish between viral and the total amount of

gene expressed, different sets of primer pairs were designed. To quantify only the transgenes present in a certain sample, forward primer flanked the 5' region of the gene of interest and the reverse primer flanked the 3' region of the IRES. On the other hand, to quantify the total expression of viral + endogenous genes, the primers designed flanked an identical region. Specific primers to identify the sole expression of an endogenous gene were not possible to be built in the situations viral and native cDNAs were identical. All reverse transcription quantitative Real-time PCR (RT-qPCR) primers used in this study are detailed in Table 6.

Table 6 – Sequence of primers used for amplification of cDNA by Real-Time PCR and resultant amplification product. *H-Homo sapiens*, *M-Mus musculus*, *C-Cricetulus griseus*; GAPDH primers were designed to amplify a cDNA region common to both mouse and human variants; Pabpn1 and Vezt were taken from Bahr *et al.* (2009).

	Primer	Denomination	Reference	Species	Forward Primer (5'-3')	Reverse Primer (5'-3')	Product (bp)
Reference genes	TBP	TATA box Binding Protein	NM_003194.4	H	GACGAGTTCCAGCGCAAGGGTT	GCACCCTGAGGGGAGGCCAA	110
	Tbp	TATA box Binding Protein	NM_013684.3	M	AATAGTGATGCTGGGCACTGCGG	GTGCGTCAGGCGTTCGGTGG	113
	GAPDH/ Gapdh	Glyceraldehyde 3-phosphate dehydrogenase	NM_002046.4/ NM_008084.2	H/M	CGGAAGGCCATGCCAGTGAGC	TGCCAAGGCTGTGGGCAAGG	63
	Pgk1	Phosphoglycerate kinase 1	NM_008828.2	M	CTGACTTTGGACAAGCTGGACG	GCAGCCTTGATCCTTTGGTTG	110
	Pabpn1	Poly(A) binding protein, nuclear 1	NM_019402	C	GTGGCCATCCTAAAGGGTTT	CGGGAGCTGTTGTAATTGGT	205
	Vezt	Vezatin, adherens junctions transmembrane protein	NM_172538	C	GTGTGAAAGTGGGGCTGAAT	GTTCTGCATGGTGGTGAAT	200
Transgenes	dTomato	dTomato red fluorescent protein	-	-	TGAAGATGCGCGGCACCAACT	TGGTGGATCTCGCCCTCAGCA	124
	eGFP	Enhanced Green fluorescent Protein	-	-	GAAGTTCATCTGCACCACCG	GCTTCATGTGGTCGGGGTAG	107
	F_IRES	Construct specific ferritin heavy chain-1_IRES	-	-	TACGCAAGATGGGTGCCCTGA	ATTCCAAGCGGCTTCGGCCA	140
	T_IRES	Construct specific transferrin receptor-1_IRES	-	-	GGGAGTCGCAAATGCCCTCT	ATTCCAAGCGGCTTCGGCCA	113
	MagA	MagA	AB001699.1	-	GGCGAGTTGGAAACGCCGGT	AGATCGGCGGGCAGCAACAC	125
Endogenous genes	Total_F	Ferritin heavy chain-1	NM_010239.2/ XM_003513182.1	M/C	TGAGGAGAGGGAGCATGCCGA	CCAGTCATCACGGTCTGGTTT	100
	Total_T	Transferrin Receptor-1	NM_011638.4	M	TGAGTGGCTACCTGGGCTAT	CTCCTCCGTTTCAGCCAGTT	74
	CHO_T	Transferrin Receptor-1	NM_001246819	C	CAGGCAATTCAGAAATCATCCAAGA	CAGCTGCTTGATGGTGTCAAGT	128

Sample preparation and quantitative PCR

Cell lyses and RNA extraction, DNase treatment and cDNA synthesis by reverse transcriptase were performed at each point as per manufacturer's instructions of Fast SYBR® Green Cells-to-CT™ Kit. For the RT-qPCR reaction set up, 4 µl of cDNA were mixed with 10 µl of Fast SYBR® Green Master Mix (one of the kit's components), forward and reverse primers specific to the gene of interest to a final concentration of 200 nM, and finally, molecular biology water up to a reaction volume of 20 µl. For each cDNA analysed, two technical replicates were prepared. In each run, 500 pg of each construct (pHIV-dTomato_Fth-1, pHIV-dTomato_MagA, pHIV-eGFP_TfR-1) were included as a positive control for transgene amplification. As negative controls, non-template controls (NTC) were performed for every gene evaluated and no reverse transcriptase (NRT) controls were also included to verify the complete elimination of genomic DNA. RT-qPCR was performed using a Real-Time PCR machine *Stratagene MxP005* for the study in Chapter 6 (p.178) and a *Biorad CFX Connect Real-Time PCR Detection System*, for all other studies. The cycling conditions were the following: enzyme activation at 95°C, for 20 s, followed by a 2-step PCR cycle of 95°C for 3 s and 60°C for 30 s (annealing temperature, Ta). Ta was 60°C for all primers, with the exception of F_IRES and T_IRES, which was of 65°C for better specificity. At the end of the PCR reaction, a dissociation curve was constructed (0.5°C increase every 5 s, detecting the product's melting temperature from 65°C to 95°C). Relative expression levels were evaluated using *Bio-Rad CFX System Test Software* and verified using *Excel (Microsoft)* through the Pfaffl method (Pfaffl *et al.*, 2002) to represent the fold change in mRNA levels.

2.5.2 Immunofluorescence

Cells were seeded in 8-well glass chamber slides at different densities, depending on the cell type. Cells were left to attach and grow, at least overnight, before fixation with 4% formaldehyde, which was performed for 15 min at RT. Cells were then washed three times with PBS, permeabilised with 0.1% Triton-X 100, and blocked with 10% serum (either goat, chicken or donkey), depending on the host animal in which the secondary antibody (Ab) was raised. The blocking step was performed for 1h at RT. After another three washes with PBS, the primary Abs were applied in a solution containing 1% of specific serum and 0.1% Triton-X 100, and left at 4°C, overnight, in a humidified chamber. The following day, the cells were washed three times in PBS and the secondary Ab was applied and incubated for 2h at RT, protected from light. After washing again three times in PBS the cell's nuclei was stained for 10 min with DAPI (300 nM in PBS). Negative controls were included to test the secondary Ab specificity to the primary Ab. Therefore, during the primary Ab incubation, negative controls were kept in the same solution as previously described without the primary Ab and from that step onwards they were treated exactly as all the other samples. Primary and secondary Abs used, as well as specific dilutions, can be found in Table 7. Slides were mounted using Dako Fluorescence Mounting Media and micrographs acquired under epifluorescence illumination using a *Leica DM2500 microscope* coupled to a *Leica DFC420C camera*.

Table 7 – Description of primary and secondary Abs used in immunofluorescence (IF) and western blot (WB).

Type	Description	Application	Dilution	Reactivity	Company, Cat. no.
Primary	Rabbit Polyclonal Anti-ferritin heavy chain-1	IF WB	1:500 1:250	Mouse, human	Abcam, ab65080
	Rabbit Polyclonal Anti-transferrin receptor-1	IF WB	1:1000 1:3000	Mouse, human	Abcam, ab84036
	Rabbit Polyclonal Anti-actin	WB	1:1500	Mouse, others	Abcam, ab1801
Secondary	Alexa Fluor® 594 Goat Anti-Rabbit IgG (H+L) Antibody	IF	1:1000	Rabbit	Life Technologies, A-11012
	Alexa Fluor® 488 Chicken Anti-Rabbit IgG (H+L)	IF	1:1000	Rabbit	Life Technologies, A-21441
	IRDye 680RD Donkey Anti-Rabbit IgG (H + L)	WB	1:15000	Rabbit	Licor, 926-68073

2.5.3 Western Blotting

Protein extraction and quantification

Cells were harvested and counted and 10^6 cells were transferred into a microcentrifuge tube and centrifuged for 3 min, at 700 xg to concentrate the cells into a pellet. The cells were then washed with PBS and centrifuged again. Once the supernatant was discarded, 200 μ l of lysis buffer were mixed with the cells. The tubes were placed on ice with a rotation shaker for 30 min. Afterwards, the solution was centrifuged for 10 min at 13400 xg to remove cell debris. The supernatant was harvested, aliquoted and stored at -80°C until further use. Protein concentration was quantified following instructions of Pierce™ BCA Protein Assay Kit. Briefly, 10 μ l of sample were mixed with 200 μ l of working reagent, incubated for 30 min at 37°C

and cooled down to room temperature. Three technical replicates were performed per sample and for each experiment, a blank and samples with known concentrations of albumin were also measured to produce a standard curve. The absorbance measured in *Anthos labtec instruments spectrophotometer LP400* at a wavelength of 570 nm was then used to calculate the protein concentration by using the standard curve as a reference.

Sample preparation

Samples were thawed on ice and 10 µg of protein were mixed with 1x NuPAGE LDS Sample buffer, 1x NuPAGE Reducing Agent and distilled water up to a final volume of 25 µl. This solution was incubated at 70°C for 10 min in a heating block. Afterwards, a brief centrifugation was performed to collect any condensation.

Protein Electrophoresis

XCell SureLock Electrophoresis apparatus was mounted with the inside chamber filled with 200 ml of 1x MOPS running buffer together with 500 µl of NuPAGE Antioxidant and the outside chamber filled with 600 ml of 1x running buffer. For each sample, 5 µg of protein were loaded per well in a NuPAGE® Novex® 4-12% Bis-Tris Protein Gel. All samples were done in duplicate, where one of the gels was used for blotting and the other one for quantification of the total protein (see below). 3 µl of Odyssey Protein Molecular Weight Marker were included as a reference for protein size. Protein electrophoresis was performed at 200 V constant, for 50 min.

Wet Transfer

Immobilon®-FL Transfer Membranes were activated for 30 s in 100% methanol, briefly rinsed in distilled water and then placed in a container with transfer buffer until used. Sponge pads and Whatman paper were also soaked in transfer buffer before the “sandwich” was prepared as following (cathode to the anode direction): 2 pads, 2 sheets of paper, gel, the membrane, 2 sheet of paper and 2 pads. This was placed in the transferring apparatus (XCell II Blot Module) and the inside chamber was covered with transfer buffer plus 1% NuPAGE Antioxidant and the outside chamber with distilled water. The transfer was run at 30 V constant for 1 h.

Blocking and antibody incubation

After transfer, the membrane was blocked for 1h with Odyssey® Blocking Buffer, with gentle shaking. The membrane was then incubated with the primary antibodies anti-ferritin heavy chain-1, anti-transferrin receptor-1 and anti-actin (see Table 7 for dilutions, p.57) in the same blocking buffer with 0.2% Tween 20, overnight, at 4°C, in a shaker. Afterwards, the membrane was first rinsed and then washed for three times in a solution of PBS and 0.1% Tween 20. The secondary antibody used was IRDye 680RD Donkey anti-Rabbit IgG (H+L) (Table 7, p.57) and it was diluted in the same blocking buffer, with 0.2% Tween 20 and 0.01% SDS. The membrane was incubated with this solution for 1 h, at RT, with gently shanking and protected from light. After 1 h, the solution was discarded and the membrane washed three times as before. Finally, the membrane was rinsed in PBS to remove

any traces of SDS.

Total protein quantification

After electrophoresis, one of the gels was incubated in an Instant Blue solution for 1h at room temperature. Afterwards, the gel was rinsed several times with distilled water and left washing overnight.

Quantification and normalization

All membranes and stained gels were imaged with a *LICOR Odyssey® Sa Infrared imaging System*, at the 700 nm channel, 200 µm resolution and intensity of 5.0. Images were processed and analysed using *Image Studio™ Lite, Version 3.1* Software.

Whenever possible, total protein gels were used not only to verify the exact amount of protein loaded in each well, but also to serve as a reference when determining the expression of target proteins. Actin protein expression was the housekeeping gene chosen and was used to verify data normalization. In the rare cases total protein gels were not performed in conjunction with the target gel, actin alone was used to normalize target protein expression. Note that actin was not primarily used for data normalization because its expression was not stable between all cell lines studied, especially in the case of CHO K1 cells.

2.6 TRANSMISSION ELECTRON MICROSCOPY (TEM) ANALYSIS

Cells were seeded at 10% density in 3.5 cm dishes. After cell attachment, medium was replaced with normal medium to non-transduced cells; for transduced cell lines, culture medium was supplemented with 0.2 mM of ferric citrate. Cells were grown under these conditions for 4 days. The cells were then fixed with 4% formaldehyde and 2.5% glutaraldehyde in 0.1 M phosphate buffer for 1h under the fume hood. Cells were subsequently washed with PBS and osmicated by adding 4-5 drops of 1% Osmium tetroxide (made in water) for 1h. After three washes with 1x PBS, 30 min each, cells were dehydrated in increasing ethanol concentrations, as follows: i) 30% EtOH for 30 min; ii) 4-5drops of 0.5% Uranyl acetate in 30% EtOH; iii) and then followed by 30, 60, 70, 80 and 100% EtOH for 5 min each. Afterwards, cells were processed for epoxy resin embedding. For this, infiltration resin was pre-warmed for about 5 min at 60°C and mixed 1:1 with 100% EtOH. The bottom of the dish was covered with this preparation and left to solidify for 30 min, followed by 100% resin again for 30 min. The samples were placed inside capsules, filled with 100% resin and placed upside down in the dish. This was left at 60°C for least 48h. Finally, 70 nm sections were obtained with an ultramicrotome and collected over copper grids containing a formvar support film. Sections were imaged in *FEI 120kV Tecnai G2 Spirit BioTWIN* instrument.

2.7 CELL VIABILITY CAPACITY

Cell proliferation was determined in terms of percentage of cell number, in relation to control cells. This assay was performed to evaluate how cell proliferation responded to transduction with different viral constructs, at specific time-points post-transduction. Cells were seeded at a density of 1×10^4 cells per well of a 48-well-plate and left to proliferate for a period of 7 days. In most cases, cells were incubated under normal cell culture conditions with the exception of mMSC that were cultured under specific supplements 24h from transduction (Chapter 5, p.129). At day 7, the cell number was measured with Cell Counting Kit-8 Solution, as described in section 2.4.1 Cell viability when exposed to ferric citrate (p. 49).

2.8 MULTILINEAGE DIFFERENTIATION

In order to verify mMSC differentiation potential after reporter gene integration, cells were induced to differentiate *in vitro* into the three standard lineages: osteogenic, adipogenic and chondrogenic. mMSC differentiation assays were performed between P12-P15 and at least 2 passages from transduction. The protocols used for differentiation are described below and were adapted from (Zhu *et al.*, 2010) and (Glennon-Alty *et al.*, 2013).

For osteogenic and adipogenic differentiation, mMSC were seeded at a density of 1×10^4 and 2×10^4 cells, respectively, per well in a 24-well-plate and left to attach overnight in α -MEM media with 10% FBS. The following morning, the

medium was replaced with osteogenic or adipogenic induction medium. Negative controls were performed, where induction media was omitted. Induction and control media were substituted every 2-3 days for a period of 14 (osteogenic) and 21 (adipogenic) days, in which the cells were not passaged. At the end of the 2 weeks, cells were washed with PBS and fixed with 4% formaldehyde for 10 min. In case of osteoblast differentiation, calcium deposits were stained with 2% Alizarin Red S solution for 2 min. In the case of adipocyte differentiation, after fixation, cells were equilibrated with 60% of isopropanol for 5 min at RT. Afterwards, a freshly prepared and filtered solution of 0.5% Oil-red-O (made in isopropanol) diluted in water at 3:2 ratio, was used to stain fat deposits for 10 min. Both conditions were then washed several times with water and visualized with a light microscope.

For chondrogenic differentiation, 2×10^5 cells, initially cultured as adherent cells were transferred into 15 ml centrifuge tubes and pelleted by a 3 min centrifugation, at 162 *xg*. Cells were left to incubate for a day in the centrifuge tubes with standard mMSC medium. The mMSC pellets were then transferred to 96-well-plate for suspension cells and washed with PBS, before adding the specific chondrogenic induction media. This was replaced every 2-3 days up to a total of 21 days. Negative controls were performed, in which mMSC pellets were maintained in standard mMSC media. After the supplementation period, pellets were washed with PBS, fixed with 4% formaldehyde for 20 min, washed again and incubated with 15% sucrose (made in PBS) for 20 min at room temperature. Pellets were then mounted using Bright Cryo-m-Bed embedding medium and frozen in dry

ice for cryosectioning. Sections 7 µm in thickness were rinsed in 1% acetic acid for 10 s and stained with Safranin-O for 5 min, washed several times in distilled water and visualized under a light microscope.

2.9 ANIMAL WORK

Cells to be injected were incubated with ferric citrate, in case of HEK 293TN cells, or ferric citrate and other iron-related supplements, for all other cell types, for 3 days in normal conditions. Afterwards, cells were trypsinized as usual and resuspended in Dulbecco's Modified Eagle's Medium (DMEM) with 30% 1:1 ratio of deoxyribonuclease I : fast green. Cells were kept on ice until injection.

White Leghorn chicken eggs (*Gallus gallus*) were employed as an animal model. Fertilized eggs were kept at 12°C until use for a period up to 2 weeks. Once incubation started, eggs were maintained in an incubator at 38°C with 40% humidity. All animal work followed standard ethical guidelines according to UK regulations (Consolidated version of ASPA 1986) and embryos were not allowed to develop beyond embryonic day 5 (E5). At E3, eggs were windowed and approximately 2×10^5 transduced cells in 2 µl of the above solution were first introduced into a microcapillary pipette and injected in the brain ventricle of the chick embryo using an aspirator tube assembly for calibrated microcapillary pipettes. Embryos were allowed to develop for a further 2 days, at which point they were harvested and imaged using a fluorescence dissection *Leica M165FC stereomicroscope*. Bright field and fluorescence images were

acquired as projections of the whole embryo, equally on the right and left sides. Both bright field and fluorescent pictures were then overlaid using ImageJ software, and the location of cell clusters were able to be precisely identified and used as guidance for MR imaging of chick embryos. After fluorescent imaging, embryos were fixed overnight with 4% formaldehyde and washed several times with PBS. Embryos were kept at 4°C, in PBS, until further use.

2.10 MAGNETIC RESONANCE IMAGING

2.10.1 Sample preparation

In vitro cultured transduced cells were grown either in iron-supplemented or non-supplemented (negative controls) medium. A total of 10^7 cells from each condition were harvested, fixed with 4% formaldehyde and transferred to 0.2 ml polypropylene tubes and centrifuged at 13400 xg for 30 min. Afterwards, supernatant was substituted with 1% low-melting temperature agarose. Fixed chick embryos were embedded in 1% low-melting temperature agarose and mounted in 0.5 ml microcentrifuge tubes.

2.10.2 Imaging

Cell pellets and chick embryos were imaged using a *Bruker 7 T Avance III MRI* instrument with a 38 mm transmit/receive quadrature volume coil, as described in Taylor *et al.* (2014). Both sample types were positioned for axial imaging using a sample holder. T2-weighted MRI images were initially acquired for cell pellets. After

outlining a specific region within the cell pellet, T1/T2 maps were produced in order to obtain the longitudinal relaxivity data between the different samples. This was acquired using a modified Rapid Acquisition with Refocused Echoes (RARE) sequence, with the following repetition times (TR): of 5000, 3000, 1500, 800, 400 and 200 ms, and echo times (TE): 11, 22, 55, 77 and 99 ms. Imaging of animal embryos was performed to acquire anatomical images only (T2-weighted) and no relaxivity studies were performed on these samples. All images were equally processed using ImageJ software.

2.11 ERROR BARS AND STATISTICAL ANALYSIS

Standard deviation (SD) error bars were used when a descriptive analysis was performed and standard error of the mean (SEM) when inferential statistics were used, with a minimum number (n) of 3 independently conducted experiments ($n \geq 3$). SD and SEM were calculated using *OriginPro 9.0.0* (OriginLab Corporation).

Student t-test was calculated using *Microsoft Excel* and employed to evaluate statistical significances between two groups of samples. The statistical probability is demonstrated in terms of p -value (p), which was considered “significant” when $p < 0.05$ (*); “very significant” when $0.01 > p > 0.001$ (**) and “very highly significant” when $p < 0.001$ (***)).

CHAPTER 3

STABLE INTEGRATION OF REPORTER GENES INTO ESTABLISHED CELL LINES

3.1 INTRODUCTION

3.1.1 Transfection methods

Over the years, several methods to integrate genes of interest into specific cell lines have been used. One of the most routinely used methods is electroporation, which can be described as a physical method for transgene delivery, in which an electric field is externally applied creating transient pores in the cellular membrane allowing the entrance of foreign elements as, for example, plasmid DNA. Even though this method is a mechanical transfection and can be used in a wide range of cell lines, if the current is not optimal it can result in cell death (Neumann *et al.*, 1982). A more recent approach for physical transfection is using magnetic beads. The negatively charged transgene DNA is mixed with positively charged magnetic particles and delivered to the cells by magnetic force (Isalan *et al.*, 2005). Another very common method is chemical transfection and this can be achieved using reagents based on cationic lipids (or liposomes, mostly known as lipofection) (Felgner *et al.*, 1987) or calcium phosphate (Graham and van der Eb, 1973), amongst others. The transgenes are believed to be incorporated by the cells through endocytosis or phagocytosis, although the underlying mechanism of how nucleic acids cross the cell membrane or reach the nucleus is still unknown

(Kim and Eberwine, 2010). In all these transfection methods described above, the transgene is effectively incorporated inside the host cell, but is it not directly integrated in the nuclear genome, and therefore, in most cases it leads to a transient expression. This might be either due to degradation of the gene delivered and/or its dilution as mitosis takes place. Even if there is a selection marker, like a drug resistance gene, only rarely the transgene integrates with the host genome and becomes a stable transfection (Dimitrov, 2012). An approach to overcome these shortcomings is the stable chromosomal integration of the genes of interest using virus-mediated transfection, mostly known as transduction.

Firstly used as an expression mechanism in 1979 (Hamer and Leder, 1979), transduction is a biological method to incorporate genetic material into a host cell using a viral vector. There are several choices of viral vectors possible to use such as adenoviruses or adeno-associated viral vectors (AAVs), retroviral vectors (RVs) or lentivirus-based vectors (LVs), amongst others (Kay *et al.*, 2001). Adenoviruses are of episomal origin and usually lack of replication ability and thus the signal derived from these vectors is only transient (Adamson *et al.*, 2011), while RVs are unable to efficiently infect non-dividing cells (Yamashita and Emerman, 2006). Therefore, LVs, such as the human immunodeficiency virus type 1 (HIV-1), are many times preferred in detriment of others due to its effective mechanism to introduce foreign DNA into the host genome of dividing as well as non-dividing cells (Naldini *et al.*, 1996; Roe *et al.*, 1993). Also, they can accommodate transgenes up to 10 Kb, while in AAVs the packaging limit is about 5 Kb (Trono, 2000).

3.1.2 Lentiviral-mediated transduction

Transgene incorporation takes place in the nucleus, where just the target material between specific sites of the viral vector, named long terminal repeats (LTRs), is integrated into the host cell's genome. In order for this mechanism to be safe for the user, the HIV-1 genome was "disassembled" and genes involved with unwanted characteristics, like virulence and replication, were removed, leading to an elimination of about 60% of the genome. Only genes absolutely necessary for virus assembly, reverse transcription and target gene integration (*gag*, *pol* and *rev* genes) were used, and these were distributed in several plasmids to allow a safe handling of the viral components (Dull *et al.*, 1998). These viral components together with the vector holding the transgene can then be transfected into a "producer" cell line that will express all proteins necessary for the assembly of the lentiviral particles. Once assembled, these viral particles are secreted in the culture medium that can then be directly used to infect other cells. This method typically yields high titers, of about 10^7 transducing units (TU) per ml, and this can be further increased by concentrating the particles, using techniques such as ultracentrifugation (Kutner *et al.*, 2009).

Other characteristics that make lentiviral vectors an ideal method of incorporating foreign DNA into a cell, besides safety and high titer production, are the minimal interaction with the normal physiology of the cell, stability and reproducibility and the ability to transduce a wide range of cell types, including non-dividing and difficult to transfect cells (Mátrai *et al.*, 2010; Trono, 2000). Also,

genetic engineering has made it possible to design lentiviral vectors that contain a drug resistant gene or an imaging traceable gene, such as a fluorescent gene reporter, in order to allow a rapid and easy identification of successfully transduced cells.

LVs have been widely used not only in molecular biology as a means to up- or down-regulate a certain gene in a study, but also as delivery agents for gene therapies in the clinical field. At the moment, in the United Kingdom alone, five clinical trials using lentiviral gene therapy are being led specially to correct monogenic diseases, such as X-Linked Severe Combined Immune Deficiency (Trial UK-0198 registered under [Gene therapy clinical trials worldwide](#)). In spite of the efficiency and applicability of this method, one concern remains with the use of any viral vector in medical therapies, namely, the risk of insertional mutagenesis (IM) resulting from the random nature of LV integration. For instance, random gene integration may possibly activate silenced oncogenes or disrupt tumour suppressor genes (Woods *et al.*, 2002). IM has been associated with some unwanted effects reported in gene therapy trials (Hacein-Bey-Abina *et al.*, 2003) and has led to a reassessment of the risks associated with gene therapies involving viruses. Some work has been done on integration preferences of HIV and its engineered lentiviral vector counterpart but the results are controversial. For instance, it has been shown by different groups that HIV-1 is likely to integrate at clusters of highly active genes, particularly those which were activated due to HIV-1 infection (Schröder *et al.*, 2002; Wu *et al.*, 2003). On the other hand, more recent studies using HIV-lentiviral

based vectors have found that the lentiviruses were more prone to integrate within introns, rather than active transcription sites or CpG islands (Ustek *et al.*, 2012; Yang *et al.*, 2008). Nevertheless, there are also studies focused on controlling this phenomenon and directing the integration site of lentiviruses (Bushman, 2002).

3.1.3 Choice of lentiviral vectors

There is an enormous choice of lentiviral transfer vectors in the market, and one must decide on which one to choose depending on the specific application desired. Here, we used pHIV-dTomato and pHIV-eGFP due to some particular features of the vectors, such as (i) the presence of a MCS to introduce our gene of interest upstream of an IRES and fluorescent reporter, allowing an equivalent expression of both genes; (ii) the relatively small size of about 7.7 kb; and (iii) the EF1- α promoter. The EF1- α promoter was selected because in MSCs, it has been reported to maintain a stable transgene expression over 20 population doublings without interfering with differentiation potential (Lee *et al.*, 2004). Also, it has been shown to be the most stable promoter during mESC-derived embryoid body differentiation (Norrman *et al.*, 2010). On the other hand, at high MOIs (≥ 100), it has been described to transiently arrest the cell cycle at S phase and also to decrease transgene expression during mESC differentiation *in vitro* (Hong *et al.*, 2007; Lee *et al.*, 2004).

In this chapter, a HIV-based lentiviral approach is described to stably introduce magnetic and fluorescent reporter genes into established cell and stem cell lines, creating a means of tracking cells using fluorescence methods

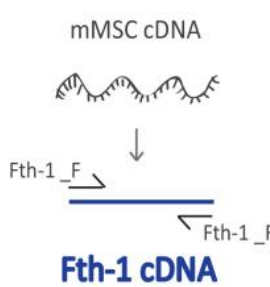
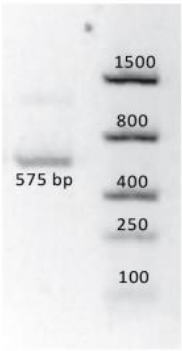
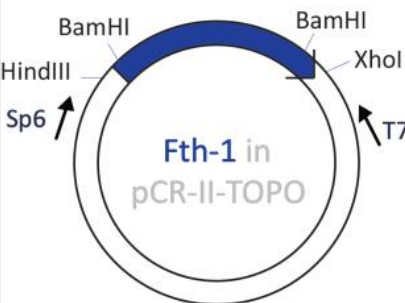
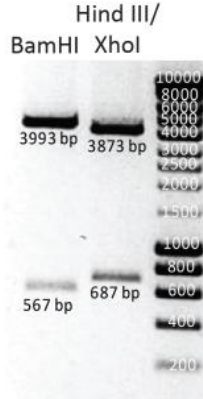
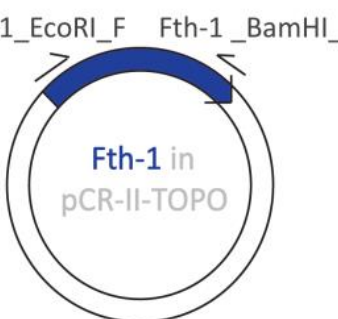
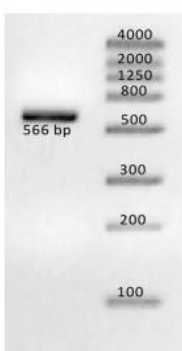
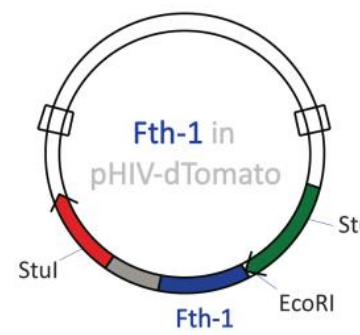
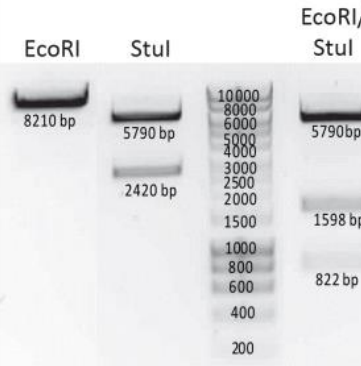
in vitro and MRI technology in animal embryos. The effect of the use of different concentrations of iron (in the form of ferric citrate) as a culture medium supplement on the viability of several cell lines is also investigated in order to define safe (non-toxic) conditions to achieve high intracellular iron concentrations. However, iron by itself cannot enter the cell and in high concentrations can become toxic due to its oxidative potential. For this reason, other components, such as transferrin and ascorbic acid, were also evaluated as a means to assist iron in entering the cell, and their effects are described in this chapter.

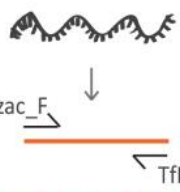
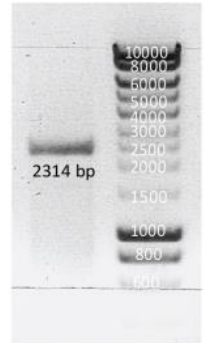
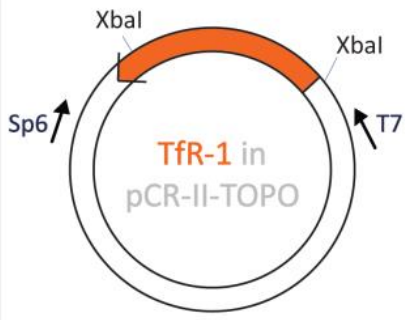
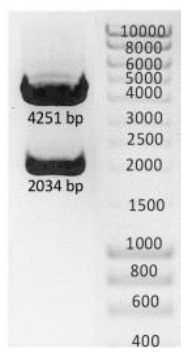
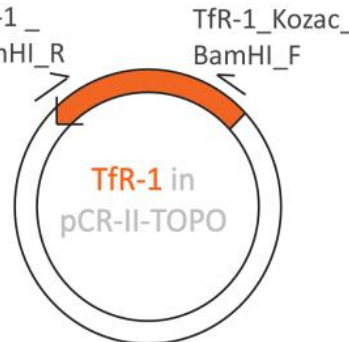
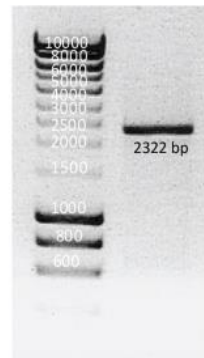
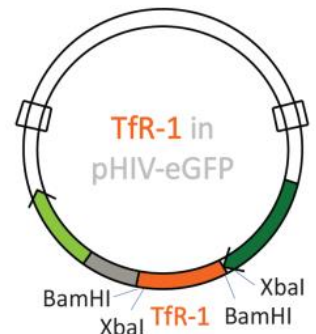
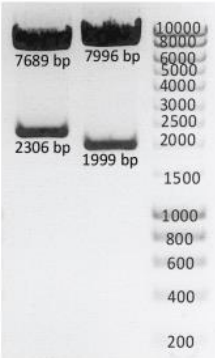
3.2 RESULTS

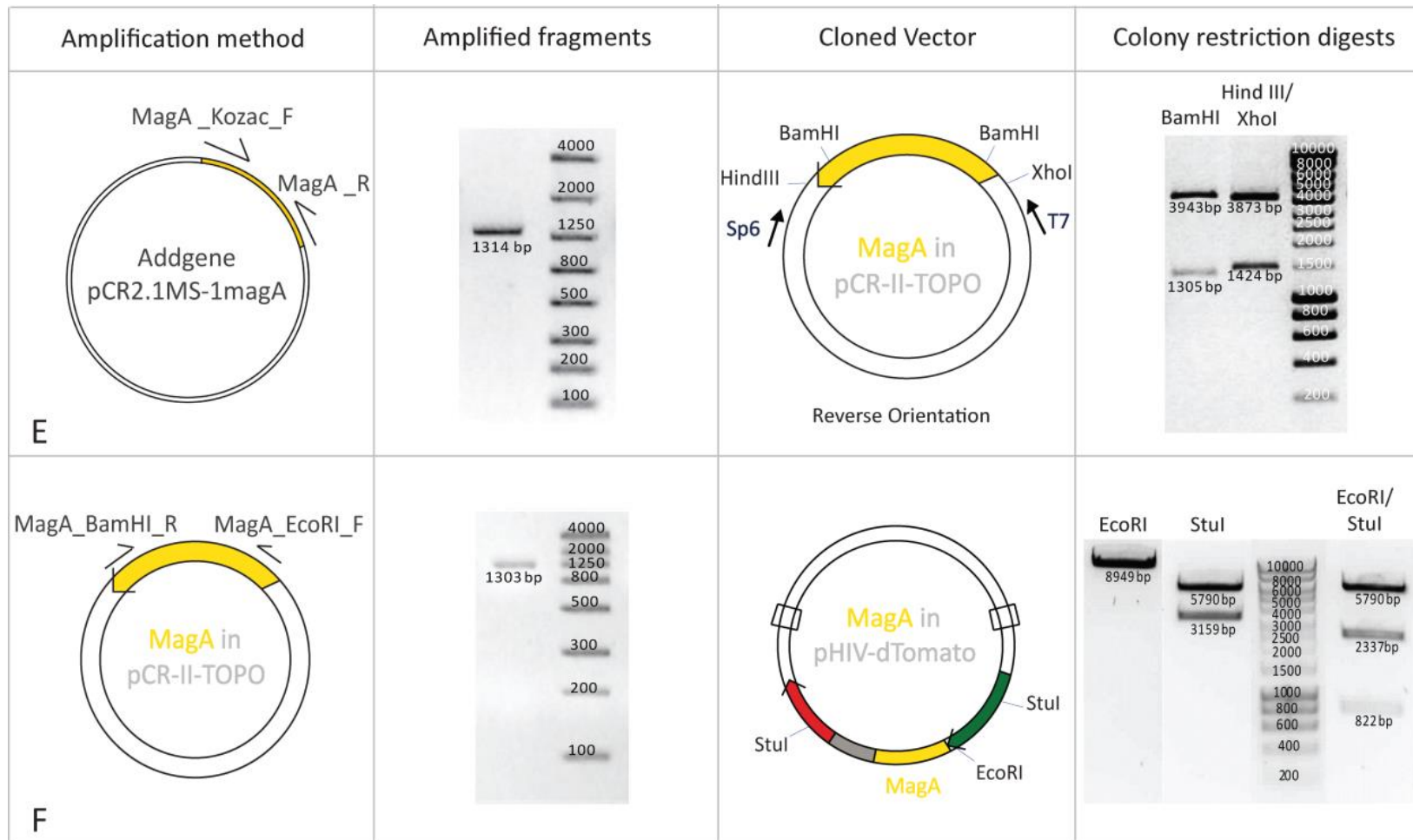
3.2.1 Generation of lentiviral constructs

To obtain Fth-1, TfR-1 and MagA transgenes, the cDNAs were PCR amplified with specific primers. In the case of Fth-1 and TfR-1, primers were purposely designed to exclude both untranslated regions (see sequences in Appendix I, p.242), as these regions are known to have an influence at the post-transcriptional level, inhibiting the translation of the mRNA. A synthetic Kozac sequence (GCCACC) was included when designing specific primers for TfR-1/MagA cDNA amplification, as it is known to promote the initiation of the translation process (Kozak, 1981). This was not necessary for the Fth-1 gene as it has a native Kozac sequence. Amplification strategies are shown in Table 8 (**A**, **C** and **E**), together with PCR fragments of cDNAs that were run on an electrophoresis gel.

Table 8 – Cloning strategies, including the amplification method, electrophoresis of amplified fragments and colony restriction digests performed to create and evaluate individual constructs containing Fth-1 (A and B), TfR-1 (C and D) and MagA (E and F) cDNAs. Half arrows represent forward (F) or reverse (R) primers. Components of the lentiviral vectors: red – dTomato gene; grey – IRES; dark green - EF1- α promoter; light green – GFP gene.

Amplification method	Amplified fragments	Cloned Vector	Colony restriction digests
<p>A</p> 		 <p>Forward Orientation</p>	
<p>B</p> 			

Amplification method	Amplified fragments	Cloned Vector	Colony restriction digests
<p data-bbox="302 446 638 734"> mMSC cDNA  TfR-1 cDNA </p> <p data-bbox="302 750 347 798">C</p>	 <p data-bbox="817 558 907 582">2314 bp</p>	 <p data-bbox="1209 750 1433 782">Reverse Orientation</p>	 <p data-bbox="1646 399 1713 422">XbaI</p>
 <p data-bbox="302 1212 347 1260">D</p>	 <p data-bbox="929 997 1019 1021">2322 bp</p>		 <p data-bbox="1635 837 1780 861">BamHI XbaI</p>



After PCR amplification with a proof-reading enzyme, both transgenes were introduced into a feasible working cloning vector, pCR[®]II-TOPO[®]. The cloning method chosen, in this case, was TA cloning, in which inserts are cloned in a non-directional way. Colony restriction digests were performed to select constructs containing an insert with the expected Fth-1/Tfr-1/MagA cDNA size. The restriction enzymes used are detailed within the cloned vectors' illustration and respective fragment products with the estimated band sizes are shown on the right hand side of Table 8 (A, C and E). Enzyme digestions showed that Tfr-1 cDNA was cloned in the reverse orientation into pCR[®]II-TOPO[®]. This was possible to determine due to the presence of two Xba I sites, outside and inside Tfr-1 cDNA insert. For pCR[®]II-TOPO[®]-Fth-1 and pCR[®]II-TOPO[®]-MagA the insert cloning orientation was determined by sequencing analysis using a T7 promoter, where it was possible to verify that Fth-1 insert was cloned in the forward direction and MagA insert in the reverse direction. The positive constructs were also sequenced to verify the sequence integrity of the inserts. Sequencing analysis revealed two point mutations in the MagA gene, which were also present in the parental vector from which it had been cloned (provided by Addgene). These mutations were identified as being silent mutations, not altering amino acid sequence. However, Addgene reported two amino acid substitutions (S94L and P390S) in MagA gene which do alter amino acid coding and are not conservative substitutions. The impact that these substitutions have on the normal function of MagA gene is unknown, but it is thought to be the same cDNA as used in previous studies (see Chapter 6, p.173). MagA cDNA

sequence and point mutations details are provided in Appendix I, p.242).

Due to the high recombination frequency between the long terminal repeats (LTRs) present in the lentiviral vectors (pHIV-dTomato/pHIV-eGFP), inserts were initially introduced into pCR®II-TOPO. This facilitated the synthesis of inserts, *i.e.*, by simply expanding the plasmid in a bacterial culture, followed by a plasmid DNA preparation. To generate lentiviral constructs, all cDNAs were once again PCR amplified with a new set of primers to include specific restriction enzymes in both 5' and 3' ends, which allowed a directional cloning of Fth-1/MagA into the pHIV-dTomato lentiviral vector. The cloning of TfR-1 into pHIV-eGFP was non-directional due to the lack of available restriction enzymes (only BamHI was present in the parental vector). Amplification strategies and PCR fragments of cDNAs were run on an electrophoresis gel and are shown in Table 8 (**B**, **D** and **F**). As previously, cells were transformed, expanded and colonies with the expected insert size were selected after an initial restriction digest step and the resulting products are shown in the electrophoresis gel on the right hand side of Table 8 (**B**, **D** and **F**). Whole sequencing analysis of final lentiviral plasmid constructs revealed that sequences of interest were successfully cloned into the lentiviral plasmids, without new mutations being introduced. Lentiviral constructs were then ready to be used in the production of lentiviral particles. The parental vectors are from now on described simply as dT or GFP and the constructs as dT_F (for Fth-1), GFP_T (for TfR-1) and dT_M (for MagA) (Figure 5).

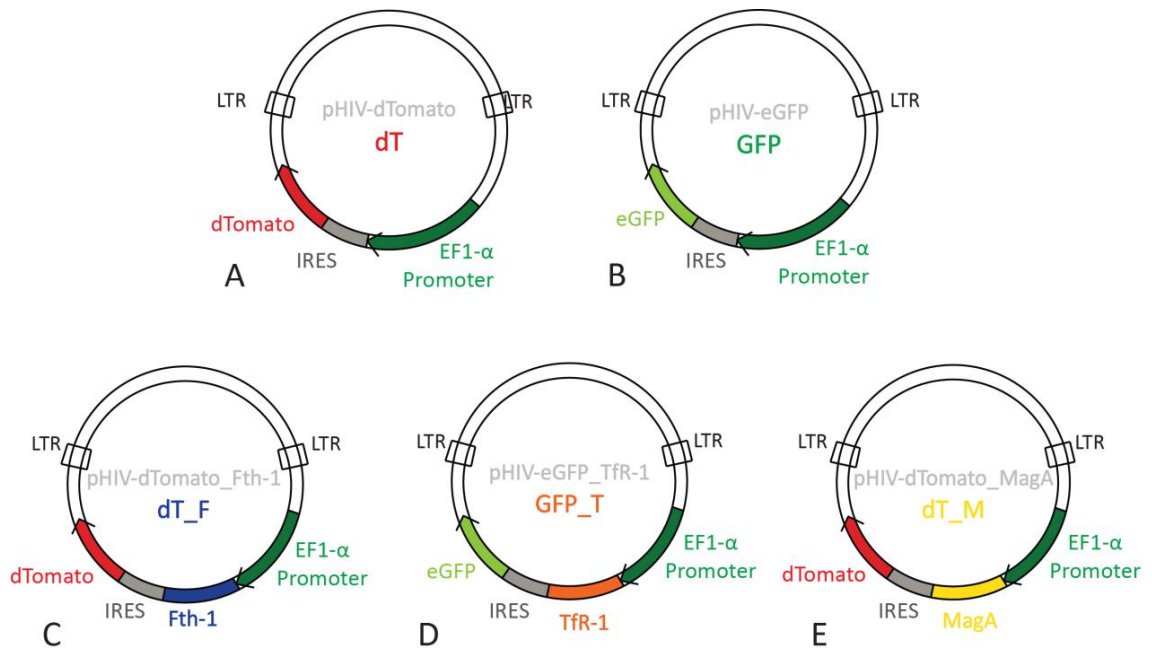


Figure 5 – Plasmid maps of parental vectors dT (**A**) and GFP (**B**) and lentiviral constructs dT_F (**C**), GFP_T (**D**) and dT_M (**E**). Some key features are represented, such as the fluorophore of each plasmid (dTomato or eGFP transgene) connected to the gene of interest (Fth-1/TfR-1/MagA) through an IRES to allow bicistronic expression of both genes. Also represented is the promoter elongation factor 1-alfa (EF1- α) to initiate the constitutive expression and the HIV-long terminal repeats (LTR), which flank the region to be incorporated into the host's cell genome.

As the following chapters describe several cell types transduced with either single (dT, GFP, dT_F, GFP_T, dT_M) or multiple viral preparations (dT_F + GFP_T) there was a necessity to clone the chosen genes in lentiviral vectors with different fluorophores. Hence, when working with multiple viral preparations, transduction was easily followed-up by the expression of two different fluorescent proteins.

3.2.2 Production of lentiviral particles

In a lentiviral packaging system involving multiple plasmids, the optimization of relative amounts of each plasmid involved allows for an efficient production of high titers of lentiviral particles. For this reason, several mass ratios of the transfer

(dT/GFP), packaging (psPAX2) and envelope (pMD2.G) plasmids were tested by cotransfection of the producer cell line HEK 293T(N). Afterwards, the resultant particles were transduced into the same cell line with an equal volume of viral supernatant, in order to evaluate the production efficiency for each condition. The results were analysed using flow cytometry (Figure 6) to detect the percentage of fluorescent cells in the population.

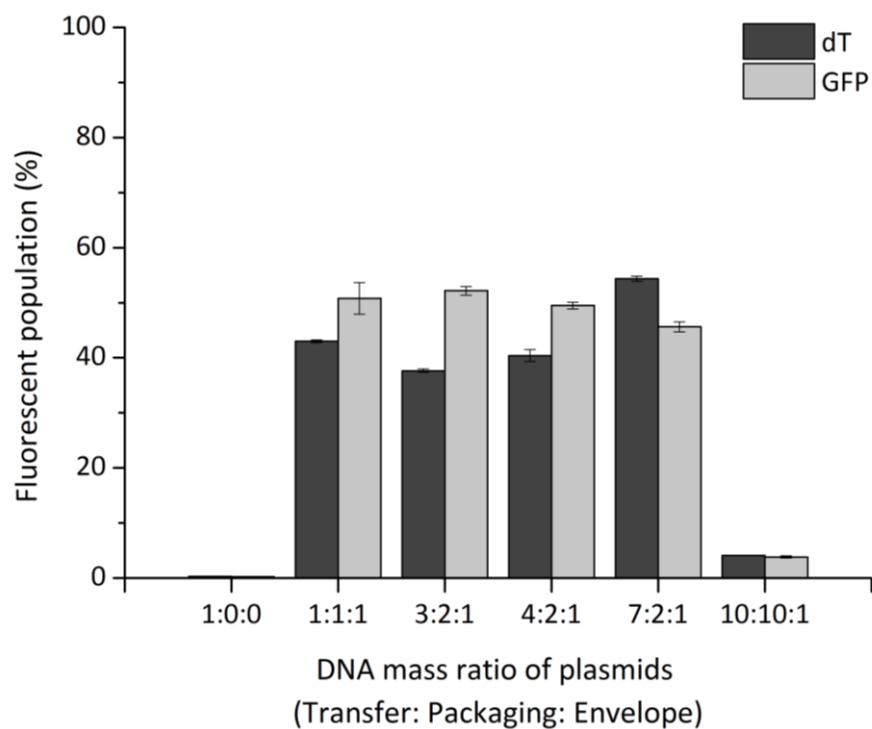


Figure 6 – Flow cytometry analysis of red (dT) and green (GFP) fluorescent populations of HEK 293T(N) cells after being transduced with the same volume of viral supernatant, produced with different plasmid ratios. Error bars represent SEM ($n=3$) (M&M, p.43).

Figure 6 shows that the mass ratios 1:1:1, 3:2:1, 4:2:1 and 7:2:1 gave rise to similar production efficiencies, with 40 to 50% of cells being transduced with both viral particles types. A ratio of 10:10:1 was less efficient, and as expected, when packaging and envelope vectors were not present (1:0:0), the transfer vector alone

was unable to form efficient lentiviral particles, confirming the safety of this lentiviral production system. A plasmid ratio of 4:2:1 was thus chosen as it offered a good yield with both vectors and this ratio was used for producing lentiviral particles with the parental vectors and the constructs containing the magnetic reporter genes.

3.2.3 Determination of viral titer of lentiviral particles

In order to transduce cells of interest with a specific multiplicity of infection (MOI) the viral titer for each batch of lentiviral particles was determined. To do this, 5×10^4 HEK 293T(N) cells were transduced with different amounts of unconcentrated (concentrated in the case of MagA) lentiviral particles and the number of fluorescent cells was determined by flow cytometry. Figure 7 shows the results obtained for different transducing particles in HEK 293T(N) cells.

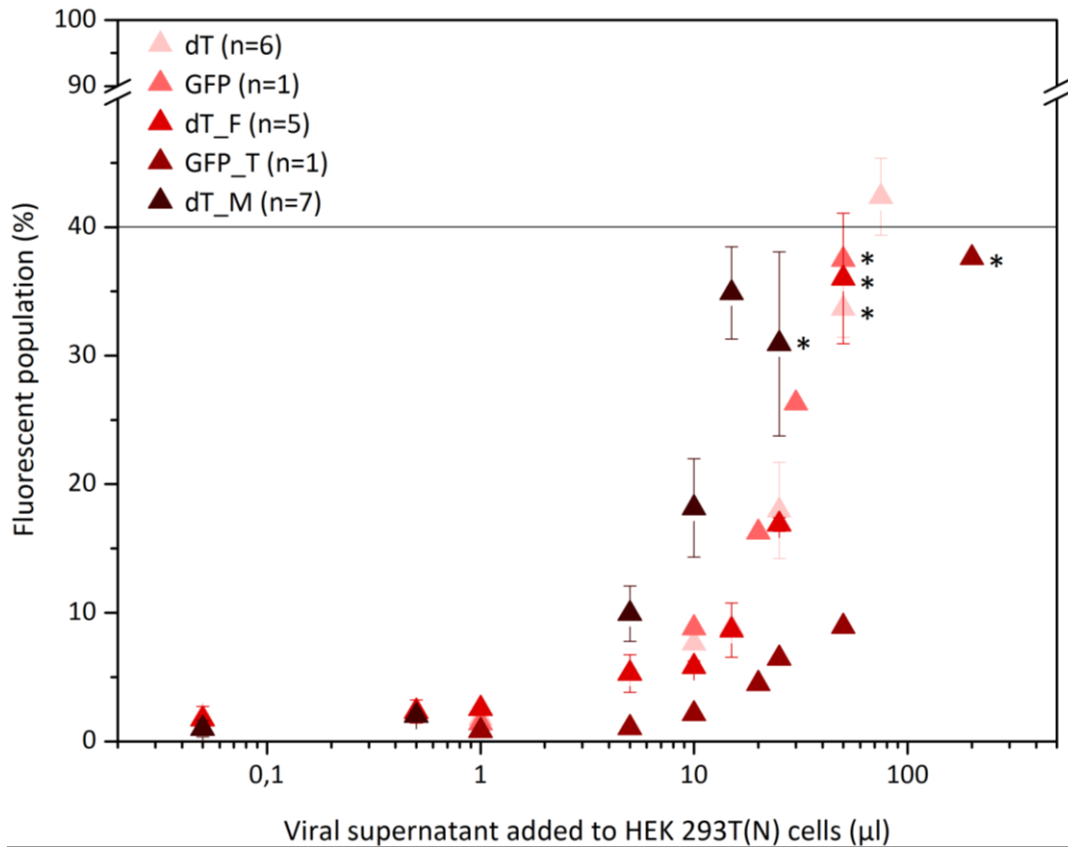


Figure 7 – Flow cytometry analysis of red (dT, dT_F and dT_M) and green (GFP, GFP_T) fluorescent cells in relation to the volume of lentiviral particles used for transduction of HEK 293T(N) cells. A 40% fluorescent threshold was set and the chosen value for titration is annotated with a *. Error bars represent SEM (number of biological replicates are indicated in the legend) (M&M, p.46).

The results obtained with flow cytometry show an expected rise in the percentage of fluorescent cells with the increasing volume of lentiviral particles. To calculate accurate titrations, a value that fitted the linear relationship between the fluorescent population and the volume of viral supernatant added was chosen. Therefore, only volumes that gave rise to less than 40% fluorescent cells were taken into consideration (Kutner *et al.*, 2009). According to Equation 2 (p.47), the number of transducing units per ml of solution was determined and results are shown in Figure 8.

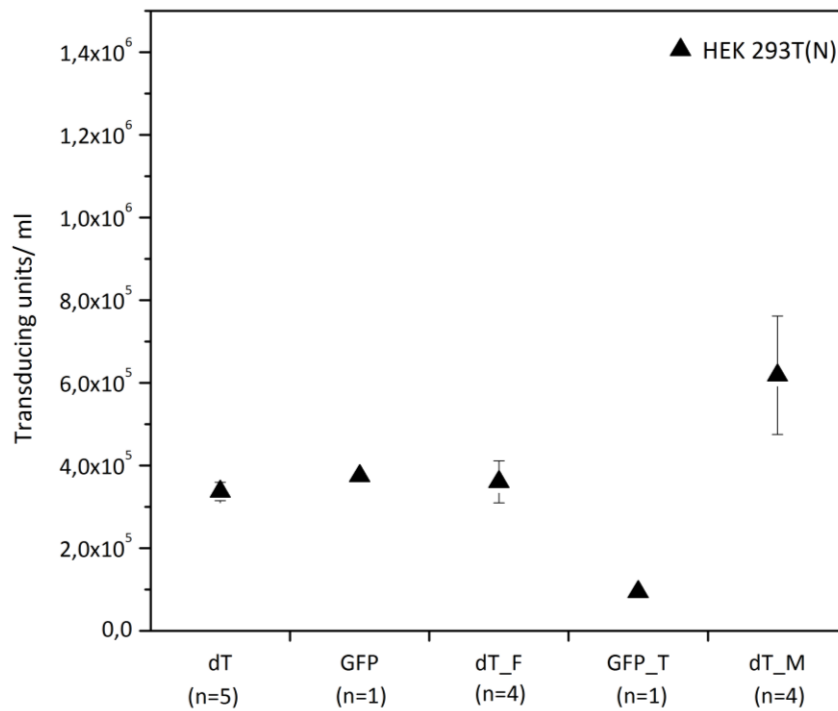


Figure 8 – Viral titer of different lentiviral preparations determined in HEK 293T(N) cells. Error bars represent SEM (number of biological replicates are indicated in the X-axis) (M&M, p.47).

3.2.4 Transduction efficiency between cell lines

To evaluate transgene integration efficiency of lentiviral particles in the different cell lines used in this study, 5×10^4 cells were transduced with the same amount of viral particles and the results were analysed with flow cytometry (Figure 9).

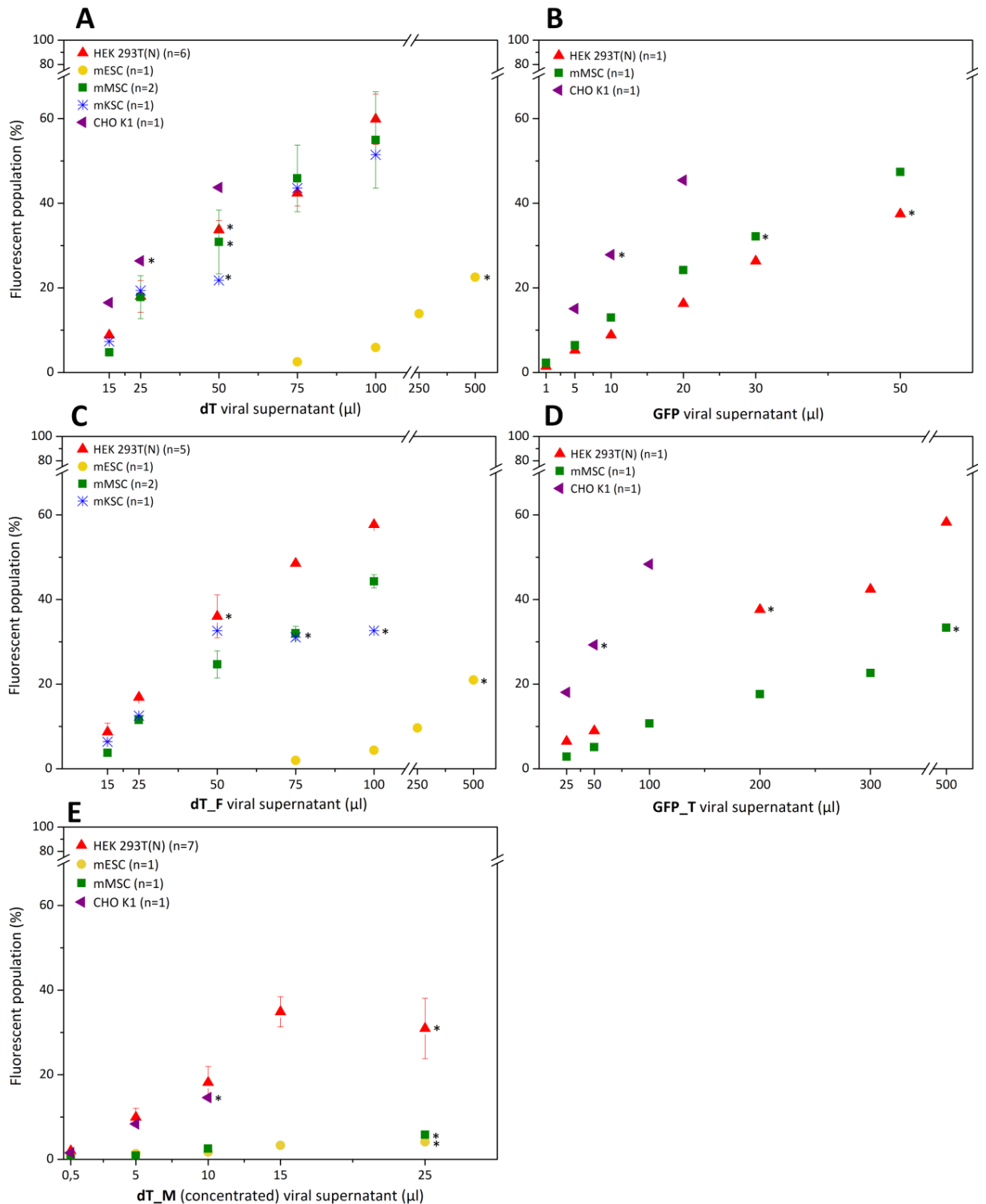


Figure 9 – Flow cytometry analysis of populations of fluorescent cells after transduction with different viral preparations, such as dT (A), GFP (B), dT_F (C), GFP_T (D) and dT_M (E) in several types of cells, demonstrating the variation of transduction efficiency between cell lines. As previously, the chosen value to calculate the viral titer was below the 40% fluorescent threshold and is annotated with a *. Error bars represent SEM where possible (numbers of biological replicates are indicated on the graphs) (M&M, p46).

Figure 9 shows that there is a prominent difference in transduction efficiency if the same virus amount is used on different cells. This is especially true for mESC, which proves to be the least transducible cell line, independent of lentiviral construct used. For the other cell lines, HEK 293T(N), mMSC, mKSC and CHO K1 cells, the difference in transduction efficiency is not so prominent. It should be noted that not all cell lines were used to evaluate the integration efficiency of the different constructs as this was performed as necessary according to the work described in the following chapters. When identifying the theoretical number of transgenes that have integrated, it is important that differences between specific cell lines are accounted for. For this reason, the most correct way to proceed is to not only rely on the titration performed on the producer cell line, HEK 293T(N), but also to take into account the efficiency of transgene integration dependent of each cell line.

After integration efficiency was determined individually in each cell line, the number of transducing units per ml of supernatant was once again calculated and is shown in Figure 10.

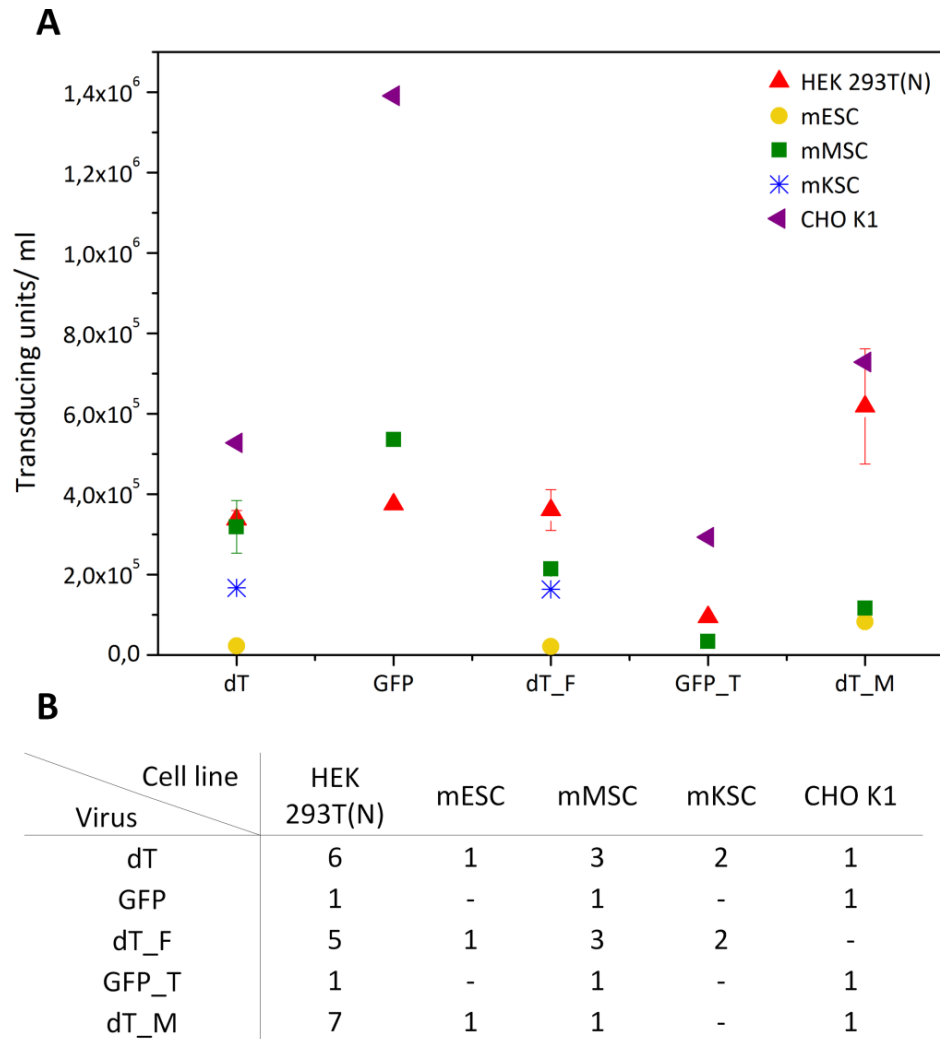
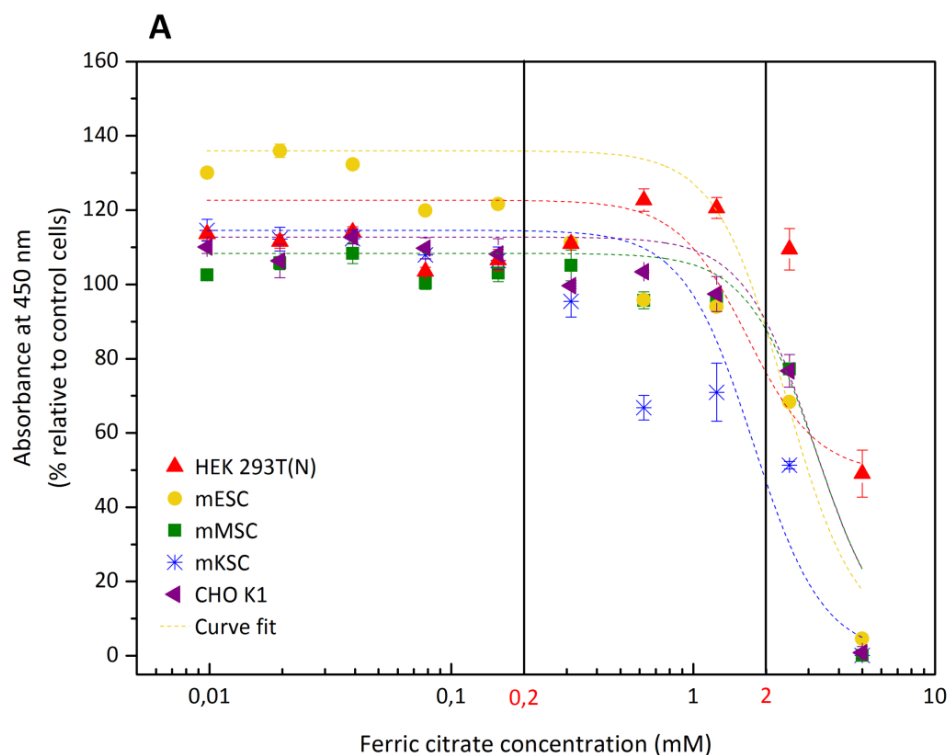


Figure 10 – Viral titer of different lentiviral preparations specifically determined for each cell line (**A**). Error bars represent SEM where possible. Numbers of biological replicates are indicated in the table in **B** (M&M, p47).

The multiplicity of infection (MOI) used for each condition was tested on a case-by-case basis and depended on the lentiviral integration ability without compromising cell health and proliferative capacity of a specific cell type. In order to do this, a range of different MOIs were tested in target cell lines and cell counting assay was performed (see 2.7 Cell viability capacity, p.62). The highest MOIs that were able to maintain proliferation of cells in comparable levels to controls were chosen to use subsequent experiments (data not shown).

3.2.5 Optimization of Intracellular Iron Loading

To optimize the suitable iron supplementation that allows a significant increase in intracellular iron content, five wild-type (WT) cell lines used in the course of this study were exposed to increasing amounts of ferric citrate concentrations, from 10 μ M up to 5 mM. A cell counting assay was performed to detect the percentage of viable cells in each condition tested (Figure 11).



B

	HEK 293T(N)	mESC	mMSC	mKSC	CHO K1
EC50	1,67	2,41	3,25	1,77	3,16
EC80	2,66	3,82	5,15	2,81	5,01

Figure 11 – Cell viability evaluation of several cell lines, when exposed to increasing amounts of ferric citrate for a period of 24h (**A**). Absorbance is shown in relation to control cells (cultured without supplementation). The best logistic fit for each cell line is represented in the cell's correspondent colour. The 0.2 and 2 mM marks display the chosen concentrations of ferric citrate used in further experiments, supported by the table in **B**. EC50 and EC80 represent the ferric citrate concentration (mM) that causes 50 and 80% cell reduction relative to control. Error bars represent SEM ($n=3$) (M&M, p49).

As shown by Figure 11, when supplemented with low iron concentrations (0.01-0.2 mM), all cell lines maintain a 100% or higher living capacity in relation to a non-supplemented control. Relying on these results and on the iron supplementation values commonly described in the literature, an optimum concentration of 0.2 mM of ferric citrate was used to supplement cells of interest. Furthermore, in order to fully determine the reporter gene potential of accumulating intracellular iron, a ten-fold higher concentration of 2 mM was also used in the following work. However, as shown in Figure 11, 2 mM of ferric citrate decreases cell viability in two cell lines, in HEK 293T(N) to about 80% and in mKSC to approximately 50% cell viability. Other cell lines studied are only slightly below 100% viability when ferric citrate is incubated at 2 mM. Nevertheless, it is speculated that once cells are overexpressed with iron-clustering genes, such as ferritin heavy chain-1, they may be more resistant to the effects promoted by high concentrations of ferric citrate. In relation to the iron concentration which is normally present in the cell culture medium (approximately 300 nM of ferric nitrate) the supplementations with 0.2 or 2 mM of ferric citrate provide, respectively, a 700 or 7000-fold increase of iron.

Besides ferric citrate, other supplements such as L-ascorbic acid (Lane *et al.*, 2013) or holo-transferrin (Deans *et al.*, 2006) have also been described in the literature to play a role in the cellular iron loading process. To test if either of these supplements would contribute to increase intracellular iron, four cell lines were exposed to different supplementations. The concentrations used were: 0.2 mM of

ferric citrate, as determined previously, 50 μ M of L-ascorbic acid, as it was described to be an approximation to physiological conditions (Lane *et al.*, 2013) and 1.28 mM of human holo-transferrin, equivalent to 100 μ g/ml. For this last supplement, even though some reports suggest its use in concentrations of 1 mg/ml and higher (Deans *et al.*, 2006; Iordanova *et al.*, 2010), optimization experiments showed that concentrations higher than 1.28 mM did not have a significant impact in terms of cellular iron loading (data not shown). As demonstrated in Figure 12, the condition that proved to have the best iron loading capacity was the co-supplementation of ferric citrate, L-ascorbic acid and holo-transferrin. This was particularly true for mMSC and mKSC, where significant increases in intracellular iron concentrations were observed with the combination of all three supplements. For this reason, these components were included in all iron loading experiments described in the next chapters. HEK 293T(N) are the only exception, where no benefit was seen with the use of L-ascorbic acid and holo-transferrin and thus ferric citrate was the only supplement used for iron loading.

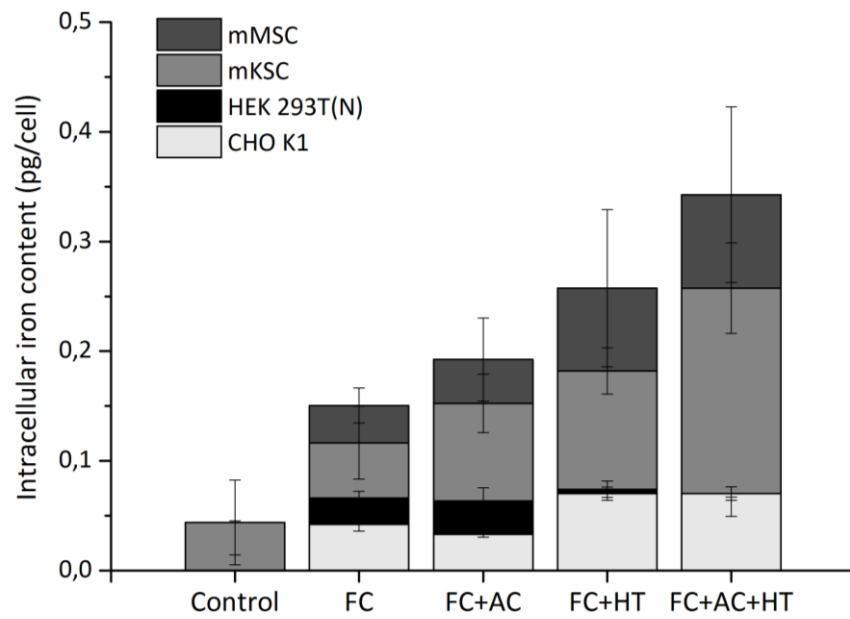


Figure 12 – Measurement of intracellular iron content of mMSC, mKSC, HEK 293T(N) and CHO K1 with different supplements: FC-0.2 mM of ferric citrate, AC-50 μ M L-ascorbic acid, HT-1.28 mM human holo-transferrin. Error bars represent SEM ($n=3$).

3.3 DISCUSSION

The iron content inside any organism needs to be tightly controlled in order for it to function properly, and to achieve this, the expression of key proteins involved in iron metabolism is tightly regulated. For instance, Fth-1 and TfR-1 possess iron responsive elements (IRE) in their 5' and 3' UTR, respectively (Appendix I). These elements have the ability to inactivate Fth-1 mRNA and stabilize TfR-1 translation if iron is not present in the cell and do the reverse when iron is in excess (Figure 1). While generating the lentiviral constructs, untranslated regions from Fth-1 and TfR-1 cDNAs were intentionally excluded from amplification, to allow a constitutive expression of viral Fth-1 and TfR-1 genes, bypassing the cell's gene regulation mechanisms. The rationale behind this procedure was to increase the cellular uptake of iron and its accumulation inside ferritin cages, safely increasing the cell's iron content and thus providing a good contrast in MRI. In the case of MagA, since it has a bacterial origin, this cDNA does not possess untranslated regions and only an artificial Kozac sequence was included in cDNA amplification.

Following cloning of lentiviral constructs with the specific target genes, individual amounts of each plasmid required for the viral assembly were optimized and the plasmid ratio of 4:2:1 (transfer: packaging: envelope vectors) was selected as the best choice for producing the lentiviral particles. Once all the lentiviral batches were produced and before transducing the cells of interest, the concentration of virions in the supernatant was calculated to make the transduction

process standardized and reproducible over time. As expected, distinct viral preparations had different efficiencies when transducing the same cell line HEK 293T(N) (Figure 7). These results can be translated in terms of viral titer for each preparation, and they are demonstrated in Figure 8. Differences in the resultant viral titers can be explained, in part, due to the construct size, as it is known that the bigger the lentiviral construct, the less efficient it is (Urbinati *et al.*, 2009). This can be observed in the case of GFP_T (10 kb), with approximately 1×10^5 TU/ml and its parental vector, GFP (7.7 kb), with 3.75×10^5 TU/ml. Such is not observed between dT_F (3.6×10^5) and its original construct dT (3.37×10^5). This effect is even more prominent in the case of the dT_M construct, with an initial unconcentrated version of 1.14×10^4 TU/ml (data not shown). Only after concentration was it possible to achieve a value similar to the other viral productions, with 6.18×10^5 TU/ml. This poor production efficiency seen in dT_M cannot alone be explained by insert size and is much more significant than that observed with GFP_T. It can be hypothesized, however, that this outcome is related to a potential toxic effect of MagA expression in HEK 293T(N) cells, although this has not been explored in detail in the course of this work.

It is not only important that transduction with different viral preparations are reproducible (achieved by calculating the viral titer), but one also needs the transduction to be similarly efficient between cell lines. This means that MOI must be calculated taking into account the transgene integration efficiency, thus contributing for a more similar transgene expression between cell lines, in order to

allow results to be compared. For this reason, we calculated the efficiency of transduction by titration of each viral preparation in the specific cell line to be transduced. Even though the use of this method is more accurate, it is not perfect and we still can perceive some variation when the viral genes are quantified at the mRNA level (later chapters). Also, other factors may contribute to certain variability. For example, target genes may be inserted in places where gene expression is not active, leading to variable expressions in different cells. On the other hand, this may also pose as an advantage in stem cell biology because in a therapeutic setting, stem cells might differentiate and epigenetic changes could silence the transgenes depending on their site of integration.

In this chapter, three potential magnetic reporter genes were successfully introduced into a variety of stem cell lines. Target genes were cloned alongside a fluorescent gene (dT or GFP) to allow bicistronic expression, thus allowing an easy identification of transduced cells by flow cytometry. The influence of iron concentration on cell number for a variety of different cell lines was also determined. It was found that low concentrations of iron are actually beneficial for cell proliferation and this observation reinforces the notion that iron is a crucial element for cell health and perhaps should be used in routine cell culture conditions (Figure 11, p.87). Also, and as expected, each cell line has its own individual resistance to higher concentrations of ferric citrate and that the use of supplements, such as holo-transferrin and/or L-ascorbic acid, also aid in iron incorporation in most cells studied.

CHAPTER 4

TRANSFERRIN RECEPTOR-1 AS A REPORTER GENE FOR MRI TRACKING OF CELLS

4.1 INTRODUCTION

TfR-1 is a membrane glycoprotein which has an indispensable role in maintaining iron homeostasis, serving as a mediator in the iron uptake by most cells through the internalization of iron-bound transferrin (Aisen, 2004).

4.1.1 Studies targeting transferrin receptor-1

Most studies relating to TfR-1 involve the up-regulation and/or overexpression of this gene, mainly for targeted therapeutic applications, such as using this receptor and its conjugate (transferrin) as a drug delivery system (Moore *et al.*, 2001; Qian *et al.*, 2002; Wang *et al.*, 2010). This is based on the fact that tumour/cancer cell lines often have very high numbers of TfR-1 on their membrane, when compared to most healthy tissues within an organism (Inoue *et al.*, 1993). TfR-1 can therefore be targeted by two different approaches: i) to deliver a therapeutic agent to a malignant cell, promoting cytotoxic effects; or ii) inhibiting TfR-1 at the cellular surface with specific molecules, therefore directly promoting cell death (Daniels *et al.*, 2012). Therefore, this system proves to be advantageous in terms of drug tissue distribution, preferentially targeting high expressing TfR-1 cells and avoiding non-specific toxicity. Also, extended half-life of the drug when

combined with transferrin would bypass its spreading into the blood stream. Finally, a somewhat “controlled” intracellular drug release would then be possible (Daniels *et al.*, 2012; Qian *et al.*, 2002). However, this use of TfR-1 is mainly focused on cancer therapeutics and to a lesser extent on cell tracking applications.

4.1.2 Transferrin receptor-1 as an MRI reporter gene

One of the earliest cell tracking studies based on TfR-1 levels was performed by Moore *et al.* (1998), where gliosarcoma cells were stably transfected with an engineered human transferrin receptor-1 (ETR). This engineered gene lacked the 3' untranslated region containing the iron responsive elements responsible for post-transcriptional regulation of TFR-1 in iron uptake regulation. These cells were exposed to a conjugation of dextran-coated monocrystalline iron oxide nanoparticles (MION) with transferrin (Tf-MION). In the first instance, the group showed that when Tf-MION was presented as an iron source, it was internalized by TFR-1 mediated endocytosis and did not interfere with ETR expression levels. Later on, ETR was overexpressed again in a gliosarcoma cell line using a lentiviral approach and cells were non-invasively monitored with MRI in a mouse model, where the cells gave a distinct contrast as a result of the higher iron uptake. This was then the first research group to primarily explore TFR-1 as an MRI reporter gene (Ichikawa *et al.*, 2002; Moore *et al.*, 1998; Moore *et al.*, 2001; Weissleder *et al.*, 2000).

Since then, another two groups have investigated the role of TfR-1 as a cell tracking probe for visualization with MRI. However, one of these studies was mostly

focused on targeted delivery of cancer therapies using a breast cancer cell line (Wang *et al.*, 2010). The other report is the only one which has evaluated TfR-1 as a potential MRI reporter gene in the field of cell tracking. This was performed by Deans *et al.* (2006), where human TFR-1 in conjunction with human ferritin heavy chain-1 (FTH-1) were stably transfected by electroporation into an immortalized mouse cerebellar progenitor cell line (also known as C17 cell line). Both transgenes were deprived of 3' and 5' UTR in TFR-1 and FTH-1, respectively, to allow constitutive expression. When analysing transgene integration, human TFR-1 and FTH-1 were investigated at mRNA and protein level. It was found that in transgenic cells, FTH-1 was increased 2.5-fold more than in controls when both cell types were iron supplemented. However, since this study overexpressed TFR-1 and FTH-1 genes from human origin into a mouse cell line, the authors failed to investigate if the endogenous levels of these genes (mouse TfR-1 and Fth-1) were affected. Therefore, they did not show if the transgenic cells were compensating the overexpression by down-regulating their own TfR-1 and Fth-1 levels, in order to maintain iron homeostasis. Nevertheless, in this study it was found that cells expressing both transgenes stored more intracellular iron than controls, without affecting cell viability. This intracellular iron accumulation resulted in an increase in T_2 and T_2^* contrast both *in vitro* and *in vivo* when transgenic cells were transplanted into mouse (Figure 13) (Deans *et al.*, 2006).

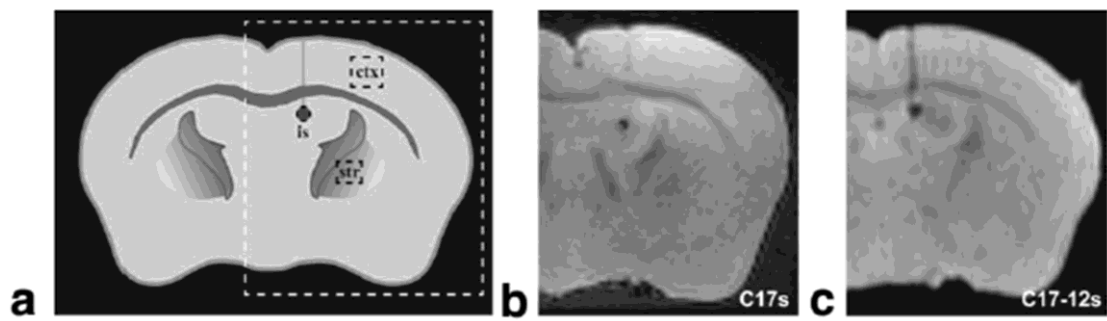


Figure 13 – Control (C17s) and TFR-1/FTH-1 transfected cells (C17-12s) were supplemented with iron (1 mM of ferric citrate and 1 mg/ml holo-transferrin) for 48h before transplantation into an adult mouse brain. **a** – schematic representation of a coronal section of a mouse brain, indicating the injection site (is), control regions in the cortex (ctx) and striatum (str). **b** and **c** – Magnetic resonance (7 T) T_2^* -weighted images of *ex vivo* mouse brain sections, 20 days after injection. A clear contrast is observed between injected cells and the surrounding brain tissue; analysing regions of interest within the injection site, a significant signal loss is detected for C17-12s ($n=3$), when compared to C17s ($n=2$). Reproduced with [permission](#) from Deans *et al.* (2006).

In this chapter, mouse transferrin receptor-1 gene is evaluated for its potential as a reporter gene for MRI tracking of cells. To do this, first, a stable and long-term overexpression was evaluated in a model cell line, CHO K1. Transduced cells were then compared to controls in terms of cell viability and also iron homeostasis, by investigating endogenous and total levels of TfR-1. Finally, iron retention capacity of TfR-1 transduced cells and the feasibility of imaging these cells using MRI are also evaluated.

4.2 RESULTS

Transferrin receptor-1 was initially assessed as a potential magnetic reporter in several cell lines such as HEK 293(N), CHO K1, mouse fibroblast cells STO (ATCC® CRL-1503™) and MEF-1 (ATCC® CRL-2214™), and stem cell lines such as mESC and mMSC. The most promising results were obtained using HEK 293T(N) (data not shown), CHO K1 and mMSC. Therefore, the present chapter describes CHO K1 as a model cell line to explore the full potential of TfR-1 as an MRI reporter and in the following chapter TfR-1 is assessed in mMSC (Chapter 5).

CHO K1 cells were transduced with lentiviral particles encoding either for GFP, to serve as control, or GFP_T, to evaluate the potential of transferrin receptor-1 as a magnetic reporter. These cells were transduced with a MOI=100 and were not subjected to FACS sorting. Three independent transductions were carried out for each condition and represent, therefore, three biological replicates ($n=3$).

4.2.1 Evaluation of reporter gene integration

Transgene expression, in the form of green fluorescence due to the presence of a GFP reporter, was monitored over several passages using fluorescence microscopy (Figure 14) and flow cytometry (Figure 15).

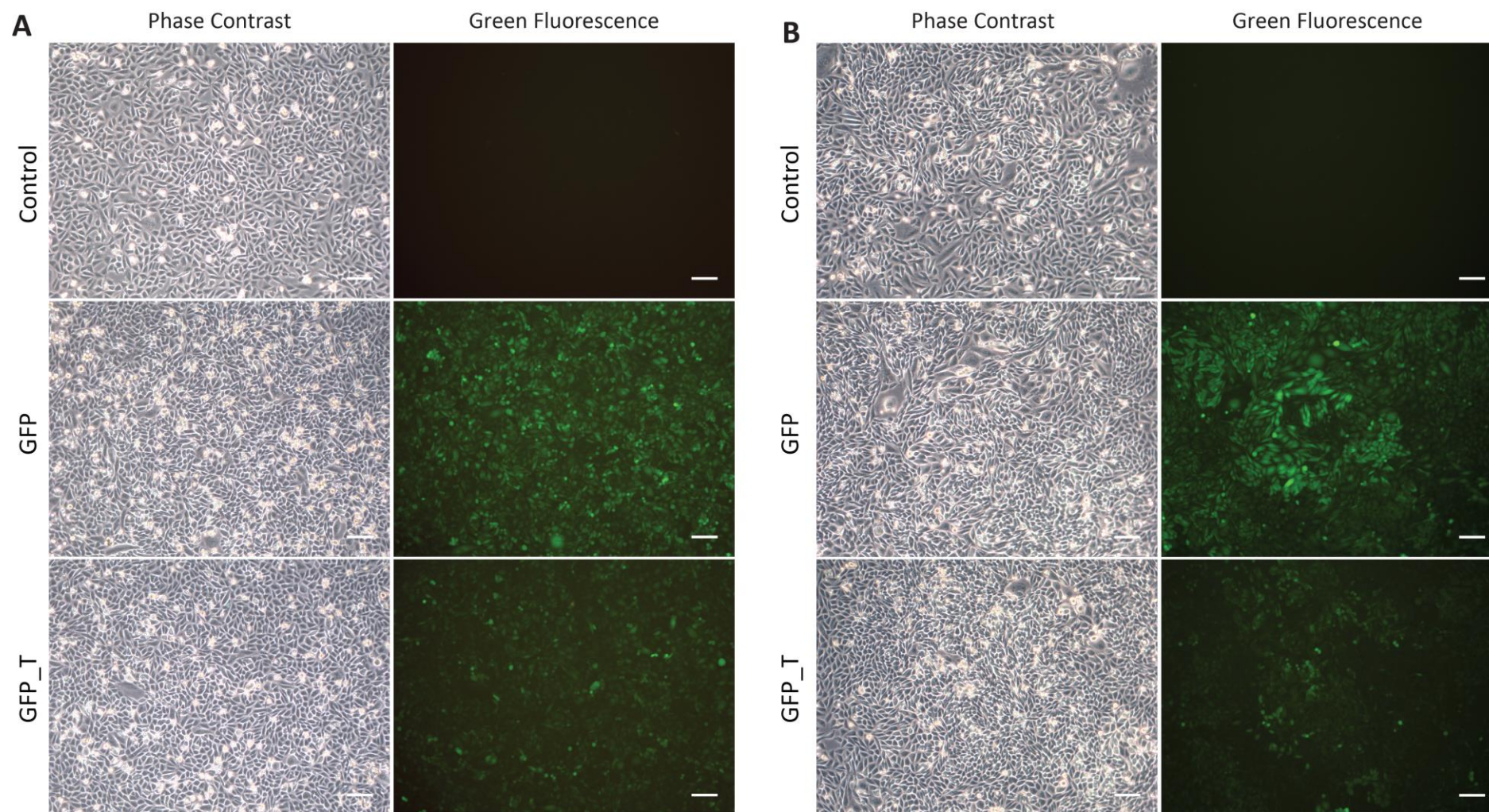


Figure 14 – Representative pictures of CHO K1 cells, at P3 (**A**) and P8 (**B**) post-transduction, and control cells (untransduced) at an equivalent passage. GFP corresponds to GFP transduced cells and GFP_T to TfR-1 transduced cells. All green fluorescent pictures were taken with the same exposure conditions. Scale bars correspond to 100 μm .

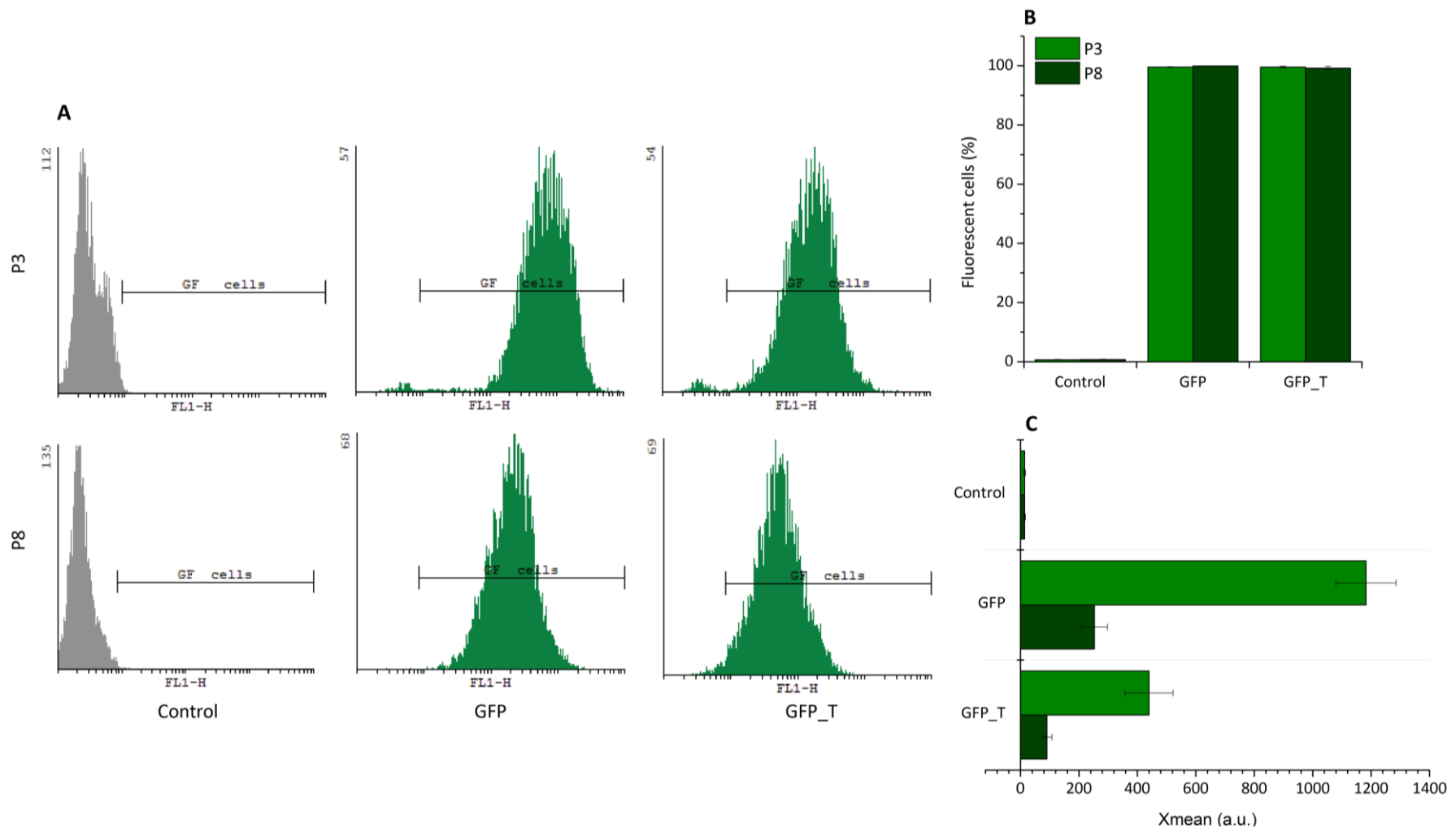


Figure 15 – Flow cytometry histograms of **(A)** CHO K1 cells, at P3 and P8 after transduction. Histograms show the number of events (cells) counted (y-axis) versus the fluorescence intensity (x-axis). Green fluorescence (GF) gate represents GFP-positive cell population plotted in **B**. The Xmean **(C)** represents the mean fluorescence obtained from the gated region (GFP cells). Error bars represent SEM ($n=3$); a.u. - arbitrary units; (M&M, p.48).

Figure 14 and Figure 15 demonstrate that GFP and GFP_T transductions were very efficient in both conditions as cells are nearly 100% GFP-positive and maintain green fluorescence over the period of time studied. A small difference in the brightness of green fluorescence is also perceptible between GFP-control cells and GFP_T cells (Figure 14). This is further evaluated with flow cytometry (Figure 15, C), where the mean fluorescence intensity not only has a clear shift between GFP and GFP_T at P3, meaning that GFP_T are less bright than GFP control, but also between P3 and P8, where there is a decrease in green fluorescence intensity for both conditions, even though they are still almost 100% GFP-positive.

To additionally complement integration stability evaluation and its effects on the native TfR-1, the transgenes GFP/ viral transferrin receptor-1 (Viral_T) as well as endogenous TfR-1 (here named as CHO_T) were also assessed at P1 and P3 with RT-qPCR (Figure 16). Because the integrated transgene was derived from a mouse cell line, whose sequence is not completely homologous to Chinese hamster, viral (Viral_T) and endogenous (CHO_T) TfR-1 mRNA transcripts could be detected individually by RT-qPCR. The total amount of TfR-1 (Total_T) expressed in the cell at a certain condition was later determined by protein quantification. For RT-qPCR evaluation Pabpn1 and Vezt genes were used as a reference for CHO K1 cells to normalize Ct values obtained for target genes.

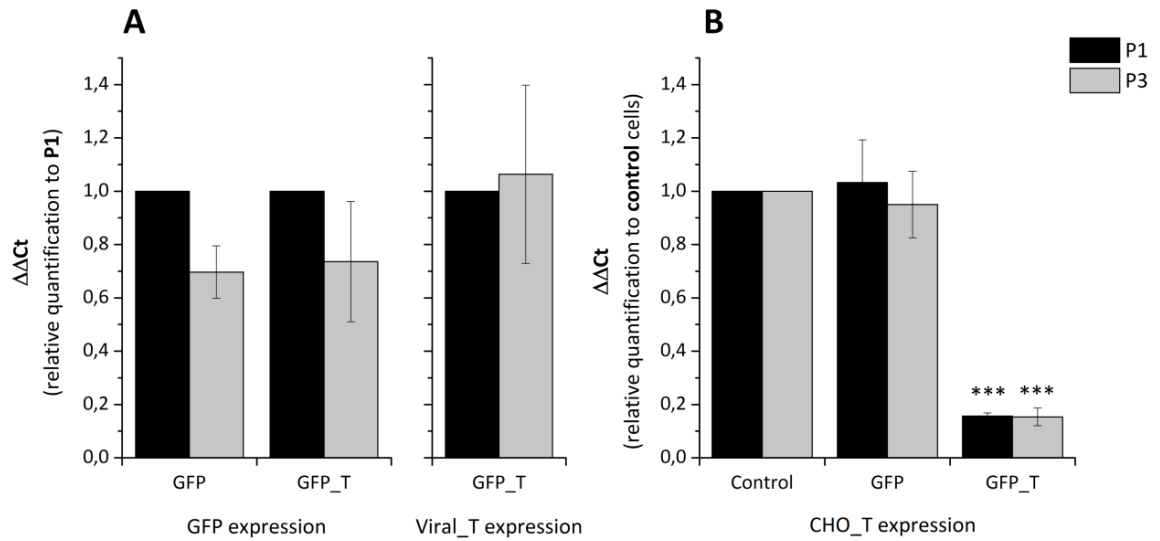


Figure 16 – RT-qPCR relative quantification of GFP, Viral_T and CHO_T targets in control, GFP and GFP_T transduced CHO K1 cells at P1 and P3 post-transduction. GFP and Viral_T expression values are normalised to P1 (**A**) and endogenous CHO_T to control cells (**B**). A very significant statistical decrease of endogenous TfR-1 is observed only in TfR-1 overexpressed cells (GFP_T), both at P1 and P3. Error bars represent SEM ($n=3$) (M&M, p.52).

The data presented in Figure 16, **A** confirms the observation with flow cytometry (Figure 15, **C**), in which GFP expression decreases in both cell lines over time. The same, however, is not confirmed for Viral_T expression, which appears relatively stable from P1 to P3. This suggests that the bicistronic expression in this case might not be equivalent for both transgenes. Also, the data in Figure 16, **B** shows that the endogenous TfR-1 (CHO_T) expression is stable in control and GFP cells over the period of time studied, while there is a very significant decrease in GFP_T cells, due to the overexpression of TfR-1 transgene. This decrease is maintained from P1 to P3.

4.2.2 Cell viability

In order to understand to what extent GFP and/or TfR-1 transgene integration was affecting cell health and proliferative capacity, a viability assay was performed on GFP and GFP_T transduced cells. This was done at two time-points, P1 and P4, having control cells as a reference for comparison. Results are presented in Figure 17.

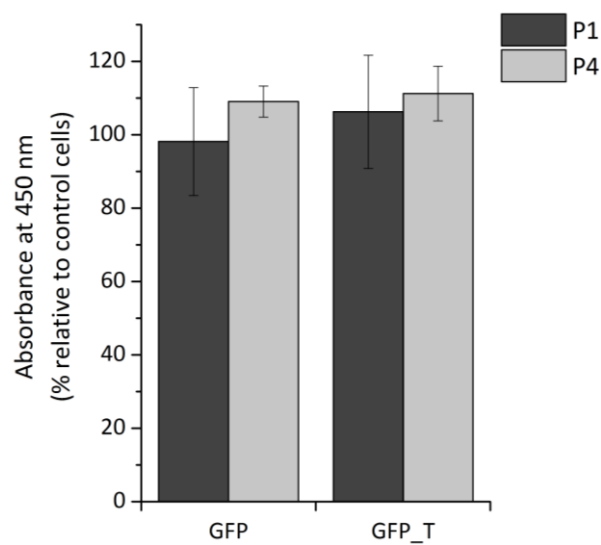


Figure 17 – Viability of GFP and GFP_T transduced CHO K1 cells at P1 and P4 post-transduction. Data points are normalised to Control (untransduced) cells. Error bars represent SEM ($n=3$) (M&M, p.62).

Figure 17 shows that cells transduced with either GFP or GFP_T have a viability/ proliferation capacity in similar levels to control cells, both at P1 (7 days post-transduction) and at P4. This suggests that transgene overexpression is not causing any cellular survival.

4.2.3 Iron homeostasis

To estimate how the cell's iron homeostasis was being affected due to the integration of TfR-1 transgene, GFP and viral TfR-1 (Viral_T) expression were explored. Moreover, the endogenous TfR-1 (CHO_T) mRNA transcripts were also quantified by RT-qPCR and the total TfR-1 (Total_T) expression, comprising both endogenous and viral TfR-1, was quantified at the protein level by WB. To do this, control, GFP and GFP_T cells were exposed to an iron concentration of 0.2 mM, previously determined (Figure 11 – Chapter 3) (+ 1.28 mM holo-transferrin; + 50 μ M L-ascorbic acid – not mentioned from here on), alongside a non-supplemented control (0 mM) for a period of 4 days (Iron supplementation, p.50). Target genes were evaluated at the mRNA level by RT-qPCR (Figure 18 and Figure 19 A, C) and at the protein level by WB (Figure 19 B, D and Supplementary figure 1). For RT-qPCR amplification, the reference genes used were the same as previously described. For WB detection, actin and total protein gels were used as references for data normalization.

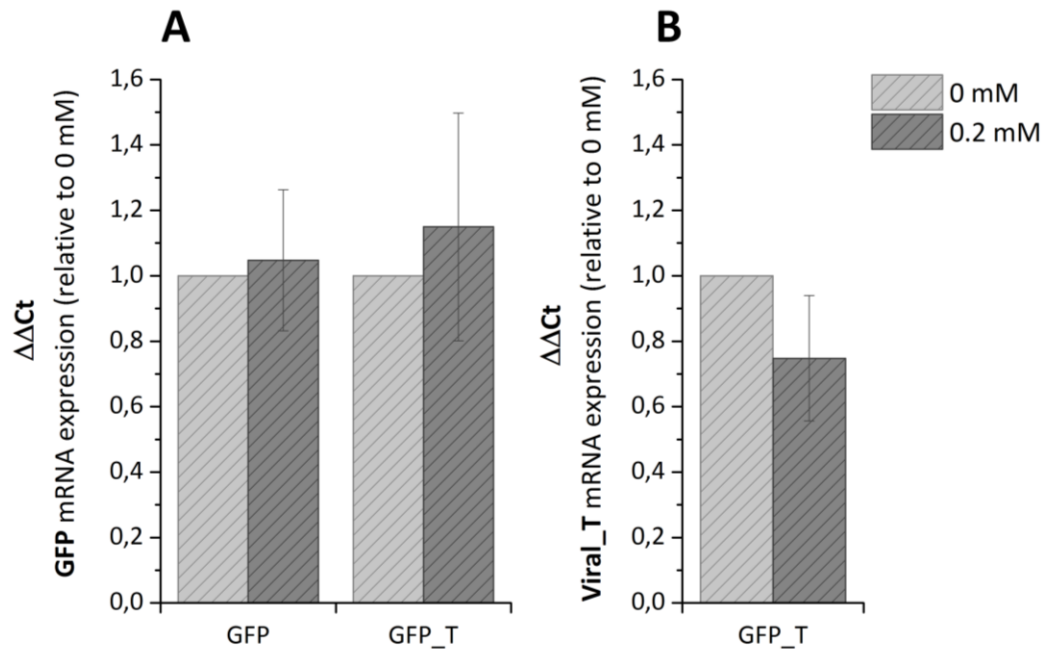


Figure 18 – RT-qPCR relative quantification of transgenes GFP (A) and Viral_T (B) when GFP and GFP_T transduced cells were exposed to 0 and 0.2 mM of iron. Error bars represent SEM ($n=3$) (M&M, p.52).

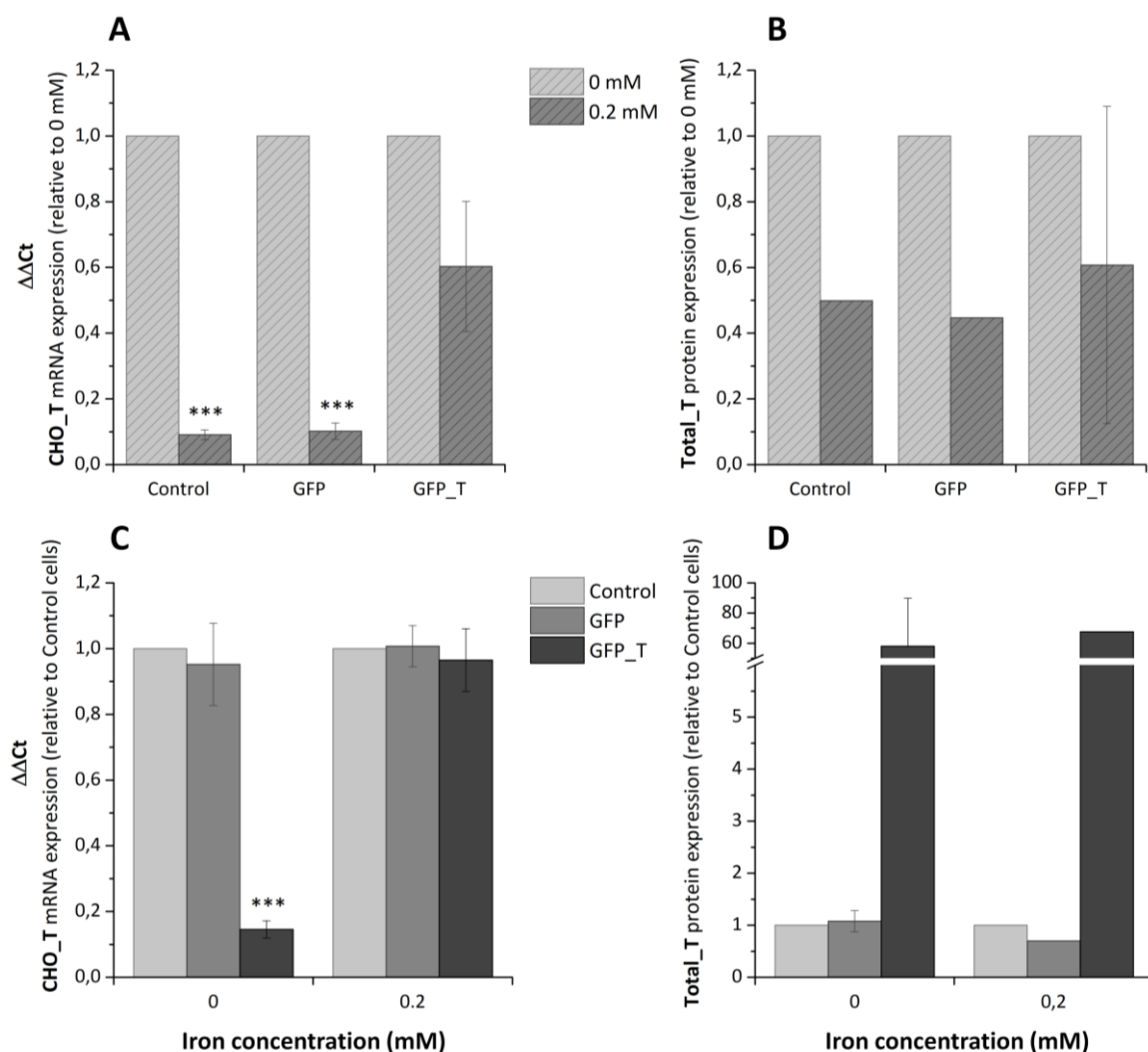


Figure 19 – Relative quantification of endogenous TfR-1 (CHO_T) expression obtained via RT-qPCR (**A** and **C**) and of total (endogenous + viral) TfR-1 (Total_T) protein levels obtained via WB (**B** and **D**), when control, GFP and GFP_T transduced cells were exposed to different iron concentrations of 0 and 0.2 mM (M&M, p.50). Graphs **A** and **B** evaluate target expression levels when each cell line is exposed to different iron concentrations and graphs **C** and **D** the difference between cell lines when exposed to the same iron concentration. Error bars represent SEM ($n=3$) (M&M, p.52 for RT-qPCR and p.57 for WB).

In Figure 18, GFP (graph **A**) and Viral_T (graph **B**) target expression was plotted against a non-supplemented control for each condition (GFP and GFP_T) in order to evaluate transgene expression when iron was present at a concentration of 0.2 mM. The results show that GFP and TfR-1 transgene expression is stable with

0.2 mM of iron, with no significant differences between the two conditions. A further evaluation in TfR-1 levels was performed, in which mRNA transcripts were quantified at the endogenous level (*i.e.*, TfR-1 derived from CHO K1 origin only) (Figure 19, **A** and **C**) and the total expression of TfR-1 (endogenous and viral origin) was quantified at the protein level (Figure 19, **B** and **D**). The results displayed in Figure 19, graph **A**, show that when comparing individual conditions with different iron concentrations, the natural tendency would be that when iron is present in high concentrations, the TfR-1 mRNA transcripts are cleaved by endonucleases (Figure 1– Chapter 1) and thus the mRNA levels are decreased when compared to a non-supplemented control. This is seen for control and GFP cells with a high statistical significance. The same is observed at the protein level (Figure 19, graph **B**) for the same conditions, with the total TfR-1 protein levels being decreased to about half. However, for GFP_T transduced cells there is no significant decrease in endogenous and total TfR-1 levels when iron is present and this may be explained by the results demonstrated in Figure 19, graph **C**. Here, at each supplementation condition (without or with iron), GFP and GFP_T transduced cells are compared to control cells. Interestingly, without iron supplementation, GFP_T cells are the only ones with a very significant decrease of endogenous mRNA TfR-1 levels. At 0.2 mM of iron, the levels in GFP_T cells are very similar to control cells which explain why there is no decrease in graph **A**, because endogenous mRNA levels are already low to begin with. At the protein level, in Figure 19, graph **D**, the scenario is totally opposite, in which the quantification of total TfR-1 shows a 60 to 70-fold

overexpression of this gene in GFP_T cells when compared to controls, both without and with 0.2 mM iron supplementation, respectively. These results clearly show that insertion of GFP_T virus is influencing the overall expression levels of TfR-1.

To further confirm TfR-1 overexpression levels of GFP_T in relation to controls (control, GFP) and to specifically localize the TfR-1 protein within the cell, immunofluorescence was performed. Control, GFP and GFP_T cells with no iron supplementation were immunostained with rabbit anti-TfR-1 primary Ab and then visualized with a red fluorophore linked to an anti-rabbit secondary Ab. DNA was stained with DAPI in order to visualize the nuclear region. The results obtained for GFP_T cells are displayed in Figure 20. Immunofluorescence pictures of other conditions (Control, GFP), as well a negative control to confirm the specificity of the secondary to the primary Ab, are shown in Supplementary figure 2.

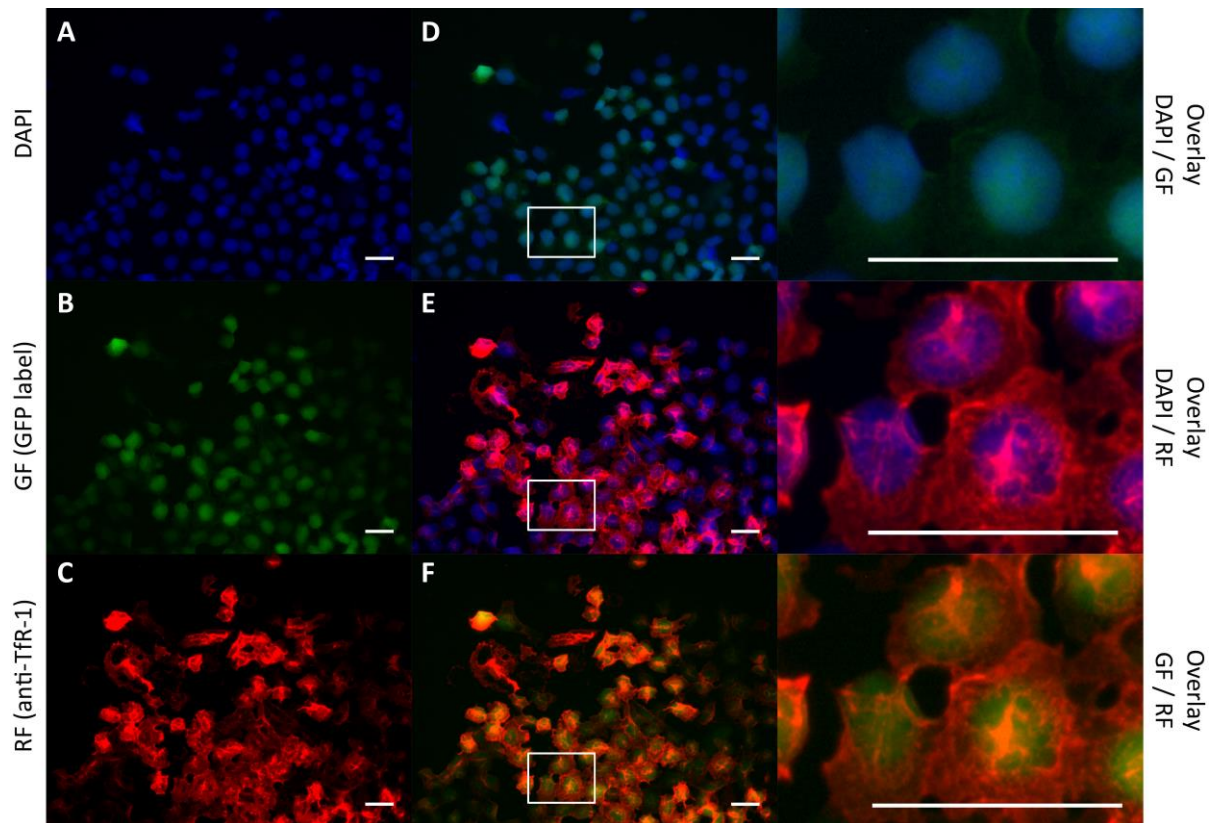


Figure 20 – Representative immunofluorescence pictures of GFP_T transduced CHO K1 cells, showing nuclear staining with DAPI (**A**), green fluorescence (GF) obtained by GFP reporter (**B**) and the detection of TfR-1 proteins, visualized by red fluorescence (RF) (**C**). The overlay between these conditions shows that GFP reporter is mainly expressed in the nucleus (**D**), TfR-1 is present outside the nuclear region, more likely localized at the cellular membrane (**E**) and that there is a mixed population in (**F**), where only the high expressing GFP cells also have an overexpression of TfR-1. A higher magnification of the insets is presented on the right hand side pictures. Scale bars: 25 μ m; (M&M, p.56).

In Figure 20, the precise localization of TfR-1 is not very clear, but it is predicted to be identified at the cellular membrane (**E**), while the GFP expression is only seen in the nuclei (**D**). The overexpression of TfR-1 is identified in **F**, where there is a mixed population of GFP/viral TfR-1 cells. The cells highly expressing GFP also show a high detection of TfR-1, while cells expressing a low GFP present a lower level of detection of TfR-1. All the same, when compared with control and GFP cells in Supplementary figure 2, there is a clear TfR-1 overexpression in GFP_T cells.

Another important complex responsible for keeping iron homeostasis is ferritin, also tightly controlled by the cell through the IRP/IRE regulatory system (Figure 1 – Chapter 1). To evaluate the cell's control over ferritins when transgenes were introduced, ferritin heavy chain-1 expression levels (here named as Total_F) were analysed in the same conditions as previously described at the mRNA (by RT-qPCR, Figure 21, **A** and **C**) and at the protein level (by WB, Figure 21, **C, D** and Supplementary figure 1). Reference genes and proteins used for data normalization of RT-qPCR and WB, respectively, are the same as described above.

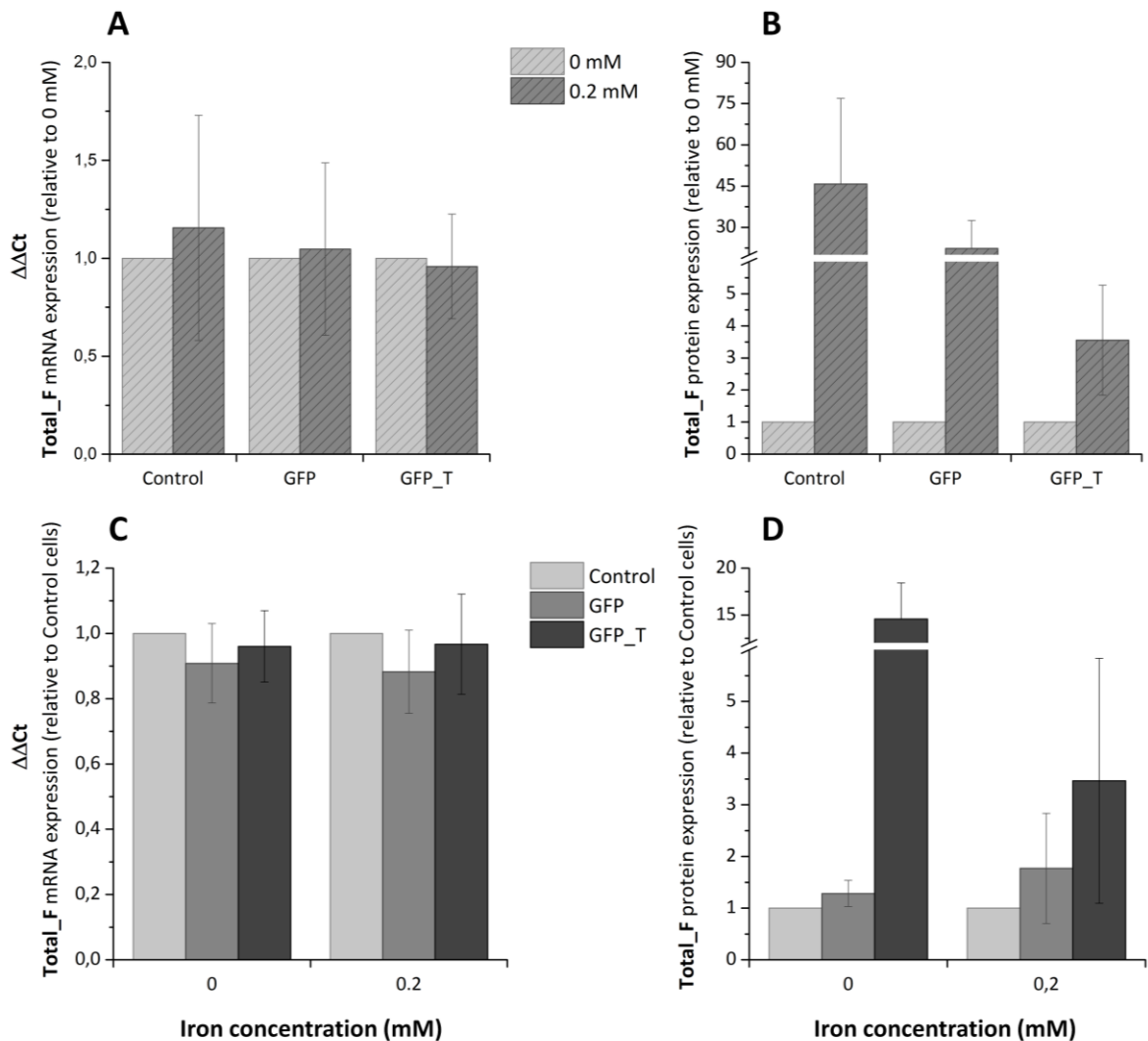


Figure 21 – Relative quantification of Fth-1 (Total_F) expression obtained via RT-qPCR (**A** and **C**) and the respective protein levels obtained via WB (**B** and **D**), when Control, GFP and GFP_T transduced cells were exposed to different iron concentrations of 0 and 0.2 mM. Graphs **A** and **B** evaluate Total_F expression levels when each cell line is exposed to different iron concentrations and graphs **C** and **D** the difference between cell lines when exposed to the same iron concentration. Error bars represent SEM ($n=3$) (M&M, p.52 for RT-qPCR and p.57 for WB).

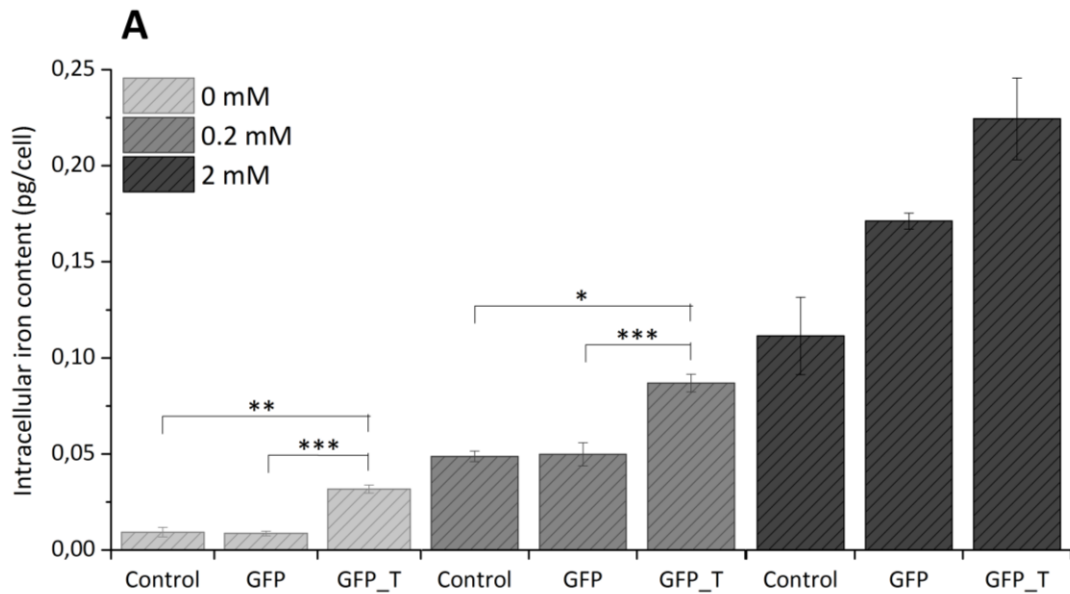
The results displayed in Figure 21 show that at the mRNA level there is not much variation of Fth-1 and the levels are maintained relatively constant either when iron is supplemented for each cell line (comparing to a non-supplemented control) (graph **A**) or when GFP and GFP_T are compared to control cells, at each

supplementation condition (graph **C**). In contrast, at the protein level, Fth-1 protein expression is elevated for each cell line when iron is added (graph **B**). Note that in graph **B**, while control and GFP cells have an up-regulation of 45 and 25-fold respectively in relation to non-supplemented cells, GFP_T cells have only a 3.5-fold increase. Similarly to the down-regulation of TfR-1 mRNA levels, this smaller increase may be explained by the results presented in graph **D**, where Fth-1 protein levels are much higher in GFP_T cells when compared to controls (Control, GFP), at both supplementation conditions. This contrast between mRNA and protein expressions may be explained by the post-transcriptional regulation of Fth-1 (*i.e.*, when iron is present in excess, translation of Fth-1 is promoted).

The results presented above show the effect of integrated GFP and/or TfR-1 transgenes on cellular iron homeostasis, through the analyses of endogenous and viral TfR-1, as well as the endogenous Fth-1. The results obtained suggest that GFP cells are very similar to control cells, while GFP_T cells express high levels of TfR-1, also leading to an endogenous overexpression of Fth-1. Next, the intracellular iron present in each condition was evaluated.

4.2.4 Intracellular Iron Uptake *in vitro*

The capacity of GFP_T to retain more iron than controls (Control, GFP) was explored by measuring the intracellular iron content of Control, GFP and GFP_T transduced CHO K1 cells non-supplemented or supplemented with 0.2 and 2 mM of iron. Results are displayed in Figure 22, where the intracellular amount of iron is shown as a function of iron supplementation.



B

	In relation to Control		In relation to GFP	
	fold	SEM	fold	SEM
0 mM	4,48	0,83	3,77	0,311
0.2 mM	1,80	0,13	1,81	0,14
2 mM	2,18	0,46	1,20	0,06

Figure 22 – Intracellular iron content of CHO K1 cells determined with the Ferrozine assay (A). Control, GFP and GFP_T transduced cells were supplemented with different iron concentrations of 0, 0.2 and 2 mM for 4 days prior to measurement (Iron supplementation, p.50). Fold-differences between GFP_T cells and Control or GFP are presented for each supplementation condition in B. Error bars represent SEM ($n=3$) (M&M, p.50).

Figure 22 (A) shows an increased capacity of GFP_T cells to retain intracellular iron when compared to controls. This capacity is statistically significant for 0 and 0.2 mM of iron supplementation conditions. With 2 mM of iron an increase is also observed, although it is not statistically significant. The fold-differences presented in table B (Figure 22) show that GFP_T cells have a higher difference to controls when iron is not supplemented, *i.e.*, relying only in the iron/ transferrin available in cell culture medium (Iron supplementation, p.50), with around 4-fold increase. These results suggest that TfR-1 might be a promising

reporter gene for MRI, as it increases intracellular iron accumulation when compared to controls.

4.2.5 MRI

To study the potential of TfR-1 transgene as an MRI reporter, cell pellets of control, GFP and GFP_T were scanned using T2-weighted sequences. To do this, 10^7 cells were centrifuged at high speed to form a compact cell pellet and imaged via MR, where T1/T2 maps were produced for relaxivity studies. Results are displayed in Figure 23.

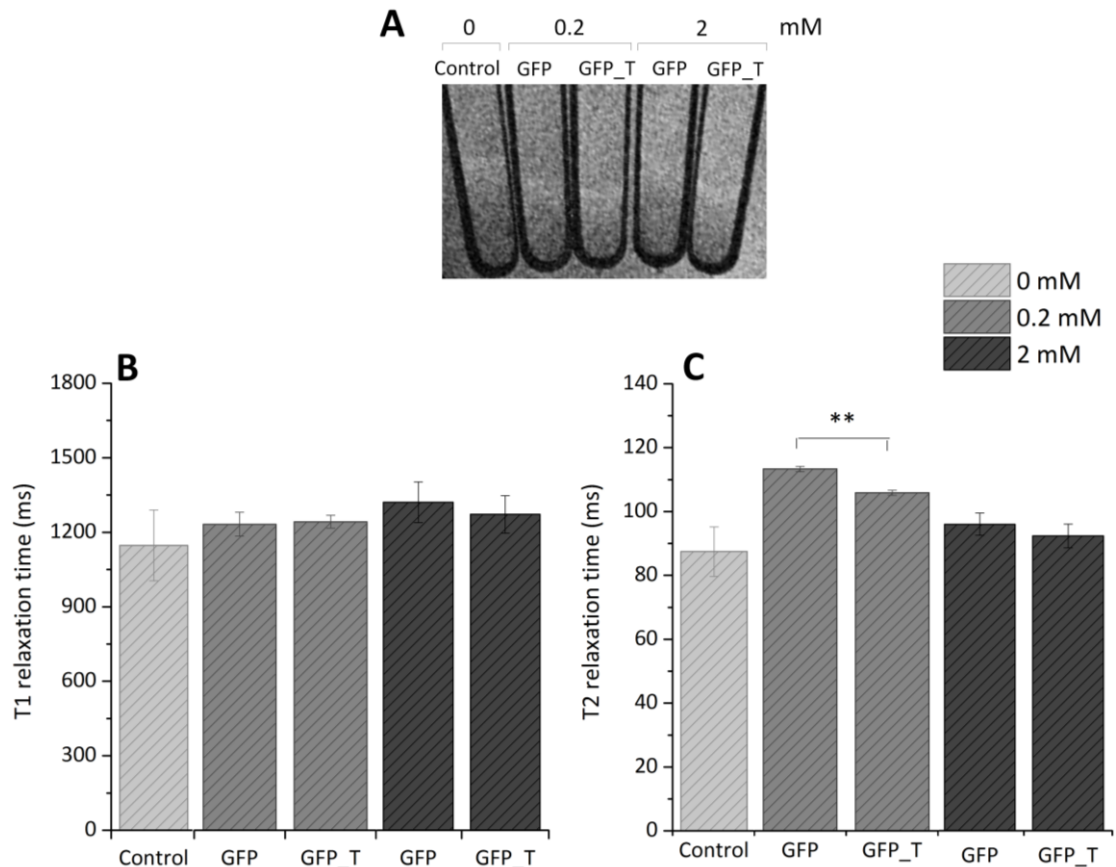


Figure 23 – MR imaging of cell pellets of CHO K1 cells. **A** is a T2-weighted representative MR image obtained with the MRI of control with no iron supplementation (0 mM), GFP and GFP_T both supplemented with 0.2 and 2 mM of iron (Iron supplementation, p.50). Relaxation times T1 and T2 were quantified on a specific region of the cell pellet and are represented in **B** and **C**, respectively. Error bars represent SEM ($n=3$) (M&M, p.65).

Figure 23 shows that at 0.2 mM condition, GFP_T cells when compared to GFP control were able to produce a statistically very significant ($p=0,002$) T2 shortening effect, presented in graph **C**. Nevertheless, this difference may not be sufficient to detect an MRI contrast once cells are introduced *in vivo*. Again, at 2 mM condition, even though it is not statistically significant, a small T2 shortening effect is still observed. Also, in graph **C**, 0 mM control condition appears not to be correct, since the signal loss is even more intense than for the other conditions supplemented with iron. None of these differences are perceptible in MR image **A**,

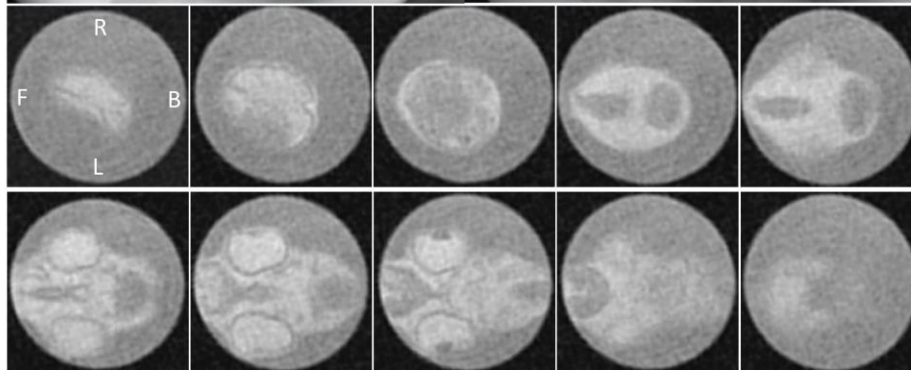
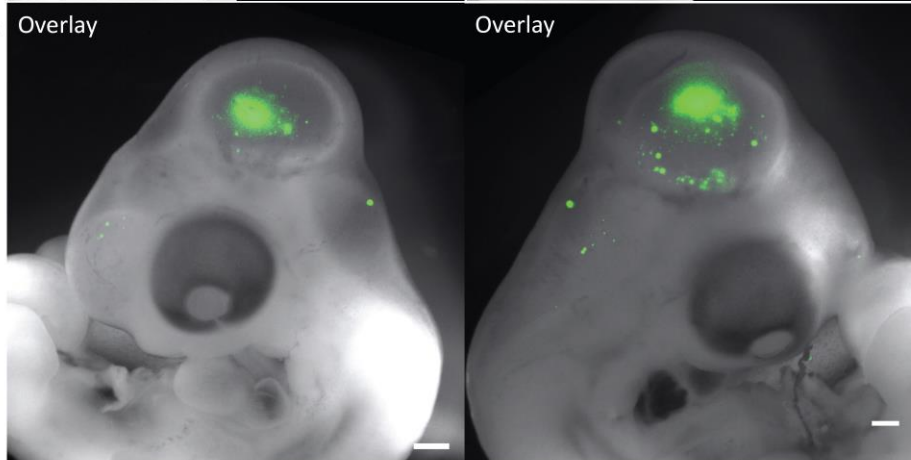
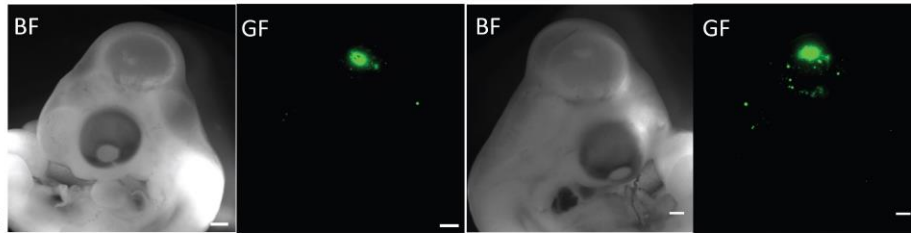
where the signal intensity obtained is very much alike in all conditions.

Then, GFP and GFP_T cells were injected into the brain of chick embryos *in ovo*, the model organism used in this work. 2×10^5 cells were microinjected into the midbrain of the chick embryo at embryonic day 3 (E3). Both cell types were either incubated in normal cell culture conditions (0 mM) or supplemented with 0.2 or 2 mM of iron for 3 days prior to injection. At E5, embryos were imaged with two complementary platforms: by fluorescence microscopy to detect green fluorescence derived from the GFP gene, and by MRI, by observing hypointense regions derived from iron retained in transduced cells, which was influenced by extracellular iron supplementation and/or due to TfR-1 overexpression (Figure 24).

A) CHO K1 - GFP (0 mM iron supplementation)

Left View

Right View



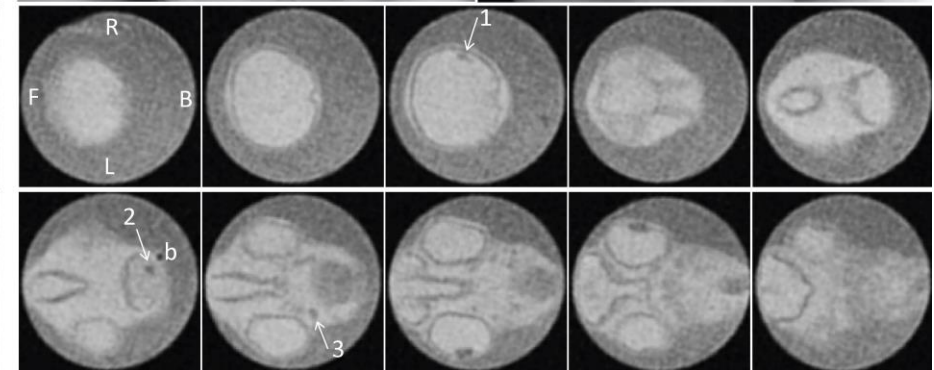
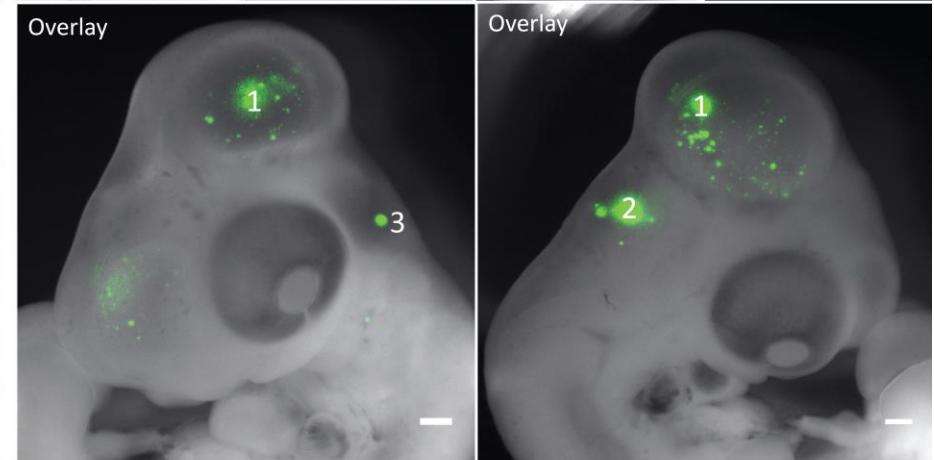
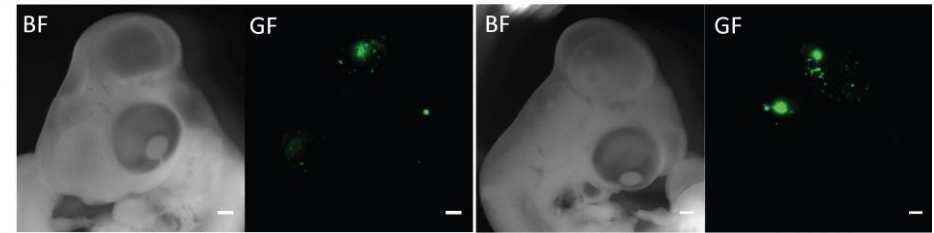
Fluorescence Imaging

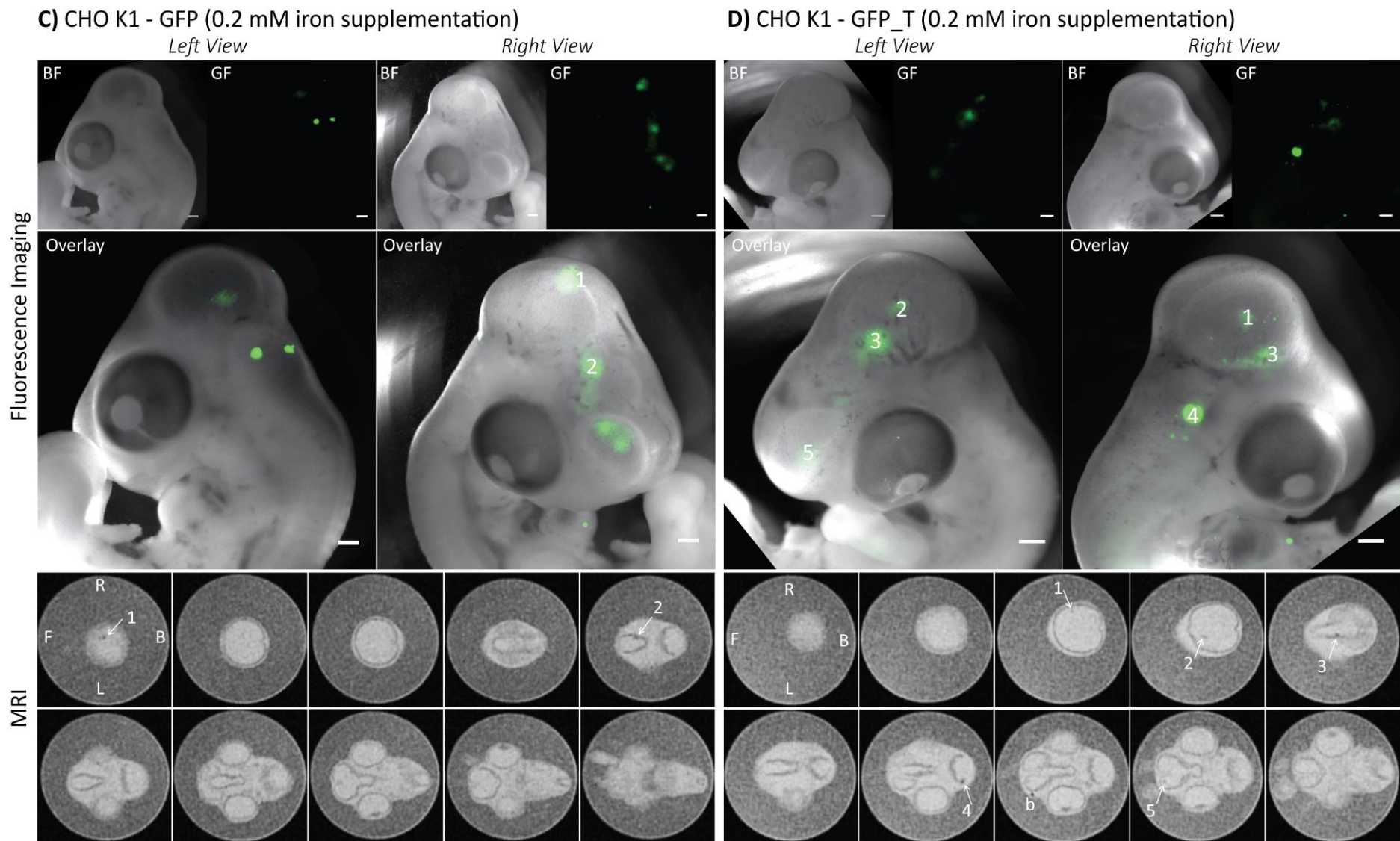
MRI

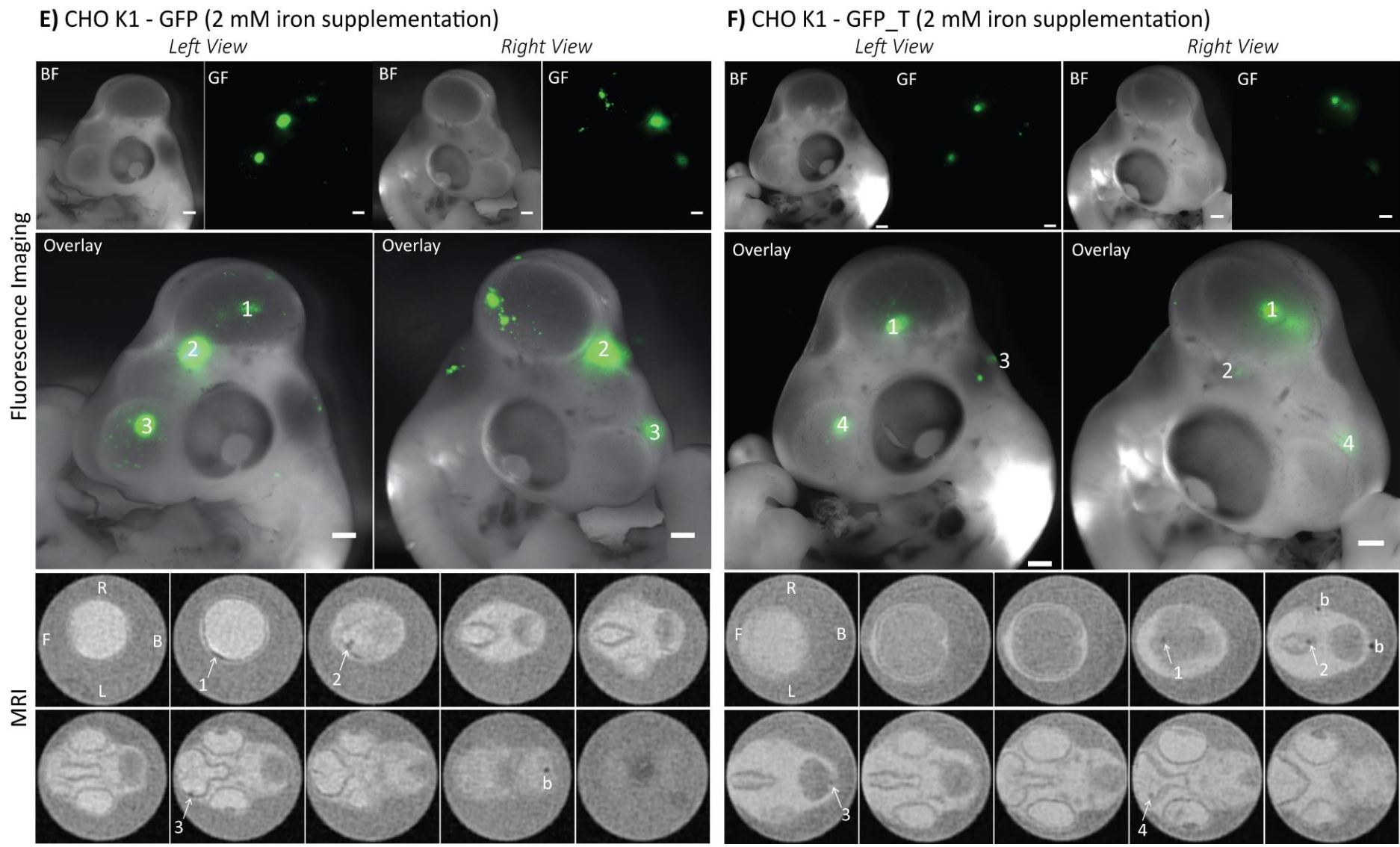
B) CHO K1 - GFP_T (0 mM iron supplementation)

Left View

Right View







Fluorescence Imaging			MRI		
Iron conc.	Transduction condition	Biological rep. (technical rep.)	Iron conc.	Transduction condition	Biological rep. (technical rep.)
0 mM	GFP	n=1 (1)	0 mM	GFP	n=1 (1)
	GFP_T	n=2 (5)		GFP_T	n=1 (2)
0.2 mM	GFP	n=1 (3)	0.2 mM	GFP	n=1 (1)
	GFP_T	n=1 (2)		GFP_T	n=1 (1)
2 mM	GFP	n=2 (2)	2 mM	GFP	n=2 (2)
	GFP_T	n=2 (3)		GFP_T	n=2 (3)

Figure 24 – Fluorescence and MR imaging of GFP (**A**, **C** and **E**) and GFP_T (**B**, **D** and **F**) transduced CHO K1 cells, 2 days after injection in the midbrain of a chick embryo (E5). Cells were injected after culture with or without iron supplementation (0, 0.2 and 2 mM of iron for 3 days) (Iron supplementation, p.50). In the fluorescence imaging panel, bright field (BF) and green fluorescence (GF) are projection images from the whole embryo; overlays are presented for both left and right views and were used as a reference guidance for MR imaging; scale bars correspond to 1 mm. In the MRI panel, anatomical images are displayed as transverse sections along the rostrocaudal axis of the embryo (left to right); 10 sections are displayed for each embryo. All images are representative from the results obtained and were equally processed with ImageJ software. Arrows indicate T2 shortening effect; b – bubble of air. Position of the embryo: F – front; B – back; R – right; L – left; number of biological and technical replicates is indicated in the table above (M&M, p.65).

In some areas in Figure 24, tiny bubbles of air (designated as “b”) got trapped in the agarose during sample preparation, resulting in areas with no signal in close proximity to the embryo, and are indicated in the images. To identify if transduced cells integrated into chick embryo’s brain, first, bright field and fluorescence imaging were performed on whole embryos. Due to the presence of fluorescent reporters, transduced cell clusters were easily identified and located within the brain. This served as a guideline to identify hypointense cell clusters with MR imaging. Without this support, identifying cell clusters based only on anatomical images would have proven to be much more difficult.

In Figure 24, when iron supplementation was not provided (panels **A** and **B**),

it was only possible to detect hypointense regions in GFP_T cells, corresponding to the location of fluorescent cells in embryos. On the other hand, no hypointense region was found when embryos were injected with GFP control, even though green fluorescent cell clusters are observed. A similar situation is detected for 0.2 mM condition (panels **C** and **D**), in which only two clusters of cells are identified in GFP control, even though there are many others imaged with fluorescence microscopy. On the other hand, all GFP_T cell clusters first identified with green fluorescence, were able to be correlated and identified using MR imaging. Surprisingly, when iron was supplemented at 2 mM (panels **E** and **F**), the most concentrated condition of the three, hypointense regions were found for both GFP and GFP_T cells, but the contrast was not noticeably stronger when compared to GFP_T with low iron concentrations (**B** and **D**). Also, no obvious difference is found between GFP and GFP_T hypointense regions. Overall, these results suggest that when using such a high iron supplementation, as 2 mM, there might be an overload of iron present in the cell, disguising the influence of TfR-1 overexpression. Therefore, in order to use TfR-1 as a valuable reporter gene, *in vitro* iron supplementation prior to injection may not even be necessary to visualize GFP_T cells under MRI.

4.3 DISCUSSION

Over the past two decades, TfR-1 has been investigated as an MRI reporter, mostly for targeted cancer therapies, using nanoparticles to encapsulate chemotherapeutical agents and TfR-1 as a drug delivery system (Moore *et al.*, 1998; Qian *et al.*, 2002). Only once the use of TfR-1 as an MRI reporter was focused on stem cell tracking and it was performed in conjunction with Fth-1 overexpression, in a mouse neural stem cell line (Deans *et al.*, 2006). In this chapter, the sole overexpression of mouse TfR-1 was used to increase intracellular iron content in CHO K1, a model cell line chosen to evaluate TfR-1 as a potential reporter gene for MRI tracking of cells.

In Chapter 3, TfR-1 cDNA was cloned into a pHIV-eGFP lentiviral vector. Because this cDNA was originally obtained from mouse cells, viral and endogenous TfR-1 transcripts were possible to be individually detected in the current study. Also, a primer pair to detect simultaneously viral and endogenous TfR-1 mRNA transcripts was attempted; however, even though the predicted homology between the two cDNAs is 88%, it was not possible to find a common region. Nevertheless, at the protein level, the antibody chosen to target TfR-1 was able to detect simultaneously the endogenous and viral TfR-1 proteins, allowing for a quantification of the total TfR-1 (or Total_T).

GFP/ Viral_T transgene integration was evaluated in CHO K1 cells initially over several passages (P3 to P8) (Figure 14, Figure 15 and Figure 16) and then when

supplemented with two concentrations of iron (0 and 0.2 mM) (Figure 18). It was found that transduction was very effective with nearly 100% of cells GFP-positive and stable irrespective of iron supplementation. However, in Figure 16, a small decrease in GFP expression was found when analysing GFP and GFP_T cells over the course of the study (P1 to P3), which was not seen for Viral_T expression in GFP_T cells. This might be explained by the fact that, within the transfer lentiviral vector, GFP transgene is located downstream of the internal ribosome entry site (IRES), which also flanks upstream the reporter gene of interest, in this case TfR-1. Therefore, the promoter EF1- α is about 3 kb upstream from GFP transgene, possibly not permitting efficient transcription in this region. Also in Figure 16, a significant decrease in the endogenous expression of TfR-1 (CHO_T) is observed in GFP_T cells, both at P1 and P3, when compared to control and GFP cells. The same is seen likewise in Figure 19 (graph **A** and **C**), where the endogenous TfR-1 mRNA levels are decreased in GFP_T cells, when compared to controls, both with and without iron supplementation. This decrease might be due to the presence of iron responsive elements (IREs) present in 3'UTR of the endogenous TfR-1, allowing the cell to have a post-transcriptional control over the mRNA cleavage, and therefore decreasing TfR-1 mRNA transcripts available. Nevertheless, as viral TfR-1 transgene was deprived of IREs from the untranslated region, as described in Chapter 3, this allowed for a constitutive expression without the cell's control (Figure 19, **D** and Figure 20). Supplementary figure 2 also demonstrates that the integration of mouse TfR-1 transgene (GFP_T) leads to an overexpression of this gene, while controls

(Control and GFP) remain with basal levels.

As opposed to TfR-1, where there is an endonucleolytic cleavage for mRNA stability control, and thus mRNA transcripts may be decreased or increased depending on iron availability, the way the IRP/IRE system regulates ferritins is to either allow or block the translation process. Therefore, whether iron is present or not, the total amount of Fth-1 mRNA transcripts may be relatively constant, as seen in Figure 21 (graphs **A** and **C**). However, at the protein level is where the cell's control over ferritins is quite distinctive. When total protein Fth-1 levels are compared between the different conditions, at a defined iron concentration (Figure 21, graph **D**), an up-regulation of 15 and 3.5-fold is observed for GFP_T cells, when supplemented with 0 and 0.2 mM of iron, respectively. A similar up-regulation was described by Deans *et al.* (2006), where protein levels of human FTH-1 were increased 2.5-fold in TFR-1/FTH-1 transfected cells when supplemented with iron, compared to control cells. However, their supplementation conditions were far greater, with 1 mg/ml of holo-transferrin and 1 mM of ferric citrate, ten and five times more than used here. They also mention that when cells were not supplemented, FTH-1 protein levels were decreased in TFR-1/FTH-1 transfected cells. On the contrary, our results indicate that at low iron concentrations, such as 0 mM (relying only in the iron/transferrin present in cell medium and FCS) (please see Iron supplementation on p.50), Fth-1 protein levels are increased. This difference might be due to the fact that in this study, only TfR-1 was overexpressed, while in Deans *et al.* (2006), both TFR-1 and FTH-1 were overexpressed in

conjunction. It is very likely that due to the presence of high levels of TfR-1, GFP_T cells have an increased Fth-1 protein expression both with and without iron supplementation, which may indirectly result in an increase in ferritin light chain expression, leading to an increase in the number of ferritin heteropolymers available within the cell. Immunofluorescence was also employed in detecting Fth-1 proteins, but no differences were found between GFP_T and control conditions (data not shown). Overall, these results suggest that, in GFP_T transduced cells, the iron available may be entering the cells through the accessible overexpressed TfR-1 and then clustering in ferritin cages, as a consequence of the normal iron homeostasis regulation process.

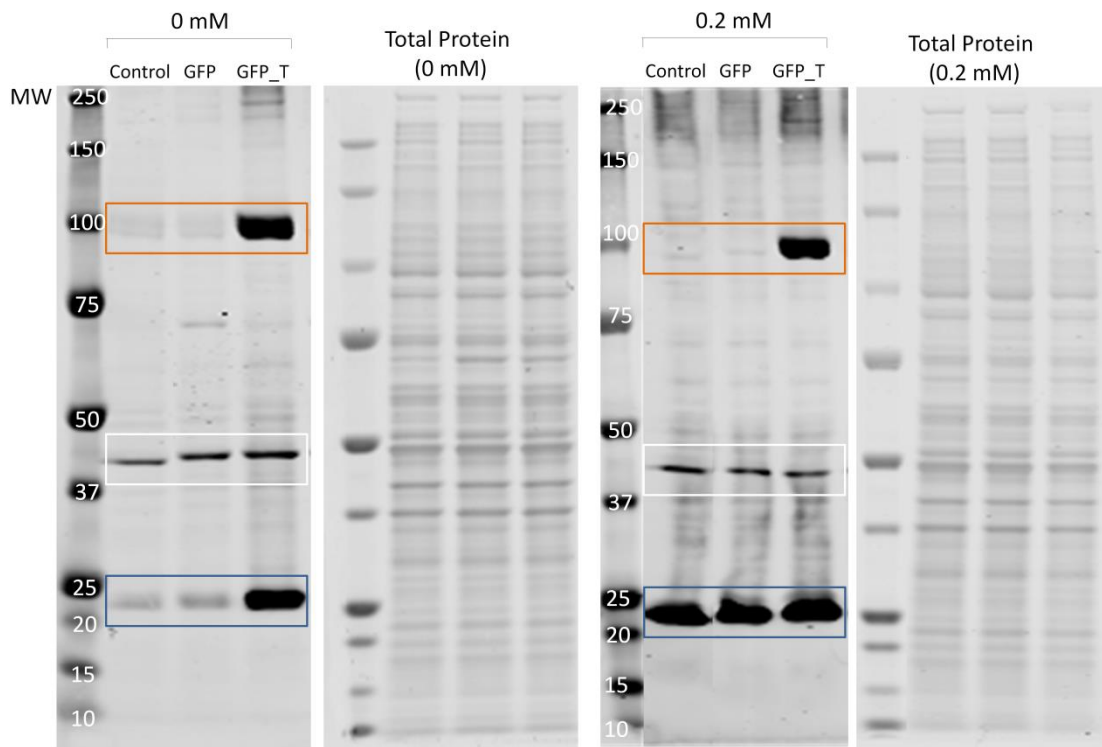
Next, intracellular iron was measured and it was found that GFP_T cells have a higher capacity to retain iron than controls (Control and GFP cells), with statistical significance for two concentrations tested (0 and 0.2 mM) (Figure 22). Also, when cell pellets were evaluated with MR imaging at 0.2 mM of iron a significant T2 shortening effect was observed for GFP_T cells (Figure 23). The results suggest that because both TfR-1 and Fth-1 levels were up-regulated in GFP_T cells when compared to controls, intracellular iron content was also reasonably increased. This reinforces the hypothesis that ferritins might be clustering iron inside the cell and in a non-toxic way (Figure 17).

To complement this study, GFP and GFP_T cells injected in chick embryos were imaged with fluorescence microscopy and MRI. Interestingly, only when cells were either not supplemented or supplemented with 0.2 mM of iron prior to

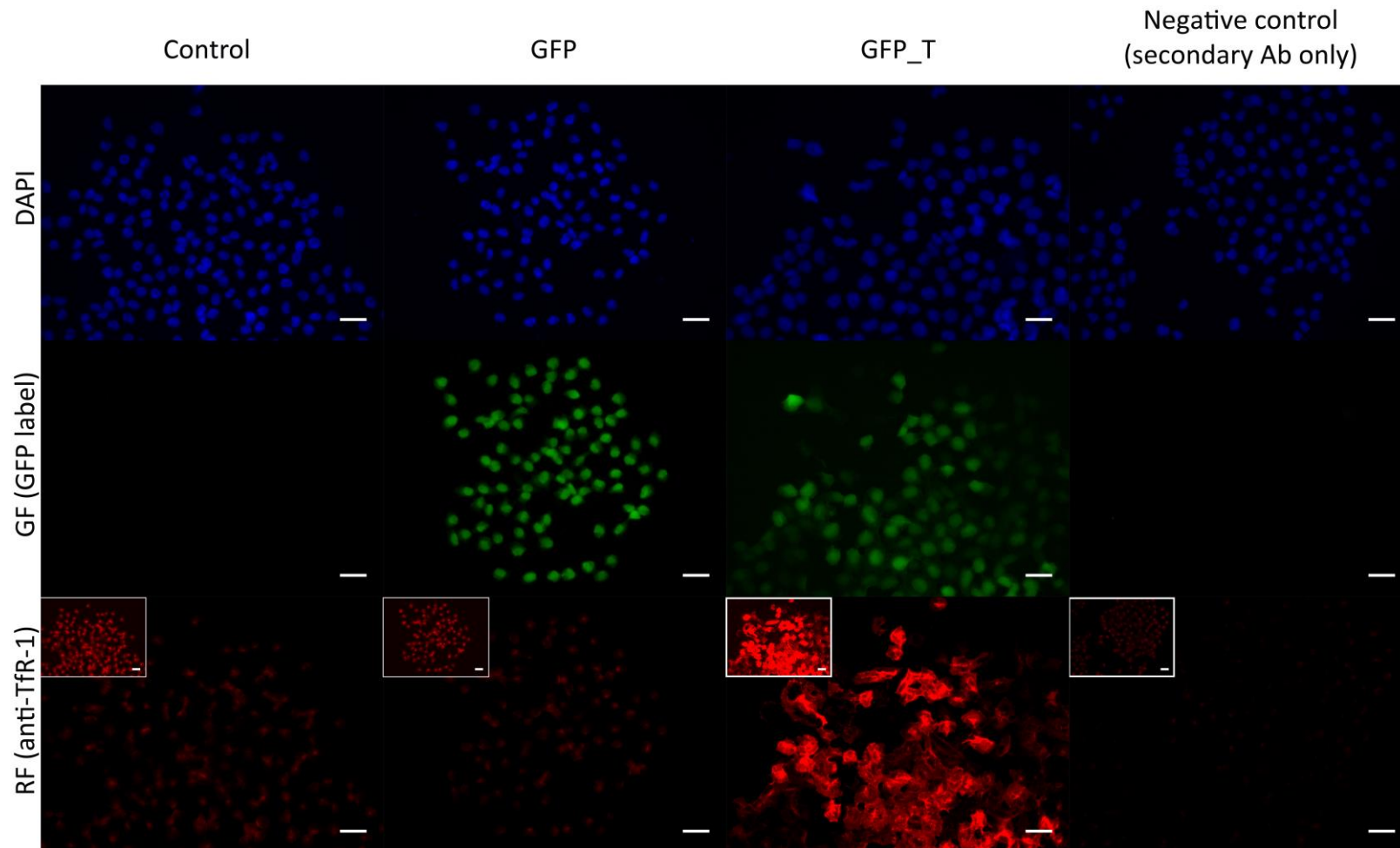
injection that a distinguishable contrast was observed for GFP_T cells, but not for GFP control (Figure 24, **A-B** and **C-D**). This is comparable with the previous results of iron retention capacity, obtained with the intracellular iron measurement and MRI imaging of cell pellets. Such a difference was not so evident when cells were supplemented with 2 mM (Figure 24, **E** and **F**), suggesting that at this concentration there might be an excess of iron present and TfR-1 overexpression in GFP_T cells is no longer noticeable. Also, the use of TfR-1 as a reporter gene for cell tracking might not even need iron supplementation prior to cell injection. This would prove to be a very useful feature in a reporter gene, as long-term studies would be possible without adding any iron-related supplementation.

In summary, TfR-1 gene was overexpressed in a model cell line, CHO K1, and analysed for its potential as an MRI reporter. The targeted overexpression was first found to up-regulate the overall TfR-1 levels in cells, without interfering with their viability and allowing iron to enter the cell in a constitutive manner. The results indicate that iron homeostasis was affected by TfR-1 overexpression and was able to adjust by inducing an increase in the ferritins available. This resulted in higher intracellular iron retention of TfR-1 transduced cells relative to controls, in particular with low levels of iron (0 and 0.2 mM), thus facilitating detection with MRI. Therefore, TfR-1 gene overexpression in mammalian cells can be a useful tool to track cells with MRI technology.

4.4 SUPPLEMENTARY DATA



Supplementary figure 1 – Representative western blots and correspondent total protein gels from control, GFP and transferrin receptor-1 (GFP_T) transduced CHO K1 cells, supplemented for 4 days with 0 or 0.2 mM of iron. Orange rectangle highlights total Tfr-1 (endogenous + viral, here described as Total_T) protein expression, with a predicted molecular weight (MW) of 100 kDa; white rectangle corresponds to actin expression with 42 kDa and blue rectangle to Fth-1 (or Total_F) with 21 kDa. Protein quantification was normalized using total protein gels and confirmed using actin as a reference protein (M&M, p.57).



Supplementary figure 2 – Representative immunofluorescence pictures of Control, GFP and GFP_T transduced CHO K1 cells, showing nuclear staining with DAPI, green fluorescence (GF) originating from the GFP reporter and the detection of TfR-1 proteins, visualized with a red fluorescent antibody (RF). A clear protein overexpression of TfR-1 is found in GFP_T. All pictures sets were taken with the same exposure conditions. RF pictures with a longer exposure time are shown in the insets. A negative control targeting only the secondary Ab is included to confirm the specificity to the primary Ab. Scale bars: 25 μm ; (M&M, p.56).

CHAPTER 5

FERRITIN HEAVY CHAIN-1 AND TRANSFERRIN RECEPTOR-1 AS REPORTER

GENES FOR MRI TRACKING OF CELLS

5.1 INTRODUCTION

TfR-1 is transmembrane glycoprotein responsible for internalizing iron-bound transferrin which is then released and stored in a non-toxic form inside metalloprotein complexes, called ferritins. This is only possible due to the ferroxidase activity present in the heavy subunit of ferritin (Fth-1), which not only incorporates but also transforms cytoplasmic ferrous iron into a safe ferric iron configuration. Both TfR-1 and Fth-1 are known to have a significant role in iron metabolism and thus, have been targeted as a means to increase intracellular iron concentration of specific cell types. This would prove useful in particular for MRI tracking studies, using iron as a natural contrast agent.

5.1.1 Studies targeting ferritin heavy chain-1

The first evidence of using ferritin heavy chain-1 gene as an overexpression system was reported by Picard *et al.* (1996), in which a mouse erythroleukemia cell line was stably transfected with Fth-1. The transgene included two point mutations in the IRE site, and showed a decrease of 20 to 30% of heme in haemoglobin production in cells overexpressing Fth-1, indicating iron starvation as a consequence of iron accumulation within ferritins. They also demonstrated that the labile iron

pool (LIP) was significantly reduced in these cells and they were more resistant to H₂O₂ oxidative damage (Picard *et al.*, 1998; Picard *et al.*, 1996).

Next, a study published by Cozzi *et al.* (2000), confirmed the massive reduction in the LIP in cells overexpressing human wild-type FTH-1, even though the iron uptake by transferrin receptor-1 was increased. It was demonstrated that FTH-1 overexpression increased the resistance to formation of reactive oxygen species. Furthermore, they generated a human FTH-1 mutant with an inactivated ferroxidase centre, which when overexpressed in cells did not obtain the same results as wild-type FTH-1, thus providing evidence for the importance of ferroxidase activity in iron incorporation. This paper describes an important observation on culturing cells with FTH-1 overexpression, namely that cell proliferation appears to be slower than in normal cells. They also state that this could be simply overcome by long-term iron supplementation (Cozzi *et al.*, 2000).

5.1.2 Ferritin heavy chain-1 gene as an MRI reporter gene

Although Fth-1 overexpression was shown to allow an increase of intracellular iron above background levels (Cozzi *et al.*, 2000; Picard *et al.*, 1996), it was only in 2005 that two different research groups investigated if ferritin complex could be a potential reporter for MR imaging (Cohen *et al.*, 2005; Genove *et al.*, 2005). Genove *et al.* (2005) engineered both human heavy and light ferritin subunits, removing IRE regulatory regions to allow free overexpression of both proteins without interference of the IRP/IRE regulatory system. This way, they obtained the necessary contrast needed for MRI without introducing any exogenous

contrast agents. Then, ferritin-overexpressing cells were inoculated into a mouse brain and monitored *in vivo* for 5 weeks. The results obtained with MRI were also validated with histological staining (Genove *et al.*, 2005). The other study was from Cohen *et al.* (2005), who overexpressed solely the mouse Fth-1 in rat glioma cells, again with the IREs removed, and under the control of a tetracycline promoter. After inoculation of ferritin-expressing cells in the hind limb of mice, tumours formed and were left to grow up to 6 mm. Just like in the previous study, Fth-1 alone allowed sufficient contrast for MRI detection and their findings could be correlated with histology (Cohen *et al.*, 2005).

Over the following years, a few more studies described the use of Fth-1, often associated with fluorescent proteins, as a novel reporter gene for use in MRI. Many cell types were used: several types of cancer cells (Aung *et al.*, 2009; Feng *et al.*, 2012; Iordanova *et al.*, 2010; Kim and Eberwine, 2010; Ono *et al.*, 2009), a mouse embryonic stem cell (ESC) line (Liu *et al.*, 2009), cardiac cell lines (Campan *et al.*, 2011; Naumova *et al.*, 2010) and neural stem/ progenitor cells (Vande Velde *et al.*, 2012). To introduce human/mouse Ferritin heavy chain-1 gene into the cell, different methods were used such as virus transduction (Genove *et al.*, 2005, Vande Velde *et al.*, 2011), transfection (Aung *et al.*, 2009) or electroporation (Deans *et al.*, 2006). Parameters like proliferation, viability, cytotoxicity and differentiation potentials were assessed by most studies and overall, no differences in relation to control cells were observed. In fact, in one case, it was reported that Fth-1 overexpression induced a decrease in iron toxicity when compared to control cells,

suggesting an antioxidant protective role against iron toxicity (Genove *et al.*, 2005). Also, the intracellular iron retention of transgenic cells in relation to controls was very often studied before transplantation into an animal model. In most cases, iron was supplemented *in vitro* in the form of ferric citrate or nitrate, with concentrations ranging from 0.2 to 1 mM, with additional 1-2 mg/mL of human holo-transferrin, for periods between 1-4 days (Deans *et al.*, 2006; Genove *et al.*, 2005; Iordanova *et al.*, 2010; Kim and Eberwine, 2010; Naumova *et al.*, 2010).

More recently, researchers have developed engineered ferritins in order to increase the contrast obtained with MRI, for example, a chimeric ferritin, comprising of a unique polypeptide with heavy and light chain subunits (L*H) fused together. This chimeric fused ferritin was found to have a significantly higher iron incorporating capacity than wild-type and even Fth-1 overexpressing cells and consequently, a higher relaxation rate when imaged with T2-weighted MRI (Iordanova *et al.*, 2010). The same authors went a step further and reported an even greater iron accumulating ferritin, by modifying a specific site in the mitochondrial ferritin (MtF) allowing it to localize into the cytoplasm instead of the mitochondria (Iordanova *et al.*, 2013). MtF is known to have a ferroxidase centre and an iron binding capacity similar to the native heavy-chain of ferritin. This was found by Corsi *et al.* (2002), when the transfection of HeLa cells with MtF lead to a higher iron uptake, specifically located in the mitochondria, as it was reported that transferrin receptors-1 were up-regulated, allowing the iron to enter the cell and, at the same point, the cytoplasmic ferritins were reduced (Corsi *et al.*, 2002).

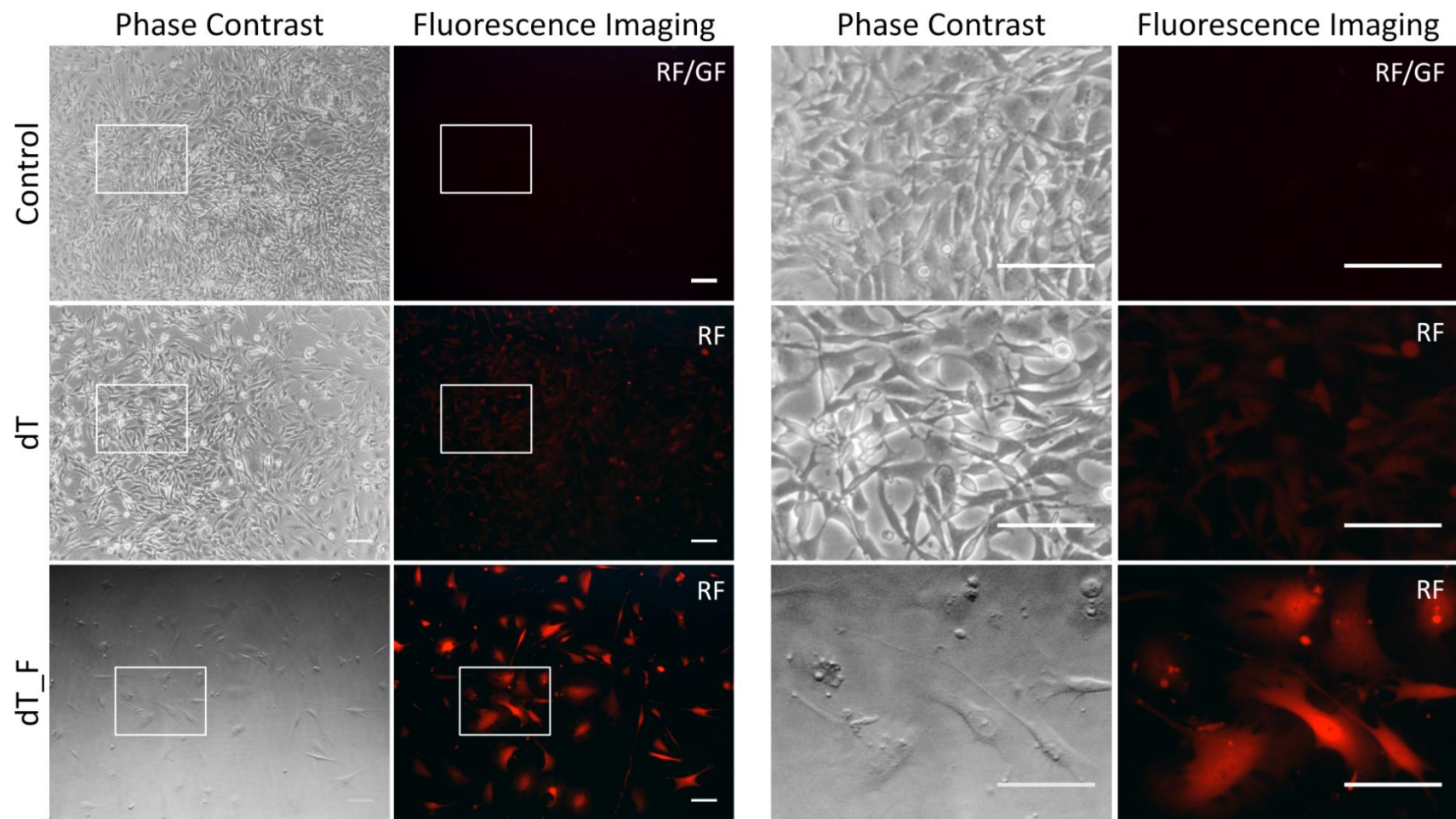
Even though Fth-1 seems to be a very promising MRI reporter gene for long-term *in vivo* investigations, more studies are needed in order to explore the full potential of this gene and in particular, to validate its efficacy with cell lines that are relevant for regenerative therapies. Here, mouse Fth-1 and TfR-1 are explored as potential reporters for MRI tracking studies, both individually and in conjunction, in a mouse mesenchymal stem cell line.

5.2 RESULTS

As described in Chapter 3, Fth-1 was cloned in a dTomato lentiviral plasmid (dT_F), allowing for red fluorescence when transduced into cells. On the other hand, TfR-1 was cloned together with a GFP reporter (GFP_T), thus producing green fluorescence upon transduction. In the current chapter, mMSC were transduced with individual lentiviral particles, encoding for either dT or GFP, to serve as controls, and dT_F or GFP_T, to evaluate the potential of Fth-1 and TfR-1, respectively, as magnetic reporters. Also, a mMSC line in which dT_F and GFP_T lentiviral particles were transduced in conjunction was created and is designated as dT_F+GFP_T. These cells were transduced with MOI=50, including dT_F+GFP_T with MOIs=50+50, and were subjected to FACS sorting at P6 after transduction to obtain highly expressing dT or GFP-positive populations. Three independent transductions and FACS sorting were carried out for each condition and represent, therefore, three biological replicates ($n=3$).

5.2.1 Reporter gene integration in normal cell culture conditions

Transgene expression, in the form of red or green fluorescence, due to the presence of dTomato or GFP reporter, respectively, was initially monitored using fluorescence microscopy. Figure 25 displays phase contrast and fluorescence microscopy images taken 7 days after transduction (here designated as P1 post-transduction), in which cells were grown in standard (without iron supplementation) cell culture medium.



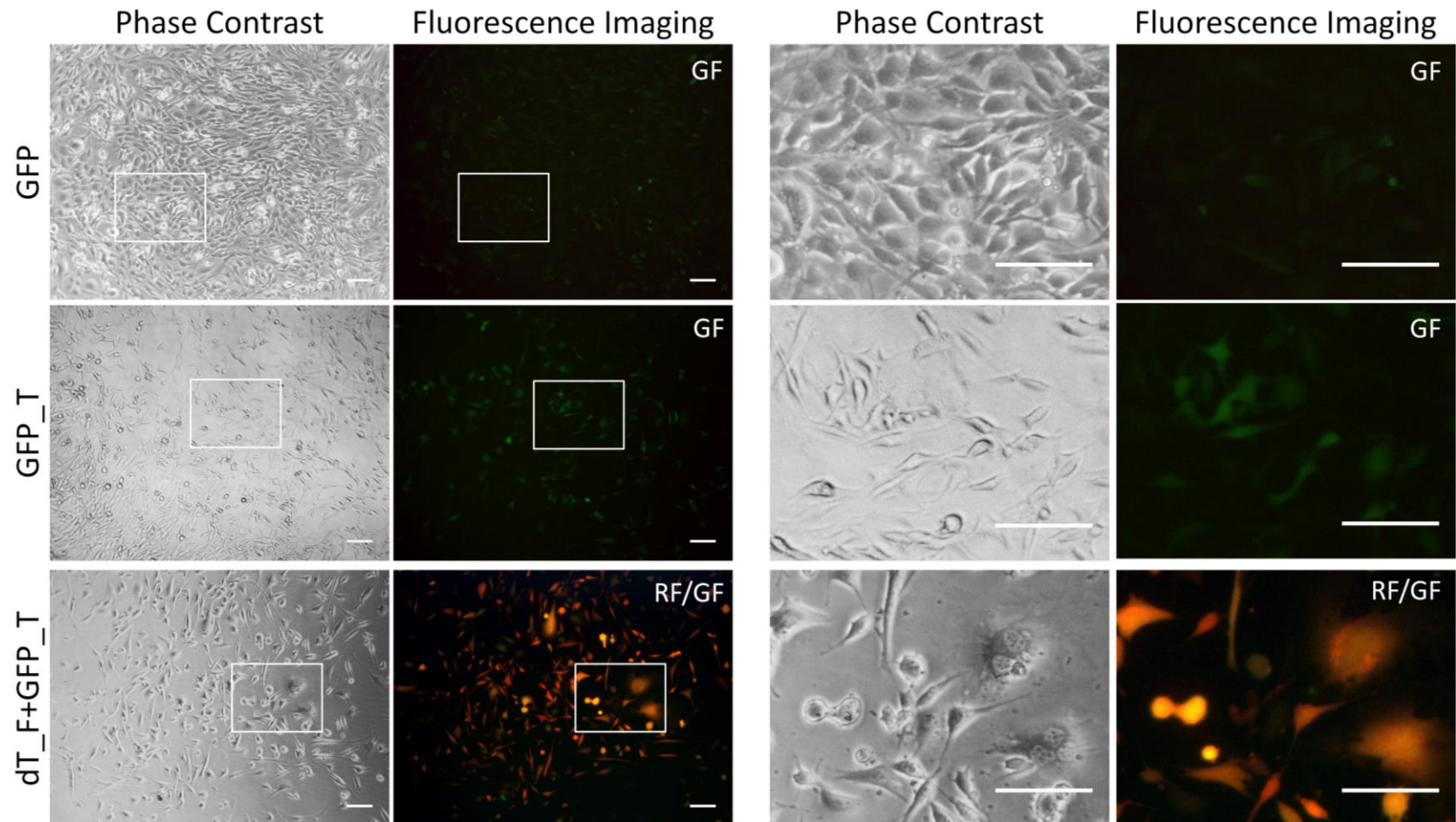


Figure 25 – Representative pictures of mMSC at P1 post-transduction. Control cells (untransduced) are displayed at an equivalent passage. dT corresponds to dTomato transduced cells; dT_F to Fth-1 transduced cells; GFP to GFP transduced cells; GFP_T to TfR-1 transduced cells and dT_Fth-1+GFP_T to cells transduced in conjunction with Fth-1 and TfR-1. All sets of pictures were taken with the same exposure conditions. A higher magnification of the insets is presented on the right hand side panel. RF - Red fluorescence; GF - Green fluorescence; RF/GF - Merge. Scale bars correspond to 100 μ m.

Figure 25 shows that mMSC were efficiently transduced with specific lentiviral particles, however not all transduced cells behaved similarly to Control cells. This was the case, for example, for dT_F transduced cells, which had a very different morphology when compared to control and dT cells, displaying a very large cytoplasm as opposed to an elongated shape typical of mMSC. This may be due to the overexpression of Fth-1, since dT cells were morphologically similar to untransduced cells (Control). However, in terms of transduction efficiency, even though both conditions were subjected to the same MOI, a difference in red fluorescence is quite outstanding, with dT_F cells being much brighter than dT control cells. The same atypical morphology was present in dT_F+GFP_T cells, even though in a smaller number. Also in this condition, the transduction of two lentiviral particles in conjunction appears to be comparable, in terms of red and green fluorescence, to the parental transductions (dT_F and GFP_T). As for GFP and GFP_T, morphologically these cells were very similar to control cells even though GFP_T cells were present in a much lower number and only on the side of the well, thus the phase-contrast picture being a bit distinct from the others. At this specific time-point (P1), it was clear that cells exposed to different transduction conditions had different proliferation rates. This partially had to do with the transduction process, which by itself may disturb the normal cell cycle, but the integrated transgene could also be responsible. A viability assay was performed at this point (7 days after transduction) and is presented in Figure 26.

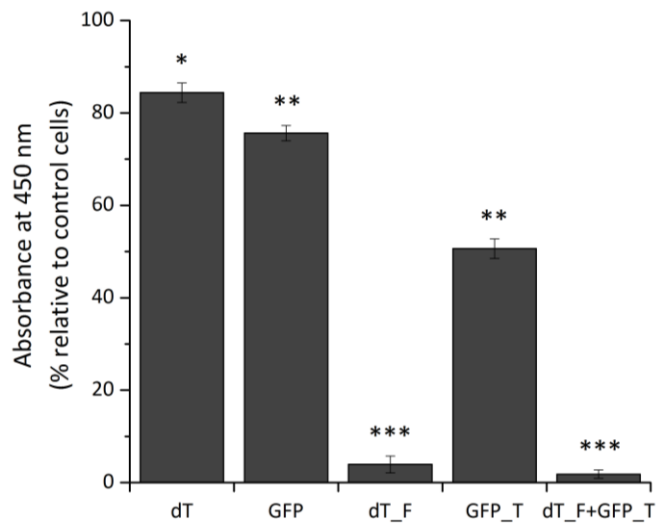


Figure 26 – Viability assay on transduced mMSC at P1 post-transduction with normal cell culture conditions. Data points and statistics are presented in relation to Control (untransduced) cells. Error bars represent SEM (n=3) (M&M, p.62).

The viability assay demonstrated in Figure 26 assessed proliferative capacity of mMSC cell line transduced with different viral preparations and compared to untransduced cells. This assay corroborated the results shown in Figure 25, in which all transduced cells had a decrease in the proliferation rate, however some cell lines, such as dT_F and dT_F+GFP_T, are more affected than others. Therefore, Fth-1 overexpression in mMSC may be contributing to a deregulation in iron homeostasis and indirectly promoting proliferative arrest. All cell lines were monitored with fluorescence microscopy over several passages and a decrease in transgene expression in the form of red or green fluorescence was never observed for transduced cells (data not shown). However, while dT/GFP controls proliferated normally when compared to untransduced mMSC, cells overexpressing with Fth-1 transgene never recovered from a slower proliferation capacity. Thus, in this condition, the population was enriched for low-expressing dT_F or untransduced

cells given their higher proliferation rate effectively diluting the fraction of the population consisting of high-expressing dT_F. As for cells transduced with TfR-1, such as GFP_T, viability rate was also significantly decreased, relative to untransduced cells, as all the other cell lines. However, GFP_T viability rate is comparable to its GFP control, only with a slight decrease, possibly due to a larger insert within the lentiviral construct, as discussed previously in Chapter 3.

In order to try and overcome this problem, mMSC were again transduced and cultured in either normal conditions or with iron supplementation from 24h post-transduction. As described in Chapter 3, iron supplementation included 0.2 mM ferric citrate, 1.28 mM holo-transferrin and 50 μ M L-ascorbic acid. To compare both culture conditions, integrated transgenes (dTomato, Viral_F, GFP and Viral_T) were evaluated over two passages (from P1 to P3) with RT-qPCR and results are displayed in Figure 27. For RT-qPCR, Tbp and Pgk1 genes were used as a reference for mMSC to normalize Ct values obtained for target genes.

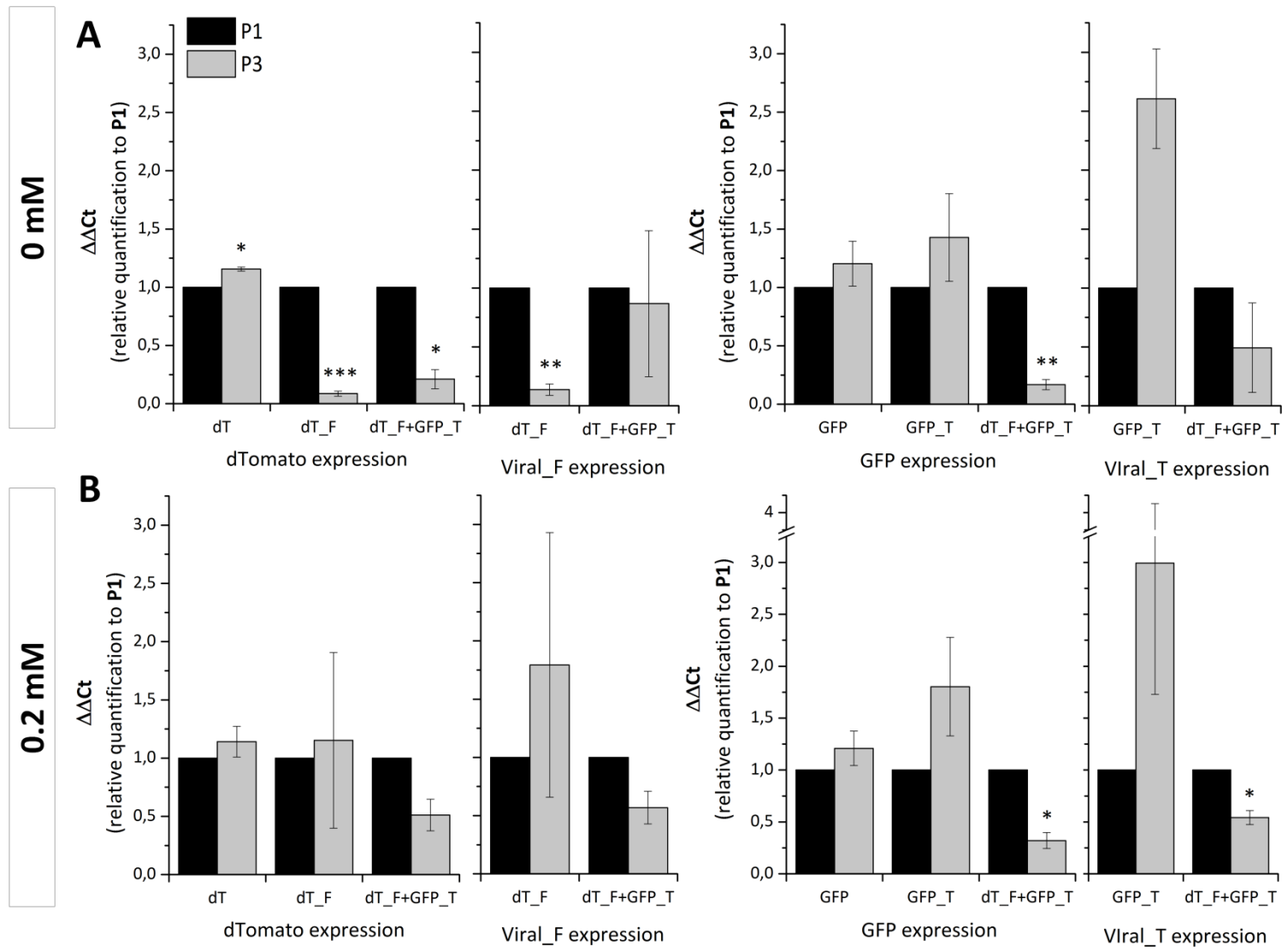


Figure 27 – RT-qPCR relative quantification of dTomato, Viral_F, GFP and Viral_T targets in transduced mMSC at P1 and P3 post-transduction (without FACS sorting). Expression values of target genes are plotted against P1 without (A) and with (B) iron supplements from 24h post-transduction. Error bars represent SEM ($n=3$) (M&M, p.52).

Results displayed in Figure 27 show that without iron supplementation (**A**) mMSC integrated with dTomato and Fth-1 (dT_F and dT_F+GFP_T) were not able to keep high expression levels neither from dTomato or Viral_F transgenes, with a statistically significant reduction. Additionally, a reduction in GFP and Viral_T expression levels from P1 to P3 was also observed for dT_F+GFP_T cells. This may be as well due to Fth-1 overexpression in these cells, since GFP_T maintain expression levels constant of both transgenes from P1 to P3, with even a 2.5-fold increase in Viral_T expression at P3, however with no statistical significance. As previously mentioned, Fth-1 overexpression may be promoting an iron homeostasis deregulation, leading to a population decrease of cells transduced with Fth-1. This appears to be partially overcome by adding iron supplements to the cells from 24h after transduction (**B**). In this case, dT_F transduced cells maintained relatively constant dTomato and Viral_F expression levels from P1 to P3. As for dT_F+GFP_T cells, even though not statistically significant, a small decrease both in dTomato and Viral_F target genes remained present. Similarly, GFP and Viral_T expression levels were still significantly reduced.

From this point onwards, all data presented was obtained using iron supplemented cells as described above, from 24h post-transduction.

5.2.2 Reporter gene integration with iron supplementation

mMSC transduced with specific lentiviral particles and iron supplemented from 24h post-transduction were given a few passages to recover and expand and

were then FACS sorted at P6 post-transduction. Figure 28 shows phase contrast and fluorescence microscopy images from the different transduced cell lines after FACS sorting for high expressing dT or GFP-positive population. Flow cytometry was then performed to confirm FACS sorting and results are illustrated in Figure 29.

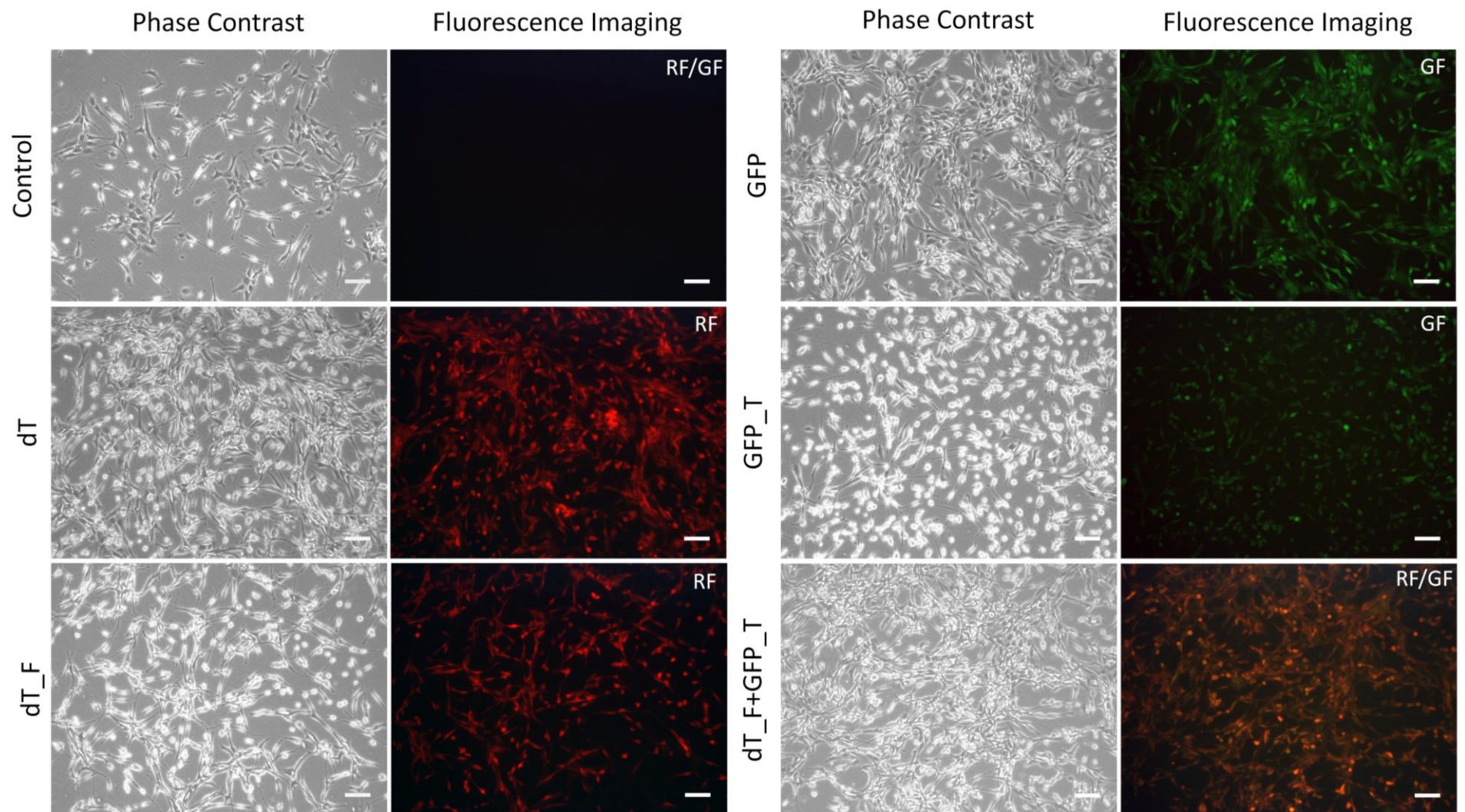


Figure 28 – Representative pictures of mMSC at P7 post-transduction and FACS sorted, as well as control cells (untransduced) at an equivalent passage. All sets of pictures were taken with the same exposure conditions. RF-Red fluorescence; GF-Green fluorescence; RF/GF - Merge. Scale bars correspond to 100 μ m.

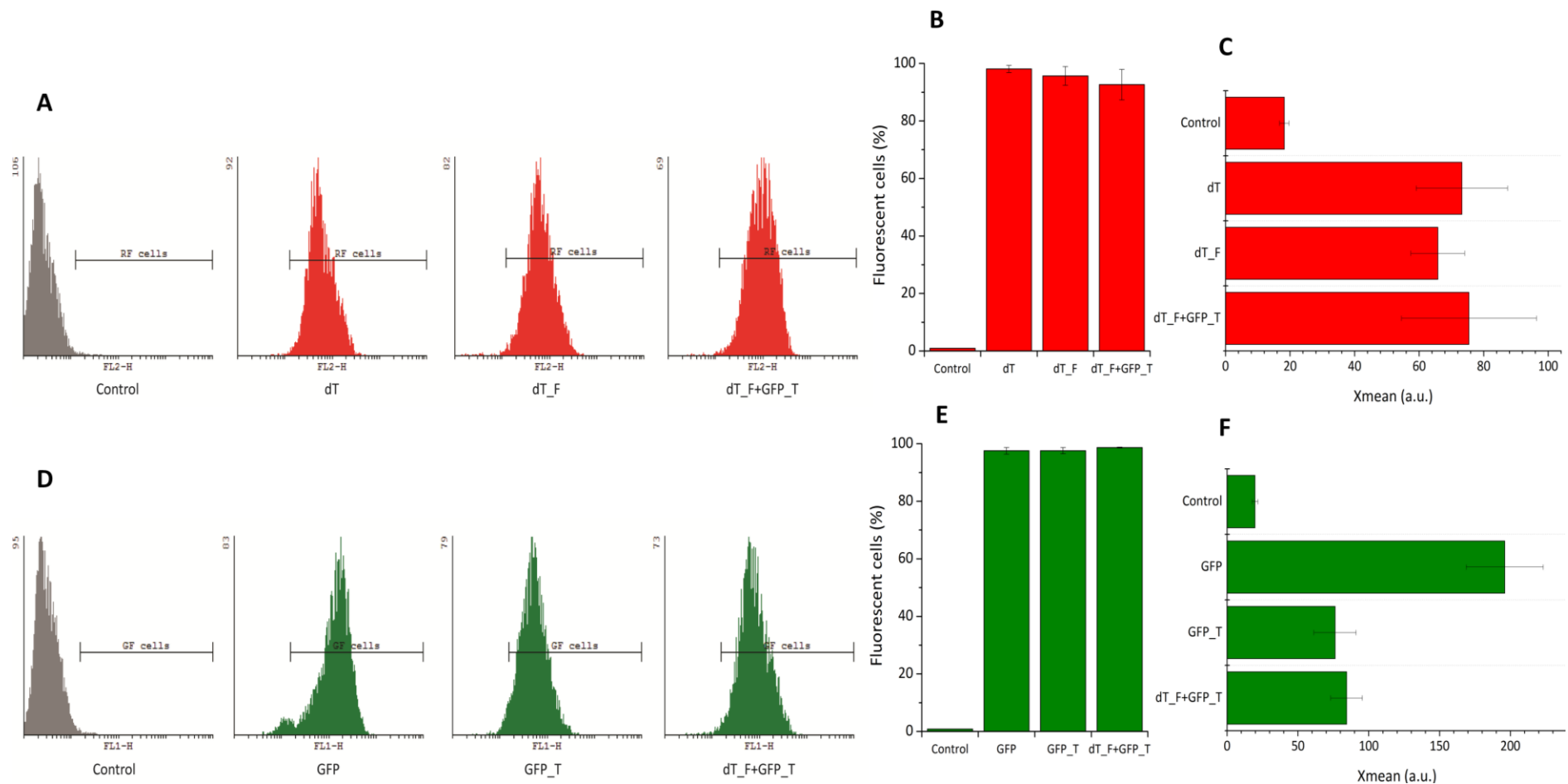


Figure 29 – Flow cytometry histograms (**A** and **D**) of mMSC cells, at P8 post-transduction and after FACS sorting. Histograms show the number of events (cells) counted (y-axis) versus the fluorescence intensity (x-axis). Red/ green fluorescence (RF/GF) gate represents dTomato/GFP-positive cell population plotted in **B** and **E**. The Xmean (**C** and **F**) represents the mean fluorescence obtained from the gated region (dTomato/ GFP cells). Error bars represent SEM ($n=3$). a.u-arbitrary units; M&M, p.48.

Figure 28 demonstrates that with iron supplementation, all transduced cells appear morphologically very similar to untransduced mMSC. Also, with FACS sorting, dT and GFP-positive cells are much more uniform in fluorescence expression, with all nearly 100% positive (Figure 29, **B** and **E**). Only a difference in brightness of green fluorescence is observed between GFP-control cells and the other GFP-transduced cells (GFP_T and dT_F+GFP_T) (Figure 28). This was also quantitatively measured by flow cytometry (Figure 29, **F**), where the mean fluorescence intensity for GFP cells is more than double compared to the other transduction conditions.

5.2.3 Cell viability

In order to evaluate to what extent transgene integration was affecting long-term cell health and proliferative capacity, the same viability assay shown previously in Figure 26, was again performed to cells iron supplemented from 24h post-transduction and evaluated not only at P1 (7 days after transduction), but also at P8, after FACS sorting. The results are displayed in Figure 30.

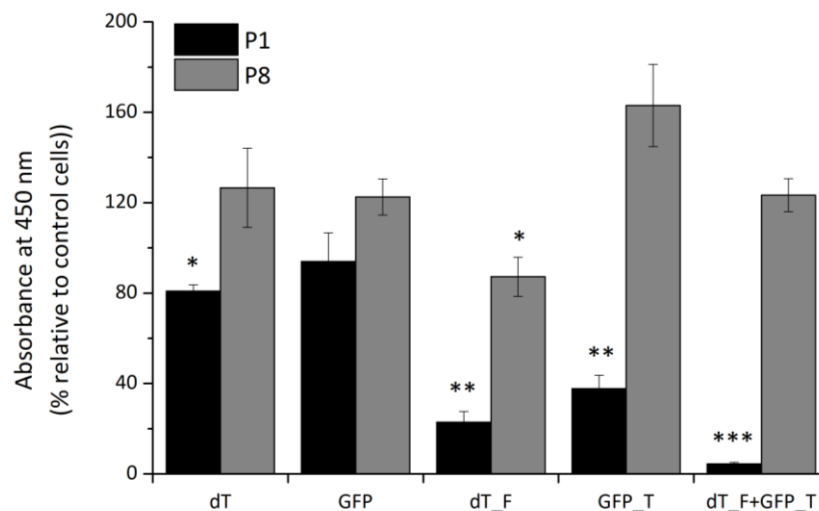


Figure 30 – Viability of transduced mMSC at P1 and P8 post-transduction when supplemented with iron. Cells at P8 were already FACS sorted. Data points and statistics are presented in relation to Control (untransduced) cells, cultured in the same conditions. Error bars represent SEM ($n=3$) (M&M, p.62).

Just like it was observed without iron supplementation (Figure 26), there is a statistically significant reduction in cell viability at P1. However, for dT_F transduced cells with iron supplementation the viability reduction was not so prominent than without iron addition, with an increase from 4 to 22% at P1. By P8, a highly pure dT-positive population, such as that shown in Figure 29, recovered up to 87% of viability, even though it was still a significantly reduced when compared to Control cells. As for dT_F+GFP_T cells, iron supplementation did not play a significant role in the increase of viability at P1, having about only 4% of proliferative and healthy cells. Nevertheless, over several passages these cells were able to recover to levels comparable to controls. On the contrary and as mentioned before, dT_F transduced cells without iron supplementation (Figure 25 and Figure 26) were never able to recover their viability state and over passages the dT_F-positive population was diluted by low expressing dT_F cells or untransduced cells. For this reason, the

viability of these cells was not evaluated at P8, as it would not represent a pure population of dT_F transduced cells. As for GFP_T cells, while without iron supplementation (Figure 26) the viability rate was around 50% at P1, when adding iron following transduction, the viability suffered a slight decrease, with values of about 40%. Perhaps iron supplementation is influencing these cells, promoting a small decrease in their viability. Still, at P8, GFP_T cells present an ever higher proliferative/health rate than controls, although not statistically significant. Overall, while cells appear to go through a sensitive period a few days after transduction, if iron is added to the culture media, overexpression of Fth-1 does not seem to interfere so much with normal cell functions and cells can recover up to normal levels in a few passages. To fully verify if transduced cells behaved similarly to the untransduced parental cell line, differentiation potential was assessed at P8 post-transduction, again after FACS sorting. This was done by directing mMSC differentiation into osteogenic, adipogenic and chondrogenic lineages. Results are displayed in Supplementary figure 3 and no apparent differences were found between conditions.

5.2.4 Overexpression of reporter genes at mRNA and protein level

To estimate the overexpression of genes involved in the iron pathway, such as TfR-1 and Fth-1, endogenous and viral transcripts of these genes were evaluated. Since Fth-1 transduced cells (dT_F and dT_F+GFP_T) did not proliferate in the absence of iron, a comparison between cells cultured with and without iron supplementation was not possible, as in the previous chapter. Instead, the total

mRNA expression levels of TfR-1 and Fth-1, designated as Total_T and Total_F, were measured in control and transduced iron supplemented cells, from P1 to P3 post-transduction by RT-qPCR (Figure 31). For RT-qPCR amplification, the reference genes used were the same as previously described.

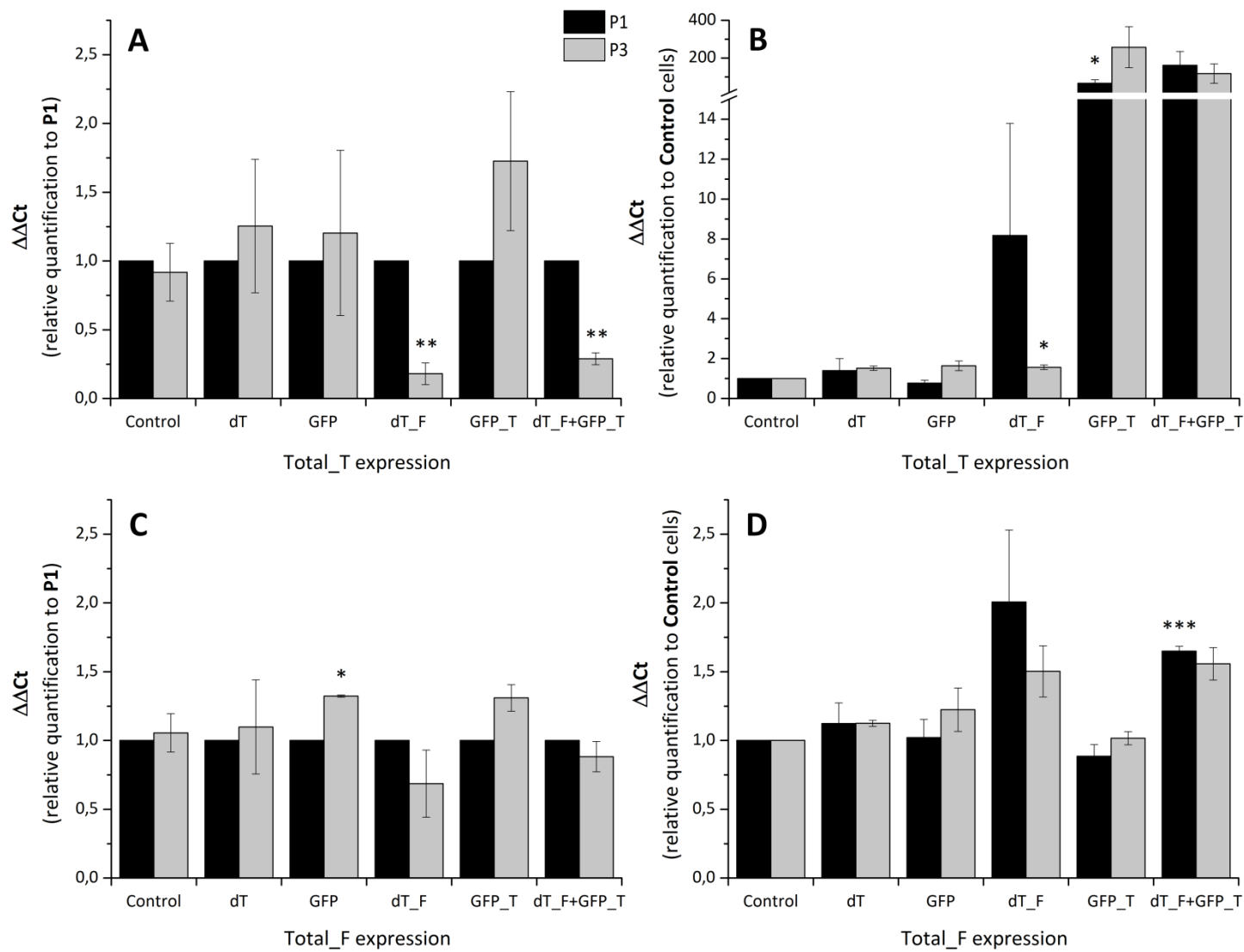


Figure 31 – RT-qPCR relative quantification of endogenous and viral TfR-1 transcripts (Total_T, **A** and **B**) and of endogenous and viral Fth-1 transcripts (Total_F, **C** and **D**) in Control and transduced mMSC at P1 and P3 post-transduction. Expression values of target genes are normalized in relation to P1 (**A** and **C**) and to Control cells (**B** and **D**). Error bars represent SEM ($n=3$) (M&M, p.52).

In Figure 31, total mRNA expression levels of TfR-1 and Fth-1 were quantitatively measured, comparing for each condition from P1 to P3 post-transduction (**A** and **C**) and also, at each passage, transduced cells were compared to control cells (**B** and **D**). In graph **A**, the results obtained show that the Total_T expression for controls, i.e., Control, dT and GFP, is relatively constant from P1 to P3. The same is observed for Total_F mRNA expression levels in graph **B**, however with a slight increase in GFP cells. On the other hand, with the overexpression of Fth-1 in dT_F and dT_F+GFP_T cells, there is a statistically significant reduction of Total_T expression, even though there is no change in Total_F expression from P1 to P3. As for when expression levels at each passage are compared to Control cells, in graph **C** and **D**, the results show that again levels between controls (Control, dT and GFP) are maintained relatively constant, but the overexpression of iron related genes alters the expression of Total_T and Total_F. More specifically, for dT_F cells at P1 there is an up-regulation both of Total_T and Total_F when compared to Control cells; at P3, even though levels of both target genes have decreased, there is still a significant up-regulation of Total_T expression in dT_F cells. These results suggest that an overexpression of Fth-1 may be also promoting an up-regulation of TfR-1. In the case of GFP_T cells, a substantial increase is shown for total mRNA TfR-1 levels, both at P1 and at P3 with 65 and 257-fold increase, respectively, when compared to Control cells. However, at both passages Total_F levels are not significantly different than control cells. This indicates that even though many more TfR-1 transcripts are being formed, Fth-1

mRNA transcripts are maintained at constant levels. At last, the transduction of TfR-1 and Fth-1 in conjunction (dT_F+GFP_T) resulted in an up-regulation of both Total_T and Total_F targets, with a very significant increase of Total_F, at P1 ($p=0.00037$).

These changes observed at the mRNA level were then assessed at the protein level by WB (Figure 32 and Supplementary figure 4) and immunofluorescence (Figure 33). Cells used for this evaluation were collected at P8 post-transduction and after FACS sorting. For WB detection, actin and total protein gels were used for data normalization.

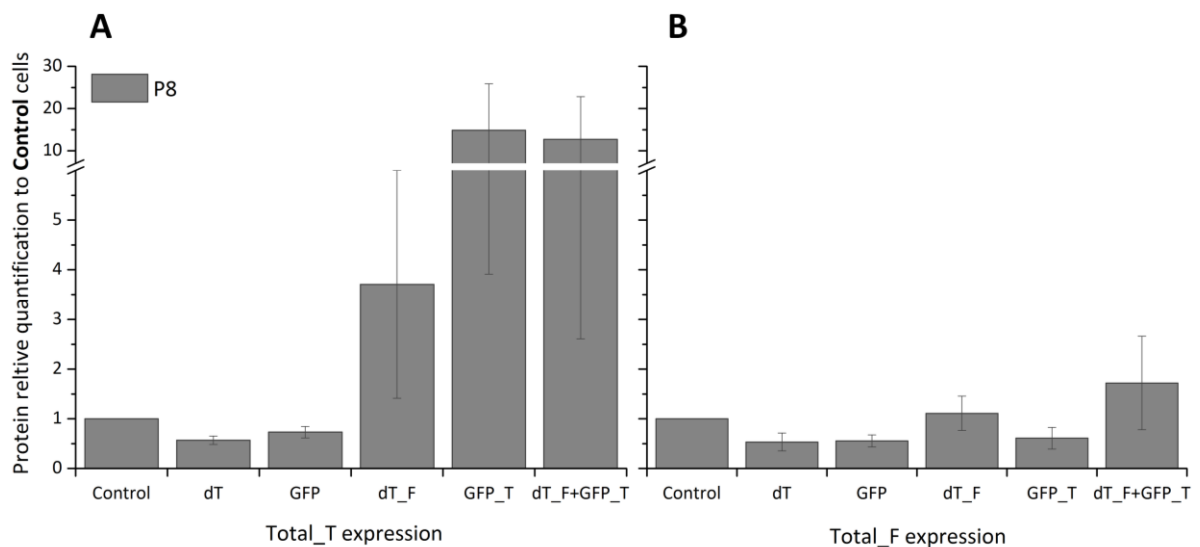


Figure 32 – WB relative quantification of Total_T (A) and Total_F (B) targets in Control and transduced mMSC at P8 post-transduction and after FACS sorting. Error bars represent SEM ($n=3$) (M&M, p. 57).

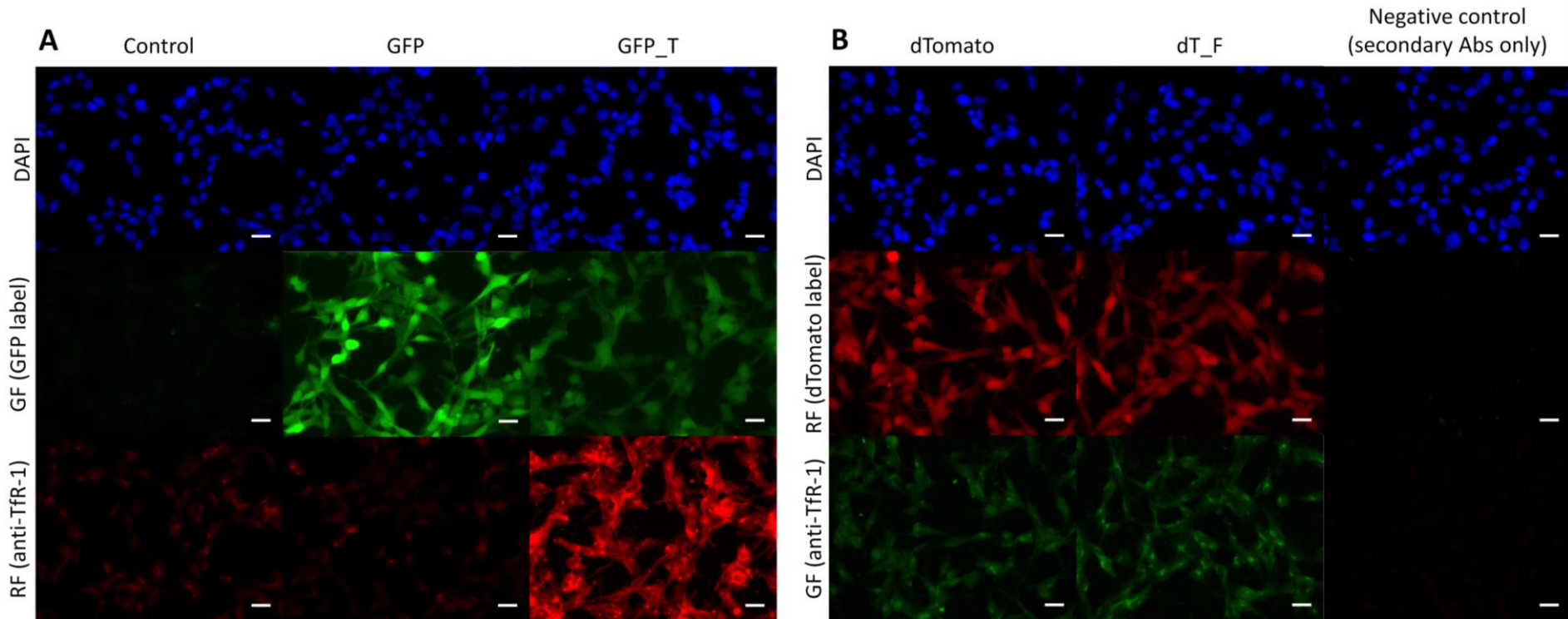


Figure 33 – Representative immunofluorescence pictures of Control, GFP and GFP_T in panel **A** and dT, dT_F and negative control in panel **B**, at P8 post-transduction and after FACS sorting. Nuclear region is shown by DAPI staining. In panel **A**, green fluorescence (GF) is originated from the GFP reporter and the detection of TfR-1 proteins is visualized with a red fluorescent antibody. On the contrary, in panel **B**, red fluorescence (RF) is obtained due to the presence of dTomato reporter and the detection of TfR-1 proteins is visualized with a green fluorescent antibody. dT_F+GFP_T condition was not possible to be evaluated by IF due to the presence of both GFP and dTomato reporters. All pictures sets were taken with the same exposure conditions. Negative controls targeting only the secondary Abs used are included to prove specificity to the primary Ab. Scale bars: 25 μ m; M&M, p.56.

Protein quantification data obtained by WB (Figure 32) shows that, similarly to the mRNA quantification data, Control, dT and GFP cells have constant protein levels of both Total_T and Total_F targets, while dT_F has a 3.5-fold up-regulation of Total_T, possibly promoted by Fth-1 overexpression. Also, Total_T is up-regulated in GFP_T and dT_F+GFP_T cells with 15 and 13-fold increases, respectively. However, for Total_F protein quantification, differences between transduced magnetic reporters and control cells are not so distinctive, with only dT_F+GFP_T cells having a slight 1.7-fold increase in relation to Control cells, although this was not statistically significant. Data obtained with immunofluorescence (Figure 33) confirms that a clear TfR-1 overexpression is present in GFP_T cells, when compared with controls (Control and GFP). Also, expression levels of TfR-1 appear to be slightly higher in dT_F cells, when compared to its dT control, as observed for WB. Immunofluorescence staining for Fth-1 was also performed in transduced cells in the same conditions, but no difference was found (data not shown).

Overall, these techniques show a clear overexpression of TfR-1 in GFP_T and dT_F+GFP_T cells, both at the mRNA and protein level. However this is not the case with Fth-1 overexpression in dT_F and dT_F+GFP_T cells. Next, the capacity of TfR-1 and/or Fth-1 transduced cells to retain more iron than controls (Control, dT and GFP) is explored measuring the intracellular iron concentration.

5.2.5 Intracellular Iron Uptake *in vitro*

The capacity of dT_F, GFP_T or dT_F+GFP_T transduced cells to accumulate more iron than controls (Control, dT and GFP) was evaluated by measuring the intracellular iron content of these cells with Ferrozine assay. To do this, control and transduced cells (grown with 0.2 mM of iron from 24h post-transduction) were compared to cells that received an extra supplementation of 2 mM of iron for four days. Also, untransduced mMSC cultured without iron supplementation were included for comparison. Results are displayed in Figure 34, where the intracellular amount of iron is shown as a function of iron supplementation.

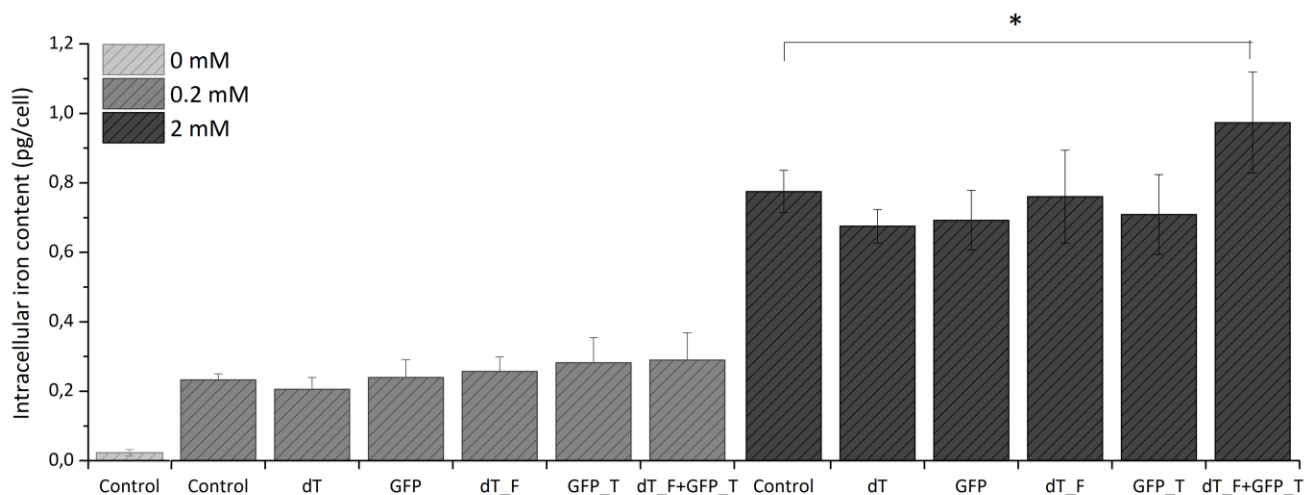


Figure 34 – Intracellular iron content of mMSC cells determined with the Ferrozine assay. Control and transduced cells were supplemented with different iron concentrations of 0.2 mM from 24 post-transduction or 2 mM for 4 days prior to measurement (Iron supplementation, p.50). A non-supplemented (0 mM) Control was also included. Error bars represent SEM ($n=3$) (M&M, p.50).

Figure 34 shows that mMSC have a great capacity for iron incorporation, reaching up to approximately 0.2 and 0.8 pg/cell, when untransduced cells are incubated with 0.2 and 2 mM of iron, respectively. With 0.2 mM, no differences in

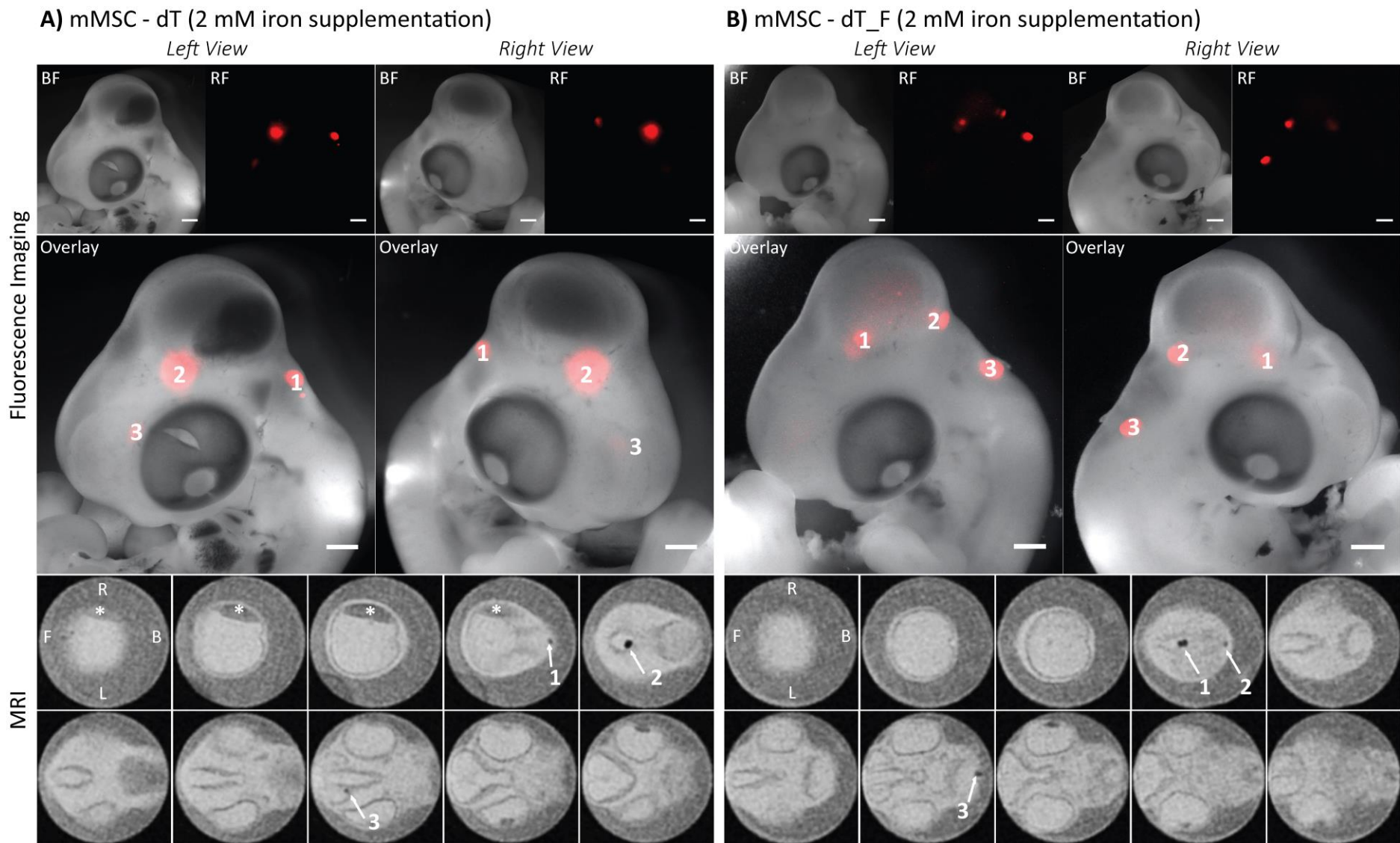
iron accumulation capacity are detected between the different cells. However, with 2 mM iron supplementation, dT_F+GFP_T cells demonstrate an increased capacity of intracellular iron retention relative to other transduced cells, with a statistically significant difference relative to control cells. Therefore, TfR-1 and Fth-1 used in conjunction might be a promising reporter system for MRI tracking of mMSCs.

5.2.6 MRI

To study the potential of TfR-1 and/or Fth-1 transgenes as possible MRI reporters, cell pellets from control and transduced cells were scanned using T2-weighted sequences. To do this, 10^7 cells were centrifuged at high speed to form a compact cell pellet and imaged via MR, where T1/T2 maps were produced for relaxivity studies. Results are displayed in Figure 35.

Due to such high levels of iron present in cells incubated with 2 mM of iron, as seen in Figure 34, when scanning with MRI (Figure 35, **A**), the relaxation (signal loss) was so quick for these cells that it was only possible to determine T1 and T2 relaxation times for cells with no iron supplementation (Control – 0 mM) or cells supplemented with 0.2 mM of iron (Figure 35, **B** and **C**). Relaxivity studies show that the averages of samples containing dT_F, GFP_T or dT_F+GFP_T are slightly lower than their respective controls. This is more perceptible in MRI image **A**, in which at 0.2 mM iron concentration, controls (Control, dT and GFP) appear to be the lightest pellets, followed by dT_F and GFP_T, which look much alike, and the darkest pellet, or the one with strongest loss of signal appears to be dT_F+GFP_T cells. However, none of the conditions at 0.2 mM iron supplementation were able to produce statistically significant shortening effects, either with T1 or T2 scans.

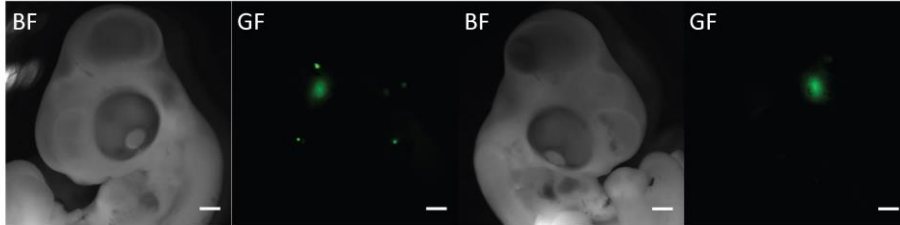
Then, 2×10^5 transduced cells were microinjected into the midbrain of the chick embryo at embryonic day 3 (E3). All transduction conditions were supplemented with 2 mM of iron for 3 days prior to injection. A non-supplemented control - dT (0 mM) was also included. At E5, embryos were imaged with two complementary platforms: by fluorescence microscopy to detect red/green fluorescence derived from the dTomato/GFP gene and by MR transversal imaging, by observing hypointense regions derived from iron retained in transduced cells, which was influenced by extracellular iron supplementation and/or due to TfR-1 and/or Fth-1 overexpression (Figure 36).



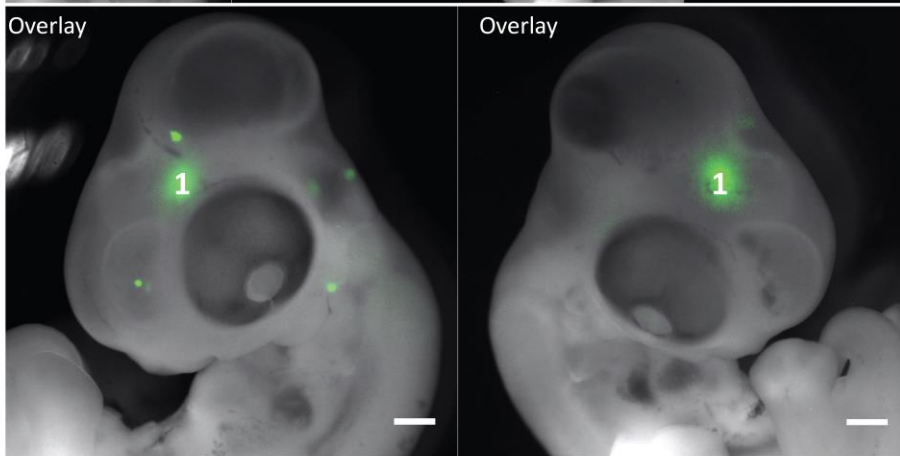
C) mMSC - GFP (2 mM iron supplementation)

Left View

Right View



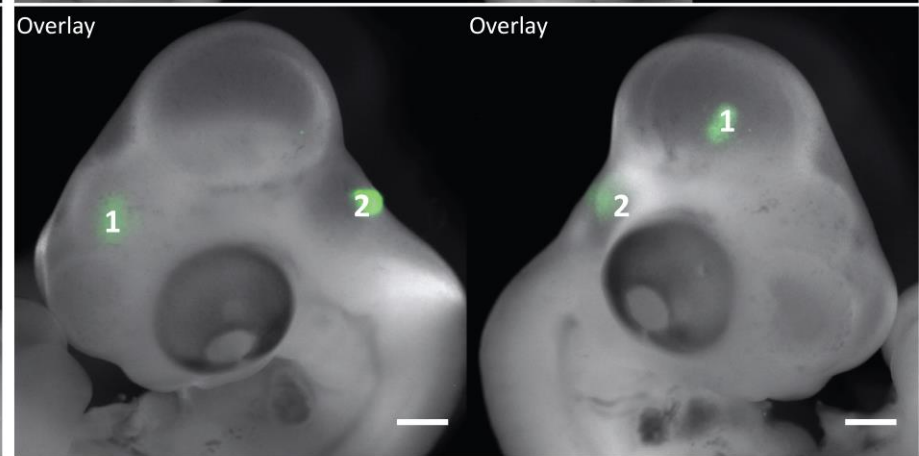
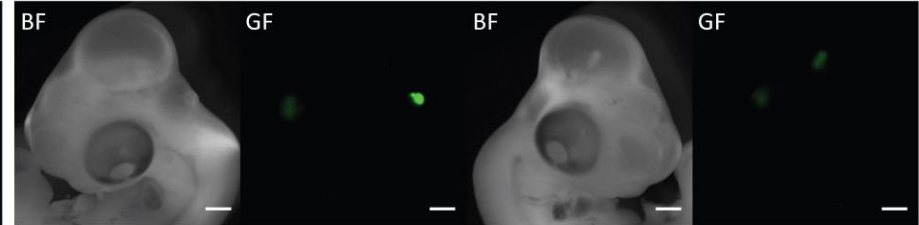
Fluorescence Imaging



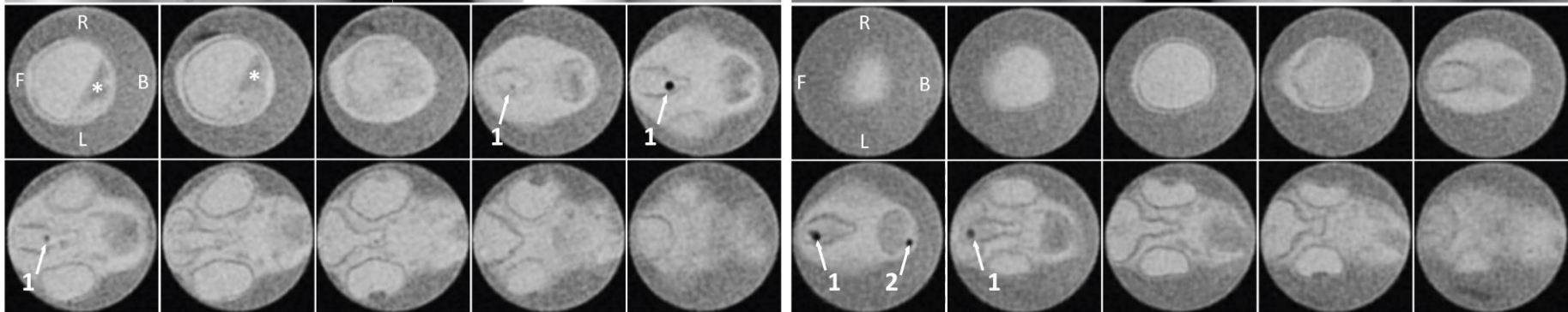
D) mMSC - GFP_T (2 mM iron supplementation)

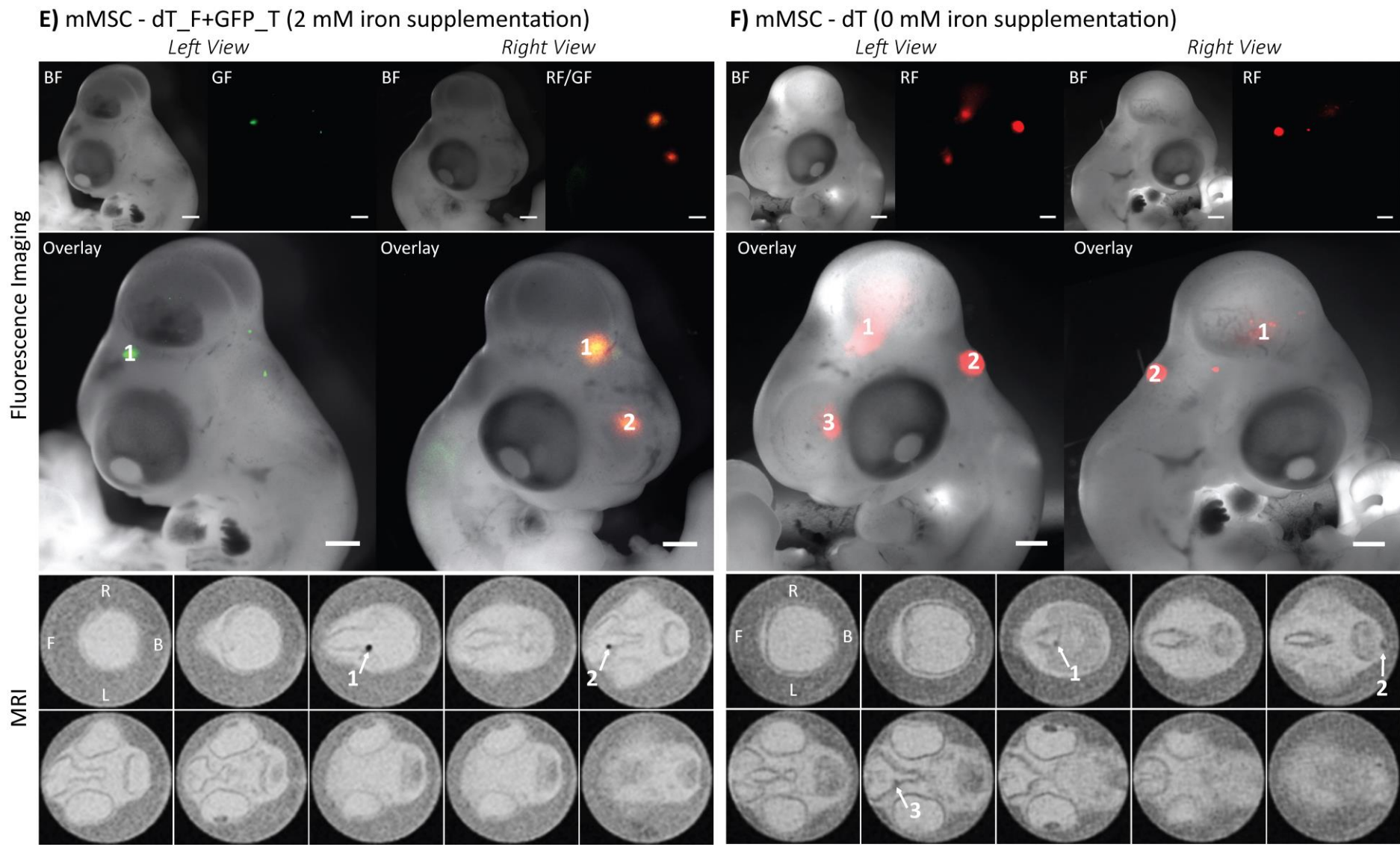
Left View

Right View



MRI





Fluorescence Microscopy			MRI		
Iron conc.	Transduction condition	Biological rep. (technical rep.)	Iron conc.	Transduction condition	Biological rep. (technical rep.)
2 mM	dT	n=3 (6)	2 mM	dT	n=2 (2)
	dT_F	n=3 (5)		dT_F	n=2 (2)
	GFP	n=2 (4)		GFP	n=1 (2)
	GFP_T	n=2 (5)		GFP_T	n=1 (2)
	dT_F+GFP_T	n=3 (5)		dT_F+GFP_T	n=2 (2)
0 mM	dT	n=1 (3)	0 mM	dT	n=1 (2)

Figure 36 – Fluorescence and MR imaging of dT and dT_F (A and B), GFP and GFP_T (C and D) and dT_F+GFP_T and dT (0 mM) (E and F) transduced mMSC cells, 2 days after injection in the midbrain of a chick embryo (E5). Cells received 2 mM of iron supplementation for 3 days prior to injection, with the exception of dT (0 mM) (F), which did not receive any supplementation (Iron supplementation, p.50). In the fluorescence imaging panel, bright field (BF) and red/green fluorescence (RF/GF) are projection images from the whole embryo; overlays are presented for both left and right views and were used as a reference guidance for MR imaging; scale bars correspond to 1 mm. In the MRI panel, anatomical images are displayed as transverse sections along the rostrocaudal axis of the embryo (left to right); 10 sections are displayed for each embryo. All images are representative from the results obtained and were equally processed with ImageJ software. Arrows indicate T2 shortening effect; b – bubble of air; * – blood. Position of the embryo: F – front; B – back; R – right; L – left; number of biological and technical replicates is indicated in the table above (M&M, p.65).

In some areas in Figure 36, tiny bubbles of air are designated as “b” and also darker areas which correspond to blood found in the brain are indicated with an asterisk (*). These blood spots are perfectly visible with bright field imaging and were likely due to a brain haemorrhage caused while injecting at E3 or perhaps while dissecting the chick embryo at E5. Due to the presence of haemoglobin which contains large amounts of iron (Ponka and Lok, 1999), the blood present in the brains containing haemorrhages promotes a loss of signal (darker contrast) relative to background when imaged. To identify if transduced cells integrated into chick embryo’s brain, first, bright field and fluorescence imaging were performed on

whole embryos. Due to the presence of fluorescent reporters, transduced cell clusters were easily identified and located within the brain. This served as a guideline to identify hypointense cell clusters with MR imaging. Without this support, identifying cell clusters based only on anatomical images would have proven to be much more difficult.

At the first instance, results in Figure 36 show that mMSC microinjected into an E3 embryo chick formed compact globular cell clusters localized at few locations within the brain. This was particularly useful in this case, as complementing two different imaging platforms, fluorescence with MR imaging, became very accurate. Also, at 2 mM iron supplementation, the iron retained by transduced cells allowed an easy identification of hypointense regions, all correlated with red and/or green fluorescence obtained with fluorescence microscopy. However, at this iron concentration no evident differences were found between the different transduction conditions (A-E). The cell clusters identified with fluorescence microscopy in the control with no iron supplementation (dT, 0 mM) were also correlated with MR imaging, but the hypointense regions found were much lighter than those with 2 mM of iron supplementation conditions. These results suggest that with MRI, 2 mM of iron supplementation to cells creates an almost complete loss of signal, *i.e.*, turns the region nearly black, and therefore at this detection limit no differences between different reporter genes can be found.

5.3 DISCUSSION

Over the past few years, several studies have evaluated the potential of TfR-1 and/or Fth-1 as MRI reporter genes designed specifically for cell tracking purposes. As described in the previous chapter, TfR-1 capacity of internalizing transferrin-bound iron makes it a suitable system for increasing intracellular iron content (Deans *et al.*, 2006). On the other hand, the heavy subunit of ferritin (Fth-1) alone or together with the light subunit (Ftl-1) has been overexpressed in a number of cell lines and used as a means to store higher levels of intracellular iron, relative to controls (Cohen *et al.*, 2005; Genove *et al.*, 2005; Iordanova *et al.*, 2010). The aim of overexpressing either gene in a certain cell line is to produce a contrast effect sufficiently high to be visualized and followed up with MRI. In this chapter, TfR-1 and Fth-1 were investigated either individually or in combination to create a suitable reporter system for MRI tracking of mouse mesenchymal stem cells.

In Chapter 3, both TfR-1 and Fth-1 cDNAs were cloned directly from mMSC and overexpressed in the same cell line using a lentiviral approach. Both magnetic reporters (TfR-1 and Fth-1) were deprived of the iron responsive elements located in their UTRs, allowing for a constitutive expression of these genes, without the cell's interference. Moreover, because these cDNAs were overexpressed in the same cell from which they originated, the sole expression of endogenous TfR-1/Fth-1 was not possible to be detected as both viral and endogenous transcripts were identical. However, a specific primer pair was designed for RT-qPCR, in which the forward primer matched the target magnetic reporter (TfR-1/Fth-1) and the reverse primer

corresponded to a segment within the IRES (internal ribosome entry site). This allowed the design of a primer pair to specifically detect only the viral transcripts of either TfR-1 or Fth-1, being therefore designated as Viral_T and Viral_F, respectively. The total levels of TfR-1 or Fth-1, determined by RT-qPCR and WB, corresponded to both endogenous and viral transcripts and were designated as Total_T for TfR-1 and Total_F for Fth-1.

Also in Chapter 3, while TfR-1 was cloned into pHIV-eGFP lentiviral vector, expressing GFP gene as a green fluorescent reporter (GFP_T), Fth-1 was cloned into pHIV-dTomato, which expressed dTomato gene as a red fluorescent reporter (dT_F). This allowed for a longitudinal monitoring of cells with fluorescence microscopy and quick identification of which magnetic reporter was present, particularly useful when both genes were overexpressed in conjunction (dT_F+GFP_T). MSC were transduced with MOI=50 for each viral preparation, which theoretically means that about 50 copies of each transgene were integrated per cell. Previous studies, when overexpressing Fth-1 gene, have used similar MOIs from 30 to 100 in order to obtain significant contrast by MRI (Genove *et al.*, 2005; Iordanova *et al.*, 2010).

Reporter gene integration in the mMSC line was evaluated initially over a period of 7 days with fluorescence microscopy, while transduced cells were cultured under normal conditions, *i.e.*, the same cell culture conditions applied to untransduced mMSC. A different morphology in dT_F transduced cells was immediately perceptible after a few days in culture (Figure 25). Also, the proliferative/health rate of transduced cells suffered a big impact, in particular for

cells transduced with Fth-1 (dT_F and dT_F+GFP_T), with only 5% of viable cells present (Figure 26). These data suggests that Fth-1 constitutive overexpression in mMSC might be unbalancing the tightly controlled iron metabolism and promoting a toxic effect on these cells. In order to overcome this issue, iron supplements were added to the culture media 24h post-transduction. Cells either iron supplemented or cultured under normal conditions were compared by evaluating transgene integration after 7 days (P1) and at P3 (Figure 27). This evaluation, performed by RT-qPCR, showed that the lack of iron supplementation promoted a decrease of the transgenes in dT_F and dT_F+GFP_T populations. This decrease in mRNA levels might be due to the higher proliferation rate of untransduced or low-expressing dT_F cells present in the population at that time-point. On the contrary, when cells were iron supplemented, dTomato and Fth-1 transgenes were kept at constant levels from P1 to P3, at least for dT_F cells. As for the other conditions that integrated GFP and/or TfR-1 transgenes, mRNA levels did not seem to be disturbed with the absence or addition of iron supplementation. In order to continue to study the evaluation of TfR-1 and/or Fth-1 as potential MRI reporter genes, only cells with iron supplementation from 24h post-transduction were used for subsequent analysis. This suggests a lack of flexibility when using Fth-1 as a reporter gene, as cells have to be on permanent iron supplementation, although it is not clear if other stem/progenitor cells would present the same limitation.

mMSC transduced and iron supplemented were evaluated after FACS sorting (Figure 28 and Figure 29), showing nearly 100% of positive dT and GFP populations

for all transduced conditions. Also, cell viability was investigated at P1 and P8 post-transduction. With iron supplementation, the decrease in viability was not as noticeable at P1 as seen previously, and with the increase in passage number most transduced conditions were able to recover to equivalent values of untransduced cells. Of note, a pure population of dT_F cells at P8 still had a small decrease in cell viability while, on the other hand, GFP_T cells had an increase, relative to Control cells. This increase in cell viability is quite interesting since TfR-1 overexpression is usually observed in malignant tumour cells, which also have an increase in cell proliferation (Ponka and Lok, 1999; Sutherland *et al.*, 1981). The viability fluctuations observed for dT_F and GFP_T cells suggest that constitutively expressing only one particular gene involved in the maintenance of iron homeostasis might create an unbalanced uptake and/or storage of iron. On the other hand, the combination of TfR-1 and Fth-1 overexpression in the same cell line, such as performed for dT_F+GFP_T cells, produces viability data at P8 that is very similar to controls (dT and GFP), possibly restoring a balanced iron homeostasis for this condition.

Next, reporter genes were evaluated at the mRNA and protein level (Figure 31 and Figure 32) and results show that when iron related genes, such as TfR-1 and Fth-1, are overexpressed in mMSC, the total levels of these transcripts vary significantly. For instance, in dT_F cells, a small up-regulation at the mRNA and protein levels are observed for Total_T when compared to Control cells, indicating that Fth-1 integration is promoting Total_T up-regulation, possibly due to the

necessity of more intracellular iron. This was confirmed by immunofluorescence, where cells were immunostained with anti-TfR-1 antibody, and dT_F cells were slightly brighter when compared to dT cells (Figure 33). However, Total_F levels are not significantly up-regulated in dT_F cells, neither at the mRNA nor at the protein level as one would expect. In the case of GFP_T cells, very high levels of Total_T are detected, both at the mRNA and protein level; however, without any change in Total_F levels. These results indicate that even though many new receptors may be formed due to TfR-1 overexpression, ferritins are not present in higher amounts than in controls. TfR-1 overexpression in GFP_T cells was confirmed using immunofluorescence (Figure 33). At last, only in dT_F+GFP_T cells is overexpression detected for both Total_T and Total_F at the mRNA level. At the protein level, an increase in Total_T is present similarly to GFP_T cells, but for Total_F only a small up-regulation is observed. This suggests that it is only when TfR-1 and Fth-1 are overexpressed together that iron homeostasis is restored.

The results obtained with the Ferrozine assay (Figure 34) confirm what was suggested and show that only when overexpressing both TfR-1 and Fth-1 in conjunction that it was possible to obtain a higher concentration of intracellular iron (2 mM), relative to Control cells. This may be the case as it might create a balanced iron system, introducing larger amounts of iron into the cell through the overexpressed TfR-1, and storing intracellular iron in a safe configuration in ferritin cages, promoted by the overexpression of Fth-1. To test if dT_F transduced cells were actually retrieving iron inside ferritin cages, these cells were deprived from

iron supplementation for a short time period (4 days). Then, the intracellular iron content of dT_F cells was compared to a non-supplemented control (untransduced cells) and no differences were found between the two conditions (data not shown). This suggests that iron may not be retrieved in ferritin cages for very long after iron supplementation is removed. Nevertheless, this assay was not performed for dT_F+GFP_T transduced cells, where a balanced iron system might have been restored.

In terms of total iron content that mMSC are able to incorporate, both with Ferrozine assay and MR imaging of cell pellets (Figure 35, **A**), it was found that mMSC have an extremely high capacity for iron incorporation. For example, untransduced mMSC can accumulate up to 0.8 pg of iron per cell, when supplemented with 2 mM of iron. For this reason, when imaging compressed cell pellets previously supplemented with 0 mM (only untransduced cells), 0.2 or 2 mM of iron concentration, it was only possible to determine T1 and T2 relaxation times for 0 and 0.2 mM conditions. However, at these iron concentrations, no significant difference was found between transduced cells, in agreement with the intracellular iron quantification obtained with the Ferrozine assay (Figure 34). Because the only statistically significant difference found was when dT_F+GFP_T cells were supplemented with 2 mM of iron, this concentration was then used to supplement cells prior to microinjection in chick embryos.

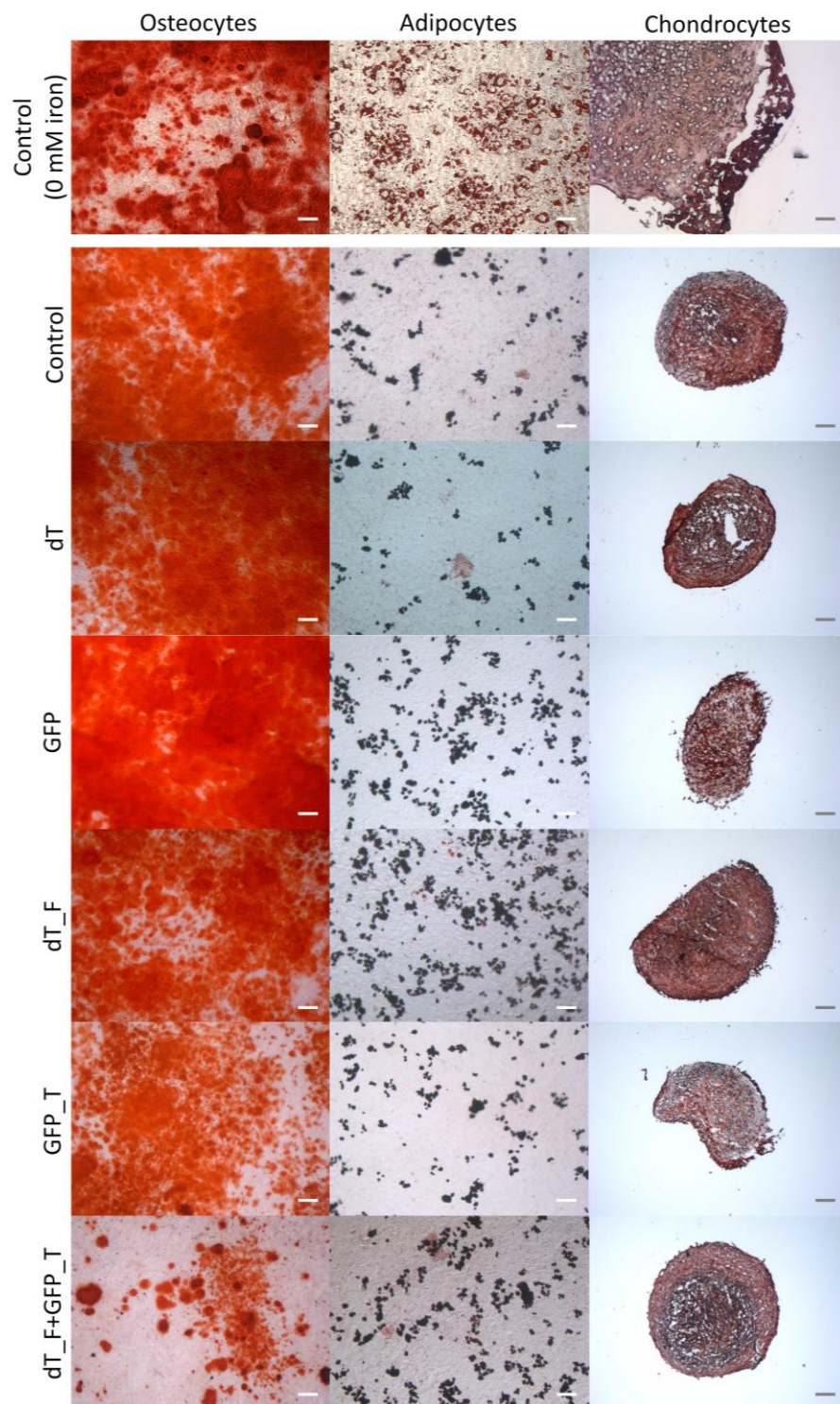
At embryonic day 5 (E5), the identification of transduced cell clusters was straightforward for all conditions analysed and with both imaging platforms

(fluorescence microscopy and MRI) (Figure 36). Fluorescence microscopy allowed for the detection of cell clusters transduced with either GFP or dTomato genes, allowing for green and red fluorescence visualization, while MRI allowed for the detection of cell clusters based on contrast differences due to iron accumulation capacity of cells. At the same supplementation conditions of 2 mM of iron, controls (dT and GFP) were not distinctive from magnetic reporters of interest (dT_F, GFP_T and dT_F+GFP_T). Even though a significantly higher intracellular iron accumulation was found for dT_F+GFP_T, when imaged with MRI, this condition did not provide a definitive contrast in relation to the remaining transduction conditions.

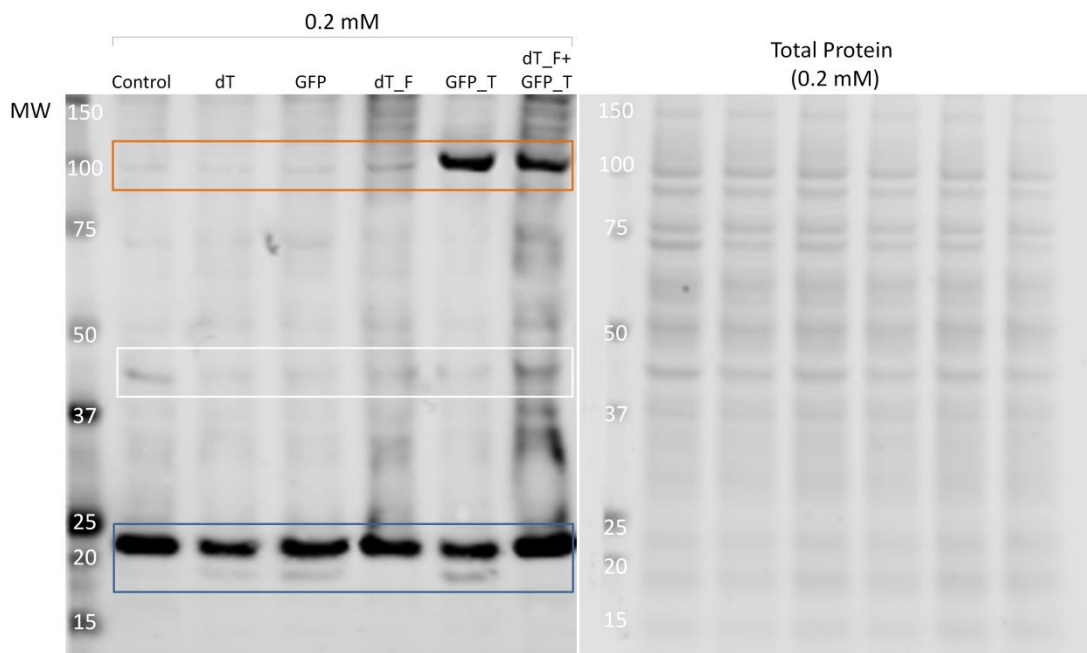
In summary, mMSC was used as a model stem cell line to evaluate the potential of TfR-1 and Fth-1, either used individually as magnetic reporter genes or in conjunction as a system to upload and store intracellular iron with a higher capacity than controls. It is clear that cell viability must be taken into consideration as it might reflect a disturbance promoted by the overexpression of a single gene involved in the iron metabolism. Also, because iron homeostasis is tightly controlled by the cell, the total levels TfR-1 and Fth-1 need to be determined and evaluated if a true overexpression is taking place. The results obtained with this study suggest that if a reporter system, like overexpression of TfR-1 and/or Fth-1, is to be used as a means of tracking mMSC through MRI, then 2 mM of iron might be too high supplementation conditions, since it completely overloads these cells and does not allow the reporter gene influence to take place. On the other hand, control mMSCs (untransduced, dT and GFP) appear to retain a very high concentration of iron by

itself creating very significant hypointense regions. These results suggest that for short-term cell tracking studies, it could be possible to detect mMSC with MRI in the absence of a contrast agent or reporter gene as long as the cells have previously been cultured in medium supplemented with iron.

5.4 SUPPLEMENTARY DATA



Supplementary figure 3 – Representative differentiation pictures of Control, dT, GFP, dT_F, GFP_T and dT_F+GFP_T incubated with 0.2 mM of iron 24h post-transduction, along with a non-supplemented Control. Differentiation potential of these cells was directed towards the formation of osteocytes, adipocytes or chondrocytes (M&M, p.62).



Supplementary figure 4 – Representative western blot and correspondent total protein gels from Control, dT, GFP, ferritin heavy chain-1 (dT_F), transferrin receptor-1 (GFP_T) and dT_F+GFP_T transduced mMSC cells, iron supplemented since 24h after transduction. Orange rectangle highlights total TfR-1 (endogenous + viral, described as Total_T) protein expression, with a predicted molecular weight (MW) of 100 kDa; white rectangle corresponds to actin expression with 42 kDa and blue rectangle to Fth-1 (endogenous + viral, Total_F) with 21 kDa. Sometimes another band is detected when targeting Fth-1, which may correspond to a post-translational modification of this protein. Protein quantification was normalized using total protein gels and confirmed using actin as a reference protein (M&M, p. 57).

CHAPTER 6

MAGA AS A REPORTER GENE FOR MRI TRACKING OF CELLS

6.1 INTRODUCTION

MagA is a gene encoding for an iron transporter protein whose role in the formation of iron oxide crystals in magnetotactic bacteria has been extensively studied for many years, although no consensus exists on whether it is an essential gene for magnetosome formation (Nakamura *et al.*, 1995b; Uebe *et al.*, 2012).

6.1.1 MagA gene as an MRI reporter gene

MagA was first proposed as a possible MRI reporter gene in 2008. So far, only two research groups have explored its suitability as an MRI reporter.

In the first study performed by Zurkiya *et al.*, in 2008, MagA overexpression was conducted in a HEK 293FT cell line (Invitrogen, R700-07), and the authors concluded that the sole overexpression of MagA, a gene thought to be involved in the magnetosome formation, was sufficient to produce “magnetic nanoparticles” within the target cells (Figure 37), giving rise to a significant contrast in MRI (Zurkiya *et al.*, 2008).

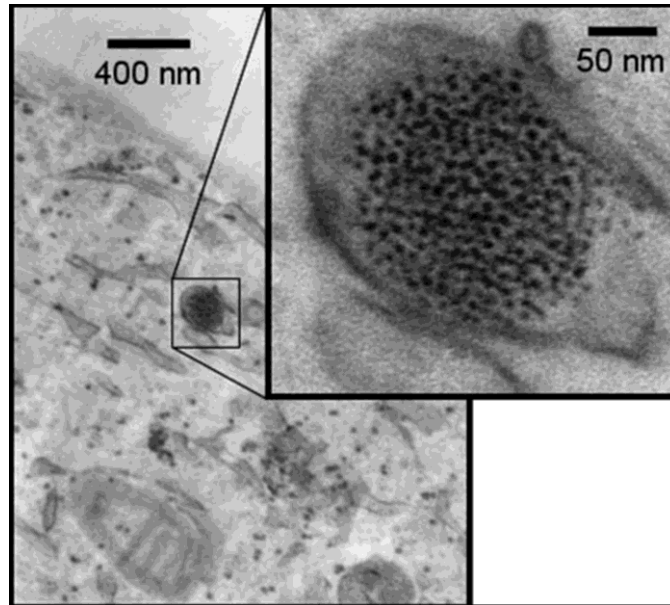


Figure 37 – Transmission electron microscopy (TEM) of HEK 293FT cells overexpressing MagA, where electron dense spots are visible (and highlighted in the inset) and have been suggested to correspond to iron oxide nanoparticles. Reproduced with [permission](#) from Zurkiya *et al.* (2008).

Furthermore, the authors characterized the produced nanoparticles and suggested that these consisted mainly of magnetite (Fe_3O_4), the same component found in iron oxide magnetosomes of *Magnetospirillum magneticum* AMB-1 bacteria (Zurkiya *et al.*, 2008). In contrast, another study showed that the MagA gene is not crucial for magnetosome synthesis and neither is part of MAI, the cluster of genes related to the organelle's formation and function (Uebe *et al.*, 2012). However, this does not exclude the fact that MagA is an iron transporter protein and could be used as a reporter gene, if it effectively aids in the accumulation of iron inside the cell.

Six years later, Zurkiya *et al.*, (2008) reported MagA inducible overexpression in mESC, controlled by a tetracycline (TET) response element. They observed an

increased contrast with MRI, and a longitudinal monitoring of engrafted stem cells was possible, but only when doxycycline (DOX) together with ferric citrate were supplemented *in vitro* (mESC in culture) or *in vivo* (mESC injected into mice). MagA expression did not appear to affect mESC pluripotency, but when assessing cell proliferation, there was a significant decrease in cell number of mESC-MagA when cells were exposed to high concentrations of DOX. This was not observed in control cells. In addition, cytotoxicity assays demonstrated that mESC-MagA were far more sensitive to the supplementation of DOX and ferric citrate than control cells. Nevertheless, this report was the first evidence of MagA being used as an MRI reporter for a stem cell line (Cho *et al.*, 2014).

Goldhawk and co-workers have also explored the possibility of using the MagA gene as an MRI reporter (Goldhawk *et al.*, 2009). Similarly to Zurkiya *et al.*, they report that MagA overexpression resulted in iron accumulation in mammalian cells, producing “magnetosome-like particles”. Initially, a mouse neuroblastoma (N2A) cell line was used and transfected with a native MagA gene and an inactivating mutant, MagA_{E137V}. Despite both conditions accumulating more intracellular iron than controls, in the MRI context, only cells expressing native MagA provided enough contrast for imaging. This report showed that overexpression of the MagA gene in this cell line did not adversely affect proliferation or viability (Goldhawk *et al.*, 2009). More recently, in 2014, another study using MagA was reported by the same group, using a human breast/melanoma (MDA-MB-435) cell line. The relaxivity of cells expressing MagA

was compared to cells expressing a modified ferritin system, comprising of both subunits with iron responsive elements removed to allow constitutive expression. In this report, the tumour cell line expressing each reporter gene was transplanted in a mouse model and tumour growth was followed using MRI. It was concluded that both reporters enhance MR contrast relative to controls, with comparable results (Rohani *et al.*, 2014). A second study involving the same experimental setup reported that both reporter systems increased the intracellular iron/zinc ratio by 20-fold when supplemented with iron but the expression of the transferrin receptor decreased by 10-fold (Sengupta *et al.*, 2014).

Here, MagA gene is evaluated to assess its potential as a reporter for MRI tracking of cells. The integration ability of MagA was initially evaluated in three stem cell lines (mESC, mMSC, mKSC) and HEK 293T(N), already described by Zurkiya *et al.* (2008), to serve as a control cell line. HEK 293T(N) cells were also evaluated alongside CHO K1 cells, which have not previously been used for this purpose. The following parameters were compared: MagA transgene integration stability over passages and when exposed to different iron concentrations; the influence of MagA overexpression in iron homeostasis; and finally, iron accumulation capacity and suitability as an MRI reporter.

6.2 RESULTS

6.2.1 Reporter gene integration in stem cell lines

mESC, mMSC and mKSC cell lines, as well as HEK 293T(N), were transduced with lentiviral particles encoding for dT or dT_M (MagA), MOI=1 to evaluate MagA integration capacity in diverse cell lines. dT condition was performed to serve as a control and dT_M to evaluate MagA gene as a potential magnetic reporter. Three independent transductions were carried out for each condition and represent, therefore, three biological replicates ($n=3$).

mESC (recently described in Cho *et al.* (2014)), mMSC and mKSC were transduced to evaluate MagA integration potential in a range of stem cells. HEK 293T(N) were also included to serve as a control cell line. RT-qPCR was used to evaluate dTomato/MagA gene expression over a period of 40 days. The cells were transduced at day 0 and RT-qPCR was performed at day 0 (before transduction), 2, 4, 6, 8 for all cell lines and at day 10, 20, 30 and 40 for HEK 293T(N) and mESC. Human/mouse TBP/Tbp and GAPDH/Gapdh genes were used as reference genes to normalize Ct values obtained for dTomato and MagA genes and results are shown in Figure 38.

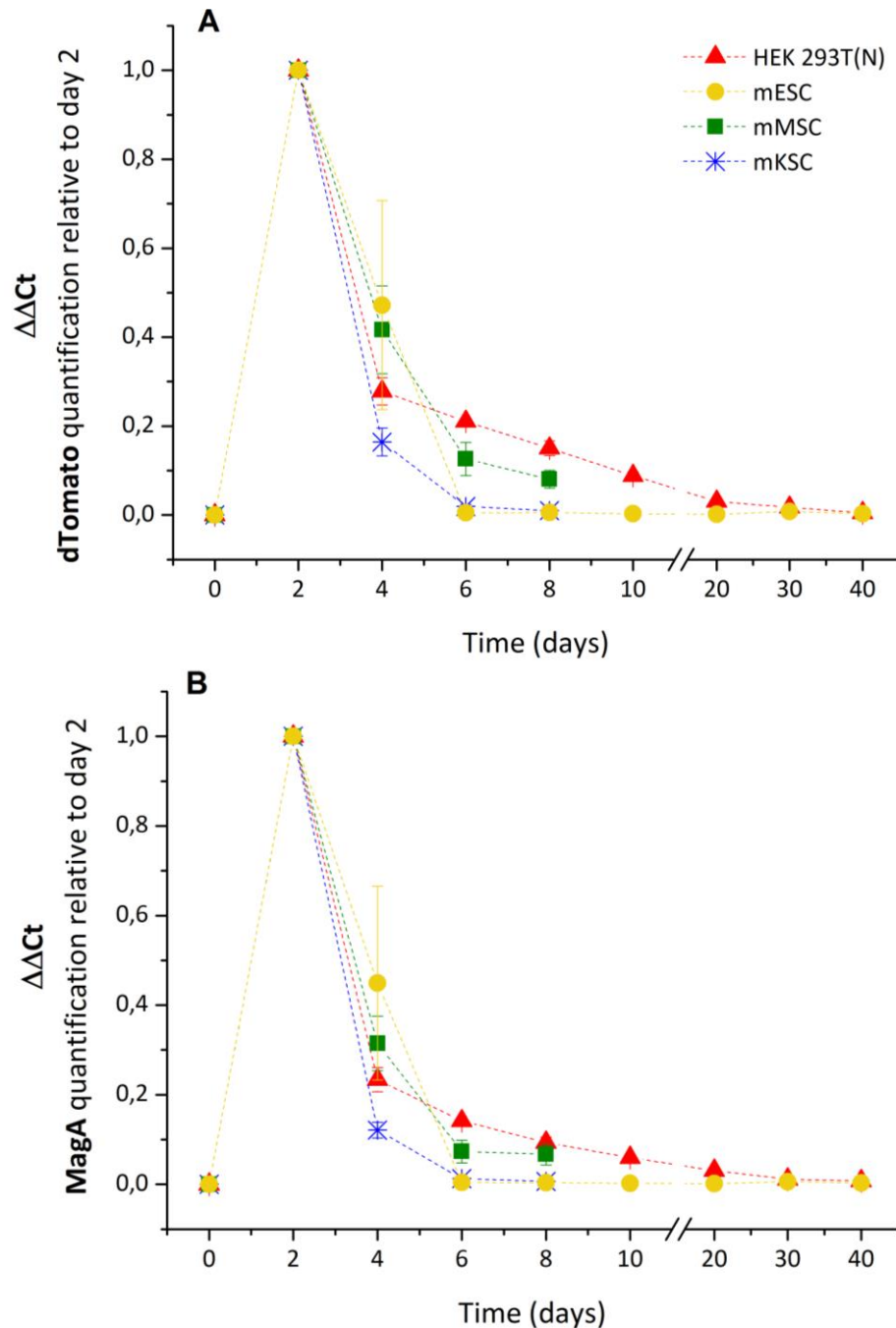


Figure 38 – RT-qPCR relative quantification of dTomato (**A**) and MagA (**B**) transgenes, evaluated in four dT_M transduced cell lines (MOI=1), including HEK 293T(N) as a reference, over a period of 40 days. Error bars represent SEM ($n=3$) (M&M, p.52).

It is possible to observe that both transgenes are transcribed at very similar levels throughout the course of the study period for all cell lines, suggesting that the bicistronic expression is effective. As expected, at day 0, no expression of the

studied genes was found, showing that mRNA expression of the test genes that was observed on all other days was due to the transduction of dT_M. At day 2, there is a peak of expression of both genes in all cell lines, which correlates with the initial appearance of red fluorescence, followed by a gradual decrease until the end of the analysis. Two cells lines, HEK 293T(N) and mESC, were able to maintain dTomato and MagA mRNA levels during a time-period of 40 days, even though slowly decreasing their expression. This has also been observed when cells were followed up daily using fluorescent microscopy to investigate expression of dT protein (results not shown). However, for the other two cell lines, mMSC and mKSC, the experiment was stopped at day 8 because these cells were mostly dead, although expression levels were detected in the very few remaining. This suggests that MagA might have a toxic effect on these cells, either by cell death or decreasing their proliferation potential. To confirm this hypothesis, cells were again transduced with dT or dT_M (MOI=1) and their viability was assessed over a period of 8 days (Figure 39).

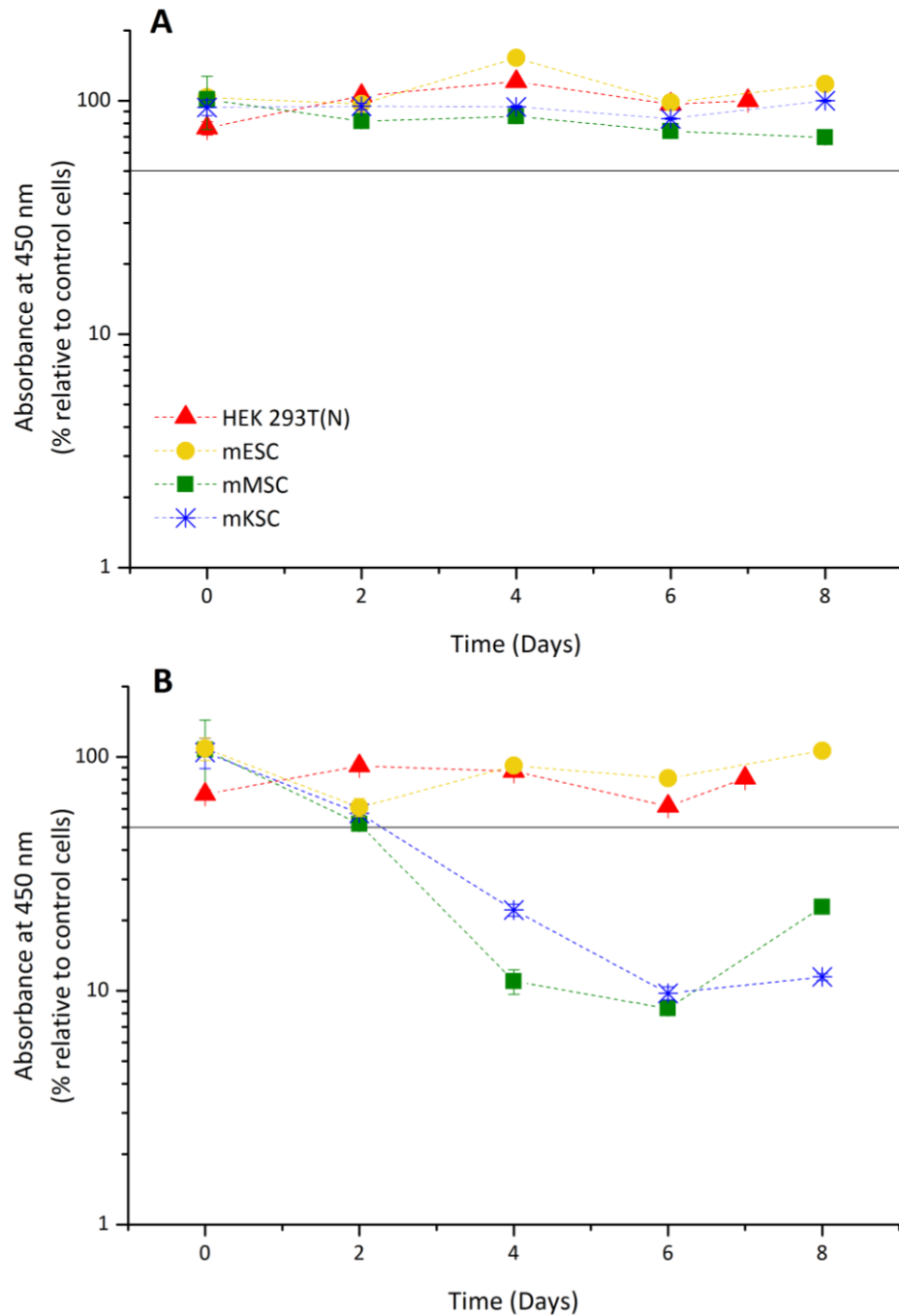


Figure 39 – Cell proliferation of HEK 293T(N), mESC, mMSC and mKSC during a period of 8 days after being transduced with dT (**A**) or dT_M (**B**) lentiviral constructs. Data points are plotted in relation to control cells. The threshold line represents 50% of cell counts. Error bars represent SEM ($n=3$) (M&M, p.62).

Figure 39 demonstrates that none of the cells have their viability or proliferation capacity impaired when transduced with dT. For dT_M transduced

cells, on the other hand, two cell lines, mMSC and mKSC, are not able to maintain proliferative capacity and fall to levels between 10-20% of controls. For this reason and together with the fact that mESC showed negligible levels of MagA expression from day 6 onwards (Figure 38), another cell line was evaluated for MagA integration potential, CHO K1.

6.2.2 Reporter gene integration in CHO K1 cell line

CHO K1 and HEK 293T(N) cells were transduced with dT or dT_M (MagA), with MOI=26 and MOI=5, respectively. Three independent transductions were carried out for each condition and represent, therefore, three biological replicates ($n=3$). MOIs were chosen in order to get a similar transgene expression level in both cell lines. Only HEK 293T(N) were possible to be FACS sorted for a high dTomato (and MagA) expressing population. FACS sorting in the same conditions was attempted on CHO K1 cells, but once these cells returned to *in vitro* culture conditions they failed to attach and did not survive.

Once transduction was performed, dTomato/MagA gene integration was initially evaluated in both cell lines using fluorescence microscopy (Figure 40) and flow cytometry (Figure 41), which allow the visualization and measurement of red fluorescence, derived from the dTomato gene.

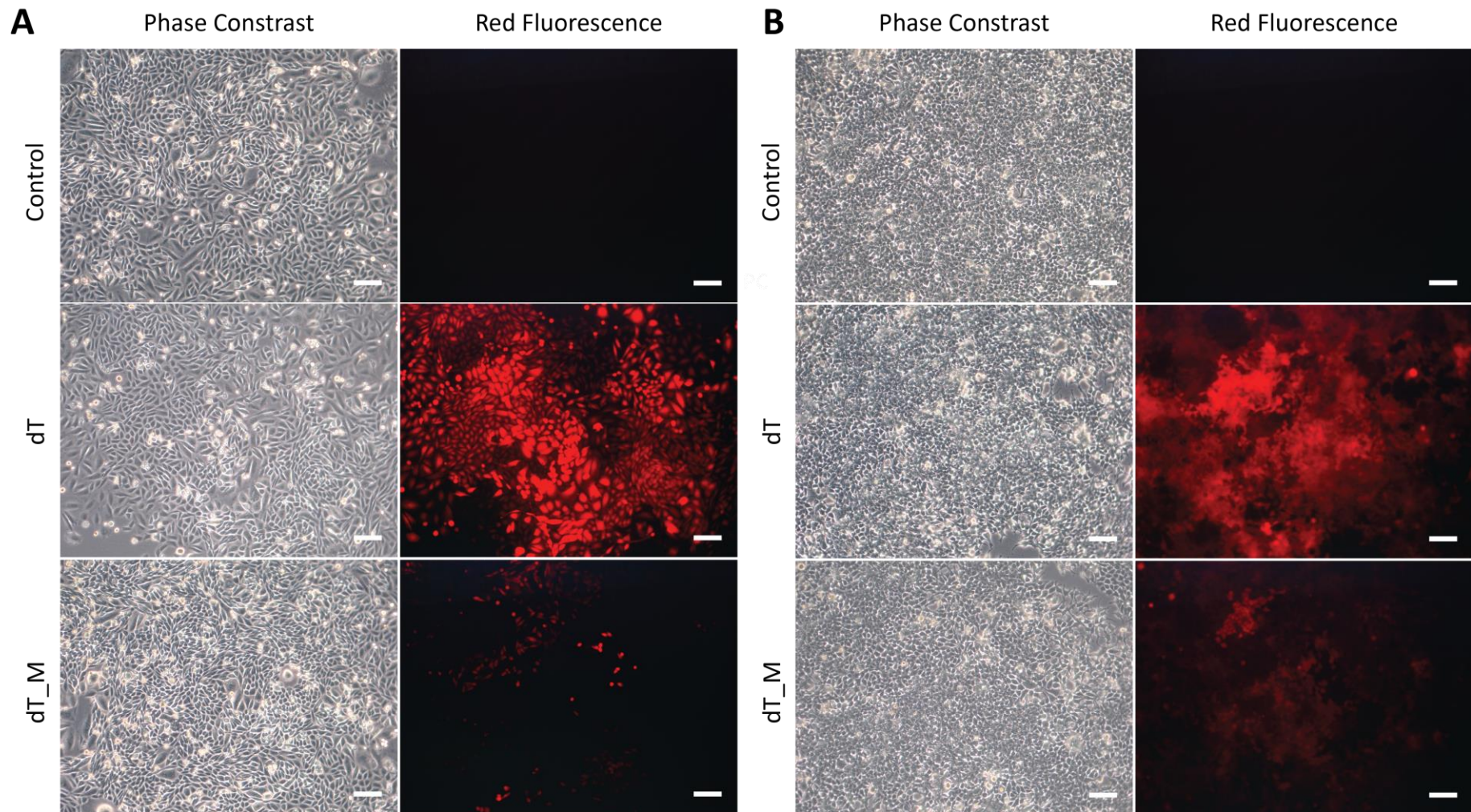


Figure 40 - Representative pictures of CHO K1 (A) and HEK 293T(N) (B) cells at P7 post-transduction, and Control cells (untransduced) at an equivalent passage. dT corresponds to dTomato transduced cells and dT_M to MagA transduced cells. All red fluorescent pictures were taken with the same exposure conditions. Scale bars correspond to 100 μm .

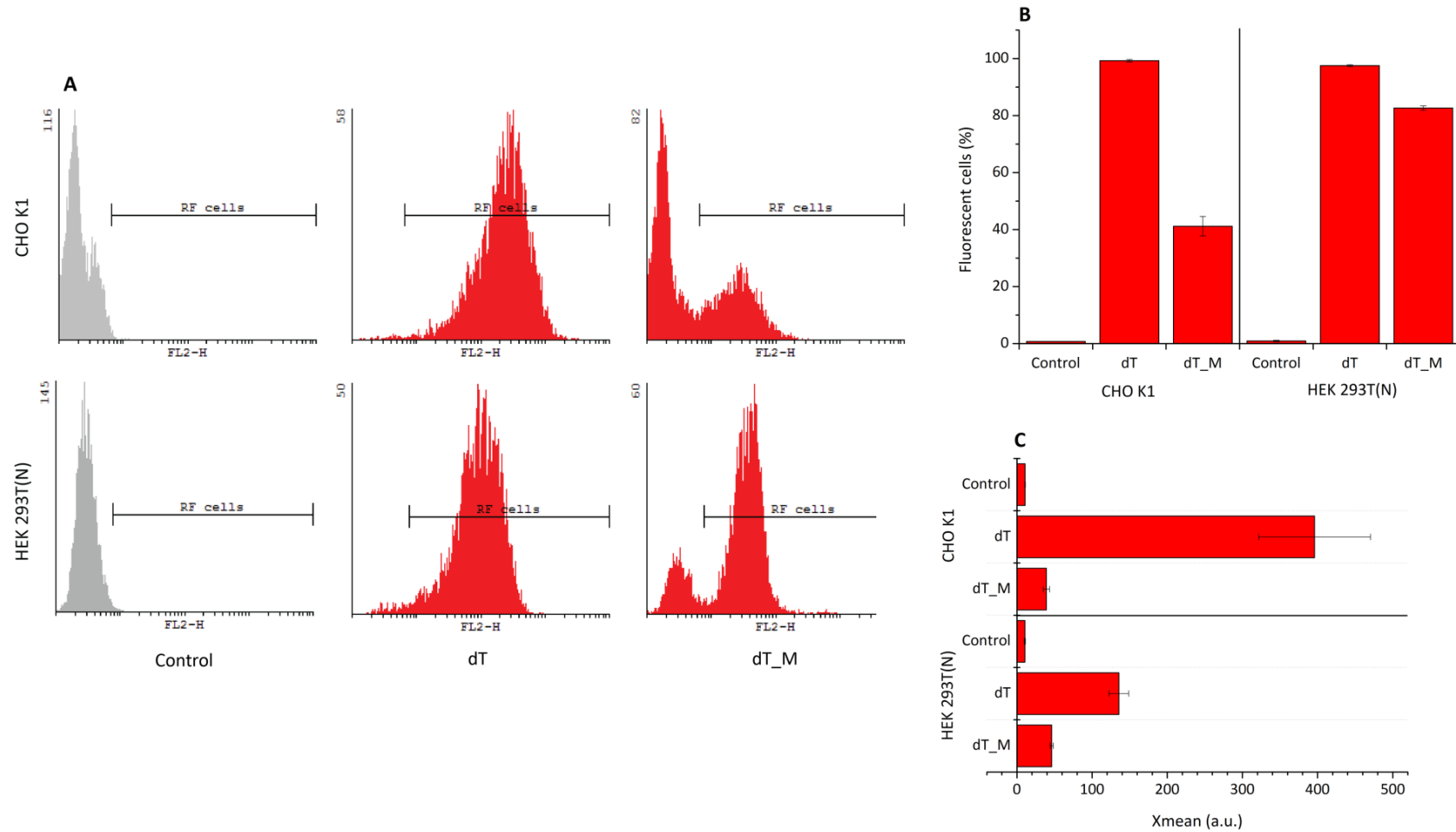


Figure 41 – Flow cytometry histograms (**A**) of CHO K1 and HEK 293T(N) cells, at P3 after transduction. Histograms show the number of events (cells) counted (y-axis) versus the fluorescence intensity (x-axis). Red fluorescence (RF) gate represents the dTomato-positive cell population plotted in (**B**). The Xmean (**C**) represents the mean fluorescence obtained from the gates region (RF cells). Error bars represent SEM ($n=3$). a.u.–arbitrary units; M&M, p.48.

Figure 40 and Figure 41 evaluate transgene expression, either by visualization or measurement of the red fluorescent cells. From these results it is clear that in relation to dT_M, transduction with dT results in a larger population of positive cells, which also tend to be brighter. The MOIs of 26 and 5 for CHO K1 and HEK 293T(N), respectively, were chosen in order for the cells to be comparable between each other. However, even though dT cells similarly express red fluorescence reaching almost 100% for both cell lines, the same is not true for dT_M, which is only expressed in about 40% of CHO K1, while in HEK 293T(N) cells, around 80% are positive (Figure 41, **B**). This difference probably has to do with the fact that HEK 293T(N) were sorted at P2 and CHO K1 cells were not, due to lack of cell survival, leading to a more diluted positive population. Also in this figure, the Xmean plot (Figure 41, **C**), which represents the cell's fluorescence intensity, shows that in case of HEK 293T(N) cells, although the difference in the percentage of positive cells between dT and dT_M is only 20%, the brightness of the dT cells is much more intense than the dT_M cells. The same point is even more evident in the case of CHO K1 cells. Nevertheless, even though only half of CHO K1 cells are transduced with dT_M when compared with HEK 293T(N) cells, both have approximately the same fluorescence intensity (Xmean). This suggests that the dT_M positive population of both cell lines may be expressing dTomato/MagA genes at the same level at this point.

To understand if the transgene expression levels in dT_M cells were stable over passages, mRNA from CHO K1 and HEK 293T(N) cells was quantitatively

evaluated by RT-qPCR at P1 and P3 after transduction. This is a direct and quantitative measurement of the transgene expression and it is shown in Figure 42. Pabpn1 and Vezt genes were used as a reference for CHO K1 cells and TBP and GAPDH genes were used as a reference for HEK 293T(N) cells.

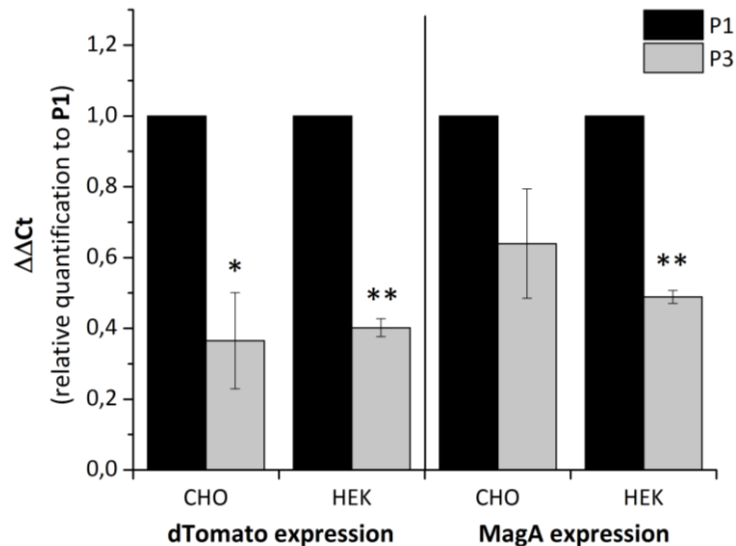


Figure 42 – RT-qPCR relative quantification of dTomato and MagA transgene expression at P1 and P3 in dT_M transduced CHO K1 cells or HEK 293T(N). For the evaluation of transgene expression over two passages, HEK 293T(N) cells were not FACS sorted. Expression values are plotted against P1. Error bars represent SEM ($n=3$) (M&M, p.52).

As seen in Figure 42, for both cell lines, the expression of integrated genes decreases from P1 to P3. Also, both transgenes appear to decrease in the same ratio, which indicates the effectiveness of the bicistronic expression system.

As previously done for stem cells, the viability was assessed for CHO K1 cells transduced with either dT or dT_M in two different time points, exactly 8 days after transduction (designated as P1) and three passages afterwards (P4). Results are displayed in Figure 43.

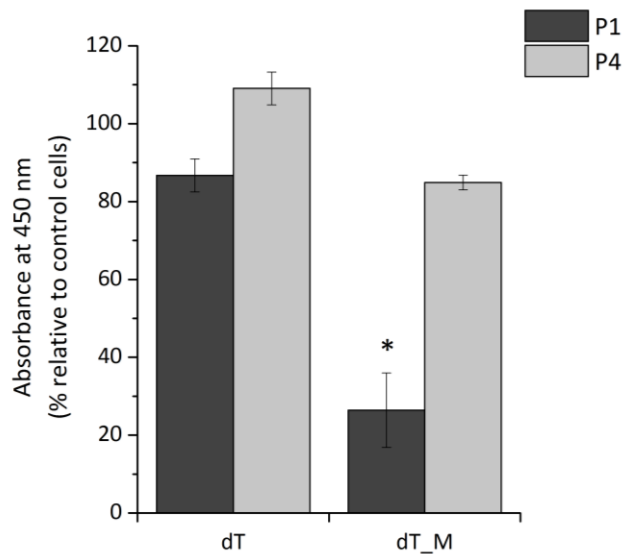


Figure 43 – Proliferation assay on dT and dT_M transduced CHO K1 cells at P1 and P4. Data points are plotted in relation to Control (untransduced) cells. Error bars represent SEM ($n=3$). A statistical difference is found in dT_M (P1) cells when compared to Control and dT cells of the same passage (M&M, p.62).

Figure 43 shows a higher sensitivity of CHO K1 to dT_M than dT overexpression when compared to Control cells at P1, which is reflected by a lower absorbance of 30% in respect to untransduced controls. However, by P4, dT_M cells have recovered and returned to the proliferation capacity equivalent to Control and dT cells, which is possibly due to the decrease of MagA expression, as seen in Figure 42.

6.2.3 Iron homeostasis

To understand if the transgenes had an effect on cellular iron homeostasis, the expression of transferrin receptor-1 and ferritin heavy chain-1, which are known to be involved in this balanced pathway, were explored. To do this, Control, dT and dT_M cells were exposed to two iron concentrations of 0.2 and 2 mM alongside a non-supplemented Control (0 mM) for a period of 4 days. Transferrin receptor-1

(Total_T) and ferritin heavy chain-1 (Total_F) were evaluated at the mRNA level by RT-qPCR (Figure 44 **A, C** and Figure 45 **A, C**) and at protein level by WB (Figure 44 **B, D**, Figure 45 **B, D** and Supplementary figure 5). For RT-qPCR amplification, the reference genes used were the same as described previously. For WB detection, actin and total protein gels were used for data normalization.

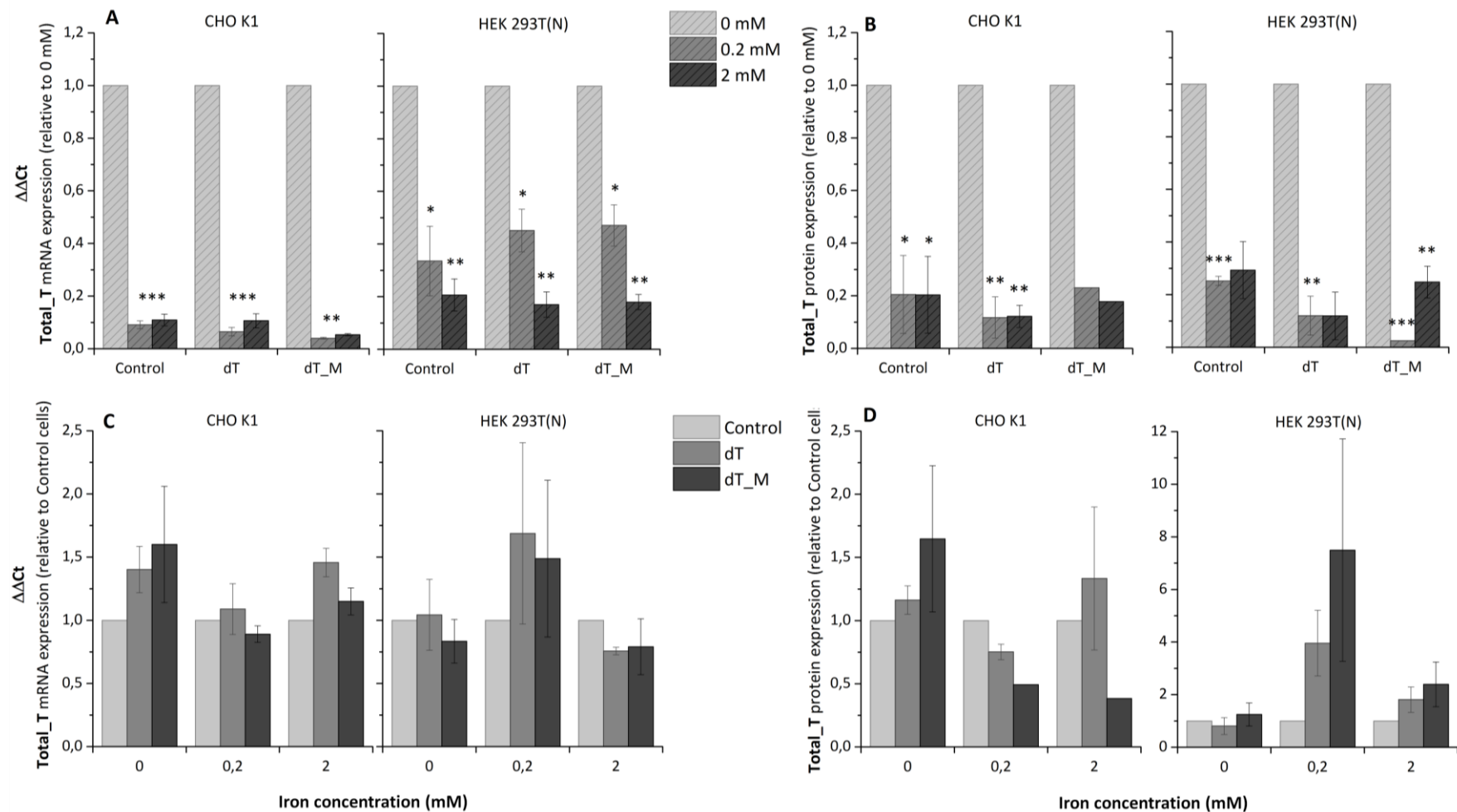


Figure 44 – Relative quantification of transferrin receptor-1 (Total_T) expression obtained via RT-qPCR (**A** and **C**) and the respective protein levels as obtained via WB (**B** and **D**), when Control, dTomato (dT) and MagA (dT_M) transduced cells were exposed to different iron concentrations of 0, 0.2 and 2 mM (Iron supplementation, p.50). Graphs **A** and **B** evaluate Total_T expression levels when each cell line is exposed to different iron concentrations and graphs **C** and **D** the difference between cell lines when exposed to the same iron concentration. Error bars represent SEM ($n=3$) (M&M, p.52 for RT-qPCR and p.57 for WB).

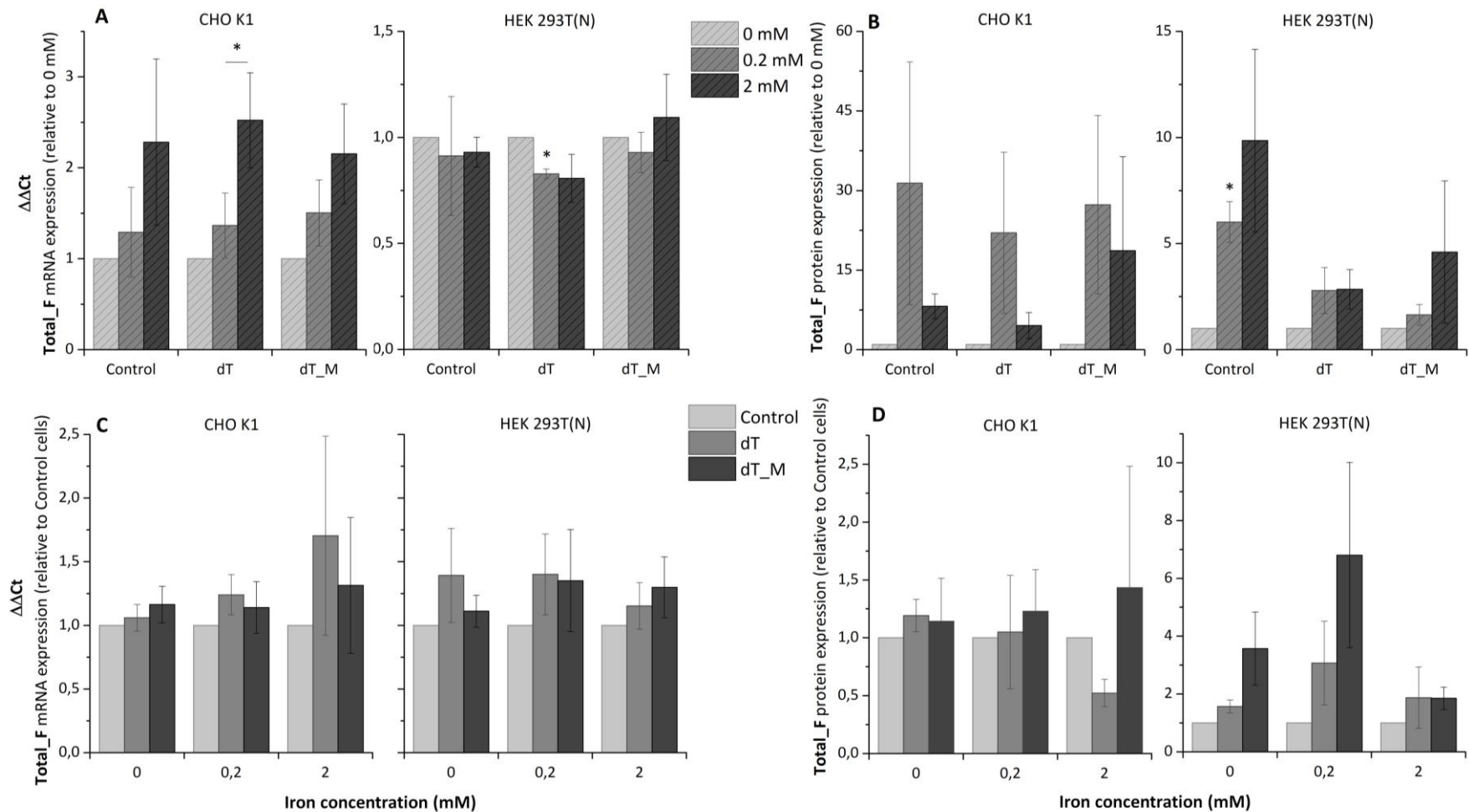


Figure 45 – Relative quantification of ferritin heavy chain1 (Total_F) expression obtained via RT-qPCR (**A** and **C**) and the respective protein levels as obtained via WB (**B** and **D**), when Control, dTomato (dT) and MagA (dT_M) transduced cells were exposed to different iron concentrations of 0, 0.2 and 2 mM ((Iron supplementation, p.50)). Graphs **A** and **B** evaluate Total_F expression levels when each cell line is exposed to different iron concentrations and graphs **C** and **D** the difference between cell lines when exposed to the same iron concentration. Error bars represent SEM ($n=3$); (M&M, p.52 for RT-qPCR and p.57 for WB).

Figure 44 shows the Total_T expression in two different scenarios, *i.e.*, how transferrin receptors-1 levels change in response to differences in iron concentration within each cell type (**A** and **B**) and to different transgenes at a specific iron concentration (**C** and **D**). For the effect of iron concentration, the results obtained with mRNA (**A**) and protein (**B**) quantification show a regular pattern for all cell lines in the study, where a statistically significant decrease in the expression of Total_T is observed with increasing of iron concentrations, relative to a non-supplemented control. This is an expected result when the IRP/IRE regulatory system is considered; that is, an influx of iron should result in reduced expression of the transferrin receptor-1 (Figure 1). In the second part, to know if the transgenes influence Total_T at a set iron concentration, mRNA expression (**C**) and protein quantification (**D**) graphs show that there is no statistically significant differences between the different cell types (Control, dT and dT_M). However, although not statistically significant, dT and dT_M HEK 293T(N) cells have an increase in Total_T expression at 0.2 mM (relative to Control cells), both at the mRNA and protein level. More interestingly, for dT_M CHO K1 cells, when there is no iron present (0 mM), Total_T appears to have an up-regulation when compared to Control and dT, both at the mRNA and protein level. Once iron is introduced (0.2 and 2 mM), even though the mRNA is relatively stable between the different samples, at the protein level, Total_T expression is down-regulated for dT_M (comparatively to Control and dT), although those differences are not statistically significant. One hypothesis for these observations is that MagA might be acting like an iron transporter, possibly

introducing more iron inside the cell, and therefore, further down-regulating Total_T expression levels.

Figure 45 evaluates Total_F, or ferritin heavy chain-1, expression levels under the same conditions. In contrast to the results observed regarding the transferrin receptor-1, the opposite trend in Total_F expression would be expected when the IRP/IRE regulatory system is considered. Panels **A** and **B** show an up-regulation of Total_F with increasing iron concentrations in all cell types, particularly at the protein level (relative to 0 mM). For the CHO K1 cells, an increase in Total_F expression is found at the mRNA level, in particular when iron is present at high concentrations (2 mM). Interestingly, at the mRNA level, HEK 293T(N) cells do not display an increase in Total_F expression and this may be explained by the readily available mRNA being translated into protein. At the protein level, both 0.2 and 2 mM of iron increase Total_F expression in each cell line, reaching up to 5 to 30-fold increase relative to a non-supplemented control. Finally, graphs **C** and **D** demonstrate if transgenes have some influence over Total_F expression. At the mRNA level, there is no evidence that dT or dT_M play a role when compared to Control cells, either for CHO K1 or HEK 293T(N). However, in HEK 293T(N) cells at the protein level, an up-regulation of Total_F expression is observed in dT_M cells, predominantly at low iron concentrations (0 and 0.2 mM).

6.2.4 Reporter gene stability with iron supplementation

To assess the effect of iron supplementation on the integration stability of dTomato and MagA transgenes, Control, dT and dT_M cells were exposed to iron

concentrations of 0, 0.2 and 2 mM for a period of 4 days. dTomato and MagA expression levels were then quantitatively measured by RT-qPCR and are displayed in Figure 46. The reference genes used here were the same as previously described for those cell lines.

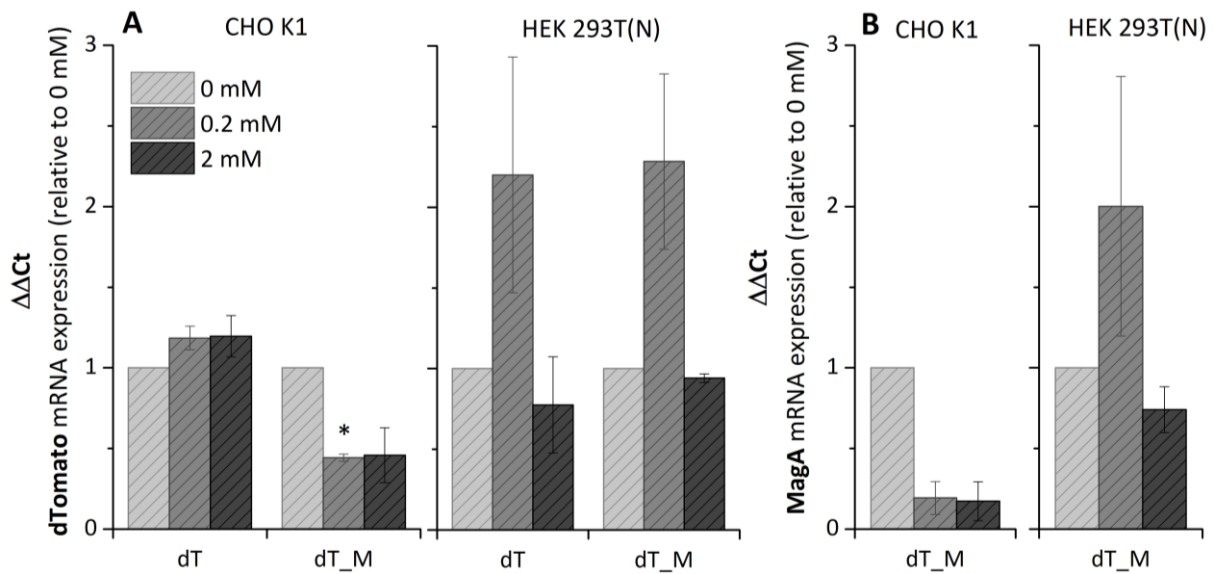


Figure 46 – RT-qPCR relative quantification of transgenes dTomato (**A**) and MagA (**B**) when dTomato (dT) and MagA (dT_M) transduced cells were exposed to 0, 0.2 or 2 mM of iron. Error bars represent SEM ($n=3$) (M&M, p.52).

It was expected that dTomato and MagA expression would be stable in the presence of increasing iron concentrations. However, the results presented in Figure 46 demonstrate that for CHO K1 cells, dTomato expression in dT transduced cells was relatively stable, but in dT_M cells, there was statistically significant down-regulation of dTomato as well as MagA expression in the presence of 0.2 mM of iron. Similar results were obtained with CHO K1 cells when exposed to ten times more iron, but these results were not statistically significant. On the other hand, HEK 293T(N) cells appeared to up-regulate MagA (and dTomato) in the presence of

0.2 mM iron, with both dT and dT_M cells following the same trend. This suggests that the two MagA transduced cell lines react differently when exposed to iron.

6.2.5 Intracellular Iron Uptake *in vitro*

In the next experiments, the ability of dT_M cells to incorporate more iron than controls (Control, dT) was explored. To this end, the intracellular iron content of Control, dT and dT_M CHO K1 and HEK 293T(N) cells was measured in non-supplemented cells as well as in cells supplemented with 0.2 and 2 mM of iron. Results are displayed in Figure 47 where the intracellular amount of iron is plotted as a function of iron supplementation.

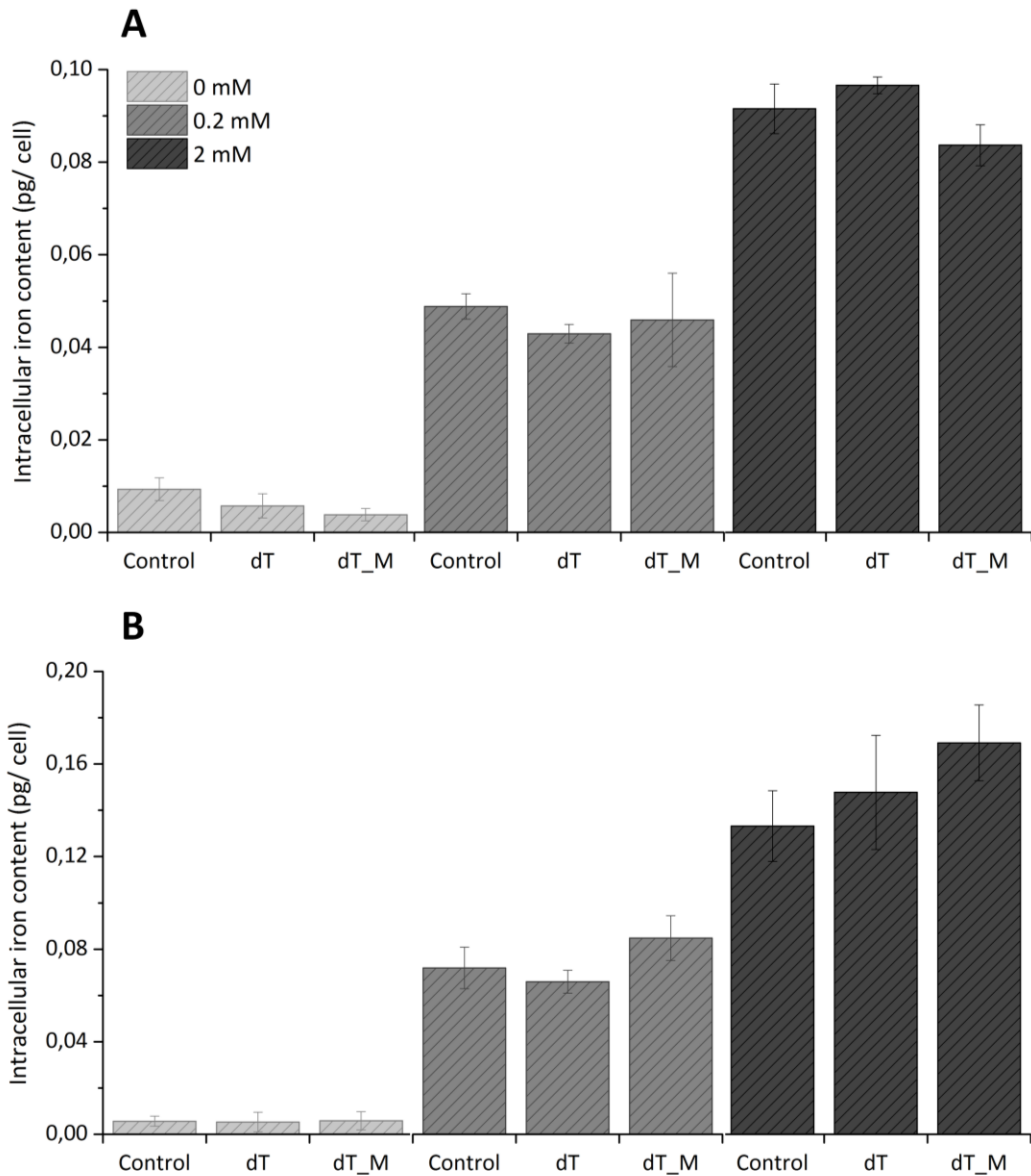


Figure 47 – Intracellular iron content of CHO K1 (**A**) and HEK 293T(N) (**B**) cells determined with the Ferrozine assay. Control, dTomato (dT) and MagA (dT_M) transduced cells were supplemented with different iron concentrations of 0, 0.2 and 2 mM for 4 days prior to measurement (Iron supplementation, p.50). Error bars represent SEM ($n=3$) (M&M, p.50).

Graphs in Figure 47 show that in relation to CHO K1 cells, HEK 293T(N) cells have double the capacity to incorporate intracellular iron. At 0.2 mM of iron, for example, intracellular amounts can reach around 0.08 pg/cell for this cell line whilst CHO K1, at the same iron concentration, only incorporates about 0.04 pg/cell. In

terms of iron accumulation between Control and transduced cells, the results show that the expression of MagA in CHO K1 did not lead to an increase in intracellular iron; in fact, in the presence of 2mM iron, a small decrease was observed relative to Control and dT cells, though this was not significant. On the other hand, dT_M HEK 293T(N) cells have slightly higher levels of intracellular iron than controls (Control, dT) when cultured in the presence of 0.2 and 2 mM iron, but the differences are not statistically significant.

To confirm the iron content in HEK 293T(N) cells, DAB-enhanced Prussian blue staining was performed on the different types of samples, in the presence of 0, 0.2 and 2 mM of iron supplementation. Prussian blue forms a dark blue pigment in the presence of iron (Ludi, 1981), the intensity of which can be enhanced by DAB, resulting in the formation of a dark brown pigmentation. The results are displayed in Figure 48 in grey scale to facilitate comparison between conditions.

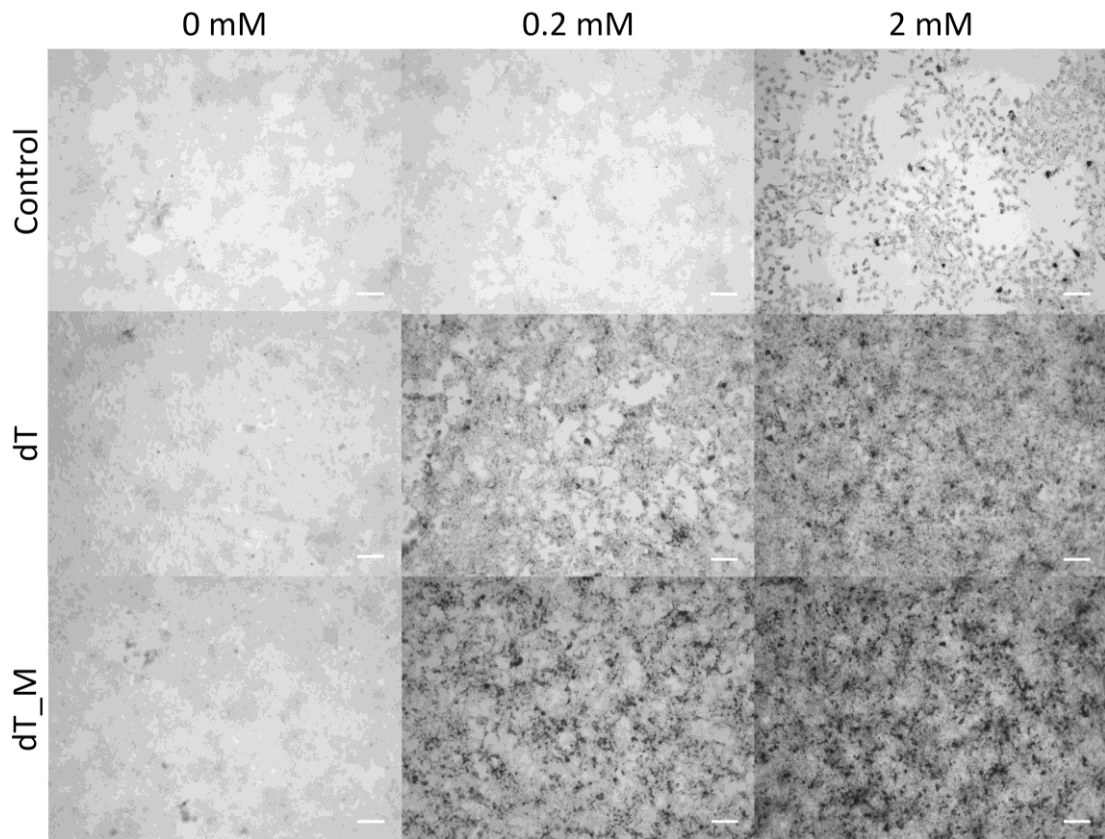


Figure 48 – Prussian blue and DAB staining of HEK 293T(N) Control, dTomato (dT) and MagA (dT_M) cells exposed to different iron concentrations of 0, 0.2 and 2 mM (Iron supplementation, p.50), M&M, p.51.

The data in Figure 48 show the same trend as seen with the Ferrozine assay for intracellular iron determination; that is, cells with no iron supplementation have negligible iron staining and the staining intensity rises with increasing iron concentrations. Also, as seen with the Ferrozine assay dT_M cells cultured in the presence of 0.2 and 2 mM iron appear to have higher levels of intracellular iron when compared to controls (Control, dT). On the other hand, the staining in Control at 0.2 mM is less intense than expected, according to the data in Figure 47, where it should be around the same level of intracellular iron as dT 0.2 mM and instead it seems not much different than Control without any supplementation of iron.

Since MagA might be a suitable MRI reporter only for HEK 293T(N), next it was investigated if, as stated by Zurkiya *et al.* (2008) and Goldhawk *et al.* (2009), the overexpression of MagA did in fact lead to the production of magnetic nanoparticle-like structures. For this, dT_M and dT cells supplemented with 0.2 mM of iron for four days, along with a non-supplemented control (Control in 0mM) were analysed via TEM.

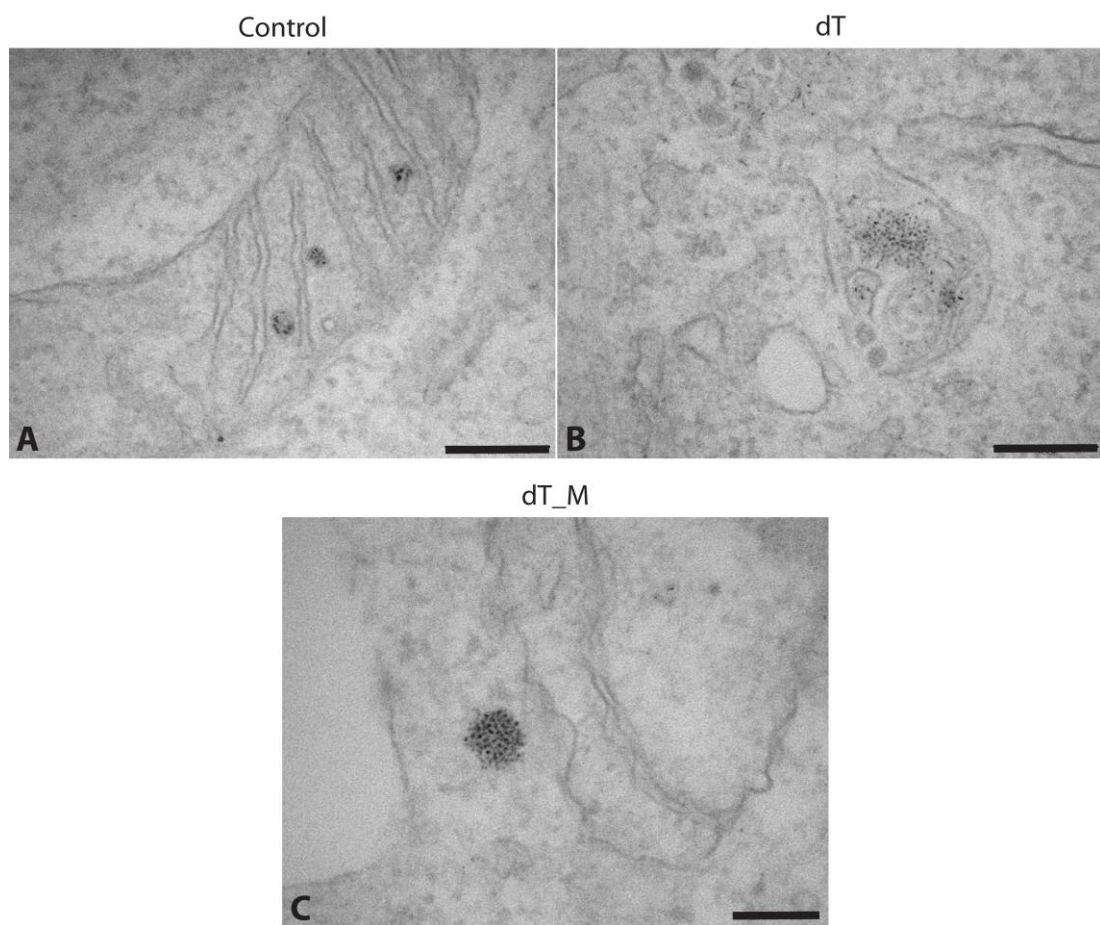


Figure 49 – Electron microscopy images of HEK 293T(N) cells. **(A)** Control cells exposed to no iron supplementation and **(B)** dTomato (dT) and **(C)** MagA (dT_M) transduced cells supplemented with 0.2 mM of iron. Electron dense spots in **A** inside mitochondria and **B** and **C** are found in the cytoplasm. Scale bars: 200 nm; M&M, p.61.

Figure 49 displays representative pictures showing the presence of electron dense spots similar to those observed by Zurkiya *et al.* (2008) (*c.f.* Figure 37), although it is not possible to assess whether they correspond to iron or other electron dense structures. These spots were observed in all conditions tested either inside mitochondria (Figure 49, **A**) and/or spread in the cytoplasm (Figure 49, **B** and **C**). The approximate size of each electron dense spot was between 5 and 8 nm, which is closely related to the average inner diameter of ferritin (8 nm), suggesting that the observed dark spots might be due to normal ferritins within a cell. With this method, no clear difference was seen between samples.

6.2.6 MRI

For MRI studies, transduced cells (dT and dT_M) supplemented with 0.2 and 2 mM of iron, along with a non-supplemented control, were scanned using T2-weighted sequences. For this purpose, 10^7 cells were centrifuged at high speed to form a compact cell pellet and imaged via MR, where T1/T2 maps were produced for relaxivity measurements (Figure 50).

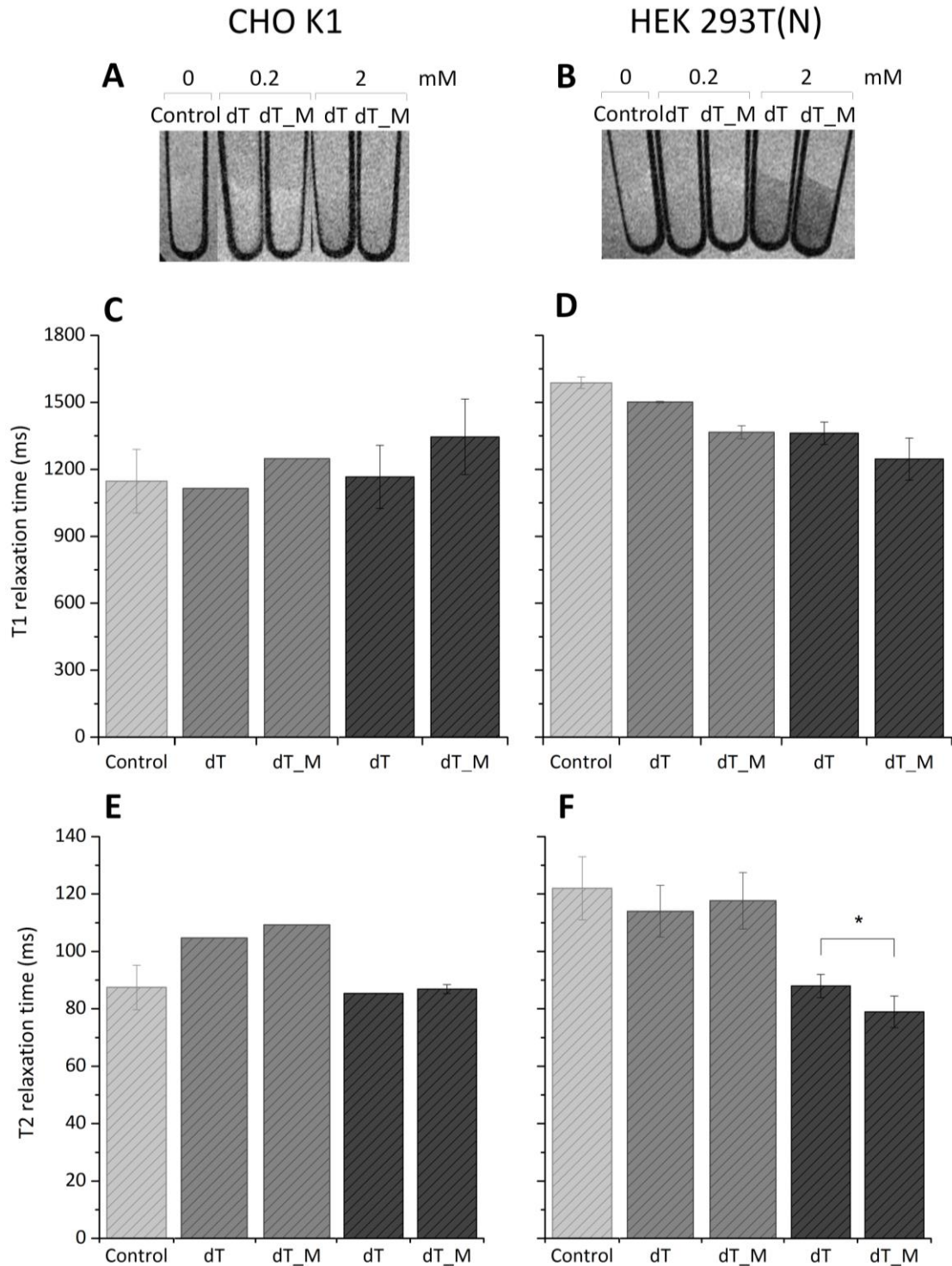


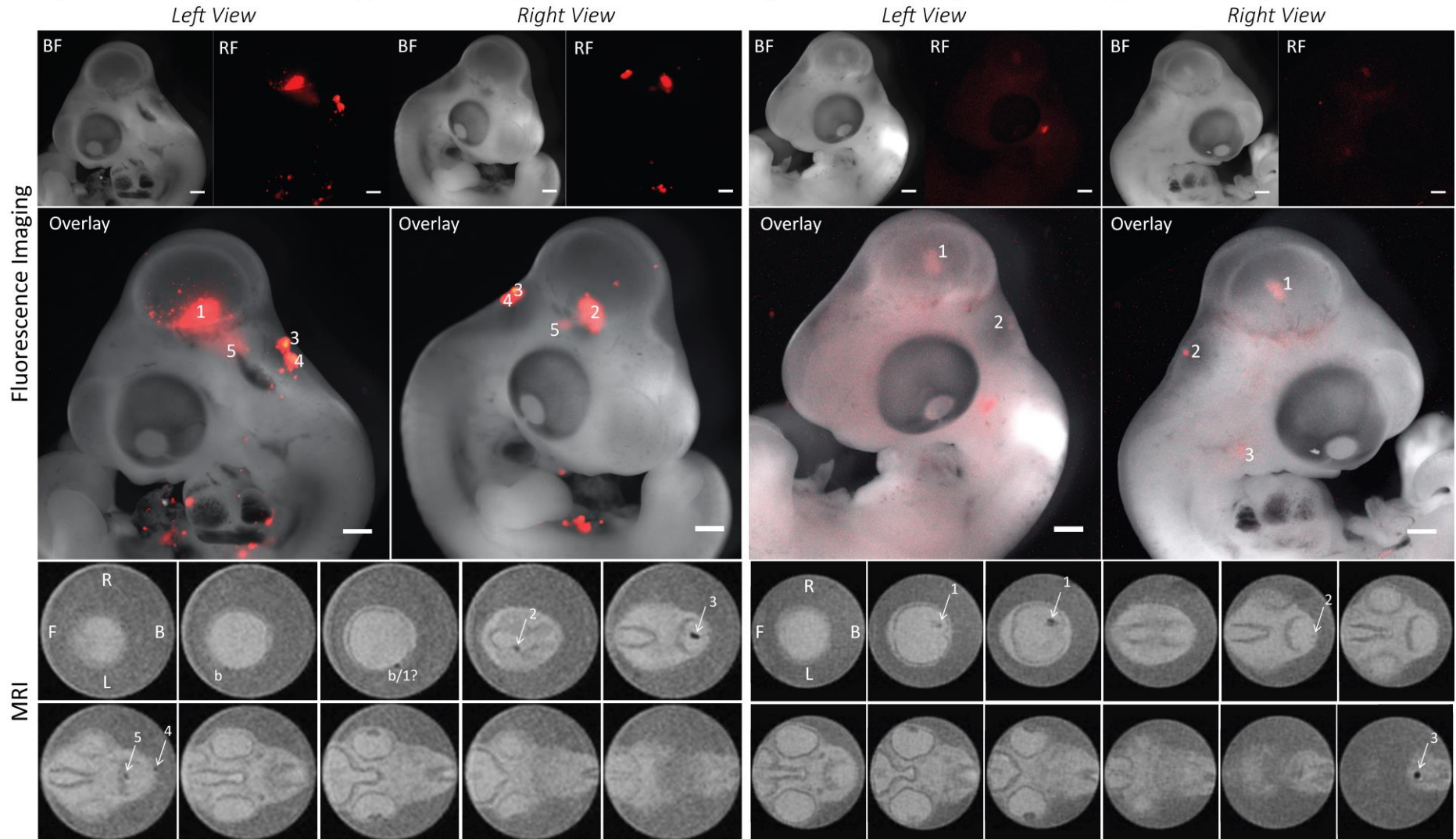
Figure 50 – MR imaging of cell pellets of CHO K1 (**A,C** and **E**) and HEK 293T(N) (**B, D** and **F**) cells. **A** and **B** are T2-weighted representative MR images obtained with MRI of Control with no iron supplementation (0 mM), dTomato (dT) and MagA (dT_M) both supplemented with 0.2 and 2 mM of iron (Iron supplementation, p.50). Relaxation times T1 and T2 were quantified on a specific region of the cell pellet and represented in **C-D** and **E-F**, respectively. Error bars represent SEM ($n=3$) (M&M, p.65).

Figure 50 shows that only dT_M transduced HEK 293T(N) cells were able to produce a statistically significant ($p=0,046$) T2 shortening effect (graph **F**) with 2 mM iron supplementation, when compared to its equivalent control (dT at 2 mM). This also can be perceptible in MRI image **B**, where dT_M at 2 mM is slightly darker than all other conditions. The same is not true for CHO K1 cells, in which there are no significant differences between dT_M and its controls.

Then, 2×10^5 dT and dT_M cells were microinjected into the midbrain of the chick embryo at embryonic day 3 (E3). Both cell types were either incubated in normal cell culture conditions (0 mM) or supplemented with 2 mM of iron for 3 days prior to injection. At E5, embryos were imaged with two complementary platforms: by fluorescence microscopy to detect red fluorescence derived from the dTomato gene, and by MRI transversal imaging, by observing electrodense spots derived from iron accumulation in transduced cells, which was influenced by extracellular iron supplementation or possibly due to MagA expression. Results are displayed in Figure 51.

C) CHO K1 - dT (2 mM iron supplementation)

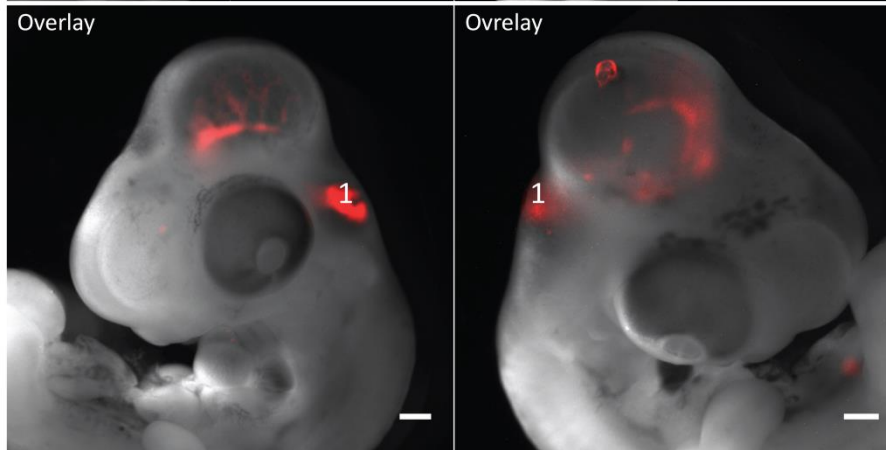
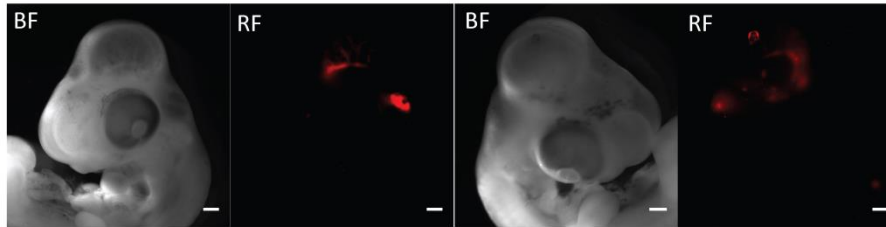
D) CHO K1 - dT_M (2 mM iron supplementation)



E) HEK 293T(N) - dT (0 mM iron supplementation)

Left View

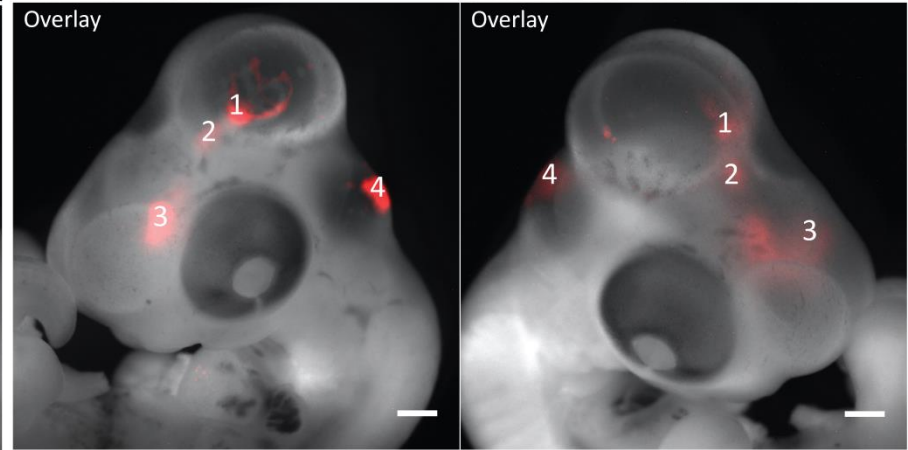
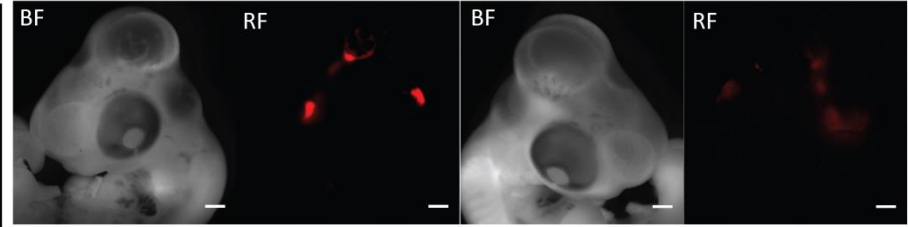
Right View



F) HEK 293T(N) - dT_M (0 mM iron supplementation)

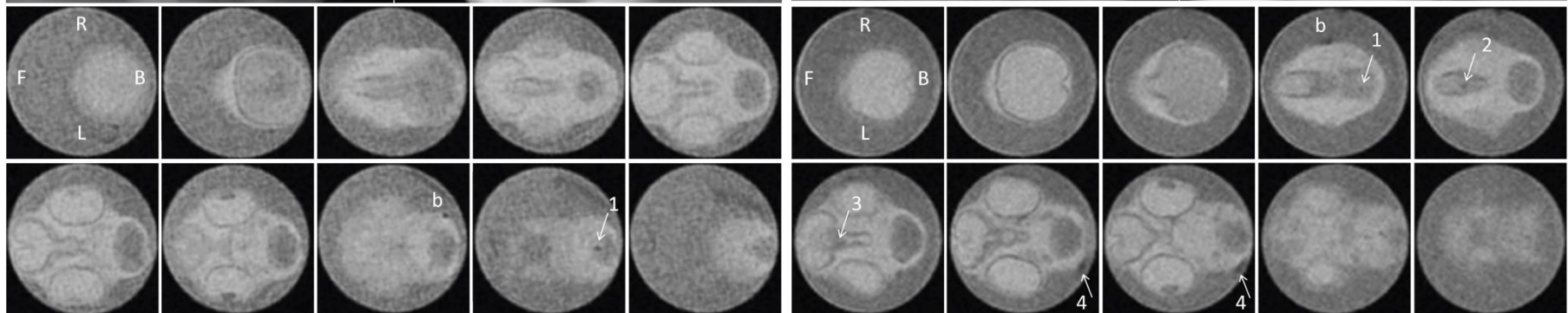
Left View

Right View



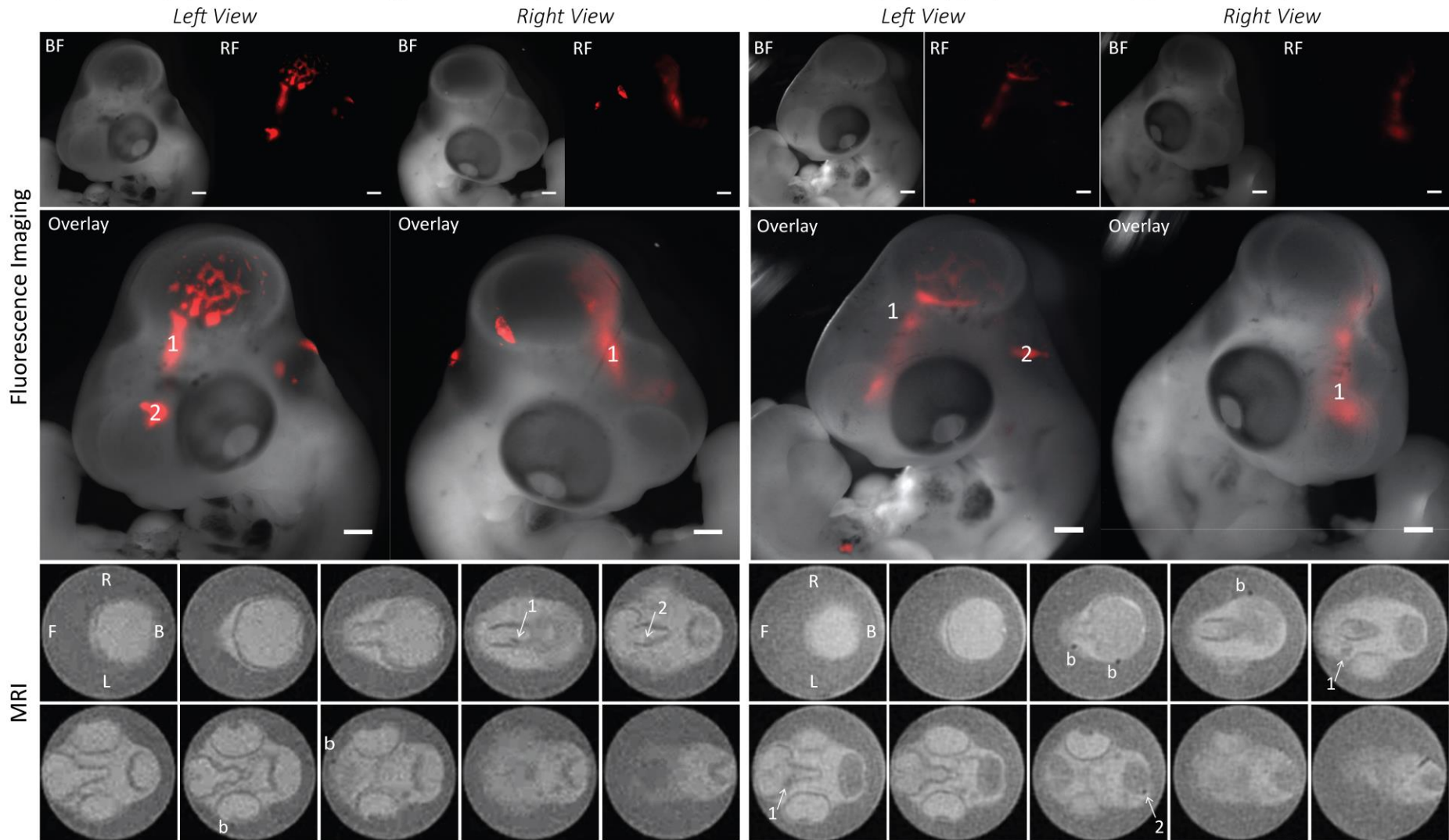
Fluorescence Imaging

MRI



G) HEK 293T(N) - dT (2 mM iron supplementation)

H) HEK 293T(N) - dT_M (2 mM iron supplementation)



Fluorescence Microscopy				MRI		
Cell type	Iron conc.	Transduction condition	Biological rep. (technical rep.)	Iron conc.	Transduction condition	Biological rep. (technical rep.)
CHO K1	0 mM	dT	n=2 (5)	0 mM	dT	n=2 (2)
		dT_M	n=2 (2)		dT_M	n=2 (2)
	2 mM	dT	n=2 (6)	2 mM	dT	n=1 (2)
		dT_M	n=2 (4)		dT_M	n=2 (2)
HEK 293T(N)	0 mM	dT	n=2 (3)	0 mM	dT	n=2 (3)
		dT_M	n=3 (5)		dT_M	n=1 (3)
	2 mM	dT	n=2 (4)	2 mM	dT	n=2 (3)
		dT_M	n=3 (7)		dT_M	n=2 (3)

Figure 51 – Fluorescence and MR imaging in CHO K1 (A, B, C and D) and HEK 293T(N) (E, F, G and H) cells, 2 days after injection in the midbrain of a chick embryo (E5). dTomato (dT) and MagA (dT_M) cells were injected with or without iron supplementation (2 mM of iron for 3 days) (Iron supplementation, p.50). In the fluorescence imaging panel, bright field (BF) and red fluorescence (RF) are projection images from the whole embryo; overlays are presented for both left and right views and were used as a reference guidance for MR imaging; scale bars correspond to 1 mm. In the MRI panel, anatomical images are displayed as transverse sections along the rostrocaudal axis of the embryo (left to right); 10 sections are displayed for each embryo, with the exception of D which has 12 images, to visualize the signal at the bottom of the neck. All images are representative from the results obtained and were equally processed with ImageJ software. Arrows indicate T2 shortening effect; b – bubble of air. Position of the embryo: F – front; B – back; R – right; L – left; number of biological and technical replicates is indicated in the table above (M&M, p.65).

To identify if transduced cells integrated into chick embryo's brain, first, bright field and fluorescence imaging were performed on whole embryos. Due to the presence of fluorescent reporters, transduced cell clusters were easily identified and located within the brain. This served as a guideline to identify hypointense cell clusters with MR imaging. Without this support, identifying cell clusters based only on anatomical images would have proven to be much more difficult.

The fluorescence imaging panel in Figure 51 suggests that CHO K1 and HEK 293T(N) cells behave differently when introduced into the brain of the chick embryo. While CHO K1 cells appear to preferentially form clusters, HEK 293T(N)

cells appear to spread and engraft in several locations within the embryo. Transduced cells are also located in different regions apart from the brain, as seen in Figure 51, panel **C**. This might be due to either migration of cells to other parts of the body or more likely to the “leakage” of cells into the amniotic sac while injecting into the ventricle cavity, having then attached to the surface of the embryo.

On what concerns the actual contrast obtained from the cells, in the case of CHO K1 (Figure 51, **A**, **B**, **C** and **D**), since the intracellular iron content results were not very promising, only two biological replicates were imaged for each condition. Comparing dT and dT_M cells exposed to the same iron concentration (0 or 2 mM), there does not appear to be any difference between control cells and those expressing MagA. Surprisingly, it was possible to detect hypointense regions corresponding to the location of fluorescent cells in embryos injected with cells that had been cultured in the absence of iron (panels **A** and **B**) However, the contrast intensity was noticeably stronger (*i.e.*, more hypointense) in embryos injected with cells that had been cultured in the presence of iron (panels **C** and **D**).

As for HEK 293T(N) (Figure 51, **E**, **F**, **G** and **H**), in all three biological replicates, for each set of embryos injected with non-supplemented dT cells (**E**), only one hypointense region corresponding to the location of fluorescent cells was detected with MRI. In contrast, in embryos injected with non-supplemented dT_M cells (**F**), all fluorescent cell clusters could also be detected via MR imaging (appearing as hypointense regions). These results imply that MagA overexpression in non-supplemented HEK 293T(N) cells may result in a higher contrast, and thus

facilitate detection with MRI. When iron supplementation was provided both to dT and dT_M cells, several of the red fluorescent cell clusters correlated with hypointense regions in MR images (**G** and **H**). However, MRI contrast of supplemented dT and dT_M clusters was very similar, suggesting that MagA transgene is not providing any advantage for these cells.

6.3 DISCUSSION

In the studies described in the literature, MagA overexpression has been conducted in several cell lines and the main outcome is that the sole expression of this gene is sufficient to increase intracellular iron content, leading to a significant contrast when imaged with MRI (Goldhawk *et al.*, 2009; Zurkiya *et al.*, 2008). Not only is the cell line where MagA has been integrated important, but also the origin of this gene. Even though the MagA gene exists in different strains of magnetotactic bacteria, the specific organism from which MagA was cloned for those studies has not always been clear. Zurkiya *et al.* (2008) did not provide specific information about the bacterial strain used in their study, although they state that it was provided by L. Bertani [supposedly *M. magnetotacticum* MS-1 bacterial strain ([GenBank AB001699.1](#))]. However, on several occasions throughout the introduction and discussion, the *M. magneticum* AMB-1 bacterial strain ([GenBank D32253.1](#)) is mentioned, leaving the reader with the impression that the MagA gene they used might have been cloned from this particular strain. On the other hand, in the first paper reported by Goldhawk *et al.* (2009), it specifically states that the strain used originated from AMB-1, and indicates that the previous study (Zurkiya *et al.*, 2008) had used the MS-1 strain. Therefore, it is still unclear which bacterial strain was used in Zurkiya *et al.* (2008). Nevertheless, neither of the reports mentions the existence of mutations present in either strain.

In this chapter, the MagA gene obtained from the magnetotactic bacterial strain MS-1, which has been deposited by L. Bertani in the Addgene repository was

used, supposedly the same as used by Zurkiya *et al.* (2008). The gene provided by Addgene had two noted missense mutations, altering amino acid coding in a non-conservative way. Also two novel silent mutations were identified by sequencing analysis and were not reported by Addgene. For more details, please see MagA gene sequence in Appendix I, p. 242. It is not known to which extent MagA gene properties were affected with these mutations and if it influenced the results presented here. MagA integration was firstly evaluated in several stem cell lines and then followed up in two cell lines: CHO K1 and HEK 293T(N) to assess MagA potential as an MRI reporter.

In the first instance, dTomato and MagA transgene integration were analysed in dT_M transduced stem cells (mESC, mMSC and mKSC) over a time period. Following these cells by fluorescent microscopy and RT-qPCR (Figure 38), it was immediately clear that two types of cells were present: some that could not survive MagA expression for more than a few days (mMSC and mKSC) and others in which MagA appeared to have no obvious toxic effects (HEK 293T(N) and mESC) (Figure 39). With these results we may suggest that mMSC and mKSC decrease their proliferation capacity over time once MagA has been introduced, dying after approximately 8 days, at which point cells still showed acceptable levels of transgene expression. On the other hand, HEK 293T(N) and mESC survive over a period of 40 days, but the transgene expression was found to decrease with time. To some extent, this may be explained by the fact that not all cells were efficiently transduced and the non-transduced cells might proliferate at a higher rate. This

would dilute the overall amount of transgene in the sample, consequently leading to the decay in its expression levels as seen via RT-qPCR (Figure 38). In the case of mESC, mRNA transcript levels were nearly null from day 6 post-transduction and the encoded dTomato protein was practically undetectable using fluorescent microscopy. mESC have been shown to silence lentiviral vectors by epigenetic mechanisms, such as DNA methylation and chromatin silencing (Yao *et al.*, 2004). Therefore, these cells were not chosen to evaluate MagA as a possible magnetic reporter. MagA integration was also unsuccessful in human MSC but successful in human ESC (data not shown). These results pose a limitation of using MagA as a reporter gene for MRI tracking of cells, as this system may not be suitable to use in all cell types.

The CHO K1 cell line was then selected to evaluate MagA gene integration capacity, and later on, its potential as an MRI reporter was assessed alongside HEK 293T(N) cells. dTomato and MagA gene integration was initially assessed by fluorescence microscopy (Figure 40) and flow cytometry (Figure 41). When comparing cell types, dT fluorescence expression in CHO K1 cells was more intense than the same condition of HEK 293T(N) cells. This may be explained by the difference in the multiplicity of infection used (CHO K1 MOI=26 vs. HEK 293T(N) MOI=5), since both cell lines have similar transduction efficiency (3.2.4 Transduction efficiency between cell lines – Figure 9). Nevertheless, this difference was not observed for dT_M transduced cells where only about half of CHO K1 cells were transduced when compared with HEK 293T(N) cells.

dTomato and MagA transgene integration was then analysed in dT_M transduced CHO K1 and HEK 293T(N) cells by RT-qPCR and it was found that from passage 1 to passage 3 after transduction, transgene expression had decreased to about half (Figure 42). This might be due either to cell death of transduced cells, slower cell proliferation relative to non-transduced cells or even to repression or down-regulation of the integrated genes. Gene silencing has been widely studied over the years, particularly in stem cells, and it can be observed mainly in three different states: (i) a complete transcriptional silencing right after transduction; (ii) an effect known as *variegation*, where genetically identical cells may either express or silence the transgene; and (iii) *extinction*, in which a progressive silencing of the transgenes may be verified in long term cultures or during differentiation of cells (Ellis, 2005; Laker *et al.*, 1998; Yao *et al.*, 2004). More recently, it was reported that even the transduction process itself with HIV-based lentiviral vectors may induce profound epigenetic modifications in human hematopoietic stem cells (Yamagata *et al.*, 2012).

As previously seen for stem cells (Figure 39), CHO K1 viability is also affected by MagA integration, particularly 8 days post-transduction (Figure 43). However, this effect is not so dramatic and cells are able to recover up to levels comparable with controls.

This overall evaluation of MagA transgene integration in the CHO K1 demonstrates that only about half of dT_M CHO K1 cells are effectively transduced at P3, comparatively with dT_M HEK 293T(N) (Figure 41, **B**), even with the

multiplicity of infection being five times superior for CHO K1 cells. This evidence together with the decrease in viability/ proliferation (Figure 43) when exposed to MagA gene suggests that this transgene integration may also be causing certain toxicity in CHO K1 as seen in stem cell lines above (Figure 39), albeit to a lower extent.

Next, it was essential to comprehend if MagA overexpression could be interfering with iron homeostasis. Figure 44 and Figure 45 demonstrate that cells reacted as expected to increasing iron concentrations. First, by down-regulating transferrin receptor-1 possibly by promoting mRNA cleavage as known from the IRP/IRE regulatory system (Figure 1) to block iron entering the cell. Second, by promoting Fth-1 mRNA translation process to occur in order to store intracellular iron present in excess. On the other hand, no statistically significant evidence was found that dT_M cells influence iron homeostasis. This influence would likely happen in two possible scenarios: i) if MagA overexpression was to produce “nanoparticles” or ferritin-like molecules accumulating intracellular iron, as proposed by Zurkiya *et al.* (2008) and Goldhawk *et al.* (2009); or ii) if MagA gene was to function as an iron transporter, as it was first described in magnetotactic bacteria (Nakamura *et al.*, 1995a). In the first case scenario, if MagA expression in mammalian cells produced biomineralized iron “nanoparticles”, it would possibly harvest intracellular iron, leading to iron depletion, which would in turn up-regulate TfR-1 levels and down-regulate Fth-1 expression. On the other hand, if it functions as an iron transporter, just like in bacteria, introducing iron in an uncontrollable

fashion into the cells' membranes (cytoplasmic, nuclear and/or mitochondrial), would be expected to lead to a decrease in TfR-1 expression and an increase in Fth-1. However, as seen in Figure 38, Figure 42 and Figure 46, to some extent, cells appear to be able to control overexpressed integrated genes. Perhaps this was the way cells found to maintain iron homeostasis since it is so important for cell survival. Therefore, this would explain why no evident differences of Total_T and Total_F were found in dT_M cells when compared to controls. It might also explain why some cells like mMSC and mKSC died and others survived. Hypothesizing a scenario where these non-surviving cells did not have any control over MagA transcription and translation processes, it would possibly lead to an uncontrollable deregulation in iron homeostasis, thus leading to cell death either by iron depletion or iron toxicity. An interesting case is observed in Cho *et al.* (2014), where increasing MagA transcription levels in TET controlled mESC-MagA are reported by qPCR, with the increase in doxycycline dosage. However, at the protein level, measured with western blot, the relative expression of MagA does not get affected with the same increase in doxycycline dosage.

Even though the exact role of MagA when overexpressed in mammalian cells and its influence on the normal cellular mechanism is yet to be verified, it is of crucial importance to know if dT_M cells could in fact have an increase in the iron load capacity, relative to control cells. For this reason, quantitative and qualitative methods were performed to access the intracellular iron content. Ferrozine assay (quantitative) showed no differences between CHO K1 cells and very small iron

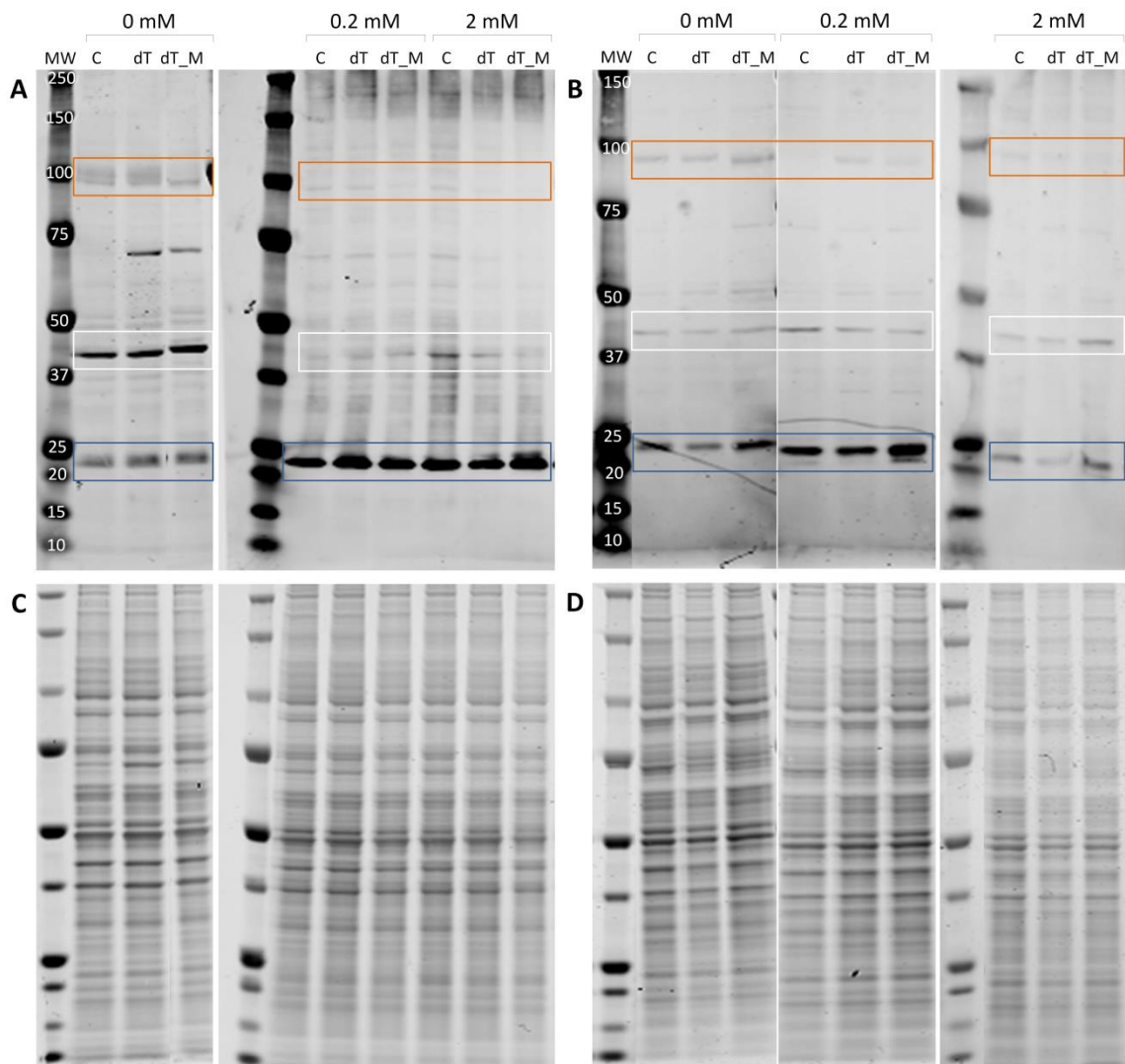
content increase in dT_M HEK 293T(N) cells (Figure 47). Equally, the qualitative method Prussian blue illustrated a higher iron accumulation capacity between different transduced and control HEK 293T(N) cells (Figure 48). Another qualitative method, TEM imaging, did not provide a great insight in terms of differences of iron content between HEK 293T(N) cell lines studied. The electron dense spots are assumed to be iron oxide crystals; however, without the means to identify the atoms present in these inclusions, there is a possibility that these spots are structures consisting of other elements of high atomic weight. Interestingly, TEM pictures shown in Figure 49 resemble the MagA-derived magnetic nanoparticles (Figure 37) presented in the study of Zurkiya *et al.* (2008), in which microanalysis showed that the particles consisted mainly of magnetite (Fe_3O_4), as seen within the magnetosomes of magnetotactic bacteria.

Finally, MRI relaxivity studies performed on cell pellets showed that only when incubated with 2 mM, dT_M HEK 293T(N) cells provided sufficient contrast to be distinguished from control cells (Figure 50, **B**, **D** and **F**). On the other hand, embryo MRI scans indicated that only when cells were not iron supplemented that a distinct contrast was found between dT and dT_M (Figure 51, **E-H**), implying that MagA overexpression is somehow contributing to an increase in MRI contrast. Also, the T2 shortening effect of HEK 293T(N) cells implanted in the chick embryo is very similar, irrespective of iron supplementation, suggesting that supplementation previous to injection might not even be necessary for this cell line. In case of CHO K1 cells, MRI studies did not demonstrate a higher contrast capacity of dT_M,

relative to control cells (Figure 50, **A**, **C** and **E**; Figure 51, **A-D**). Nonetheless, in these cells the T2 shortening effect observed in embryo MRI scans is much more striking relative to HEK 293T(N), even though the same is not observed when measuring intracellular iron content (Figure 47) or in relaxivity studies performed on cell pellets (Figure 50). This might be due to the cluster formation observed in CHO K1, leading to a more intense loss of signal when imaged with MR, contrary to HEK 293T(N) cells which preferentially spread within the chick embryo brain.

In summary, MagA gene overexpression in mammalian cells might be a useful reporter for MRI tracking, as seen here in HEK 293T(N) cells and in previous reports (Goldhawk *et al.*, 2009; Zurkiya *et al.*, 2008), but it is definitely dependent on the cell type used. Caution must be taken when introducing this bacterial gene, as it might promote a toxic effect on certain cell lines and/or disturb the cell's iron equilibrium. For this reason, if using this gene as an MRI reporter, it is important to understand how it functions within the cell, and therefore, further work needs to be done.

6.4 SUPPLEMENTARY DATA



Supplementary figure 5 – Representative western blots (**A** and **B**) and correspondent total protein gels (**C** and **D**) from Control, dTomato (dT) and MagA (dT_M) transduced CHO K1 (**A** and **C**) and HEK 293T(N) (**B** and **D**) cells, supplemented for 4 days with 0, 0.2 or 2 mM of iron. Orange rectangle highlights Tfr-1 (or Total_T) protein expression, with a predicted molecular weight (MW) of 100 kDa; white rectangle corresponds to actin expression with 42 kDa and blue rectangle to Fth-1 (or Total_F) with 21 kDa. Sometimes another band is detected when targeting Fth-1, which may correspond to a post-translational modification of this protein. Please note that because actin was not stable in different blots, particularly in the case of CHO K1 cells (**A**), protein quantification was normalized using only total protein gels for this cell line (M&M, p. 57).

CHAPTER 7

GENERAL DISCUSSION AND CONCLUSION

In the current work, reporter gene technology was evaluated as means to track cells within a model organism using MR imaging. This relied on the potential magnetic properties of specific genes, such as: i) transferrin receptor-1 (TfR-1), known to be an iron transporter located on the membrane of mammalian cells; ii) ferritin heavy chain-1 (Fth-1), an integral part of the ferritin complex which is responsible for storing intracellular iron in a safe configuration, and, iii) MagA, identified as an iron transporter in the membrane of magnetotactic bacteria and possibly involved in the formation of magnetosomes. The concept behind this work was that overexpression of any of these genes in a certain cell line would be sufficient to increase intracellular iron content and thus lead to a significant MRI contrast of these cells when compared to controls and to background levels.

The work presented here was conducted by using a HIV-based lentiviral method to stably overexpress potential magnetic reporters (TfR-1, Fth-1 or MagA), along with fluorescent reporters (GFP and dTomato) in several established cell lines. Due to the lentiviral construct design, shown in Figure 5, Chapter 3, an internal ribosome entry site (IRES) was present between the magnetic and fluorescent reporters, allowing for bicistronic expression of both genes. TfR-1 was cloned into a GFP-containing lentiviral vector (green fluorescence), while Fth-1 and MagA were cloned into a dTomato-containing lentiviral vector (red fluorescence). When

integrated in specific cell lines, the presence of fluorescent reporters allowed for a longitudinal monitoring *in vitro* by fluorescence-based methods. However, this only allowed for verification of the expression levels obtained from fluorescent reporters. In some situations, even though cells were transduced with the same MOI, when comparing controls with target genes, for example GFP with GFP_T transduced in CHO K1 cells (Chapter 4) or in mMSC (Chapter 5), the control normally appeared with brighter fluorescence than the other transduction condition. This can potentially be explained by the fact that, within the lentiviral vector, the fluorescent reporter is located downstream of the IRES and is thus furthest from EF1- α promoter. In case of another gene of interest being present, the location of the fluorescent gene can influence this one to have weaker expression relative to the magnetic reporter, which in turn is located upstream of the IRES and is the first to be expressed by the promoter. Nevertheless, the only way to know if both integrated genes were being represented at the same level was to evaluate transgene expression by RT-qPCR. Results using this technique showed that for most transductions performed, the lentiviral system used here provided a robust bicistronic expression of both transgenes.

An initial evaluation of the cell viability status a few days after transduction comprised both cell proliferation capacity and cell health and appeared to be decreased for all transduction conditions. This may not only be due to the transduction process itself or an influence derived from the integrated transgenes, as discussed on a case-by-case basis, but also due to the presence of the EF1- α

promoter. This promoter, present in all lentiviral constructs studied here, has been reported to transiently arrest the cell cycle at S phase in mesenchymal stem cells, when high MOIs of HIV-1 derived lentiviral preparations were used. However, the same publication also registered that, when EF1- α promoter was used, a significant increase in expression with advancing passages was observed and that transduced cells had the same differentiation capacity as untransduced cells (Lee *et al.*, 2004).

After analysing the overall transgene integration capacity and its effects on the viability status of a cell, the evaluation of how iron homeostasis is kept in response to the target transgene overexpression is also crucial. Taking a general overview of all results obtained in this study, some main points need to be taken in consideration. For instance, a balanced iron metabolism should always be a priority, confirming if cells are able to adjust its metabolic needs to the overexpression of iron related genes. This was observed when TfR-1 was overexpressed in CHO K1 cell line, in Chapter 4, where an internal increase of Fth-1 compensated TfR-1 overexpression, maintaining an iron homeostasis state. However, in some cases this does not occur so easily, as observed when analysing mMSC overexpressed with Fth-1, in Chapter 5. Therefore, it is crucial to understand the impact on the cell's normal behaviour, either when overexpressing a gene involved in the iron metabolism, such as TfR-1 or Fth-1, or when integrating a gene which may possibly disturb the normal iron metabolism, like MagA gene, studied in Chapter 6. In this case, there was no confirmation that iron homeostasis was adjusting to the new needs potentially promoted by MagA overexpression and therefore, the true

function of MagA when overexpressed in mammalian cells remains elusive.

In order to investigate the potential cause of toxicity in cells when transduced with MagA transgene, the surviving and non-surviving cell lines were compared side by side in culture. It was noticed that these two groups of cells performed different cellular respiration pathways and this could potentially be responsible for determining either cell death or cell survival. Even though all cell lines used in this work were cultured under glucose-containing medium, the surviving cell lines, such as HEK 293T(N), mESC and hESC, after a few days in culture turned the medium into a yellow colour. This was most likely due to a drop in pH caused by the secretion of lactic acid, a biowaste product from the glycolytic pathway (anaerobic respiration). On the other hand, non-surviving cells, like mMSC, hMSC and mKSC, although metabolites are also secreted into the culture medium, the colour always remained the same, even after long periods of time, indicating there were no changes in the pH. In this case, cells might preferentially use oxidative phosphorylation (aerobic respiration) to meet their energy needs. In order to understand if the cellular respiration pathways had any influence on the survival of some cell lines in detriment of others, a hypothesis was approached to try to explain why cells who most likely use of mitochondria for oxidative phosphorylation, fail to survive after MagA transduction. The hypothesis contemplated that the lack mitochondrial function of these cells after MagA transduction might potentially be the underlying reason for the non-survival. Therefore, glucose-deprivation experiments (substituting glucose with galactose) were performed to one cell line from each group (mESC and mKSC). The production of energy through the glycolytic pathway under galactose-supplemented conditions, rather than glucose,

yields no net ATP and therefore cells are forced to use the oxidative phosphorylation pathway to produce energy. For both cell lines, mKSC and mESC, an obvious decrease in proliferation was immediately detected when comparing galactose-supplemented media with normal media conditions (data not shown). This was somewhat expected since not only the cells probably need some time to adjust to the new metabolic conditions, but also it is known that oxidation phosphorylation pathway requires more time for energy production, not allowing such a fast growth rate. However, the fact that mESC, when transduced with MagA, were not able to proliferate under aerobic conditions (data not shown) provides some insight of a possible mitochondrial functional loss after MagA gene was introduced. Nevertheless, further work needs to be done to understand the reason for toxicity upon MagA integration in some cell lines in detriment of others.

The capacity of cells transduced with magnetic reporters to retain more iron than controls was evaluated by measuring the intracellular iron content of each cell, using a Ferrozine assay. GFP_T transduction into CHO K1 cells (Chapter 4) promoted a higher intracellular iron accumulation relative to untransduced and GFP control cells; however, when GFP_T viral particles were transduced in mMSC (Chapter 5) the same results were not observed. While CHO K1 cells were transduced with MOI=100, mMSC had only MOI=50. This might partially explain why TfR-1 overexpression led to an iron content increase in some cell lines but not others. Also, in CHO K1 cells, iron homeostasis adjusted to GFP_T integration, promoting an increase in Fth-1 mRNA/ protein levels, indirectly meaning that the number of ferritins available increased due to the sole overexpression of TfR-1. This potentially

led to more iron entering the cell due to high numbers of receptors available, and clustering in ferritins in a safe configuration.

An interesting observation between all these studies was the variation of iron accumulation capacity amongst the different cell lines studied. All cell lines were incubated with 2 mM of iron for a period of 4 days prior to measurement. The CHO K1 cell line has the least retention capability, with only 0.1 pg/cell, similarly to HEK 293T(N) cells with 0.13 pg/cell, but greatly surpassed by mMSC, with 0.78 pg/cell. These values refer to untransduced cells only. In a work published by Heyn *et al.*, (2003), calculations of the minimum amount of iron needed for MRI detection of a single cell lead to a conclusion that for 100x100x200 μ m (2nL) voxel resolution, using a 1.5 T MRI with a 3DFIESTA pulse sequence, the range would have to be between 1.4 and 3 pg/cell (Heyn *et al.*, 2003). Although MR imaging conditions were different for the present study, and cells were not detected on a single basis but rather as a cluster, it is good to take into consideration that the influence magnetic reporter genes may possibly have on iron acquisition into cells is very likely to be on the borderline for minimum MRI detection capacity.

When analysing cell pellets with MRI, the results show that MRI contrast is dependent not only on the overexpressed transgene as desired, but very much influenced by the cell type and iron supplementation conditions used. The fact that mMSC have such great iron retention aptitude, makes it possible for them to create markedly increased MRI contrast when supplemented with iron, without the further need of contrast agents or magnetic reporter genes.

To further complete this study, magnetic target genes and respective controls were injected into the midbrain of an E3 chick embryo. Up to now, no other research study has investigated the potential of MRI reporter genes using the chick embryo *in ovo* as a model organism. At embryonic day 5, embryos were harvested and imaged both with fluorescence microscopy and MRI. In terms of the fluorophores chosen for this study, GFP and dTomato, the best to use particularly in an *in vivo* setting was dTomato, created by Shaner *et al.* (2004). While eGFP (Cubitt *et al.*, 1999) produces a green fluorescence protein with an excitation peak of 488 nm, dTomato gene gives rise to a red fluorescence protein with an excitation peak of 554 nm. The longer excitation wavelength makes dTomato produce less phototoxicity and penetrate deeper into the tissue (Shaner *et al.*, 2007), circumventing more efficiently the biological tissue autofluorescence than eGFP.

In conclusion, the field of magnetic reporter genes is yet to be fully explored. While other MRI imaging systems require exogenous contrast agents, such as SPIONS, magnetic reporter gene technology would allow for long-term MRI cell tracking studies, without signal dilution upon cell division or false positive signalling. The promise of a global magnetic reporter gene for MRI tracking of any cell type might never come to a reality, as one needs to evaluate on a case-by-case basis, if a certain reporter gene is influencing the normal behaviour of a specific cell line. A pitfall of using reporter genes for cell tracking is the low sensitivity when compared to exogenous agents such as SPIONS (Vande Velde *et al.*, 2011). However, studies have reported adverse effects on cell differentiation when exposed to particles such

as SPIONs (Chen *et al.*, 2010). Furthermore, the inevitable dilution over time of these particles does not allow a longitudinal tracking study over the course of weeks or months (Taylor *et al.*, 2014). An alternative approach would be to join together both tracking methods, combining the high sensitivity of SPIONs in early tracking studies to precisely determine the location of cell engraftment, allied with the magnetic reporter gene technology for long-term monitoring. Possibly the magnetic nanoparticle dissolution with time would allow for sufficient iron dispersion to be taken up by complexes such as ferritins, whose numbers may be increased due to overexpression of TfR-1, as seen in Chapter 4, or perhaps of Fth-1, as described by a number of previous studies (Cohen *et al.*, 2005; Deans *et al.*, 2006; Genove *et al.*, 2005). Another setback is the necessity to use a retroviral system to stably introduce and overexpress magnetic reporters of interest. This has long been known to pose potential risks, such as insertional mutagenesis, and may not be applicable in the clinical setting. For this reason, increasing research on gene integration directed targeting is being explored, aiming to avoid the random insertion pattern, typical of virus-based integration systems (Nielsen *et al.*, 2009; Qasim *et al.*, 2010; Qi *et al.*, 2013). Also, several studies are testing the efficacy and safety of non-viral DNA transfer systems, creating the next generation of gene delivery tools (Yin *et al.*, 2014).

Other reporter genes with potential MRI contrast properties may also be explored for cell tracking purposes. One example is the divalent metal transporter, DMT-1, known to be involved in the uptake of manganese and recently presented

as a novel reporter for manganese-enhanced MRI, or MEMRI (Bartelle *et al.*, 2012). Another protein yet to be explored as a magnetic reporter is Scara5+, initially reported by Jiang *et al.* (2006) as a class A scavenger receptor. Later it was identified by Li *et al.* (2009) to be expressed in the mesenchymal, stromal and capsule compartments of the embryonic kidney, serving as an endocytosis-mediated receptor of extracellular ferritin, representing therefore a mechanism for non-transferrin iron delivery. This protein could potentially be used in other cell types to introduce ferritin complexes into the cell, allowing for intracellular iron accumulation in a safe configuration and contributing to a significant increase in contrast with MRI. Therefore, reporter gene technology may one day be a robust system for tracking of cells.

At last, from the three magnetic reporters for MRI cell tracking investigated in this study, TfR-1 proved to be a suitable reporter in the CHO K1 cell line (Chapter 4), particularly when used with low iron supplementation conditions. However, the same suitability was not verified for mMSC (Chapter 5). In fact, for this particular cell line, none of the reporter genes investigated promoted a contrast difference using MRI, neither when TfR-1 and Fth-1 were overexpressed independently or in conjunction. Also, as described in Chapter 6, stem cell lines failed to incorporate MagA gene (mKSC, hMSC, mMSC) or decreased its expression levels to null a few days after transduction (mESC). The product derived from MagA overexpression in mammalian cells and potential cytotoxicity remains unknown. Nevertheless, this system does not appear to be adequate for stem cell studies, but

rather for other cell lines, perhaps with a more robust iron metabolism, easily adjusting its needs. As previously stated in the study of Zurkiya *et al.* (2008), the MagA gene provided a distinct contrast with MRI in HEK 293T(N) cells and when iron supplementation was not provided. Even though the same was not observed for CHO K1 cell line, the potential use of MagA (or TfR-1) without any iron-related supplementation conditions would provide a useful advantage for long-term tracking of cells.

BIBLIOGRAPHY

- Adamson, A.D., Jackson, D., Davis, J.R.E., 2011. Novel approaches to *in vitro* transgenesis. *The Journal of endocrinology* 208, 193-206.
- Ahrens, E. T., Bulte, J. W. M., 2013. Tracking immune cells *in vivo* using magnetic resonance imaging. *Nature Reviews. Immunology* 13(10), 10.1038/nri3531.
- Aisen, P., 1998. Transferrin, the transferrin receptor, and the uptake of iron by cells. *Metal ions in biological systems* 35, 585-631.
- Aisen, P., 2004. Transferrin receptor 1. *The international journal of biochemistry & cell biology* 36, 2137-2143.
- Aisen, P., Enns, C., Wessling-Resnick, M., 2001. Chemistry and biology of eukaryotic iron metabolism. *The international journal of biochemistry & cell biology* 33, 940-959.
- Alfke, H., Stöppler, H., Nocken, F., Heverhagen, J., Kleb, B., Czubayko, F., Klose, K., 2003. *In Vitro MR Imaging of Regulated Gene Expression*. *Radiology* 228, 488492.
- Arosio, P., Ingrassia, R., Cavadini, P., 2009. Ferritins: a family of molecules for iron storage, antioxidation and more. *Biochimica et biophysica acta* 1790, 589-599.
- Arosio, P., Levi, S., 2002. Ferritin, iron homeostasis, and oxidative damage. *Free radical biology & medicine* 33, 457-463.
- Aung, W., Hasegawa, S., Koshikawa-Yano, M., Obata, T., Ikehira, H., Furukawa, T., Aoki, I., Saga, T., 2009. Visualization of *in vivo* electroporation-mediated transgene expression in experimental tumors by optical and magnetic resonance imaging. *Gene therapy* 16, 830-839.
- Bahr, S., Borgschulte, T., Kayser, K., Lin, N., 2009. Using microarray technology to select housekeeping genes in Chinese hamster ovary cells. *Biotechnology and bioengineering* 104, 1041-1046.
- Bailey, D.L, Townsend, D.W., Valk, P.E., Maisey, M.N. (2005). *Positron Emission Tomography: Basic Sciences*. Secaucus, NJ: Springer-Verlag.
- Bartelle, B.B., Szulc, K.U., Suero-Abreu, G.A., Rodriguez, J.J., Turnbull, D.H., 2012. Divalent metal transporter, DMT1: A novel MRI reporter protein. *Magnetic resonance in medicine : official journal of the Society of Magnetic Resonance in Medicine / Society of Magnetic Resonance in Medicine*.
- Bazylinski, D., Garratt-Reed, A., Frankel, R.B., 1994. Electron microscopic studies of magnetosomes in magnetotactic bacteria. *Micros. Res. Tech.* 27, 389-401.
- Bazylinski, D.A., Frankel, R.B., 2004. Magnetosome formation in prokaryotes. *Nature reviews. Microbiology* 2, 217-230.

- Benoit, M.R., Mayer, D., Barak, Y., Chen, I.Y., Hu, W., Cheng, Z., Wang, S.X., Spielman, D.M., Gambhir, S.S., Matin, A., 2009. Visualizing implanted tumors in mice with magnetic resonance imaging using magnetotactic bacteria. *Clinical cancer research : an official journal of the American Association for Cancer Research* 15, 5170-5177.
- Bhirde, A., Xie, J., Swierczewska, M., Chen, X., 2011. Nanoparticles for cell labeling. *Nanoscale* 3, 142-153.
- Blakemore, R.P., 1975. Magnetotactic bacteria. *Science* 190, 377-379.
- Bothwell, T.H., 1995. Overview and mechanisms of iron regulation. *Nutrition reviews* 53, 237-245.
- Boyd, D., Vecoli, C., Belcher, D.M., Jain, S.K., Drysdale, J.W., 1985. Structural and functional relationships of human ferritin H and L chains deduced from cDNA clones. *J Biol Chem* 260, 11755-11761.
- Bulte, J., Douglas, T., van Gelderen, P., Lewis, B., Frank, J., 2001. Magnetodendrimers allow endosomal magnetic labeling and in vivo tracking of stem cells. *Nature Biotechnology* 19, 1141-1147.
- Bulte, J., Kraitchman, D., 2004. Iron oxide MR contrast agents for molecular and cellular imaging. *NMR in Biomedicine* 17, 484-499.
- Bushman, F.D., 2002. Integration site selection by lentiviruses: biology and possible control. *Current topics in microbiology and immunology* 261, 165-177.
- Campan, M., Lionetti, V., Aquaro, G.D., Forini, F., Matteucci, M., Vannucci, L., Chiappesi, F., Di Cristofano, C., Faggioni, M., Maioli, M., Barile, L., Messina, E., Lombardi, M., Pucci, A., Pistello, M., Recchia, F.A., 2011. Ferritin as a reporter gene for in vivo tracking of stem cells by 1.5-T cardiac MRI in a rat model of myocardial infarction. *American journal of physiology. Heart and circulatory physiology* 300, 50.
- Campillos, M., Cases, I., Hentze, M., Sanchez, M., 2010. SIREs: searching for iron-responsive elements. *Nucleic acids research* 38, 7.
- Chasteen, N., Harrison, P., 1999. Mineralization in Ferritin: An Efficient Means of Iron Storage. *Journal of Structural Biology* 126, 182194.
- Chen, Y.C., Hsiao, J.K., Liu, H.M., Lai, I.Y.Y., Yao, M., Hsu, S.C., Ko, B.S., Chen, Y.C., Yang, C.S., Huang, D.M., 2010. The inhibitory effect of superparamagnetic iron oxide nanoparticle (Ferucarbotran) on osteogenic differentiation and its signaling mechanism in human mesenchymal stem cells. *Toxicology and applied pharmacology* 245, 272-279.
- Cherry, S., 2004. In vivo molecular and genomic imaging: new challenges for imaging physics. *Physics in Medicine and Biology* 49.
- Cho, I.K., P., M.S., Paudyal, R., Piotrowska-Nitsche, K., Cheng, P.H., Zhang, X., Mao, H., Chan, A.W.S., 2014. Longitudinal Monitoring of Stem Cell Grafts In

- VivoUsing Magnetic Resonance Imaging with Inducible Maga as a Genetic Reporter. *Theranostics* 4, 972989.
- Cohen, B., Dafni, H., Meir, G., Harmelin, A., Neeman, M., 2005. Ferritin as an Endogenous MRI Reporter for Noninvasive Imaging of Gene Expression in C6 Glioma Tumors. *Neoplasia* 7, 109117.
- Corsi, B., Cozzi, A., Arosio, P., Drysdale, J., Santambrogio, P., Campanella, A., Biasiotto, G., Albertini, A., Levi, S., 2002. Human mitochondrial ferritin expressed in HeLa cells incorporates iron and affects cellular iron metabolism. *Journal of Biological Chemistry*.
- Cozzi, A., Corsi, B., Levi, S., Santambrogio, P., Albertini, A., Arosio, P., 2000. Overexpression of wild type and mutated human ferritin H-chain in HeLa cells: in vivo role of ferritin ferroxidase activity. *Journal of Biological Chemistry*.
- Cubitt, A.B., Woollenweber, L.A., Heim, R., 1999. Understanding structure-function relationships in the Aequorea victoria green fluorescent protein. *Methods in cell biology* 58, 19-30.
- Daniels, T.R., Bernabeu, E., Rodríguez, J.A., Patel, S., Kozman, M., Chiappetta, D.A., Holler, E., Ljubimova, J.Y., Helguera, G., Penichet, M.L., 2012. The transferrin receptor and the targeted delivery of therapeutic agents against cancer. *Biochimica et biophysica acta* 1820, 291-317.
- Deans, A., Wadghiri, Y., Bernas, L., Yu, X., Rutt, B., Turnbull, D.H., 2006. Cellular MRI contrast via coexpression of transferrin receptor and ferritin. *Magnetic resonance in medicine : official journal of the Society of Magnetic Resonance in Medicine / Society of Magnetic Resonance in Medicine* 56, 51-59.
- Dimitrov, D., 2012. Therapeutic Proteins, in: Voynov, V., Caravella, J.A. (Eds.), *Therapeutic Proteins*. Humana Press, pp. 1-26.
- Dull, T., Zufferey, R., Kelly, M., Mandel, R.J., Nguyen, M., Trono, D., Naldini, L., 1998. A third-generation lentivirus vector with a conditional packaging system. *Journal of virology* 72, 8463-8471.
- Ellis, J., 2005. Silencing and variegation of gammaretrovirus and lentivirus vectors. *Human gene therapy*.
- Engstrom, P.F., Sigurdson, E.R., Evans, A.A., et al., 2003. Imaging Modalities. In: Kufe D.W., Pollock R.E., Weichselbaum R.R., et al., editors. *Holland-Frei Cancer Medicine*. 6th edition. Hamilton (ON): BC Decker.
- Fehling, H., Lacaud, G., Kubo, A., Kennedy, M., Robertson, S., Keller, G., Kauskoff, V., 2003. Tracking mesoderm induction and its specification to the hemangioblast during embryonic stem cell differentiation. *Development* 130, 4217-4227.

- Felgner, P., Gadek, T., M., H., Roman, R., Chan, H., Wenz, M., Northrop, J., Ringold, G., Danielsen, M., 1987. Lipofection: a highly efficient, lipid-mediated DNA-transfection procedure. *Proceedings of the National Academy of Sciences of the United States of America* 84, 7413-7417.
- Feng, Y., Liu, Q., Zhu, J., Xie, F., Li, L., 2012. Efficiency of ferritin as an MRI reporter gene in NPC cells is enhanced by iron supplementation. *Journal of biomedicine & biotechnology* 2012, 434878.
- Fenton, H.J.H., 1894. LXXIII.-Oxidation of tartaric acid in presence of iron. *Journal of the Chemical Society, Transactions* 65, 899-910.
- Ferreira, C., Bucchini, D., Martin, M.E., Levi, S., Arosio, P., Grandchamp, B., Beaumont, C., 2000. Early Embryonic Lethality of H Ferritin Gene Deletion in Mice. *Journal of Biological Chemistry* 275, 3021-3024.
- Fleming, M.D., Andrews, N.C., 1998. Mammalian iron transport: an unexpected link between metal homeostasis and host defense. *The Journal of laboratory and clinical medicine* 132, 464-468.
- Ford, G.C., Harrison, P.M., Rice, D.W., Smith, J.M., Treffry, A., White, J.L., Yariv, J., 1984. Ferritin: design and formation of an iron-storage molecule. *Philosophical transactions of the Royal Society of London. Series B, Biological sciences* 304, 551-565.
- Frankel, R., Blakemore, R., Wolfe, R., 1979. Magnetite in freshwater magnetotactic bacteria. *Science (New York, N.Y.)* 203, 1355-1356.
- Fukuda, Y., Okamura, Y., Takeyama, H., Matsunaga, T., 2006. Dynamic analysis of a genomic island in *Magnetospirillum* sp. strain AMB-1 reveals how magnetosome synthesis developed. *FEBS letters* 580, 801-812.
- Ganz, T., Nemeth, E., 2012. Hepcidin and iron homeostasis. *Biochimica et biophysica acta* 1823, 1434-1443.
- Gatter, K.C., Brown, G., Trowbridge, I.S., Woolston, R.E., Mason, D.Y., 1983. Transferrin receptors in human tissues: their distribution and possible clinical relevance. *Journal of Clinical Pathology*.
- Genove, G., DeMarco, U., Xu, H., Goins, W., Ahrens, E., 2005. A new transgene reporter for in vivo magnetic resonance imaging. *Nature Medicine* 11, 450-454.
- Gilad, A., McMahon, M., Walczak, P., Winnard, P., Raman, V., van Laarhoven, H., Skoglund, C., Bulte, J., van Zijl, P., 2007a. Artificial reporter gene providing MRI contrast based on proton exchange. *Nature biotechnology* 25, 217-219.
- Gilad, A., Winnard, P., van Zijl, P., Bulte, J., 2007b. Developing MR reporter genes: promises and pitfalls. *NMR in biomedicine* 20, 275-290.
- Glennon-Alty, L., Williams, R., Dixon, S., Murray, P., 2013. Induction of mesenchymal

- stem cell chondrogenesis by polyacrylate substrates. *Acta biomaterialia* 9, 6041-6051.
- Goldhawk, D., Lemaire, C., McCreary, C., McGirr, R., Dhanvantari, S., Thompson, R., Figueredo, R., Koropatnick, J., Foster, P., Prato, F., 2009. Magnetic Resonance Imaging of Cells Overexpressing MagA, an Endogenous Contrast Agent for Live Cell Imaging. *Molecular Imaging* 8(3), 129-139.
- Gomme, P.T., McCann, K.B., Bertolini, J., 2005. Transferrin: structure, function and potential therapeutic actions. *Drug Discovery Today* 10, 267-273.
- Gould, S.J., Subramani, S., 1988. Firefly luciferase as a tool in molecular and cell biology. *Analytical biochemistry* 175, 5-13.
- Graham, F.L., van der Eb, A.J., 1973. A new technique for the assay of infectivity of human adenovirus 5 DNA. *Virology* 52, 456-467.
- Graham, R.M., Reutens, G.M., Herbison, C.E., Delima, R.D., Chua, A.C., Olynyk, J.K., Trinder, D., 2008. Transferrin receptor 2 mediates uptake of transferrin-bound and non-transferrin-bound iron. *Journal of hepatology* 48, 327-334.
- Haacke E. M., Brown R. W., Thompson M. R., Venkatesan R., 1999. *Magnetic resonance imaging: physical principles and sequence design*. John Wiley & Sons.
- Hacein-Bey-Abina, S., von Kalle, C., Schmidt, M., Le Deist, F., Wulffraat, N., McIntyre, E., Radford, I., Villeval, J.L., Fraser, C.C., Cavazzana-Calvo, M., Fischer, A., 2003. A serious adverse event after successful gene therapy for X-linked severe combined immunodeficiency. *The New England journal of medicine* 348, 255-256.
- Hamer, D.H., Leder, P., 1979. Expression of the chromosomal mouse Beta major globin gene cloned in SV40. *Nature* 281, 35-40.
- Harney, A., Meade, T., 2010. Molecular imaging of in vivo gene expression. *Future medicinal chemistry* 2, 503-519.
- Harrison, P.M., Arosio, P., 1996. The ferritins: molecular properties, iron storage function and cellular regulation. *Biochim Biophys Acta* 1275, 161-203.
- Harrison, P.M., Ford, G.C., Rice, D.W., Smith, J.M., Treffry, A., White, J.L., 1987. Structural and functional studies on ferritins. *Biochem Soc Trans* 15, 744-748.
- Hawrylak, N., Ghosh, P., Broadus, J., Schlueter, C., Greenough, W. T., Lauterbur, P. C., 1993. Nuclear-magnetic-resonance (NMR) imaging of iron oxide-labeled neural transplants. *Exp Neurol* 121, 181-192.
- Henkelman, R. M. , Stanisiz, G. J. , Graham, S. J., 2001. Magnetization transfer in MRI: a review. *NMR Biomed* 14, 57-64.
- Hémadi, M., Kahn, P.H., Miquel, G., El Hage Chahine, J.M., 2004. Transferrin's mechanism of interaction with receptor 1. *Biochemistry* 43, 1736-1745.

- Hentze, M.W., Kuhnt, L.C., 1996. Molecular control of vertebrate iron metabolism: mRNA-based regulatory circuits operated by iron, nitric oxide, and oxidative stress. *Proceedings of the National Academy of Sciences* 93, 8175-8182.
- Hentze, M.W., Muckenthaler, M.U., Andrews, N.C., 2004. Balancing acts: molecular control of mammalian iron metabolism. *Cell* 117, 285-297.
- Herman, G. T., 2009. *Fundamentals of computerized tomography: Image reconstruction from projection*, Springer, 2nd edition.
- Heyn, C., Bowen, C.V., Rutt, B.K., Gareau, P.J., 2003. Single cell detection with FIESTA: effect of iron loading and distribution. *Proc. Int. Soc. Magn. Reson. Med.* 11, 805.
- Hong, S., Hwang, D.Y., Yoon, S., Isacson, O., Ramezani, A., Hawley, R.G., Kim, K.S., 2007. Functional Analysis of Various Promoters in Lentiviral Vectors at Different Stages of In Vitro Differentiation of Mouse Embryonic Stem Cells. *Molecular Therapy* 15, 1630-1639.
- Ichikawa, T., Högemann, D., Saeki, Y., Tyminski, E., Terada, K., Weissleder, R., Chiocca, E.A., Basilion, J.P., 2002. MRI of Transgene Expression: Correlation to Therapeutic Gene Expression. *Neoplasia* 4.
- Inoue, T., Cavanaugh, P.G., Steck, P.A., Brünner, N., Nicolson, G.L., 1993. Differences in transferrin response and numbers of transferrin receptors in rat and human mammary carcinoma lines of different metastatic potentials. *Journal of cellular physiology* 156, 212-217.
- Iordanova, B., Hitchens, T.K., Robison, C.S., Ahrens, E.T., 2013. Engineered mitochondrial ferritin as a magnetic resonance imaging reporter in mouse olfactory epithelium. *PLoS one* 8.
- Iordanova, B., Robison, C.S., Ahrens, E.T., 2010. Design and characterization of a chimeric ferritin with enhanced iron loading and transverse NMR relaxation rate. *Journal of biological inorganic chemistry : JBIC : a publication of the Society of Biological Inorganic Chemistry* 15, 957-965.
- Isalan, M., Santori, M.I., Gonzalez, C., Serrano, L., 2005. Localized transfection on arrays of magnetic beads coated with PCR products. *Nature methods* 2, 113-118.
- Jang, S. I., & Lee, D. K., 2014. Contrast-enhanced endoscopic ultrasonography: advance and current status. *Ultrasonography* 33(3), 161–169.
- Jiang, Y., Oliver, P., Davies, K.E., Platt, N., 2006. Identification and characterization of murine SCARA5, a novel class A scavenger receptor that is expressed by populations of epithelial cells. *Journal of Biological Chemistry* 281, 11834-11845.
- Jing, S.Q., Trowbridge, I.S., 1987. Identification of the intermolecular disulfide bonds

- of the human transferrin receptor and its lipid-attachment site. *The EMBO journal* 6, 327-331.
- Jordan, A., Reichard, P., 1998. Ribonucleotide reductases. *Annual review of biochemistry* 67, 71-98.
- Jung, C. W., Jacobs, P., 1995. Physical and chemical properties of superparamagnetic iron oxide MR contrast agents: ferumoxides, ferumoxtran, ferumoxsil, *Magnetic Resonance Imaging* 13(5), 661-74.
- Kawabata, H., Yang, R., Hiramata, T., Vuong, P.T., Kawano, S., Gombart, A.F., Koeffler, H.P., 1999. Molecular Cloning of Transferrin Receptor 2 A NEW MEMBER OF THE TRANSFERRIN RECEPTOR-LIKE FAMILY. *Journal of Biological Chemistry*.
- Kay, M.A., Glorioso, J., Naldini, L., 2001. Viral vectors for gene therapy: the art of turning infectious agents into vehicles of therapeutics. *Nature Medicine* 7, 3340.
- Kim, T.K., Eberwine, J.H., 2010. Mammalian cell transfection: the present and the future. *Analytical and bioanalytical chemistry* 397, 3173-3178.
- Komeili, A., Li, Z., Newman, D., Jensen, G., 2006. Magnetosomes Are Cell Membrane Invaginations Organized by the Actin-Like Protein MamK. *Science* 311, 242-245.
- Koorts, A.M., Viljoen, M., 2007. Ferritin and ferritin isoforms I: Structure–function relationships, synthesis, degradation and secretion. *Archives Of Physiology And Biochemistry* 113, 3054.
- Kostura, L., Kraitchman, D., Mackay, A., Pittenger, M., Bulte, J., 2004. Feridex labeling of mesenchymal stem cells inhibits chondrogenesis but not adipogenesis or osteogenesis. *NMR in biomedicine* 17, 513-517.
- Kozak, M., 1981. Mechanism of mRNA recognition by eukaryotic ribosomes during initiation of protein synthesis. *Current topics in microbiology and immunology* 93, 81-123.
- Kutner, R., Zhang, X., Reiser, J., 2009. Production, concentration and titration of pseudotyped HIV-1-based lentiviral vectors. *Nature Protocols* 4.
- Laker, C., Meyer, J., Schopen, A., Friel, J., Heberlein, C., Ostertag, W., Stocking, C., 1998. Host cis-mediated extinction of a retrovirus permissive for expression in embryonal stem cells during differentiation. *Journal of virology* 72, 339-348.
- Lane, D.J.R., Chikhani, S., Richardson, V., Richardson, D.R., 2013. Transferrin iron uptake is stimulated by ascorbate via an intracellular reductive mechanism. *Biochimica et biophysica acta* 1833, 1527-1541.
- Lang, C., Schüler, D., 2006. Biogenic nanoparticles: production, characterization, and application of bacterial magnetosomes. *Journal of Physics: Condensed*

Matter 18.

- Lawrence, C.M., Ray, S., Babyonyshev, M., Galluser, R., Borhani, D.W., Harrison, S.C., 1999. Crystal structure of the ectodomain of human transferrin receptor. *Science* 286, 779-782.
- Lawson, D., Treffry, A., Artymiuk, P., Harrison, P., Yewdall, S., Luzzago, A., Cesareni, G., Levi, S., Arosio, P., 1989. Identification of the ferroxidase centre in ferritin. *FEBS letters* 254, 207-210.
- Lee, C.I., Kohn, D.B., Ekert, J.E., Tarantal, A.F., 2004. Morphological Analysis and Lentiviral Transduction of Fetal Monkey Bone Marrow-Derived Mesenchymal Stem Cells. *Molecular Therapy* 9, 112-123.
- Levi, S., Arosio, P., 2004. Mitochondrial ferritin. *The international journal of biochemistry & cell biology* 36, 1887-1889.
- Levi, S., Luzzago, A., Cesareni, G., Cozzi, A., Franceschinelli, F., Albertini, A., Arosio, P., 1988. Mechanism of ferritin iron uptake: activity of the H-chain and deletion mapping of the ferro-oxidase site. A study of iron uptake and ferro-oxidase activity of human liver, recombinant H-chain ferritins, and of two H-chain deletion mutants. *J Biol Chem* 263, 18086-18092.
- Levy, J.E., Jin, O., Fujiwara, Y., Kuo, F., Andrews, N.C., 1999. Transferrin receptor is necessary for development of erythrocytes and the nervous system. *Nature genetics* 21, 396-399.
- Li, J.Y., Paragas, N., Ned, R.M., Qiu, A., Viltard, M., Leete, T., Drexler, I.R., Chen, X., Sanna-Cherchi, S., Mohammed, F., Williams, D., Lin, C.S., Schmidt-Ott, K.M., Andrews, N.C., Barasch, J., 2009. Scara5 is a ferritin receptor mediating non-transferrin iron delivery. *Developmental cell* 16, 35-46.
- Liu, J., Cheng, E., Long, R., Wang, Y., Cheng, P., Yang, J., Wu, D., Mao, H., Chan, A., 2009. Noninvasive monitoring of embryonic stem cells in vivo with MRI transgene reporter. *Tissue engineering. Part C, Methods* 15, 739-747.
- Louie, A., Huber, M., Ahrens, E., Rothbacher, U., Moats, R., Jacobs, R., Fraser, S., Meade, T., 2000. In vivo visualization of gene expression using magnetic resonance imaging. *Nature Biotechnology* 18, 321-325.
- Ludi, A., 1981. Prussian blue, an inorganic evergreen. *Journal of Chemical Education*.
- Mann, S., Sparks, N., Frankel, R., Bazylinski, D., Jannasch, H., 1990. Biomineralization of ferrimagnetic greigite (Fe₃S₄) and iron pyrite (FeS₂) in a magnetotactic bacterium. *Nature* 343, 258-260.
- Mannucci, S., Ghin, L., Conti, G., Tambalo, S., Lascialfari, A., Orlando, T., Benati, D., Bernardi, P., Betterle, N., Bassi, R., Marzola, P., Sbarbati, A., 2014. Magnetic Nanoparticles from *Magnetospirillum gryphiswaldense* Increase the Efficacy of Thermotherapy in a Model of Colon Carcinoma. *PLoS one* 9.
- Martel, S., Mohammadi, M., Felfoul, O., Lu, Z., Pouponneau, P., 2009. Flagellated

- Magnetotactic Bacteria as Controlled MRI-trackable Propulsion and Steering Systems for Medical Nanorobots Operating in the Human Microvasculature. *The International journal of robotics research* 28, 571-582.
- Mátrai, J., Chuah, M.K., VandenDriessche, T., 2010. Recent advances in lentiviral vector development and applications. *Molecular therapy : the journal of the American Society of Gene Therapy* 18, 477-490.
- Matsunaga, T., Nakamura, C., Burgess, I., Sode, K., 1992. Gene transfer in magnetic bacteria: transposon mutagenesis and cloning of genomic DNA fragments required for magnetosome synthesis. *J Bacteriol* 74, 2748-2753.
- Moore, A., Basilion, J.P., Chiocca, E.A., Weissleder, R., 1998. Measuring transferrin receptor gene expression by NMR imaging. *Biochimica et biophysica acta* 1402, 239-249.
- Moore, A., Josephson, L., Bhorade, R.M., Basilion, J.P., Weissleder, R., 2001. Human transferrin receptor gene as a marker gene for MR imaging. *Radiology* 221, 244-250.
- Mora, C., Ranghini, E., Bruno, S., Bussolati, B., Camussi, G., Wilm, B., Edgar, D., Kenny, S., Murray, P., 2012. Differentiation of podocyte and proximal tubule-like cells from a mouse kidney-derived stem cell line. *Stem cells and development* 21, 296-307.
- Muckenthaler, M.U., Galy, B., Hentze, M.W., 2008. Systemic iron homeostasis and the iron-responsive element/iron-regulatory protein (IRE/IRP) regulatory network. *Annual review of nutrition* 28, 197-213.
- Murat, D., Byrne, M., Komeili, A., 2010. Cell biology of prokaryotic organelles. *Cold Spring Harbor perspectives in biology* 2.
- Nakamura, C., Burgess, J., Sode, K., Matsunaga, T., 1995a. An iron-regulated gene, *magA*, encoding an iron transport protein of *Magnetospirillum* sp. strain AMB-1. *The Journal of biological chemistry* 270, 28392-28396.
- Nakamura, C., Kikuchi, T., Burgess, J., Matsunaga, T., 1995b. Iron-regulated expression and membrane localization of the *magA* protein in *Magnetospirillum* sp. strain AMB-1. *Journal of biochemistry* 118, 23-27.
- Naldini, L., Blomer, U., Gallay, P., Ory, D., Mulligan, R., Gage, F.H., Verma, I.M., Trono, D., 1996. In vivo gene delivery and stable transduction of nondividing cells by a lentiviral vector. *Science* 272, 263-267.
- Naumova, A.V., Reinecke, H., Yarnykh, V., Deem, J., Yuan, C., Murry, C.E., 2010. Ferritin overexpression for noninvasive magnetic resonance imaging-based tracking of stem cells transplanted into the heart. *Mol Imaging* 9, 201-210.
- Neumann, E., Schaefer-Ridder, M., Wang, Y., Hofschneider, P., 1982. Gene transfer into mouse lymphoma cells by electroporation in high electric fields. *The EMBO*

journal 1, 841-845.

- Nielsen, T.T., Jakobsson, J., Rosenqvist, N., Lundberg, C., 2009. Incorporating double copies of a chromatin insulator into lentiviral vectors results in less viral integrants. *BMC biotechnology* 9, 13.
- Norrman, K., Fischer, Y., Bonnamy, B., Sand, F.W., Ravassard, P., Semb, H., 2010. Quantitative comparison of constitutive promoters in human ES cells. *PLoS one* 5.
- Ono, K., Fuma, K., Tabata, K., Sawada, M., 2009. Ferritin reporter used for gene expression imaging by magnetic resonance. *Biochemical and biophysical research communications* 388, 589-594.
- Owen, D., Kühn, L.C., 1987. Noncoding 3' sequences of the transferrin receptor gene are required for mRNA regulation by iron. *The EMBO journal* 6, 1287-1293.
- Patel, D., Kell, A., Simard, B., Deng, J., Xiang, B., Lin, H., Gruwel, M., Tian, G., 2010. Cu²⁺-labeled, SPION loaded porous silica nanoparticles for cell labeling and multifunctional imaging probes. *Biomaterials* 31, 2866-2873.
- Peacock, A.K., Cauet, S.I., Taylor, A., Murray, P., Williams, S.R., Weaver, J.V., Adams, D.J., Rosseinsky, M.J., 2012. Poly[2-(methacryloyloxy)ethylphosphorylcholine]-coated iron oxide nanoparticles: synthesis, colloidal stability and evaluation for stem cell labelling. *Chemical communications (Cambridge, England)* 48, 9373-9375.
- Pfaffl, M.W., Horgan, G.W., Dempfle, L., 2002. Relative expression software tool (REST) for group-wise comparison and statistical analysis of relative expression results in real-time PCR. *Nucleic acids research* 30.
- Picard, V., Epsztejn, S., Santambrogio, P., Cabantchik, Z.I., Beaumont, C., 1998. Role of ferritin in the control of the labile iron pool in murine erythroleukemia cells. *J Biol Chem* 273, 15382-15386.
- Picard, V., Renaudie, F., Porcher, C., Hentze, M., Grandchamp, B., Beaumont, C., 1996. Overexpression of the ferritin H subunit in cultured erythroid cells changes the intracellular iron distribution. *Blood* 87, 2057-2064.
- Ponka, P., Beaumont, C., Richardson, D.R., 1998. Function and regulation of transferrin and ferritin. *Seminars in hematology* 35, 35-54.
- Ponka, P., Lok, C.M., 1999. The transferrin receptor: role in health and disease. *The International Journal of Biochemistry & Cell Biology* 31, 1111-1137.
- Powell, A.K., 1998. Ferritin. Its mineralization. *Metal ions in biological systems* 35, 515-561.
- Qasim, W., Vink, C.A., Thrasher, A.J., 2010. Hybrid lentiviral vectors. *Molecular therapy : the journal of the American Society of Gene Therapy* 18, 1263-1267.
- Qi, X., Vargas, E., Larsen, L., Knapp, W., Hatfield, G.W., Lathrop, R., Sandmeyer, S.,

2013. Directed DNA shuffling of retrovirus and retrotransposon integrase protein domains. *PLoS one* 8.
- Qian, Z.M., Li, H., Sun, H., Ho, K., 2002. Targeted drug delivery via the transferrin receptor-mediated endocytosis pathway. *Pharmacological reviews*.
- Renshaw, P.F., Owen, C.S., McLaughlin, A.C., Frey, T.G., Leigh, J.S.J., 1986. Ferromagnetic contrast agents: a new approach. *Magn Reson Med* 3, 217-225.
- Robb, A., Wessling-Resnick, M., 2004. Regulation of transferrin receptor 2 protein levels by transferrin. *Blood* 104, 4294-4299.
- Rodriguez-Porcel, M., Wu, J., Gambhir, S., 2009. Molecular imaging of stem cells. *StemBook*.
- Roe, T., Reynolds, T.C., Yu, G., Brown, P.O., 1993. Integration of murine leukemia virus DNA depends on mitosis. *The EMBO journal* 12, 2099-2108.
- Rohani, R., Figueredo, R., Bureau, Y., Koropatnick, J., Foster, P., Thompson, R.T., Prato, F.S., Goldhawk, D.E., 2014. Imaging Tumor Growth Non-invasively Using Expression of MagA or Modified Ferritin Subunits to Augment Intracellular Contrast for Repetitive MRI. *Mol Imaging Biol* 16, 63-73.
- Rouault, T.A., 2006. The role of iron regulatory proteins in mammalian iron homeostasis and disease. *Nature chemical biology* 2, 406-414.
- Rutledge, E.A., Root, B.J., Lucas, J.J., Enns, C.A., 1994. Elimination of the O-linked glycosylation site at Thr 104 results in the generation of a soluble human-transferrin receptor. *Blood* 83, 580-586.
- Sadikot, R. T., Blackwell, T. S., 2005. Bioluminescence Imaging. *Proceedings of the American Thoracic Society* 2.6, 537–540.
- Santambrogio, P., Levi, S., Arosio, P., Palagi, L., Vecchio, G., Lawson, D.M., Yewdall, S.J., Artymiuk, P.J., Harrison, P.M., Jappelli, R., *et al.*, 1992. Evidence that a salt bridge in the light chain contributes to the physical stability difference between heavy and light human ferritins. *J Biol Chem* 267, 14077-14083.
- Santambrogio, P., Levi, S., Cozzi, A., Rovida, E., Albertini, A., Arosio, P., 1993. Production and characterization of recombinant heteropolymers of human ferritin H and L chains. *The Journal of biological chemistry* 268, 12744-12748.
- Schäfer, R., Kehlback, R., Wiskirchen, J., Bantleon, R., Pintaske, J., Brehm, B.R., Gerber, A., Wolburg, H., Claussen, C.D., Northoff, H., 2007. Transferrin receptor upregulation: in vitro labeling of rat mesenchymal stem cells with superparamagnetic iron oxide. *Radiology* 244, 514-523.
- Schröder, A.R., Shinn, P., Chen, H., Berry, C., Ecker, J.R., Bushman, F., 2002. HIV-1 integration in the human genome favors active genes and local hotspots. *Cell* 110, 521-529.

- Schüler, D., 2004. Molecular analysis of a subcellular compartment: the magnetosome membrane in *Magnetospirillum gryphiswaldense*. *Archives of Microbiology* 181, 17.
- Sengupta, A., Quiaoit, K., T., T.R., Prato, F.S., Gelman, N., Goldhawk, D.E., 2014. Biophysical features of MagA expression in mammalian cells: implications for MRI contrast. *Frontiers in Microbiology*.
- Shaner, N.C., Campbell, R.E., Steinbach, P.A., Giepmans, B.N., Palmer, A.E., Tsien, R.Y., 2004. Improved monomeric red, orange and yellow fluorescent proteins derived from *Discosoma* sp. red fluorescent protein. *Nature biotechnology* 22, 1567-1572.
- Shaner, N.C., Patterson, G.H., Davidson, M.W., 2007. Advances in fluorescent protein technology. *Journal of Cell Science* 120, 4247-4260.
- Smith, S.R., Ghosh, M.C., Ollivierre-Wilson, H., Hang Tong, W., Rouault, T.A., 2006. Complete loss of iron regulatory proteins 1 and 2 prevents viability of murine zygotes beyond the blastocyst stage of embryonic development. *Blood cells, molecules & diseases* 36, 283-287.
- Stolz, J.F., Chang, S.R., Kirschvink, J.L., 1986. Magnetotactic bacteria and single-domain magnetite in hemipelagic sediments. *Nature* 321, 849-851.
- Sutherland, R., Delia, D., Schneider, C., Newman, R., Kemshead, J., Greaves, M., 1981. Ubiquitous cell-surface glycoprotein on tumor cells is proliferation-associated receptor for transferrin. *Proceedings of the National Academy of Sciences of the United States of America* 78, 4515-4519.
- Suzuki, T., Okamura, Y., Calugay, R., Takeyama, H., Matsunaga, T., 2006. Global gene expression analysis of iron-inducible genes in *Magnetospirillum magneticum* AMB-1. *Journal of bacteriology* 188, 2275-2279.
- Taylor, A., Herrmann, A., Moss, D., Sée, V., Davies, K., Williams, S., Murray, P., 2014. Assessing the Efficacy of Nano- and Micro-Sized Magnetic Particles as Contrast Agents for MRI Cell Tracking. *PLOS ONE* 9(6), e100259.
- Taylor, A., Wilson, K.M., Murray, P., Fernig, D.G., Levy, R., 2012. Long-term tracking of cells using inorganic nanoparticles as contrast agents: are we there yet? *Chemical Society reviews* 41, 2707-2717.
- Theil, E.C., 1987. Ferritin: structure, gene regulation, and cellular function in animals, plants, and microorganisms. *Annual review of biochemistry* 56, 289-315.
- Theil, E.C., 1990. The ferritin family of iron storage proteins. *Advances in enzymology and related areas of molecular biology* 63, 421-449.
- Thomson, A.M., Rogers, J.T., Leedman, P.J., 1999. Iron-regulatory proteins, iron-responsive elements and ferritin mRNA translation. *The international journal of biochemistry & cell biology* 31, 1139-1152.

- Torti, F.M., Torti, S.V., 2002. Regulation of ferritin genes and protein. *Blood* 99, 3505-3516.
- Treffry, A., Zhao, Z., Quail, M.A., Guest, J.R., Harrison, P.M., 1997. Dinuclear center of ferritin: studies of iron binding and oxidation show differences in the two iron sites. *Biochemistry* 36, 432-441.
- Trinder, D., Baker, E., 2003. Transferrin receptor 2: a new molecule in iron metabolism. *The international journal of biochemistry & cell biology*.
- Trono, D., 2000. Lentiviral vectors: turning a deadly foe into a therapeutic agent. *Gene therapy* 7, 20-23.
- Udvardi, M., Czechowski, T., Scheible, W., 2008. Eleven golden rules of quantitative RT-PCR. *The Plant cell* 20, 1736-1737.
- Uebe, R., Henn, V., Schüler, D., 2012. The MagA protein of *Magnetospirilla* is not involved in bacterial magnetite biomineralization. *Journal of bacteriology* 194, 1018-1023.
- Ullrich, S., Kube, M., Schübbe, S., Reinhardt, R., Schüler, D., 2005. A hypervariable 130-kilobase genomic region of *Magnetospirillum gryphiswaldense* comprises a magnetosome island which undergoes frequent rearrangements during stationary growth. *Journal of bacteriology* 187, 7176-7184.
- Urbinati, F., Arumugam, P., Higashimoto, T., Perumbeti, A., Mitts, K., Xia, P., Malik, P., 2009. Mechanism of Reduction in Titters From Lentivirus Vectors Carrying Large Inserts in the 3[prime]LTR. *Mol Ther* 17, 1527-1536.
- Ustek, D., Sirma, S., Gumus, E., Arikan, M., Cakiris, A., Abaci, N., Mathew, J., Emrence, Z., Azakli, H., Cosan, F., Cakar, A., Parlak, M., Kursun, O., 2012. A genome-wide analysis of lentivector integration sites using targeted sequence capture and next generation sequencing technology. *Infection, genetics and evolution : journal of molecular epidemiology and evolutionary genetics in infectious diseases* 12, 1349-1354.
- Vande Velde, G., Rangarajan, J.R., Toelen, J., Dresselaers, T., Ibrahimi, A., Krylychkina, O., R., V., Van der Lindenv, A., Maes, F., Debyser, Z., Himmelreich, U., Baekelandt, V., 2011. Evaluation of the specificity and sensitivity of ferritin as an MRI reporter gene in the mouse brain using lentiviral and adeno-associated viral vectors. *Gene Therapy* 18, 594-605.
- Vande Velde, G., Rangarajan, J.R., Vreys, R., Guglielmetti, C., Dresselaers, T., Verhoye, M., Van der Lindenv, A., Debyser, Z., Baekelandt, V., Maes, F., Himmelreich, U., 2012. Quantitative evaluation of MRI-based tracking of ferritin-labeled endogenous neural stem cell progeny in rodent brain. *NeuroImage* 62, 367-380.
- Wang, K., Wang, K., Shen, B., Huang, T., Sun, X., Li, W., Jin, G., Li, L., Bu, L., Li, R., Wang, D., Chen, X., 2010. MR reporter gene imaging of endostatin

expression and therapy. *Molecular imaging and biology : MIB : the official publication of the Academy of Molecular Imaging* 12, 520-529.

- Weissleder, R., Moore, A., Mahmood, U., Bhorade, R., Benveniste, H., Chiocca, E.A., Basilion, J.P., 2000. In vivo magnetic resonance imaging of transgene expression. *Nature Medicine* 6, 351-355.
- de Wet, J.R., Wood, K.V., Helinski, D.R., DeLuca, M., 1985. Cloning of firefly luciferase cDNA and the expression of active luciferase in *Escherichia coli*. *Proc Natl Acad Sci USA* 82, 7870-7873.
- Wilkinson, N., Pantopoulos, K., 2014. The IRP/IRE system in vivo: insights from mouse models. *Frontiers in pharmacology* 5, 176.
- Woods, N.B., Muessig, A., Schmidt, M., Flygare, J., Olsson, K., Salmon, P., Trono, D., von Kalle, C., Karlsson, S., 2002. Lentiviral vector transduction of NOD/SCID repopulating cells results in multiple vector integrations per transduced cell: risk of insertional mutagenesis. *Blood* 101, 1284-1289.
- Worwood, M., 1990. Ferritin. *Blood Rev* 4, 259-269.
- Wu, K., Polack, A., Dalla-Favera, R., 1999. Coordinated regulation of iron-controlling genes, H-ferritin and IRP2, by c-MYC. *283(5402)*, 676-679.
- Wu, X., Li, Y., Crise, B., Burgess, S.M., 2003. Transcription Start Regions in the Human Genome Are Favored Targets for MLV Integration. *Science* 300, 1749-1751.
- Yamagata, Y., Parietti, V., Stockholm, D., Corre, G., Poinsignon, C., Touleimat, N., Delafoy, D., Besse, C., Tost, J., Galy, A., Paldi, A., 2012. Lentiviral transduction of CD34(+) cells induces genome-wide epigenetic modifications. *PLoS one* 7.
- Yamashita, M., Emerman, M., 2006. Retroviral infection of non-dividing cells: Old and new perspectives. *Virology* 344.
- Yang, S.H., Cheng, P.H., Sullivan, R.T., Thomas, J.W., Chan, A.W.S., 2008. Lentiviral integration preferences in transgenic mice. *Genesis (New York, N.Y. : 2000)* 46, 711-718.
- Yao, S., Pasceri, P., Sukonnik, T., Ellis, J., 2004. Retrovirus and Lentivirus Vectors Are Silenced in ES Cells by Dynamic Interplay of Multiple Epigenetic Modifications. *Molecular Therapy*.
- Yin, H., Kanasty, R.y.L., Eltoukhy, A.A., Vegas, A.J., Dorkin, J.R., Anderson, D.G., 2014. Non-viral vectors for gene-based therapy. *Nature reviews. Genetics* 15, 541-555.
- Yoshino, T., Maeda, Y., Matsunaga, T., 2010. Bioengineering of Bacterial Magnetic Particles and their Applications in Biotechnology. *Recent Patents on Biotechnology* 4, 214-225.
- Young, S.P., Bomford, A., Williams, R., 1984. The effect of the iron saturation of

transferrin on its binding and uptake by rabbit reticulocytes. *The Biochemical journal* 219, 505-510.

Zhu, H., Guo, Z.K., Jiang, X.X., Li, H., Wang, X.Y., Yao, H.Y., Zhang, Y., Mao, N., 2010. A protocol for isolation and culture of mesenchymal stem cells from mouse compact bone. *Nature protocols* 5, 550-560.

Zurkiya, O., Chan, A., Hu, X., 2008. MagA is sufficient for producing magnetic nanoparticles in mammalian cells, making it an MRI reporter. *Magnetic resonance in medicine : official journal of the Society of Magnetic Resonance in Medicine / Society of Magnetic Resonance in Medicine* 59, 1225-1231.

APPENDIX I

CDNA SEQUENCES

```
CAGACGTTCTCGCCCAGAGTCGCCGCGGTTTCCTGCTTCAACAGTGCTTGAACGGAACC CGGTGCTCG
ACCCCTCCGACCCCCGCCGCGCTTCGAGCCTGAGCCCTTTGCAACTTCGTGCTTCCGCCGCTCCAG
CGTCGCCACCGCGCTCGCCCCGCCGCCACCATGACCACCGCGTCTCCCTCGCAAGTGCGCCAGAACT
ACCACCAGGACGCGGAGGCTGCCATCAACCGCCAGATCAACCTGGAGTTGTATGCCTCCTACGTCTAT
CTGTCTATGTCTTGTATTTTTGACCGAGATGATGTGGCTCTGAAGAACTTTGCCAAATACTTTCTCCA
CCAATCTCATGAGGAGAGGGAGCATGCCGAGAAACTGATGAAGCTGCAGAACCGAGGAGGTGGCCGAA
TCTTCCTGCAGGATATAAAGAAAACCAGACCGTGATGACTGGGAGAGCGGGCTGAATGCAATGGAGTGT
GCACTGCACTTGGAAAAGAGTGTGAATCAGTCACTACTGAACTGCACAAACTGGCTACTGACAAGAA
TGATCCCCACTTATGTGACTTCATTGAGACGTATTATCTGAGTGAACAGGTGAAAATCCATTAAAGAAC
TGGGTGACCACGTGACCAACTTACGCAAGATGGGTGCCCTGAAGCTGGCATGGCAGAATATCTCTTT
GACAAGCACACCCTGGGACACGGTGATGAGAGCTAAGCTGACTTCCCCAAAGCCACGTGACTTTACTG
GTCACTGAGGCAGTGCATGCATGTCAGGCTGCCTTCATCTTTTCTATAAGTTGCACCAAAAACATCTGC
TTAAGTTCTTTAATTTGTACCATTTCTTCAAATAAAGAATTTTGGTACCC
```

***Mus musculus* Ferritin heavy chain-1 mRNA (NM_010239.2).** Grey area represents the untranslated regions (5' UTR and 3' UTR) and the light area the coding sequence of the Fth-1 mRNA. Note that within the 5' UTR, an iron responsive element is represented in blue. ATG and TAA in red correspond to the start and stop codons, respectively. The sequence in green is an Fth-1 native Kozac sequence. The underlined nucleotides correspond to the primer specific region used to amplify the cDNA sequence.

```
GTGCGGAAGGAAGTGACGTAGATCCAGAGGGCCGCCGGGGGTGGGGCCGAGCTATAAGCTTTGGGT
GGGAGGCAGCGCTGCCTTCAGAAGGCGTGCGGAGCGCGGGCTGCTGCATTGCGGACTGTAGAGGCGCT
TCCTAGTACTCCCTTGTAGCAGCTGAGAATGATGGATCAAGCCAGATCAGCATTCTCTAAGTTGTTTG
GTGGGGAACCATTTGTCATACACCCGTTTAGCCTTGCTCGGCAAGTAGATGGAGATAACAGTCATGTG
GAGATGAAACTGGCTGCAGATGAAGAAGAAAATGCCGACAATAACATGAAGGCTAGTGTGAGAAAACC
CAAGAGGTTTAAATGGAAGACTCTGCTTTGCAGCTATTGCACTAGTCATTTTCTTCTTGATTGGATTCA
TGAGTGGCTACCTGGGCTATTGTAAGCGTGTAGAACAAAAAGAGGAGTGTGTGAACTGGCTGAAACG
GAGGAGACAGACAAGTCAGAAACCATGGAAAACAGAGGATGTTCCCTACATCATCTCGCTTATATTGGGC
AGACCTCAAAACACTGTTGTCAGAGAAGTTGAACTCCATAGAGTTTGCTGACACCATCAAGCAGCTGA
GCCAGAATACATACACTCCTCGTGAGGCTGGATCTCAAAAAGATGAAAGTCTTGCCATTTATATTGAA
AATCAGTTCCATGAATTTAAATTCAGCAAAGTCTGGCGAGATGAACACTATGTGAAGATTCAGTGAA
AAGCAGCATTGGTCAAAACATGGTGACCATAGTGCAGTCAAATGGTAACTTAGACCCAGTGGAGTCTC
CCGAGGGTTATGTGGCATTTCAGTAAACCTACAGAAGTTTCTGGTAACTGGTCCATGCTAATTTTGGC
ACTAAAAGGACTTTGAAGAACTAAGTTATTCTGTGAATGGATCTTTAGTGATTGTTAGAGCAGGGGA
AATTACTTTTGCAGAAAAGGTTGCAAATGCCCAAAGCTTTAATGCAATTGGTGTCTCATATACATGG
ACAAGAATAAATTTCCCGTTGTTGAGGCAGACCTTGCACCTTTGGACATGCTCATCTAGGAACTGGT
GATCCATACACACCTGGCTTTCTTTCAATCATACTCAGTTTCCGCCATCTCAGTCATCAGGGTT
GCCTAATATACCTGTGCAAAACAATCTCAAGAGCTGCTGCAGAAAAGCTATTTGGAAAAATGGAAGGAA
GCTGTCTCTGCTAGATGGAACATAGATTCTTCATGTAAGCTGGAACCTTTCACAGAATCAAAATGTGAAG
CTCATTGTGAAAACGTAAGTAAAGAAAGAAATACTTAACATCTTTGGAGTTATTAAGGTTATGA
GGAACCAGACCGTTATGTTGTAGTAGGAGCCAGAGAGACGCTTTGGGTGCTGGTGTGCGGCGAAGT
CCAGTGTGGGAACAGGTCTTCTGTTGAAACTTGCCCAAGTATTCTCAGATATGATTTCAAAAGATGGA
```

TTTAGACCCAGCAGAAGTATAATCTTTGCCAGCTGGACTGCAGGCGACTTTGGAGCTGTTGGTGCCAC
TGAGTGGTTGGAGGGATACCTTTTCATCTTTGCATTTAAAAGCTTTCACTTATATTAATTTGGATAAAG
TTGTCCTTGGTACTAGTAACCTTCAAAGTTTCTGCCAGCCCCCTATTATATACACTTATGGGAAAGATA
ATGCAAGATGTAAAGCATCCAGTTGATGGAAAATCTCTATATAGAGACAGCAATTGGATTAGCAAAGT
TGAGAAACTTTCCCTTTGACAATGCTGCATATCCTTTCCCTGCATATTTCTGGAATCCCAGCAGTTTCTT
TTTGTTTTTGTGAGGATGCAGACTATCCTTATTTGGGCACTAGATTGGATACCTATGAGGCATTGACT
CAGAAAGTTCCCTCAGCTCAACCAAATGGTTTCGTACAGCAGCGGAAAGTGGCTGGTCAGCTCATTATTAA
ACTTACCCATGACGTTGAATTGAACCTGGACTATGAGATGTATAACAGCAAACTACTGTCATTTATGA
AGGATCTGAACCAGTTCAAAACAGATATCAGGGATATGGGTCTAAGTCTACAGTGGCTGTATTTCCGCT
CGTGGAGACTACTTCCGTGCTACTTCTAGACTAACAACCTGATTTTCATAATGCTGAGAAAACAAACAG
ATTTGTTCATGAGGGAAATCAATGATCGTATTATGAAAAGTGGAGTATCACTTCCCTGTCGCCCTATGTAT
CTCCAAGAGAGTCTCCTTTCCGACATATCTTCTGGGGCTCTGGCTCTCACACTCTCTCAGCTTTAGTG
GAGAACTTGAAGCTTCGTCAAAAAAATATTACTGCTTTTAAATGAAACCCCTTTCAGAAACCAGTTGGC
CCTGGCTACTTGGACTATTCAGGGAGTCGCAAATGCCCTCTCTGGTGACATTTGGAATATTGACAATG
AGTTTTAAATGTAACATGCATAATTAATAAGAGCAGGGTAGTCTGTTTCTAGACTTGTGTTGGTTGT
GCTAAATTTTCATTAGAGCTCTAAAATCTAATGTTAAAATTTCTACCCAATCATCTAATGCTTTAGGCA
GCAGCTTTTAGTGCGGGTTGGACCTACACTTCAAGTACAATGGATAACACTTTCCATGTTTGTGATA
TCTTCTCAGATTATCTTTAAAATTTTTGAGTCTTTGTAATAACTTCCCTCTTGTCTCATGGTCATGA
AAATGTCAGAACCAGTTGTAAGAACAATGCTATATGCTCTGAGGGCATTAACTAGTGTCTTTTGAGGT
AGGAGAAAGAGTGTGCTTGTGGAGGGTCAACGTGGTAGTTGGGTAGTTGGAGATTGCCCGTCTCCAT
CTGATCTTCCATTGAGCTGTATGCCCTTAAGGATGTAGCTGGTTTTGCATTTCCCTAAATTAGACAGTA
ACTTTTCAGAAGAGATGGAACCTTGTTTTTCTTGGCAGCAAGTTGAAAATAGGTCCTTAGCTGGACCAAT
TTGTCTGTTTACAGGAATAAGTAAGGCCTTACTGGTTAACCTTGGTGTTCTTTATGATGAGACCAGAA
GCCAAAGACCTCAAGTTTTCTCTCCTTGGCATCTGCCCTATAGTCTTTAGTCTTTGTTTTTATTT
TGTTTTTCTTTTTTCCCAACATTTCTGAAAAAGAACAAGTTTLAGACTCAATTTGTCAGACTTGAA
AAGAACACACTGCCAAGTTTTGGCCAAAGTGTAGTCTTCAGGAAAGCTTCTATCATTTTGGCACTG
AGATATTTATTGTTTATTTATCAGTGACAGAGTTCACTATAAATAAGTGTGTTTTTTTTTATATATA
GAAGAATAATTATCGGAAGCAGTGCCTTCCATAATTAATGACAGTTATACTGTCGTTTTCTTTAATAAA
AGCAGCATCTGCTAATGAGACCCACAGATACTGGAAGTTTTGCACTTATGGTCAGCACTTGCAACTTT
AGGAAGGAAGAATGCCACAATCCAAATAATATGAGCTAGAAGAGGATTGGGTAAATAAGAGATTCCCT
AATTGAGTTGGGGAAAAAATGATAGTTTTTCTAAGTGCAGTGTGTTGGCCAAAGTTAAATGTCATT
TAAAGGCTATGGTAGTACTTACATCTACAAAATTTTACAGCTCAATTTATTCAAGATGTAACCTAAAA
TCAATTTTGAAAATTTCCAGTACCTTTGTCACAACTTAACCTCACATTATCGGGAGCAGTGTCTTCC
ATAATGCATAAAGAACAAGGTAGTTTTTGCCTACCACAGTGTCTATATCGGAGACAGTGATCTCCATA
TGTTACACTAAGGGTGTACGTAATTATCGGGAACAGTGTCTTCCATAATTTCTTTCATGCAATGACAT
CTTCAGAGCTTGAAGATCGTTAGTATCTAACATGAATTCCTAACTTCCCTGTAGCTCCTTAGTTTTAGT
TGCAAAAAACATTTGTGGTCATTGAGCATTGGTGGGTAAAAATCAACTGCTGTAAAAATCATTACTTCC
AAGATCCTTTTTTAAAATGTGGGTATTTTGTATCTCTGGTTTATGGAATAAAAAGCATACTGTTTATAA
TGTTTTGCTGGTGACAAAAGGAATTTAACTATCTCCCTTTATTTGCATGTTACATGTTATTTCCCTAAATG
TAGTTCCTTAGAAGTTTGAATTCATTTTTGGTTTTTGGGAGGGTAGAAAAGTAGAGAATAATGGGTGTTG
GGAAGACAAAGCTTGCAAAAGGATCTTTATGTACCTGCTCATCACTATGGTGGCTATGAATTATGTAG
GTAATGAGCAAGATCACATTAACAAAGACTAGTTAACCATCATTACGCATCTAATCAGTTTTGCCATG
GGGTGAGTTCAAAGCTGCCACCTGAGAATGTCCTAGGCTCTCAGGGTCTTGGCACCCTCGCCCAAG
TTATATCCACCAGATTATTTTGGCCTCACTGAGTGTGTTTGTACTCAGTCCCTCAGTCTTCACAG
TGTTTTCTTGTACCAGTATGAGTATCACCGTGCATAATGGGATTCGAAGTCTTGAATGAAGGCATGC
ATTTTACATAGACGTCTCTGTGAAATAACCTTTGTTGTAAGTGGTGTTCAGTCAAAGCAGTAAGTT
GGTAAGGTTTAGTCTTGGGTGAAATGTGGATCTGAGTAATAAGTAGCTTCTGCTACTTATCAGGTTAT
TGTTGGTTAAAATGTAGATTTTGAAGATAAAAAATAGATCTTTTGTTCATGACTCACTGCTAGAATTTGC
ATGACCTTTACTGTGTTAGCTTTTGAATGCCTTTTTGGTTTTGGACTTGCCAACCTATACTGTCTTTGCT
GAAATGCCCTTATAAATGTATACAGCTGGTATGTAACAATGTGAAGATTCCCTACCTGACTTAATAAA
ATACTTCGATAATACTGAAAAAAA

***Mus musculus* Transferrin Receptor-1 mRNA (NM_011638.4).** Grey area represents the untranslated regions (5' UTR and 3' UTR) and the light area the coding sequence of the TfR-1 mRNA. Note that within the 3' UTR, five iron responsive elements are represented in blue. ATG and TAA in red correspond to the start and stop codons, respectively. The underlined nucleotides correspond to the primer specific region used to amplify the cDNA sequence.

```

CGTCGAGGTCATCGAAAGACGGGGGCGTCTCGTGGTCAGCCATAGGTCAGTCTCGAAATCCCCCTTC
TGGCGCTTTGGTGCCAAAAGCGCGGGCACCATAAGGTCTGGACCCACCCGTGTCAAGGACTCAAACCG
GCGAAGCCAACACGCTGAATTGCATTGGTGAATCAGGGGGTTTGCGGGGTCGCGCCATGCCGGATGCT
GCGTTGCGGCAAGATTCTTCCCACCCAAGGGGTGGCGTCAGGTGGGATTCGGCCACCGATCGCTTAT
CCCCATTTCCGTCCCAGATGATTTTCCGCCCCCTCCAGCCGCTCACTCTTGCAACATCCGCACTTTA
GACCGTGGGCTGCCTTCGTGTTAAGAACGTGCCATGGACCTGCATCATCCCGAACTGACCTATGCCGC
CATCGTCGCCCTGGCCGCCGTTCTGTGCGGGGGCTGATGACGCGCTCAAGCAACCGGCCATCGTCG
GCTATATCCTGGCCGGGGTGGTGCTGGGCCCCAGCGGCTTCGGGCTGGTGAGCAACCGCGACGCCGTG
GCCACCCTGGCCGAGTTCGGCGTGCTGATGCTGCTCGTTTCGTTCATCGGCATGAAGCTGGACATCATCCG
TTTTCTCGAAGTGTGGAAGACGGCGGTCTTACCACCGTTTTGAGATCGCGGGCTCCATCGGCACGG
CGTGCTGCTGCGCCACGGTTTGGGCTGGAACCTGGGGCTGGCGGTGGTGCTGGGCTGCGCCGTGGCG
GTGTCGTCCACCGCCGTGGTGATCAAGGTGCTGGAATCCTCGGGCGAGTTGAAACGCCGGTGGGGCG
CACCACGCTGGGCATCCTGATTGCCAGGACATGGCGGTGGTCCCATGATGCTGGTGCTGGAATCCT
TCGAGACCAAGGTGTTGCTGCCCCCGATCTGGCCCCGCTGATCCTGTCCGTGCTGTTCTGGTGCTG
CTGTTCTGGTGGCTGTCCAAGCGCCGTATCGACCTGCCGCTGACCTCCCGGCTGTGCGGGATTCCGA
TCTGGCCACCCTTTCTCCCTGGCTGGTGTCTTGGCACGGCGCCATTTCCGGGGTGTGGACCTGT
CGCCCGCCTATGGCGCCTTTCTGGGCGGCTGGTGCTGGGCAATTCCGCCAGCGGACATGCTCTTG
AAGCGCGCCAGCCCATCGGCAGCGTGCTGTTGATGGTGTTCTTCTGTCATCGGGTTGCTGCTTGA
TTTCAAGTTCATCTGGAAGAATCTGGGCACCGTTCTCACTCTTTTAGCCATGGTGACGCTGTTCAAGA
CGGCGCTGAACGTCGCCGCGCTGCGTCTGGCGCGTCAGGACTGGCCCAGCGCTTCTGGCCGGGGTG
GCCCTGGCCCAGATCGGCGAGTTCGTTTTTGGCTGGCCGATACCGCAAGGCGGTTAAGCTGATCAG
CGCCCAGGAGACCAAGCTGGTGGTGGCGGTCACCGTGCTGTCCCTGGTGTGTCGCCCTTCTGGCTGT
TCACCATGCGGCGTATGCATCGGGTGGCGGCGGTGCATGTCCATTCGTTCCGCGAATTGGTCTCGCGG
CTTTACGGCGACGAAGCCCGCACCGCGCGGGCCCCGCACCCTGGTGCGGCGGGGCTCTTGAGGGA
TGATCACAATGCCGACCTGGCACTGGAATCTGAGATCGGGGGCATCGTCTGCGGCATCGACGA

```

***Magnetospirillum magnetotacticum* MS-1 Strain MagA insert sequence (1696 bp)** originally in pCR2.1 vector (Invitrogen), Addgene, [21751](#). Grey area represents the genomic DNA surrounding the MagA gene (light area). ATG and TGA correspond to the start and stop codons, respectively. The underlined nucleotides correspond to the primer specific region used to amplify the current gene. In green, C is a mismatch from G-C and G is a new insertion, identified by sequencing analysis and not previously reported by Addgene. These mutations are silent and do not affect the amino acid coding sequence. In red, two missense mutations reported by Addgene, led to amino acid substitutions, S94L and P390S. These substitutions are not conservative and the influence it may have of normal gene coding of MagA is unknown.

APPENDIX II

BUFFERS, SOLUTIONS, MEDIA, OTHER MATERIAL

Molecular Biology	Manufacturer, catalogue number
2-propanol	Sigma, I9516
Accuzyme™ DNA Polymerase	Bioline, BIO-21051
Agarose	Helena Biosciences, 8201-07
BIOTAQ™ DNA Polymerase (5U/μl)	Bioline, BIO-21040
Calf Intestinal Alkaline Phosphatase, 10,000units/ml	NEB, M0290S
Chloroform	Sigma, C2432
dNTP Set	Bioline, BIO-39025
Ethanol	Sigma, E7023
Fast SYBR® Green Cells-to-CT™ Kit	Life Technologies, 4402956
FlashGel® Recovery Kit	Lonza, 57050
FlashGel® System	Lonza, 57067
HyperLadder™ I	Bioline, BIO-33026
HyperLadder™ IV	Bioline, BIO-33030
LB-Agar	MERCK, 1.10283.0500
Minielute PCR Purification Kit	Qiagen, 28004
Molecular biology water	Lonza, 1315
One Shot® Stbl3™ Chemically Competent <i>E. coli</i>	Invitrogen, C7373-03
Phenol: Chloroform: Isoamyl alcohol (25:24:1)	Sigma P3803
QIAprep® spin miniprep kit	QIAGEN, 27104
QIAquick gel extraction kit	QIAGEN, 28706
Random hexamers	QIAGEN, 79236
RQ1 DNase 10x reaction buffer	Promega, M198A
RQ1 DNase Stop Solution	Promega, M199A
RQ1 RNase-Free DNase	Promega, M6101A
Sodium acetate	Sigma, S5636
SuperScript™III Reverse Transcriptase	Invitrogen, 18080-044
SYBR® Safe DNA gel stain	Invitrogen, S33102
T4 DNA Ligase (1U/μl)	Roche, 10481220001
TOPO TA Cloning Kit	Invitrogen, K4650-01
TRIzol® Reagent	Invitrogen, 15596-026
X-gal (5-Bromo-4chloro-3-indolyl-β-D- galactopyranoside)	Calbiochem, 203782

Restriction enzymes

BamHI	NEB, R0136S
EcoRI-HF™	NEB, R3101S
Hind III	NEB, R0104S
Stu I	NEB, R0187S
Xba I	Promega, R618A
Xho I	NEB, R0146S

Cell Culture

Manufacturer, catalogue number

1-thyoglycerol	Sigma, M6145
2x HEPES	Sigma, 515588
Alizarin Red S	Sigma, A5533
Aspirator tube assembly for calibrated microcapillary pipettes	Sigma, A5177
Bright Cryo-m-Bed embedding medium	Bright instruments, 53581-1
Calcium Chloride 2.5 M Solution - 5 ml	Sigma, C2052
Cell Counting Kit-8 Solution	Sigma, 96992
Corning® bottle-top vacuum filter system	Sigma, CLS430767 and CLS430769
Corning® Costar® cell culture plates – 6-well, flat bottom	Sigma, CLS3516
Culture slides tissue culture 8-well	VWR, 734-0089
Deoxyribonuclease I from bovine pancreas	Sigma, D5025
DMEM: F12 (1:1) medium	Lonza, 12-719
DMSO	Sigma, D2650
DMEM	Sigma, D6546
Dulbecco's Phosphate Buffered Saline	Sigma, D8537
Fast Green FCF	Sigma, F7258
Foetal Calf Serum	PAA Laboratories, A15-609
Formaldehyde Solution	Thermo Scientific, 28908
Leukaemia Inhibitor Factor	Merck Millipore, LIF2010
L-glutamine 200mM	Sigma, G7513
Minimum Essential Medium Eagle (MEM)	Sigma, M5650
Oil-red-O	Sigma, O0625
PES filter (0.22µm)	MILLEX-GP, SLGP033RS
PES filter (0.45µm)	Sartorius Stedim, 16555
Polybrene	Sigma, H9268
Safranin-O	Sigma, S2255
Sodium Pyruvate	Sigma, S8636
Triton X-100	Sigma, T-8787
Trypan Blue Solution	Sigma, T8154
Ultracentrifuge tubes, Thinwall, UltraClear	Beckman Coulter, 344058

Cell Culture mediums:**Cell culture medium A**

Fetal Calf Serum	10%	
L-glutamine	1%	Filter with Corning® bottle-top vacuum filter system
Made in DMEM		

Cell culture medium B

Fetal Calf Serum	10%	
L-glutamine	1%	
1-thyoglycerol	100 mM	
LIF	1.5 U	Filter with Corning® bottle-top vacuum filter system
Made in DMEM		

Cell culture medium C

Fetal Calf Serum	10%	Filter with Corning® bottle-top vacuum filter system
Made in DMEM: F12		

Freezing medium

Fetal Calf Serum	30%	
DMSO	10%	
Made in DMEM		Filter with 0.22 µm PES filter

Osteogenic induction media

Dexamethasone	100 nM	
2-phospho-L-ascorbic acid trisodium salt	75 µM	
β-Glycerol phosphate	10 mM	
Fetal Calf Serum	10%	
Made in MEM		Filter with 0.22 µm PES filter

Adipogenic induction media

Dexamethasone	100 nM	
IBMX	500 nM	
Indomethacin	50 µM	
Bovine pancreas insulin	175 nM	
Fetal Calf Serum	10%	
Made in MEM		Filter with 0.22 µm PES filter

Chondrogenic induction media

TGFβ ₃	10 ng mL ⁻¹	
BMP7	100 ng mL ⁻¹	
Dexamethasone	100 nM	
2-phospho-L-ascorbic acid trisodium salt	50 μM	
Proline	40 μg mL ⁻¹	
Sodium pyruvate	1 mM	
Insulin-transferrin-selenium	1% (v/v)	
Made in DMEM		Filter with 0.22 μm PES filter

Intracellular Iron Uptake:**Iron supplements** **Manufacturer, catalogue number**

Ferric citrate	0.2/2 mM	Sigma, F3388
Human holo-transferrin	100 μg/ml (1.28 mM)	Sigma, T0665
L-ascorbic acid	50 μM	Sigma, A4403

Iron measurement

Potassium permanganate	Sigma-Fluka, 60459
Iron Standard for AAS	Sigma-Fluka, 16596

Ferrozine reagent

Ammonium acetate	5 M	Sigma, A1542
Ascorbic acid	2 M	Sigma, A0278
3-(2-Pyridyl)-5,6-diphenyl- 1,2,4-triazine- <i>p,p'</i> -disulfonic acid monosodium salt hydrate	6.5 mM	Sigma, 160601
Neocuproine	15,4 mM	Sigma, N1501

Prussian Blue

Iron stain kit		Sigma, HT20
4% potassium ferrocyanide solution	50%	Sigma, HT20-1
4% hydrochloric acid	50%	Sigma, HT20-2

DAB enhancement solution

DAB	0.025%	Sigma, D8001
Hydrogen peroxide	0,005%	Sigma, H3410
Made in PBS		

Immunofluorescence and Western Blot	Manufacturer, catalogue number
Dako Fluorescence Mounting Media	Dako, S3023
Pierce™ BCA Protein Assay Kit	Thermo Scientific, 23225
NuPAGE LDS Sample buffer (4x)	Life Technologies, NP0007
NuPAGE Reducing Agent (10x)	Life Technologies, NP0009
XCell SureLock Electrophoresis	Life Technologies, EI0001
MOPS Running Buffer (20x)	Life Technologies, NP0001
NuPAGE Antioxidant	Life Technologies, NP0005
NuPAGE® Novex® 4-12% Bis-Tris Protein Gel	Life Technologies, NP0336
Odyssey Protein Molecular Weight Marker	Licor, 928-40000
Immobilon®-FL Transfer Membranes (PVDF)	Millipore, IPFL 10100
NuPage Transfer Buffer (20x)	Life Technologies, NP0006
Sponge pad	Life Technologies, EI9052
XCell II Blot Module	Life Technologies, EI9051
Odyssey® Blocking Buffer	Licor, 927-40000

Western Blot Solutions:

Lysis Buffer for protein extraction

Tris-HCl (pH 7.5)	50 mM	
EDTA	1 mM	
EGTA	1 mM	
Sodium orthovanadate	1 mM	
Triton X-100	1%	
Sodium pyrophosphate	5 mM	
Sodium B-glycerophosphate	10 mM	Aliquot and store at -20 °C
Phosphatase inhibitor	1%	Add fresh to complete solution
Protease inhibitor cocktail	1%	

Transfer buffer

NuPage Transfer Buffer (20x)	1x	
Methanol	10%	
Made in distilled water		Add 1% NuPage Antioxidant at time of use

Other Solutions:

10x TAE

NaCl	48.4 g
Glacial Acetic Acid (17.4M)	11.4 ml
EDTA	3.7 g
H ₂ O	Up to 1L

PBS

NaCl	8 g	
KCl	0.2 g	
Na ₂ HPO ₄ dibasic	1.44 g	
KH ₄ PO ₄ monobasic	0.24 g	
H ₂ O	Up to 1 L	Adjust to pH 7.4-7.6

20% (w/v) Sucrose Solution

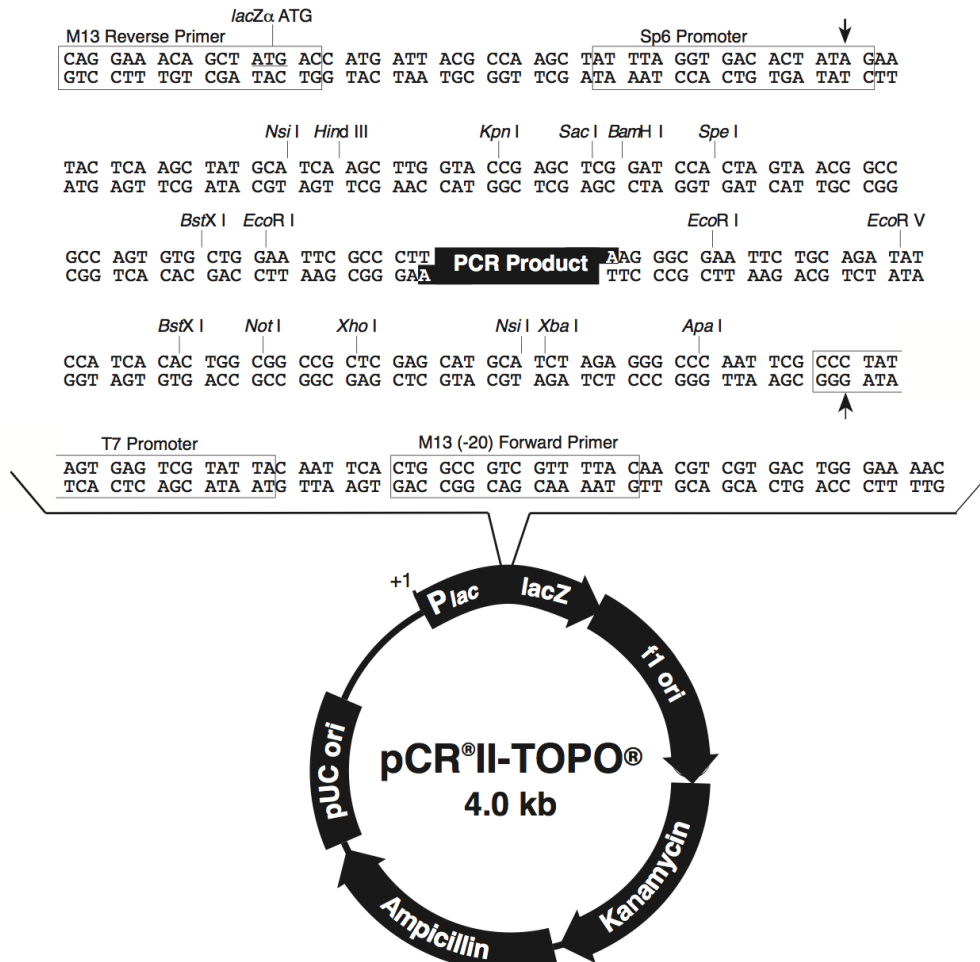
Sucrose	20%	
Sodium Chloride	0.1 M	
Sodium Chloride	0.001 M	Make in distilled water and Filter with
HEPES	0.02 M	0.22 µm PES filter

4% (v/v) formaldehyde

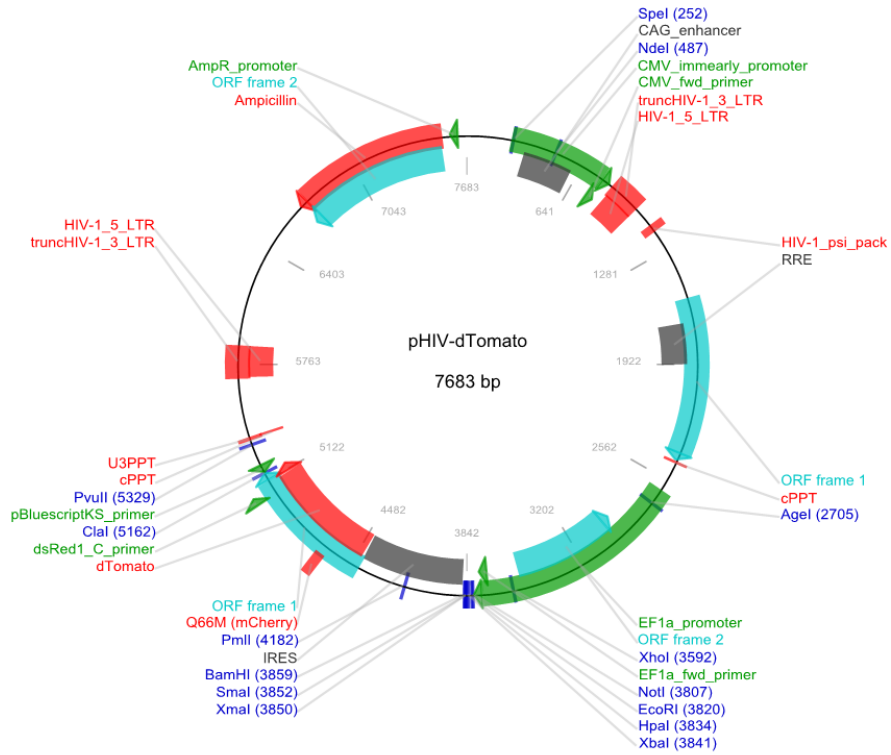
16% Formaldehyde Sol.	10 ml
PBS	30 ml

APPENDIX III

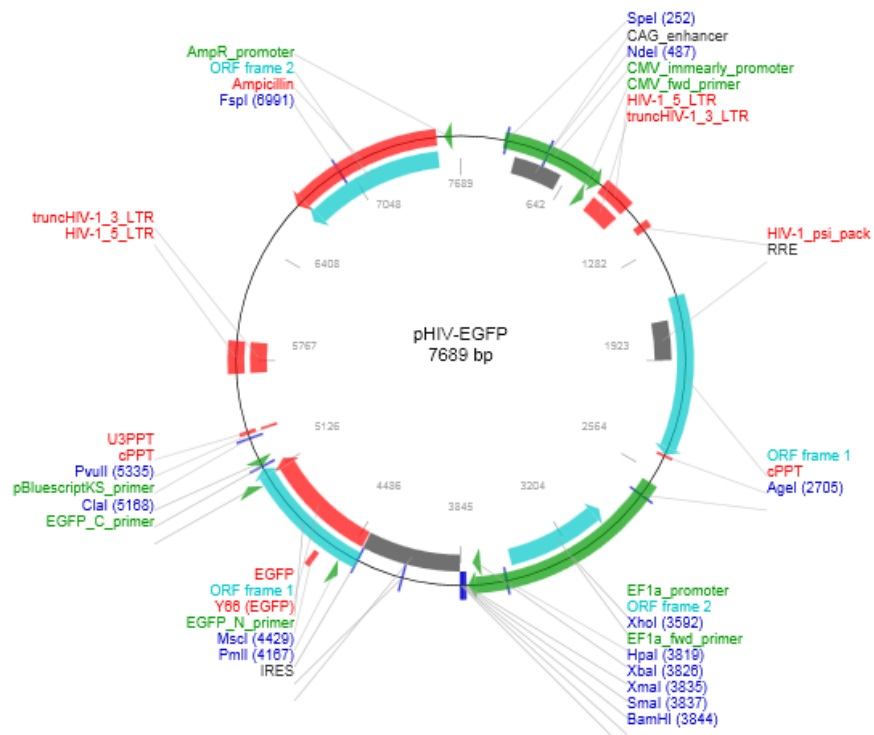
PLASMID MAPS



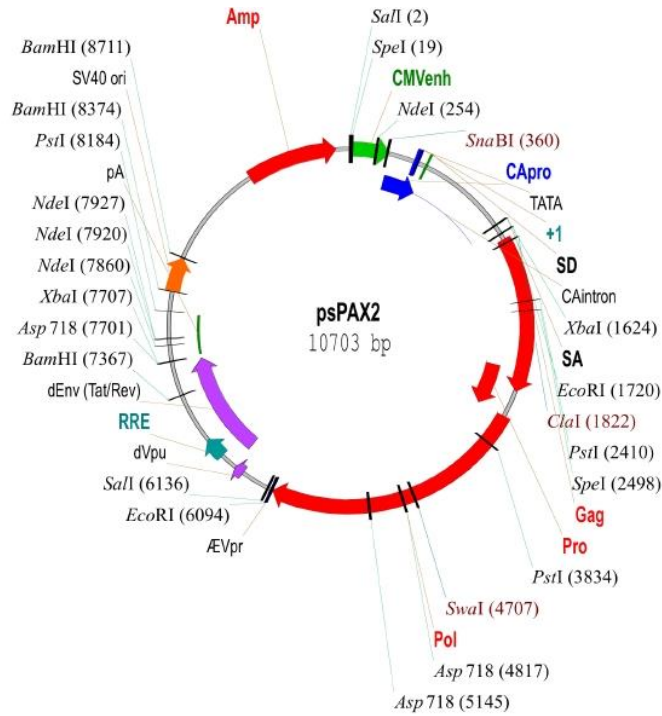
Restriction map of pCR®II-TOPO® Vector. Sequence of the multiple cloning site is annotated (TOPO TA Cloning Kit, Invitrogen).



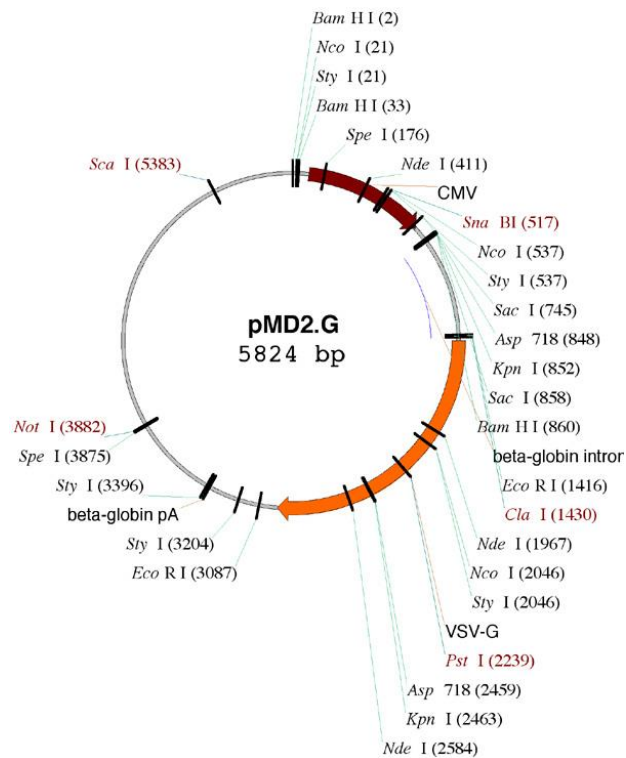
Lentiviral plasmid map of pHIV-dTomato (Addgene, 21374). Key features are annotated in the map.



Lentiviral plasmid map of pHIV-eGFP (Addgene, 21373). Key features are annotated in the map.



2nd generation packaging vector, psPAX2 (Addgene, 12260). One of the elements used to cotransfect a producer cell line, together with transfer (pHIV-dTomato/ pHIV-eGFP) and envelope (pMD2.G) plasmids in a 2nd generation HIV-based lentiviral system.



2nd generation envelop vector, pMD2.G (Addgene, 12259). One of the elements used to cotransfect a producer cell line, together with transfer (pHIV-dTomato/ pHIV-eGFP) and packaging (psPAX2) plasmids in a 2nd generation HIV-based lentiviral system.